MAGNETIC PROPERTIES OF ALKALI-BIPHENYL SINGLE CRYSTALS AND THE CALCULATION OF SPIN-SPIN INTERACTIONS

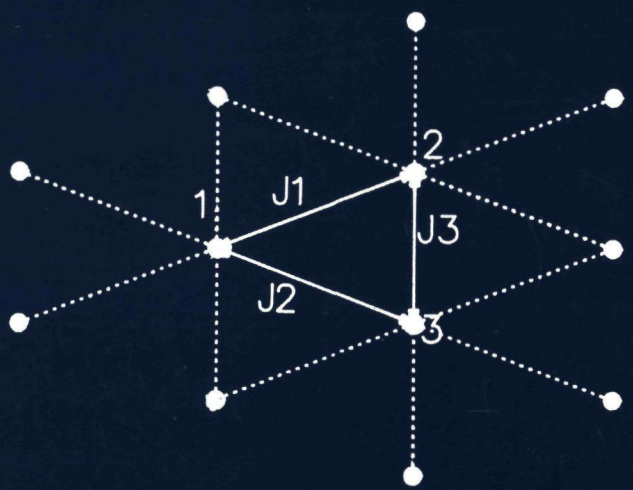

MICHIEL GRIBNAU

MAGNETIC PROPERTIES OF ALKALI-BIPHENYL SINGLE CRYSTALS AND THE CALCULATION OF SPIN-SPIN INTERACTIONS

CIP-GEGEVENS KONINKLIJKE BIBLIOTHEEK, DEN HAAG

Gribnau, Michael Carolus Maria

Magnetic properties of alkali-biphenyl single crystals
and the calculation of spin-spin interactions /
Michael Carolus Maria Gribnau. – [S.l.:s.n.]–
(Enschede : Quick Service)
Proefschrift Nijmegen.–Met samenvatting in het Nederlands.
ISBN 90-9002098-5
SISO 535 UDC 537.6 (043.3)
Trefw.: electron paramagnetic resonance (EPR) /
2-d magnetisme / spin-spin interacties.

MAGNETIC PROPERTIES OF ALKALI-BIPHENYL SINGLE CRYSTALS AND THE CALCULATION OF SPIN-SPIN INTERACTIONS

Een wetenschappelijke proeve op het gebied van de

WISKUNDE EN NATUURWETENSCHAPPEN

Proefschrift

ter verkrijging van de graad van doctor
aan de Katholieke Universiteit te Nijmegen,
volgens besluit van het College van Decanen in het
openbaar te verdedigen op
woensdag 22 juni 1988
des namiddags te 1.30 uur precies

door

Michael Carolus Maria Gribnau
geboren op 18 augustus 1959
te Heerlen

Druk : Quick Service Enschede

1988

Promotor : Prof. Dr. E. de Boer
Co-Referent : Dr. C.P. Keijzers

Voor mijn ouders
Voor Margret

A dwarf on a giant's shoulders
sees the farther of the two

Het proefschrift dat voor U ligt is het tastbare resultaat van een periode van vier jaar van intensieve samenwerking van de auteur met vele anderen. Door deze samenwerking en de daarbij behorende kruisbestuiving met de ideeën van anderen en voortbouwend op de kennis en tradities van vele generaties onderzoekers, heeft dit proefschrift zijn uiteindelijke vorm gekregen. Ik ben daarom blij om op deze plaats iedereen te kunnen bedanken met wie ik heb mogen samenwerken. Zonder iemand tekort te willen doen, wil ik enkele mensen met name noemen:

Jan Smits van de afdeling kristallografie voor zijn hulp bij het werk met de Weissenberg camera en de X-ray diffractometer.

Cees Beers van de afdeling vaste stof physica II voor de prettige samenwerking bij de susceptibiliteitsmetingen aan NaBp.2Tg en KBp.2Ttg.

Desirée van der Wey voor de snelheid en accuratesse waarmee ze het vele typewerk van de afgelopen jaren heeft uitgevoerd.

Jeroen Pikkemaat voor de inzet en het enthousiasme waarmee hij als hoofdvakstudent de metingen aan het RbBp.2Ttg heeft verricht. Veel van zijn resultaten zijn terug te vinden in hoofdstuk 4.

Ed Reijerse en Gooitzen Zwanenburg voor de vele discussies die mijn inzicht verdiept en uitgebreid hebben.

Gern möchte ich auch Dr. R. Kirmse von der Karl Marx Universität im Leipzig danken für die angenehme zusammen Arbeit wehrend seines Besuch an die Niederlande in 1986.

Een bijzonder woord van dank ben ik verschuldigd aan Adri Klaassen voor zijn assistentie bij de ESR, ENDOR en ESEEM metingen en voor het synthetiseren van de KBp.2Ttg kristallen. Zonder zijn deskundigheid en goede humeur zag dit proefschrift er heel anders uit.

Het is betreurenswaardig dat het promotiereglement mij niet toestaat dr. Kees Keijzers en prof. dr. E. de Boer te bedanken voor hun bijdragen aan dit onderzoek. Hun kennis en enthousiasme, die de voortgang van het hier beschreven onderzoek sterk bevorderd hebben, had ik dan niet onvermeld hoeven te laten.

De medewerkers van de afdeling C&CZ en Océ Nederland ben ik zeer erkentelijk voor de hulp bij het afdrukken van de eindversie van dit proefschrift.

Tenslotte wil ik de morele steun en inspiratie noemen van diegenen aan wie dit proefschrift is opgedragen.

Contents

This thesis was typeset in LaTeX on an Atari 1040ST.
The final version was printed on an Océ 6750 Laserprinter.

Chapter 1

Introduction

1.1 Historical Background and Motivation

Negative aromatic ions play a significant role in many organic reactions. Therefore, it is of fundamental importance to expand our knowledge of these anions. The study of alkali-aromatic ion pairs has been a main topic of research at the department of Molecular Spectroscopy at the university of Nijmegen for many years [1,2,3]. The goal of this research being to relate the magnetic properties, obtained from EPR, NMR and susceptibility measurements, with the molecular and electronic structures of these molecules. The magnetic resonance measurements were first carried out in liquid solutions, which have the inherent disadvantage that the information due to anisotropic interactions is lost on account of rapid molecular reorientations. Furthermore, these studies yield no direct information about the structure of these ion-pairs. The discovery by Canters in 1969 [1,4] that single crystals containing alkali-biphenyl ion pairs could be grown from highly concentrated solutions of alkali-biphenyl in polyglycoldimethylethers was the starting point of research on the solid state properties of these compounds. Among others, single crystals of NaBp.2Tg, KBp.2Ttg and RbBp.2Ttg could be prepaired. The magnetic properties of these alkali-biphenyl ion pairs were studied by Mooij [3] by EPR and susceptibility measurements. He showed that the temperature dependence of the magnetic susceptibility of NaBp.2Tg and KBp.2Ttg in the high temperature region could be described with the molecular field model for a hexagonal two-dimensional lattice [3,5], whereas the temperature dependence of RbBp.2Ttg could be described with the singlet–triplet model [6]. Thereby, he predicted a long-range ordered ferromagnetic ground-state for NaBp.2Tg and KBp.2Ttg and a ground-state with only short range order for RbBp.2Ttg. The presence of ferromagnetic exchange interactions in NaBp.2Tg and KBp.2Ttg is important as it might show the chemist a way to design a plastic ferromagnet [7,8]. In the same period the crystal structures of these compounds were solved by Noordik, Beurskens and coworkers [5,9,6]. They showed that the structures of three mentioned compounds consist of layers containing solvent separated ion-pairs: paramagnetic layers of biphenyl anions are separated by diamagnetic layers of alkalimetal-polyglycol clusters. The EPR spectra of these substances were not fully understood at that time as the anomalous angular dependence of the linewidth couldn't be explained. This problem was solved by Takizawa for NaBp.2Tg in 1980 [10]. He correlated the anisotropy in the linewidth with the pseudo two-dimensional magnetic structure of the single crystals. Thereby a new,

interesting aspect of these compounds was revealed: their low-dimensional properties. One- and two-dimensional magnetic compounds became only recently a matter of research [11], but nowadays a large variety of low-dimensional inorganic systems is known [12,13]. However, the number of organic systems with one- or two-dimensional properties is still very limited [14]. Moreover, the theories to describe the properties of these compounds are not fully developed. Therefore, model compounds are necessary to test the various theories available. These model compounds should have a small g-anisotropy. As the g-anisotropy of the various alkali-biphenyl ion pairs is smaller than 0.05% they excellently satisfy this condition [3]. Furthermore, the properties of these pure magnetic systems can be described with only three major interactions : the exchange coupling, the isotropic electron Zeeman interaction and the dipolar coupling. Therefore, these organic substances are well suited as model-systems for low-dimensional magnetism and one can fruitfully compare the theoretical predictions and experimental results for these compounds. The goal of the work described in the first part of this thesis is to expand our knowledge of the magnetic properties of the above mentioned alkali-biphenyl single crystals.

The experimentally measured EPR-spectra of paramagnetic compounds can be described by means of one or more effective electron spins within the formalism of a spin-Hamiltonian. This powerful method requires, apart from the effective electron and nuclear spins, a limited number of parameters. For the description of the experimental spectra one only needs to determine these parameters, which can , for instance, be done by a minimization procedure [15]. However, this appoach is only descriptive and doesn't yield any insight in the underlying physical mechanisms. If one wants to understand the measured properties, one has to calculate the parameters in the spin-Hamiltonian from the fundamental interactions in the actual physical Hamiltonian. The calculation of the parameters is in general not straightforward as it requires not only knowledge of the underlying fundamental interactions, but also knowledge about the importance of the various contributions to the different terms. Finally, a suitable computational procedure must be developed by which the selected contributions may be calculated. These aspects will be discussed for four of the spin-spin interactions in the spin-Hamiltonian in the second part of this thesis.

1.2 Survey of this Thesis

Part I starts with a review of the essentials of the theory of exchange narrowing in pure paramagnetic systems in chapter 2. We need this theory for the interpretation of the experimental data of the magnetic two-dimensional alkali-biphenyl single-crystals. We first discuss the relaxation theory of Kubo and Tomita [16]. This theory enables us to understand the exchange narrowing phenomena magnetic three-dimensional systems. However, it has to be extended if one wants to understand the experimental results in magnetic two-dimensional systems. The necessary extensions were first given by Richards and Salamon [17]. The theory will be applied to the three mentioned alkali-biphenyl single crystals in the next three chapters: NaBp.2Tg, KBp.2Ttg and RbBp.2Ttg. In chapter 3 we start with a discussion of the experimental results on NaBp.2Tg. These results clearly confirm the pseudo two-dimensional magnetic character of this compound above

approximately 20 K. At the lowest temperature we could reach, 1.2 K, we observed the presence of three-dimensional magnetic interactions, due to a magnetic phase–transition at 1.5 K. The static magnetic properties of NaBp.2Tg below 4.2 K can be understood on the basis of a zig-zag chain spin structure of the paramagnetic layers; this magnetic structure will be discussed as well. In the next chapter of this part we discuss the experimental data on RbBp.2Ttg. At about liquid nitrogen temperature the data are in agreement with a pseudo 2-d magnetic system. At lower temperatures the experimental results can be understood with the singlet–triplet model. At 1.2 K signals due to isolated doublets are observed. Finally a new sharp resonance line is observed at about 4.2 K at high microwave power levels. This line is attributed to the double quantum transition inside the triplet–manifold. In the last chapter of part I we will present some experimental data on KBp.2Ttg. From these data we can conclude that this compound behaves at 77 K as a 2-d magnetic system as well.

The subject of part II is the calculation of the parameters of several spin-spin interactions which occur in the spin-Hamiltonian. As an introduction to this subject we start in chapter 6 with a short review of the formalism of the spin-Hamiltonian. In chapter 7 we will discuss the computation of the exchange parameter which occurs in the Heisenberg exchange interaction. We pay especially attention to the possibility to compute the exchange constant in a pair of biphenyl anions. We conclude that this two-electron property is hard to calculate on the basis of the currently available theoretical methods. The calculation of the two major contributions to the zero field splitting (ZFS) is the subject of the next two chapters. In chapter 8 we first discuss the calculation of the spin-orbit contribution to the ZFS for a weakly coupled $S = 1/2$ dimer. Subsequently, we pay attention to the computation of the electron-electron dipolar interaction to the ZFS tensor in chapter 9. We especially discuss the question under which circumstances one cannot confine oneself to the calculation of the two-centre contributions to this tensor. We show that one should also include the one-centre contributions in the case of halide–bridged copper dimers. We also present two computer programs by which one can calculate the one- and two-centre terms of the dipolar contribution to the ZFS. We, finally, treat the calculation of the hyperfine tensor in the last chapter of this thesis. The calculated hyperfine tensors show a very satisfying agreement with the experimental ones even if the nucleus concerned has a small spin density. From these results one can conclude that one can calculate this one-electron property also with very approximate theoretical methods if one uses a correct procedure.

Bibliography

[1] G.W. Canters.
NMR Investigations on Solutions and Single Crystals of Alkali Radical Ion Pairs.
PhD thesis, University of Nijmegen, 1969.

[2] B.M.P. Hendriks.
Nuclear Magnetic Relaxation in Solutions of of Alkali Aromatic Ion Pairs.
PhD thesis, University of Nijmegen, 1973.

[3] J.J. Mooij.
Single Crystals of Alkali-Aromatic ion-pairs.
PhD thesis, University of Nijmegen, 1976.

[4] G.W. Canters, A.A.K. Klaassen, and E. de Boer.
Journal of Physical Chemistry, 74:3299, 1970.

[5] J.H.Noordik, J. Schreurs, R.O. Gould, J.J. Mooij, and E. de Boer.
Journal of Physical Chemistry, 82:1105, 1978.

[6] J.J. Mooij, A.A.K. Klaassen, E. de Boer, H.M.L. Degens, Th.E.M. van den Hark, and J.H.Noordik.
Journal of the American Chemical Society, 98:680, 1976.

[7] Yu.V. Korshak, T.V. Medvedeva, A.A. Ovchinnikov, and V.N. Spector.
Nature, 326:370, 1987.

[8] R. Friend.
Nature, 326:335, 1987.

[9] J.H. Noordik, P.T. Beurskens, Th.E.M. van den Hark, and J.M.M. Smits.
Acta Crystallographica B, 35:621, 1979.

[10] O. Takizawa, R. Srinivasan, and E.de Boer.
Molecular Physics, 44:677, 1981.

[11] P. Day.
Chemistry in Britain, 1983:306, 1983.

[12] L.J. de Jongh and A.R. Miedema.
Advances in Physics, 23:1, 1974.

[13] J. Reedijk.
Chemisch Magazine, 135. 1988.

[14] A. Benoit, J. Flouquet, B. Gillon, and J. Schweizer.
Journal of Magnetism and Magnetic Materials, 31-34:1155, 1983.

[15] C.P. Keijzers.
Spin-spin interactions in weakly interacting dimers.
In M.C.R. Symons, editor, *Electron Spin Resonance, Specialist Periodical Reports*, page 1, Royal Society of Chemistry (London), 1987.

[16] R. Kubo and K. Tomita.
Journal of the Physical Society of Japan, 9:888, 1954.

[17] P.M. Richards and M.B. Salamon.
Physical Review B, 9:32, 1974.

Part I

Magnetic Properties of Alkali-Biphenyl Single-Crystals

Chapter 2

Exchange-Narrowing in 2-d Magnetic Systems

2.1 Principal Quantum-Mechanical Interactions

The experimental phenomena observed in alkali-biphenyl single-crystals will be described and interpreted by means of the spin-Hamiltonian formalism. The spin-Hamiltonian for a system of electron spins $S = 1/2$ and nuclear spins $I = 1/2$ can be expressed as [1,2] :

$$\mathcal{H}_S = \mathcal{H}_{ex} + \mathcal{H}_{eZ} + \mathcal{H}_{dip} + \mathcal{H}_{hyp} + \mathcal{H}_{nZ} \tag{2.1}$$

with

$$\mathcal{H}_{ex} = -\sum_{i \neq j} \vec{\mathbf{S}}_i \cdot \bar{\mathbf{J}}_{ij} \cdot \vec{\mathbf{S}}_j \tag{2.2}$$

$$\mathcal{H}_{eZ} = \mu_B \sum_i \vec{\mathbf{B}} \cdot \bar{\bar{\mathbf{g}}} \cdot \vec{\mathbf{S}}_i \tag{2.3}$$

$$\mathcal{H}_{dip} = \sum_{i \neq j} \sum_{m=-2}^{2} F_{ij}^{(m)} T_{ij}^{(m)} \tag{2.4}$$

$$\mathcal{H}_{hyp} = \sum_i \sum_\alpha \vec{\mathbf{S}}_i \cdot \bar{\bar{\mathbf{A}}}_{i\alpha} \cdot \vec{\mathbf{I}}_\alpha \tag{2.5}$$

$$\mathcal{H}_{nZ} = -\gamma_N \hbar \sum_\alpha \vec{\mathbf{B}} \cdot \vec{\mathbf{I}}_\alpha \tag{2.6}$$

The various terms in these equations describe the Heisenberg-exchange coupling, the electron-Zeeman interaction, the electron-electron dipolar coupling, the hyperfine interaction and the nuclear-Zeeman interaction, respectively. The first term $\mathcal{H}_{ex}$ represents the quantum-mechanical exchange coupling between two electron spins i and j. The strength of this interaction is given by the tensor $\bar{\bar{\mathbf{J}}}_{ij}$, which depends highly upon distances and relative orientations of the molecules or ions on which the electron-spins are localized. As the magnitude of this interaction decreases very rapidly with increasing distance between the electron spins , the summation can be limited to the nearest-neighbour spins. Furthermore, the spin-orbit interaction in the alkali-biphenyl ion pairs is very small as has

m	$F_{ij}^{(m)}$	$T_{ij}^{(m)}$
0	$r_{ij}^{-3}(3\cos^2\theta_{ij}-1)$	$\frac{1}{4}\gamma_e^2\hbar^2(\vec{\mathbf{S}}_i\cdot\vec{\mathbf{S}}_j-3S_{iz}S_{jz})$
±1	$r_{ij}^{-3}\sin\theta_{ij}\cos\theta_{ij}\exp(\mp i\phi_{ij})$	$-\frac{3}{4}\gamma_e^2\hbar^2(S_{iz}S_{j\pm}+S_{i\perp}S_{jz})$
±2	$r_{ij}^{-3}\sin^2\theta_{ij}\exp(\mp 2i\phi_{ij})$	$-\frac{3}{8}\gamma_e^2\hbar^2S_{i\pm}S_{j\pm}$

Table 2.1: Distance dependent and spin dependent components of the electron-electron dipolar interaction tensor

been determined experimentally [3] . Consequently the symmetry in spin-space will be high and therefore the spin-spin coupling tensor $\bar{\bar{\mathbf{J}}}_{ij}$ will be almost isotropic. Therefore it is correct to describe the exchange-coupling with a scalar. This results in :

$$\mathcal{H}_{ex}=-2\sum_{i<j}J_{ij}\vec{\mathbf{S}}_i\cdot\vec{\mathbf{S}}_j \tag{2.7}$$

The electron-Zeeman interaction $\mathcal{H}_{eZ}$ describes the interaction of an electron spin $\vec{\mathbf{S}}_i$ with the external magnetic field $\vec{\mathbf{B}}$. The tensor $\bar{\bar{\mathbf{g}}}$ contains the g-factors, which are almost isotropic and deviate only slightly from the free-electron value $g_e = 2.00232$ as has been shown by Mooij [3]. Therefore the spin-orbit coupling of the unpaired electron will be small.

The electron Zeeman and the Heisenberg exchange interaction are the most important interactions present in the alkali-biphenyl systems. The next largest coupling is the electron-electron dipolar interaction which is the quantum-mechanical analogue of the classical interaction between two magnetic point dipoles. The distance dependent terms $F_{ij}^{(m)}$ and the spin dependent terms $T_{ij}^{(m)}$ are tabulated in table 2.1. In contrast to the exchange interaction this coupling is also important between spins which are not nearest-neighbours.

The hyperfine interaction $\mathcal{H}_{hyp}$ couples the electron and nuclear spins and the nuclear Zeeman interaction $\mathcal{H}_{nZ}$ describes the interaction of the external magnetic field with the nuclear spins. As the magnitudes of the last two interactions are much smaller than the exchange and electron-Zeeman interactions, as well as the electron-electron dipolar interaction, these interactions may be neglected in concentrated magnetic systems. However, in diluted magnetic systems the interactions due to nuclear spins should be included.

We will conclude this section with the statement that the main properties of the alkali-biphenyl systems may be described with the Hamiltonian:

$$\mathcal{H}_S=-2\sum_{i<j}J_{ij}\vec{\mathbf{S}}_i\cdot\vec{\mathbf{S}}_j+\mu_B\sum_i\vec{\mathbf{B}}\cdot\bar{\bar{\mathbf{g}}}\cdot\vec{\mathbf{S}}_i+\sum_{i\neq j}\sum_{m=-2}^{2}F_{ij}^{(m)}T_{ij}^{(m)} \tag{2.8}$$

2.2 The Kubo-Tomita Equation

In an electron paramagnetic resonance (EPR) experiment on a concentrated magnetic system all information is contained in a single, exchange-narrowed resonance line. Therefore it is of utmost importance to describe this resonance-line accurately. The first theoretical methods which were able to describe the EPR resonance-line were the "method of moments" developed by Van Vleck [4] and the "random-frequency modulation model" of Anderson and Weiss [5]. Both models predict a Lorentzian lineshape and give formulas for the angular dependence of the first derivative peak-to-peak linewidth ΔB_{pp}. The most recent theories for the description of the resonance line in low-dimensional magnetic systems were developed by Lagendijk [6,7,8] and by Benner [9,10]. Their approach has the disadvantage that it requires a lot of computing power. Therefore we will use here a relatively simple but still powerful theory for the description of the exchange-narrowed resonance-line [11,12,13]. This theory - the linear response theory - was developed by Kubo and Tomita in 1954.

It starts with the assumption that the spin-Hamiltonian $\mathcal{H}_S$ can be divided into two parts : The leading term $\mathcal{H}_0$ includes the exchange and electron-Zeeman terms. The smaller term $\mathcal{H}'$ which acts as a perturbation with respect to the pricipal term $\mathcal{H}_0$ consists of the dipolar interaction . In formulas this may be expressed as:

$$\mathcal{H}_S = \mathcal{H}_0 + \mathcal{H}' \tag{2.9}$$

$$\mathcal{H}_0 = \mathcal{H}_{ex} + \mathcal{H}_{eZ} \tag{2.10}$$

$$\mathcal{H}' = \mathcal{H}_{dip} \tag{2.11}$$

$$\mathcal{H}' \ll \mathcal{H}_0 \tag{2.12}$$

The observed quantity in a standard CW-EPR experiment is the absorption χ''. It is well-known that in the high temperature limit $\hbar\omega \ll kT$ the following equation holds [1]:

$$\frac{\chi''(\omega)}{\omega} = \frac{1}{kT}\int_0^\infty \langle M_x(t)M_x(0)\rangle \cos\omega t \, dt \tag{2.13}$$

where k is the Boltzmann constant and T the absolute temperature. $M_x(t)$ is the x-component of the magnetisation $\vec{\mathbf{M}} = -\mu_B \sum_i \overline{\overline{\mathbf{g}}}_i \cdot \vec{\mathbf{S}}_i$ at time t in the Heisenberg-representation with respect to $\mathcal{H}_0 + \mathcal{H}'$. The brackets in this formula indicate a thermal average. By a transformation to the interaction-representation according to

$$\widetilde{M}_x(t) = e^{-i\mathcal{H}_0 t} M_x(t) e^{i\mathcal{H}_0 t} \tag{2.14}$$

in which $\widetilde{M}_x(t)$ changes only in the relatively slow timescale of $\mathcal{H}'$, one can derive that the absorption at temperatures far above the ordering-temperature is given by

$$\frac{\chi''(\omega)}{\omega} = \frac{1}{4kT}\int_0^\infty \langle \widetilde{M}_-(t)M_-(0)\rangle \cos(\omega_0 - \omega)t \, dt \tag{2.15}$$

where $\omega_0 = \gamma_e B_0$ is the resonance frequency. The change of the response with time upon an external perturbation is described by the relaxation function $\phi(t)$ which is defined as

$$\phi(t) = \frac{\langle \widetilde{M}_+(t) M_-(0) \rangle}{\langle M_+ M_- \rangle} \tag{2.16}$$

By combining the last two expressions one obtains :

$$\frac{\chi''(\omega)}{\omega} = \frac{\langle M_+ M_- \rangle}{4kT} \int_0^\infty \phi(t)\ \cos(\omega - \omega_0)t\ dt \tag{2.17}$$

Now it has been shown by Kubo [14] that $\phi(t)$ can be written as

$$\phi(t) = \exp[-\int_0^t d\tau (t-\tau)\psi(\tau) + \sum_n C_n] \tag{2.18}$$

In this equation the higher order cumulants C_n will be zero in case of a Gaussian random-process. We note that the higher order cumulants are also zero if a factorization of averages of many functions into products of simpler averages is allowed. As we will use this factorization technique in our calculation it seems consistent to ignore the higher order terms C_n as well, so that $\phi(t)$ is given exactly in terms of $\psi(\tau)$. The function $\psi(\tau)$ is the total spinmoment correlation function. It is defined by:

$$\psi(\tau) = \frac{\langle [\widetilde{\mathcal{H}}'(\tau), M_+(0)][M_-(0), \mathcal{H}'(0)] \rangle}{\hbar^2 \langle M_+ M_- \rangle} \tag{2.19}$$

where $\widetilde{\mathcal{H}}'(\tau)$ is defined by

$$\widetilde{\mathcal{H}}'(\tau) = e^{i\mathcal{H}_0\tau} \mathcal{H}'(0) e^{-i\mathcal{H}_0\tau} \tag{2.20}$$

The Hamiltonian $\widetilde{\mathcal{H}}'(\tau)$ contains a time dependence due to the electron-Zeeman interaction and a time dependence due to the exchange interaction. It is possible to decompose $\psi(\tau)$ into terms with distinct m, where m is the total change in the electron-Zeeman quantum number, because $\mathcal{H}_{ex}$ commutes with $\mathcal{H}_{eZ}$ [13]. By a few more manipulations the time dependencies can be split, which results in the expression:

$$\psi(\tau) = \sum_{m=-2}^{2} \frac{\langle \hat{g}_m(\tau) g_m^\dagger(0) \rangle}{\langle M_+ M_- \rangle} e^{im\omega_0\tau} \tag{2.21}$$

with

$$\hat{g}_m(\tau) = e^{-i\mathcal{H}_{ex}\tau} g_m(0) e^{i\mathcal{H}_{ex}\tau} \tag{2.22}$$

and

$$g_m(0) = [F_{ij}^{(m)} T_{ij}^{(m)}, M_+] \tag{2.23}$$

The time dependence in the dipolar correlation functions $\langle \hat{g}_m(\tau) g_m^\dagger(0) \rangle$ results only from the exchange interaction. The time dependence due to the electron-Zeeman interaction is completely contained in the exponential term. The expressions for the various g_m terms are listed in table 2.2. By using the above expansion of $\psi(\tau)$ we can write the relaxation function $\phi(t)$ as :

$$-\ln \phi(t) = \int_0^t (t-\tau) \sum_{m=-2}^{2} \frac{\langle \hat{g}_m(\tau) g_m^\dagger(0) \rangle}{\langle M_+ M_- \rangle} e^{im\omega_0\tau}\ d\tau \tag{2.24}$$

This is the fundamental expression in the formalism of Kubo and Tomita [11,13].

$$
\begin{array}{|lcl|}
\hline
g_2 & = & 0 \\
g_1 & = & \frac{3}{2}\gamma_e^3\hbar^2 \sum_{i\neq j} F_{ij}^{(1)} S_{i+} S_{j+} \\
g_0 & = & \frac{3}{2}\gamma_e^3\hbar^2 \sum_{i\neq j} F_{ij}^{(0)} S_{i+} S_{jz} \\
g_{-1} & = & \frac{3}{2}\gamma_e^3\hbar^2 \sum_{i\neq j} F_{ij}^{(-1)} \{S_{i-} S_{j+} - 2S_{iz} S_{jz}\} \\
g_{-2} & = & -\frac{3}{2}\gamma_e^3\hbar^2 \sum_{i\neq j} F_{ij}^{(-2)} S_{iz} S_{j-} \\
\hline
\end{array}
$$

Table 2.2: The dipolar factors g_m

2.3 The Dipolar Correlation Functions

Inspection of the Kubo-Tomita expression shows that all the information with respect to the sample is contained in the dipolar time correlation functions $\langle \hat{g}_m(\tau) g_m^\dagger(0) \rangle$. A correct description of these functions is therefore very important. In this section we will concentrate upon the derivation of an easy expression for these functions. This will be done for the $m = 0$ term. The other terms can de treated analogously. By inserting the expressions for the g_0 terms we obtain the following formula for the $\langle \hat{g}_0(\tau) g_0^\dagger \rangle$ functions :

$$
\langle \hat{g}_0(\tau) g_0^\dagger \rangle = (\frac{3}{2}\gamma_e^3\hbar^2)^2 \sum_{i\neq j} \sum_{k\neq l} F_{ij}^{(0)} F_{kl}^{(0)*} \langle \hat{S}_{i+}(\tau) \hat{S}_{jz}(\tau) S_{k-} S_{lz} \rangle \tag{2.25}
$$

In this expression four-spin time correlation functions are involved. These functions are hard to calculate. However, a reduction is impossible because the resonating spins are not independent: The signal in an EPR-experiment on a concentrated magnetic system must be thought of as the collective response of the $q = 0$ mode of the total magnetisation, instead of one in which each spin resonates independently in its local environment. In some special cases [15,16] these functions may be calculated exactly but in most cases they are treated by a factorization scheme. In this scheme, which is known as the random-phase approximation, the four-spin correlation functions are decoupled into products of two-spin correlation functions according to [17]:

$$
\begin{aligned}
\langle \hat{S}_{i\alpha}(\tau) \hat{S}_{j\beta}(\tau) S_{k\alpha'} S_{l\beta'} \rangle \approx & \langle \hat{S}_{i\alpha}(\tau) \hat{S}_{j\beta}(\tau) \rangle \langle S_{k\alpha'} S_{l\beta'} \rangle \\
+ & \langle \hat{S}_{i\alpha}(\tau) S_{k\alpha'} \rangle \langle \hat{S}_{j\beta}(\tau) S_{l\beta'} \rangle \\
+ & \langle \hat{S}_{i\alpha}(\tau) S_{l\beta'} \rangle \langle \hat{S}_{j\beta}(\tau) S_{k\alpha'} \rangle
\end{aligned} \tag{2.26}
$$

By using this relation the above mentioned expression for the dipolar correlation functions reduces to

$$
\langle \hat{g}_0(\tau) g_0^\dagger \rangle = (\frac{3}{2}\gamma_e^3\hbar^2)^2 \sum_{i\neq j} \sum_{k\neq l} F_{ij}^{(0)} F_{kl}^{(0)*} \langle \hat{S}_{i+}(\tau) S_{k-} \rangle \langle \hat{S}_{jz}(\tau) S_{lz} \rangle \tag{2.27}
$$

$\langle \hat{g}_2(\tau) g_2^\dagger \rangle$	$=$	0
$\langle \hat{g}_1(\tau) g_1^\dagger \rangle$	$=$	$8\,(\frac{3}{2}\gamma_e^3\hbar^2)^2 \sum_q \lvert F_q^{(1)}\rvert^2 \langle \hat{S}_{qz}(\tau) S_{-qz}\rangle^2$
$\langle \hat{g}_0(\tau) g_0^\dagger \rangle$	$=$	$2\,(\frac{3}{2}\gamma_e^3\hbar^2)^2 \sum_q \lvert F_q^{(0)}\rvert^2 \langle \hat{S}_{qz}(\tau) S_{-qz}\rangle^2$
$\langle \hat{g}_{-1}(\tau) g_{-1}^\dagger \rangle$	$=$	$12\,(\frac{3}{2}\gamma_e^3\hbar^2)^2 \sum_q \lvert F_q^{(-1)}\rvert^2 \langle \hat{S}_{qz}(\tau) S_{-qz}\rangle^2$
$\langle \hat{g}_{-2}(\tau) g_{-2}^\dagger \rangle$	$=$	$2\,(\frac{3}{2}\gamma_e^3\hbar^2)^2 \sum_q \lvert F_q^{(-2)}\rvert^2 \langle \hat{S}_{qz}(\tau) S_{-qz}\rangle^2$

Table 2.3: The dipolar correlation functions $\langle \hat{g}_m(\tau) g_m^\dagger(0)\rangle$

where we used the fact that the terms of the type $\langle S_{i+} S_{lz}\rangle$ are zero. Although this expression is much simpler than the first one it is still hard to use, because it contains four summations over spinlabels. In order to circumvent these summations we perform a Fourier transformation by which we change from localized spins to the normal modes of delocalized spin waves. The Fourier-transformation is defined by

$$\vec{\mathbf{S}}_q = \frac{1}{\sqrt{N}} \sum_{j=1}^{N} \vec{\mathbf{S}}_j e^{i\vec{\mathbf{q}}\cdot\vec{\mathbf{r}}_{ij}} \tag{2.28}$$

where the spin-wave vectors $\vec{q}$ run over the complete first Brillouin zone of the crystal. If we again use the random phase approximation this expression reduces to :

$$\langle \hat{g}_0(\tau) g_0^\dagger \rangle = (\frac{3}{2}\gamma_e^3\hbar^2)^2 \sum_q \lvert F_q^{(0)}\rvert^2 \langle \hat{S}_{q+}(\tau) S_{-q-}\rangle \langle \hat{S}_{qz}(\tau) S_{-qz}\rangle \tag{2.29}$$

and subsequently to

$$\langle \hat{g}_0(\tau) g_0^\dagger \rangle = 2(\frac{3}{2}\gamma_e^3\hbar^2)^2 \sum_q \lvert F_q^{(0)}\rvert^2 \langle \hat{S}_{qz}(\tau) S_{-qz}\rangle^2 \tag{2.30}$$

In the last expression we assumed that the correlations are isotropic. This is true if the temperature of the spin-system lies much above the ordering temperature. The dipolar factors $F_q^{(m)}$ which occur in these equations are defined as:

$$F_q^{(m)} = \sum_{j=1}^{N} F_{ij}^{(m)} e^{i\vec{\mathbf{q}}\cdot\vec{\mathbf{r}}_{ij}} \tag{2.31}$$

and they represent the amplitudes of the correlation functions of eigenmode $\vec{q}$. In table 2.3 the expressions for the various components of the dipolar correlation function are listed.

Because the relation $\lvert F_q^{(m)}\rvert^2 = \lvert F_q^{(-m)}\rvert^2$ holds it is possible to combine the functions according to

$$G_0(\tau) = \frac{\langle \hat{g}_0(\tau) g_0^\dagger \rangle}{\langle M_+ M_- \rangle} \qquad \text{for} \quad m = 0 \tag{2.32}$$

$$\begin{aligned} G_0(\tau) &= \frac{27}{4}\frac{\gamma_e^4\hbar^4}{NS(S+1)}\sum_q |F_q^{(0)}|^2\langle \hat{S}_{qz}(\tau)S_{-qz}\rangle^2 \\ G_1(\tau) &= \frac{135}{2}\frac{\gamma_e^4\hbar^4}{NS(S+1)}\sum_q |F_q^{(1)}|^2\langle \hat{S}_{qz}(\tau)S_{-qz}\rangle^2 \\ G_2(\tau) &= \frac{27}{4}\frac{\gamma_e^4\hbar^4}{NS(S+1)}\sum_q |F_q^{(2)}|^2\langle \hat{S}_{qz}(\tau)S_{-qz}\rangle^2 \end{aligned}$$

Table 2.4: The dipolar correlation functions $G_m(\tau)$

$$G_m(\tau) = \frac{\langle \hat{g}_m(\tau)g_m^\dagger\rangle + \langle \hat{g}_{-m}(\tau)g_{-m}^\dagger\rangle}{\langle M_+M_-\rangle} \quad \text{for} \quad m = 1,2 \tag{2.33}$$

This gives us as expression for the relaxation function

$$-\ln\phi(t) \approx \int_0^t (t-\tau)\sum_{m-0}^{2} G_m(\tau)\cos(m\omega_0\tau)\,d\tau \tag{2.34}$$

In the last formula we restricted us to the cosinus part of the exponential function, because this part contributes to the absorption of the EPR-signal. The sinus part results in a shift of the resonance position which is only of interest at low temperatures. The expressions for the dipolar correlation functions $G_m(\tau)$ are listed in table 2.4. For this table we used the relation

$$\langle M_+M_-\rangle = \frac{2}{3}\gamma_e^2 NS(S+1) \tag{2.35}$$

2.4 The Time Dependence of $\langle \widehat{S}_{qz}(\tau)S_{-qz}\rangle$

In the previous section we first simplified the expression of Kubo and Tomita by decoupling the four-spin correlation functions into products of two-spin correlation functions and subsequently by a transformation from localized spins to the normal modes of spin waves $\vec{q}$. By these steps we reduced the calculation of the time dependence of the dipolar correlation functions $\langle \hat{g}_m(\tau)g_m^\dagger(0)\rangle$ to the calculation of the time dependence of the spin functions $\langle \hat{S}_{qz}(\tau)S_{-qz}\rangle$. These functions are connected with the autocorrelation functions $\langle \hat{S}_{iz}(\tau)S_{iz}\rangle$ according to

$$\langle \hat{S}_{qz}(\tau)S_{-qz}\rangle \approx \frac{1}{N}\sum_{i=1}^{N}\langle \hat{S}_{iz}(\tau)S_{iz}\rangle \tag{2.36}$$

The value $4\langle \hat{S}_{iz}(\tau)S_{iz}\rangle$ can be interpreted as the probability that a perturbation at site i at time $\tau = 0$ will be at the same position after a period τ. This probability can be calculated easily at time $\tau = 0$ and $\tau = \infty$. For a system of N equal spins they are given by

$$4\langle S_{iz}(0)S_{iz}\rangle = 1 \tag{2.37}$$

and

$$4\langle \hat{S}_{iz}(\infty) S_{iz} \rangle = \frac{1}{N} \tag{2.38}$$

This allows us to derive

$$\langle S_{qz}(0) S_{-qz} \rangle = \frac{1}{4} \tag{2.39}$$

and

$$\langle \hat{S}_{qz}(\infty) S_{-qz} \rangle = \frac{1}{4N} \tag{2.40}$$

For intermediate times τ the time dependence of the terms $\langle \hat{S}_{qz}(\tau) S_{-qz} \rangle$ must be approximated, because no exact expression is available. For short times τ we are able to make a Taylor-series expansion according to [18]

$$\langle \hat{S}_{qz}(\tau) S_{-qz} \rangle = \langle S_{qz}(0) S_{-qz} \rangle + \tau \langle \dot{S}_{qz}(0) S_{-qz} \rangle + \frac{1}{2}\tau^2 \langle \ddot{S}_{qz}(0) S_{-qz} \rangle + \ldots \tag{2.41}$$

Here, $\dot{S}_{qz}$ and $\ddot{S}_{qz}$ are the first and second derivative of S_{qz} with respect to time, respectively, calculated at $\tau = 0$. These static correlations can be calculated at infinite temperature. An important simplification at infinite temperature is that the terms with odd powers in τ will be zero. Therefore we can state to a good level of approximation :

$$\langle \hat{S}_{qz}(\tau) S_{\ qz} \rangle = \langle S_{qz}(0) S_{-qz} \rangle + \frac{1}{2}\tau^2 \langle \ddot{S}_{qz}(0) S_{-qz} \rangle \tag{2.42}$$

In the next step this time correlation function is fitted to a Gaussian random function which is given by

$$\langle \hat{S}_{qz}(\tau) S_{-qz} \rangle = \langle S_{qz}(0) S_{-qz} \rangle e^{-\frac{1}{2}\omega_q^2 \tau^2} \tag{2.43}$$

The frequency ω_q in this formula is of the order $J/\hbar$ and it is defined by :

$$\omega_q^2 = -\frac{\langle \ddot{S}_{qz}(0) S_{-qz} \rangle}{\langle S_{qz}(0) S_{-qz} \rangle} \tag{2.44}$$

By this procedure we have obtained an expression for $\langle \hat{S}_{qz}(\tau) S_{-qz} \rangle$ for all times. By inserting this formula in the dipolar correlation functions $G_m(\tau)$ we can obtain an expression for the relaxation function $\phi(t)$. Using this expression we are able to explain the experimental results of magnetic three-dimensional systems. However, this expression does not suffice for the interpretation of low-dimensional magnetic systems. The experimental data of EPR and NMR experiments show that the correlation functions in these systems decay slower than predicted by the above derived Gaussian decay. It is generally assumed that this slower decay rate is a consequence of the fact that perturbations in the spin system not only move according to a random fluctuations but also by spin diffusion [19,12]. The diffusion proces can be described with an equation analogous to the second law of Fick, if we replace the concentration through the spin correlation functions [13]:

$$\frac{\partial}{\partial \tau} \langle \hat{S}_{iz}(\tau) S_{iz} \rangle = D \vec{\nabla}^2 \langle \hat{S}_{iz}(\tau) S_{iz} \rangle \tag{2.45}$$

where D is the diffusion constant. It has been shown by Blume and Hubbard [20] that this equation can be solved easily in spin-space. The solution reads:

$$\langle \hat{S}_{qz}(\tau) S_{-qz} \rangle = \langle S_{qz}(0) S_{-qz} \rangle e^{-Dq^2\tau} \tag{2.46}$$

It will be clear that transport of magnetisation occurs especially via the $q \approx 0$ modes, because these modes have the longest life-times. By a Fourier transformation from spin-waves to localized spins we can calculate that in the case $\tau \rightarrow \infty$ the localized two-spin auto correlation functions $\langle \hat{S}_{iz}(\tau) S_{iz} \rangle$ decay as :

$$\langle \hat{S}_{iz}(\tau) S_{iz} \rangle = \langle S_{0z} S_{0z} \rangle \left(\frac{\tau_c}{\tau} \right)^{\frac{d}{2}} \tag{2.47}$$

In this last expression the magnetic dimension is represented by d and the correlation time τ_c is a constant which depends upon the dimesion d. This formula clearly shows that the autocorrelation functions in low-dimensional magnetic systems ($d = 1, 2$) decay slower than in three-dimensional magnetic systems ($d = 3$). Because of this slower decay the magnetic behaviour of low-dimensional magnetic systems differs from that of three-dimensional magnetic systems.

2.5 The Solution of the Kubo-Tomita Equation

In the last sections we concluded that the absorption of the exchange-narrowed EPR resonance line can be described with the relaxation function $\phi(t)$. This function is described by the equation of Kubo and Tomita :

$$-\ln \phi(t) = \int_0^t (t - \tau) \psi(\tau) \, d\tau \tag{2.48}$$

with

$$\psi(\tau) = \sum_{m=0}^{2} G_m(\tau) \cos(m\omega_0 \tau) \tag{2.49}$$

At this point we are able to discuss the solution of this equation. We will start with a discussion of the general aspects of the method and subsequently we will apply it to the case of a 3-d and a 2-d magnetic system.

The time dependence in the dipolar correlation functions $G_m(\tau)$ is determined by the time dependence of the two-spin correlation functions $\langle \hat{S}_{qz}(\tau) S_{-qz} \rangle$. In analogy to the time dependence of these correlation functions we divide the time domain of $G_m(\tau)$ in two parts - a short time region ($0 < \tau < \tau_1$) and a long time region ($\tau_1 < \tau < \infty$) -, which are matched for an intermediate time $\tau = \tau_1$. For short times τ we start with a Gaussian decay :

$$\tau \in [0, \tau_1) \quad : \quad G_m(\tau) = G_m(0) e^{-\frac{1}{2}\omega_{ex}^2 \tau^2} \tag{2.50}$$

In this expression the short-time decay rate ω_{ex}, which is of the order of $J/\hbar$, is defined as

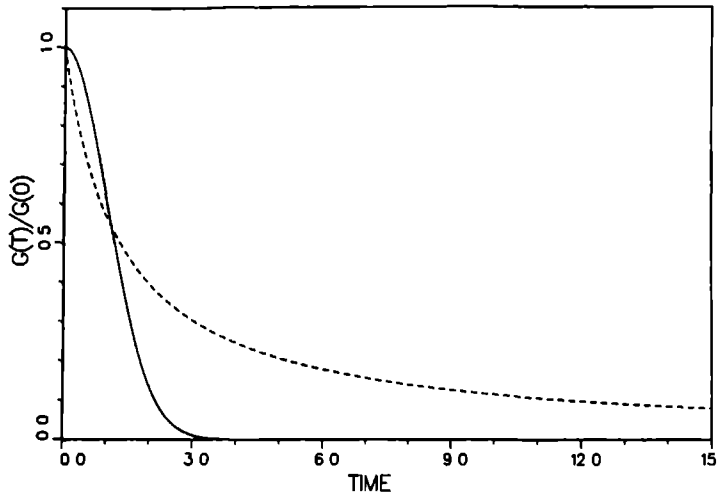

Figure 2.1: The behaviour of the short- and long-time dependence of $G_m(\tau)$

$$\omega_{ex}^2 = -\frac{\ddot{G}_m(0)}{\bar{G}_m(0)} \tag{2.51}$$

which is equal to

$$\omega_{ex}^2 = \frac{2\sum_q |F_q^{(m)}|^2 \langle \omega_q^2 \rangle \langle S_{qz}(0) S_{-qz} \rangle^2}{\sum_q |F_q^{(m)}|^2 \langle S_{qz}(0) S_{-qz} \rangle^2} \tag{2.52}$$

where the factor ω_q^2 is given by equation 2.44.

For times τ which are longer than the matching time τ_1 the long-time expression for $G_m(\tau)$ is used, This expression is based upon spin diffusion. It is given by

$$\tau \in [\tau_1, \infty) \quad : \quad G_m(\tau) = G_m(0) \frac{\sum_q |F_q^{(m)}|^2 \langle S_{qz}(0) S_{-qz} \rangle^2 e^{-2Dq^2\tau}}{\sum_q |F_q^{(m)}|^2 \langle S_{qz}(0) S_{-qz} \rangle^2} \tag{2.53}$$

Now we make the minor assumption

$$\langle S_{qz}(0) S_{-qz} \rangle e^{-2Dq^2\tau} \approx \langle S_{0z}(0) S_{0z} \rangle e^{-2Dq^2\tau} \tag{2.54}$$

which reflects the idea that in the long-time region the correlations are mainly determined by by the $q \approx 0$ modes of the spin-waves. Furthermore we introduce the factors ζ_m which are defined according to

$$\zeta_m = \frac{|F_0^{(m)}|^2 \langle S_{0z} S_{0z} \rangle^2}{\frac{1}{N} \sum_q |F_q^{(m)}|^2 \langle S_{qz}(0) S_{-qz} \rangle^2} \tag{2.55}$$

and are equal to

$$\zeta_m = \frac{|F_0^{(m)}|^2}{\frac{1}{N} \sum_q |F_q^{(m)}|^2} \tag{2.56}$$

in the limit of infinite temperature, because then we may use the equality $\langle S_{qz}(0)S_{-qz}\rangle = \frac{1}{3}S(S+1)$. At this stage we make another assumption by supposing that the dipolar factors $|F_q^{(m)}|^2$ show a Gaussian behaviour :

$$|F_q^{(m)}|^2 = |F_0^{(m)}|^2 e^{-\alpha^2 q^2} \tag{2.57}$$

The factor α in this equation is a constant. This assumption has to be made in order to be able to fit the short-time and the long-time expansion of $G_m(\tau)$ for all values of the factors ζ_m. The behaviour of $G_m(\tau)$ in the long-time region doesn't change by this assumption. By these substitutions we finally obtain for $G_m(\tau)$ in the long-time region:

$$G_m(\tau) = G_m(0)\zeta_m \frac{1}{N}\sum_q e^{-(\alpha^2 + 2D\tau)q^2} \tag{2.58}$$

In figure 2.1 the behaviour of $G_m(\tau)$ in the short-time as well as the long-time region is shown. It is clear that the decay of the correlation function is significantly changed in the presence of spin diffusion.

The Solution for a 3-*d* Spin-System

In our discussion of a 3-*d* spin system we will assume $\omega_0 > \omega_{ex}$ and focus our attention on the secular term $m = 0$. The non-secular terms $m = 1$ and $m = 2$ are averaged to zero because of the fast modulation of the $\cos(m\omega_0\tau)$ term. In case of a cubic 3-*d* spin-system the summation over the spin-waves $\vec{q}$ can be replaced by an integration over an octant of the first Brillouin zone with side π/a

$$\frac{1}{N}\sum_q \approx \frac{4\pi}{8(\pi/a)^3}\int_0^\infty q^2 dq \tag{2.59}$$

By substitution of this expression in formula 2.50 we obtain for $G_0(\tau)$ the following results

$$G_0(\tau) = G_0(0)\zeta_0 \frac{4\pi}{8(\pi/a)^3}\int_0^\infty q^2\, e^{-(\alpha^2 + 2D\tau)q^2}\, dq \tag{2.60}$$

$$G_0(\tau) = G_0(0)\zeta_0 \frac{\pi^{3/2}}{8(\pi/a)^3(\alpha^2 + 2D\tau)^{3/2}} \tag{2.61}$$

By combining the expressions 2.55,2.56 and 2.59 we can derive for the factor α^2

$$\alpha^2 = \frac{\zeta_0^{2/3}a^2}{4\pi} \tag{2.62}$$

Elimination of α^2 in equation 2.61 leads to

$$G_0(\tau) = G_0(0)\frac{\zeta_0}{\{\zeta_0^{2/3} + K\omega_{ex}\tau\}^{3/2}} \tag{2.63}$$

where the constant K is defined by

$$K = \frac{8\pi D}{a^2\omega_{ex}} \tag{2.64}$$

This constant can be calculated by using existing expressions for D and ω_{ex}. These expressions depend only on the various exchange interactions J_{ij} in the spin lattice, the lattice type and lattice distances. By inserting these expressions we obtain a value for K of about 1.

Now we have found an expression for the dipolar correlation function $G_0(\tau)$ for all times τ we are able to calculate the relaxation function $\phi(t)$. Formula 2.48 and 2.49 give :

$$\begin{aligned} -\ln\phi(t) &= \int_0^{\tau_1}(t-\tau)G_0(0)e^{-\frac{1}{2}\omega_{ex}^2\tau^2}\,d\tau \\ &+ \int_{\tau_1}^{t}(t-\tau)G_0(0)\frac{\zeta_0}{\{\zeta_0^{2/3}+K\omega_{ex}\tau\}^{3/2}}\,d\tau \qquad (2.65) \\ -\ln\phi(t) &\approx \frac{G_0(0)t}{\omega_{ex}}\sqrt{\frac{\pi}{2}}\,\mathrm{erf}\left(\frac{\omega_{ex}\tau_1}{\sqrt{2}}\right) \\ &+ \frac{2G_0(0)\zeta_0\,t}{\omega_{ex}K}\left\{\frac{1}{\{\zeta_0^{2/3}+K\omega_{ex}\tau_1\}^{1/2}}-\frac{1}{\{\zeta_0^{2/3}+K\omega_{ex}t\}^{1/2}}\right\} \\ &+ \frac{2G_0(0)\zeta_0}{K^2\omega_{ex}^2}\left\{\frac{\{2\zeta_0^{2/3}+K\omega_{ex}t\}}{\{\zeta_0^{2/3}+K\omega_{ex}t\}^{1/2}}-\frac{\{2\zeta_0^{2/3}+K\omega_{ex}\tau_1\}}{\{\zeta_0^{2/3}+K\omega_{ex}\tau_1\}^{1/2}}\right\} \qquad (2.66) \\ -\ln\phi(t) &\approx \frac{G_0(0)t}{\omega_{ex}}\left\{\sqrt{\frac{\pi}{2}}\,\mathrm{erf}\left(\frac{\omega_{ex}\tau_1}{\sqrt{2}}\right)+\frac{2\zeta_0}{K\{\zeta_0^{2/3}+K\omega_{ex}\tau_1\}^{1/2}}\right\} \qquad (2.67) \end{aligned}$$

This equation may be written as

$$-\ln\phi(t)=\eta t \qquad (2.68)$$

where

$$\eta=\frac{G_0(0)}{\omega_{ex}}\left\{\sqrt{\frac{\pi}{2}}\,\mathrm{erf}\left(\frac{\omega_{ex}\tau_1}{\sqrt{2}}\right)+\frac{2\zeta_0}{K\{\zeta_0^{2/3}+K\omega_{ex}\tau_1\}^{1/2}}\right\} \qquad (2.69)$$

This means that we obtain an exponential decaying function for $\phi(t)$. Applying a Fourier transformation to the relaxation function gives us a Lorentzian EPR resonance-line. If we neglect the second term in the above expression which may be done if $\omega_{ex}\tau_1 \gg 1$ we neglect the influence of spin diffusion. This neglect doesn't change the lineshape. The linewidth may change to a minor extent. The various terms $G_m(0)$ are tabulated in table 2.5. These terms are exactly the same as the second moment calculated by Van Vleck [4]. In fact we have rediscovered the exchange theories of Van Vleck and Anderson and Weiss. However the above described procedure, which is based on the formalism of Kubo and Tomita, is much more general in nature as will be seen in the next paragraph.

The Solution of the Kubo-Tomita Equation for a 2-d Spin-System

In much the same way as we solved the Kubo-Tomita equation in the previous paragraph we are now able to solve it for a 2-d spin-system. For the long-time region we can derive the relation [12]

$$G_0(\tau)=G_0(0)\frac{\zeta_0}{\zeta_0+K\omega_{ex}\tau} \qquad (2.70)$$

$$
\begin{array}{|rcl|}
\hline
G_0(0) & = & \frac{3}{4}\gamma_e^4\hbar^2 S(S+1)\sum_j (3\cos^2\theta_{ij}-1)^2 r_{ij}^{-6} \\
G_1(0) & = & \frac{15}{2}\gamma_e^4\hbar^2 S(S+1)\sum_j \sin^2\theta_{ij}\cos^2\theta_{ij} r_{ij}^{-6} \\
G_2(0) & = & \frac{3}{4}\gamma_e^4\hbar^2 S(S+1)\sum_j \sin^4\theta_{ij} r_{ij}^{-6} \\
\hline
\end{array}
$$

Table 2.5: The $G_m(0)$ factors

The constant K is now given by

$$K = \frac{8\pi D}{a^2\omega_{ex}} \approx 5.0 \tag{2.71}$$

for a quadratic lattice as in K_2MnF_6 and by

$$K = \frac{16\pi D}{\sqrt{3}a^2\omega_{ex}} \approx 5.8 \tag{2.72}$$

for a hexagonal lattice as in the alkali-biphenyl systems. For obtaining the numerical values we used the equality [21]

$$D = \frac{1}{3}Ja^2\sqrt{2\pi S(s+1)} \tag{2.73}$$

This supplies us with the following terms for the relaxation function :

$$
\begin{aligned}
-\ln\phi(t) &= \int_0^{\tau_1}(t-\tau)G_0(0)e^{-\frac{1}{2}\omega_{ex}^2\tau^2}\,d\tau \\
&+ \int_{\tau_1}^{t} G_0(0)\frac{\zeta_0}{\zeta_0 + K\omega_{ex}\tau}\,d\tau \qquad (2.74) \\
&\approx \frac{G_0(0)t}{\omega_{ex}}\sqrt{\frac{\pi}{2}}\,\mathrm{erf}\left(\frac{\omega_{ex}\tau_1}{\sqrt{2}}\right) \\
&+ \frac{G_0(0)\zeta_0\, t}{K\omega_{ex}}\left\{\ln\left[\frac{\omega_{ex}t}{\zeta_0/K + \omega_{ex}\tau_1}\right] - 1\right\} \qquad (2.75)
\end{aligned}
$$

The extra terms in this formula are a direct result of the presence of spin diffusion. The relaxation function $\phi(t)$ now has the form

$$-\ln\phi(t) = P\ t + Q\ t\ \ln\left(\frac{t}{t_0}\right) \tag{2.76}$$

where

$$P = \frac{G_0(0)}{\omega_{ex}}\sqrt{\frac{\pi}{2}}\,\mathrm{erf}\left(\frac{\omega_{ex}\tau_1}{\sqrt{2}}\right) - \frac{G_0(0)\zeta_0}{K\omega_{ex}} \tag{2.77}$$

$$Q = \frac{G_0(0)\zeta_0}{K\omega_{ex}} \tag{2.78}$$

and

$$t_0 = \left\{ \frac{\omega_{ex}}{\zeta_0/K + \omega_{ex}\tau_1} \right\}^{-1} \tag{2.79}$$

As will be shown below the second term is dominant. It has the consequence that the lineshape of the resonance line deviates from Lorentzian. Furthermore it also results in a dramatic change of the angular dependence of the linewidth of the EPR line . This effect will be dicussed in the next section. Up to now we only discussed the secular $m = 0$ term in the relaxation function. The non-secular terms are especially important in case $\omega_0 \leq \omega_{ex}$. Some algebra leads to the following expressions for these terms.

$$\begin{aligned} \int_0^t d\tau (t-\tau) G_m(\tau) \cos m\omega_0 \tau &= \frac{G_m(0)t}{\omega_{ex}} \sqrt{\frac{\pi}{2}} \operatorname{erf}\left(\frac{\omega_{ex}\tau_{1m}}{\sqrt{2}} \right) \\ &+ \frac{G_m(0)\zeta_m t}{K\omega_{ex}} \left\{ \ln\left(\frac{\omega_{ex}/m\omega_0}{\omega_{ex}\tau_{1m} + \zeta_m/K} \right) - 0.577 \right\} \end{aligned} \tag{2.80}$$

2.6 The Angular Dependence of the Linewidth ΔB_{pp}

We can use the relaxation function $\phi(t)$ to calculate the first derivative peak to peak resonance linewidth ΔB_{pp} of the EPR-absorption line. In theory this should be done by a Fourier transformation of the relaxation function $\phi(t)$. A complication here is that this cannot be done analytically. However, if the resonance line is Lorentzian or nearly Lorentzian we can use the following approximate procedure: First we derive expressions which are exact for a Lorentzian resonance line and subsequently we apply these formulas to our nearly Lorentzian lines.

For a purely Lorentzian resonance line the linewidth ΔB_{pp} in magnetic field units (Gauss or Tesla) is given by

$$\Delta B_{pp} = \frac{2}{\sqrt{3}} \frac{1}{\gamma_e t_e} \tag{2.81}$$

where the time t_e is given by

$$\phi(t_e) = \frac{1}{e}\phi(0). \tag{2.82}$$

For a 3-d spin system – neglecting the contribution of spin diffusion – this gives

$$\Delta B_{pp} = \sqrt{\frac{2\pi}{3}} \frac{G_0(0)}{\gamma_e \omega_{ex}} \qquad \text{for} \qquad \omega_0 > \omega_{ex} \tag{2.83}$$

and

$$\Delta B_{pp} = \sqrt{\frac{2\pi}{3}} \frac{G_0(0) + G_1(0) + G_2(0)}{\gamma_e \omega_{ex}} \qquad \text{for} \qquad \omega_0 < \omega_{ex} \tag{2.84}$$

The angular dependence is due to the dipolar factors $G_m(0)$ which are listed in table 2.5. Inspection of this table reveals that the linewidth is maximal if $\theta_{ij} \approx 0$ for all spins i and j. In case this expression was valid for a 2-d spin system , it predicts that the

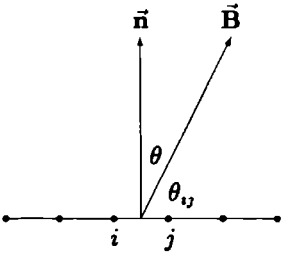

Figure 2.2: Definition of the angles θ and θ_{ij} with respect to the spinplane.

linewidth is maximal if the magnetic field $\vec{B}$ is oriented in the plane of the spins. For $\omega_0 > \omega_{ex}$ there is also a minimum in the linewidth at the magic angle $\theta_{ij} = \cos^{-1}(\frac{1}{\sqrt{3}})$. By using this 3-$d$ formula for determining the linewidth ΔB_{pp} we neglect the influence of spin diffusion. In order to include these effects we have to start from equation 2.76. In this case the angular variation of ΔB_{pp} is determined by the angular dependence of the factor Q, which in its turn contains angular variations due to $G_0(0)$ and ζ_0. The variations of G_0 and ζ_0 for a 2-d hexagonal system are tabulated in table 2.6 and 2.7, respectively. Here the angle θ is the angle between the magnetic field $\vec{B}$ and the normal to the spin plane $\vec{n}$ as depicted in figure 2.2. θ is approximately the complement of θ_{ij}. By combining the expressions for G_0 and ζ_0 we get for Q the formula

$$Q(\theta) = \frac{3}{16}\gamma_e^4\hbar^2 S(S+1)\left(\sum_j r_{ij}^{-3}\right)^2 (3\cos^2\theta - 1)^2 \tag{2.85}$$

The linewidth is obtained by a Fourier transformation of equation 2.76. This gives as an approximate expression for ΔB_{pp}

$$\Delta B_{pp} \approx \alpha + \beta(3\cos^2\theta - 1)^2 \tag{2.86}$$

where α and β are constants which depend on the temperature. This equation predicts that the linewidth is maximum as the magnetic field is oriented perpendicular to the magnetic plane ($\theta = 0$) and minimum for the magic angle $\theta = \cos^{-1}(\frac{1}{\sqrt{3}})$. The lineshape for this last orientation is Lorentzian because $Q = 0$. For all other orientations deviations from the Lorentzian lineshape are predicted. Although we used results which are only exactly valid for a hexagonal lattice, expression 2.86 is also valid for other lattice types to a good approximation. If we finally compare the expressions 2.86 and 2.83 or 2.84 it is clear that spin diffusion has a great influence upon the behaviour of the resonance line.

2.7 The Temperature Dependence of the Linewidth

In the last section we derived expressions for the relaxation-function $\phi(t)$ in 3-d and 2-d magnetic systems. Strictly speaking, these expressions are only valid at infinite temperature. Because only at that temperature the two-spin correlation functions $\langle S_{0z}S_{0z}\rangle$ are equal to $1/3S(S+1)$ for all wave-vectors $\vec{q}$. In this section we will discuss the influence of

$$
\begin{aligned}
G_0(0) &= \frac{3}{4}\gamma_e^4\hbar^2 S(S+1)\sum_j r_{ij}^{-6}\left(\frac{27}{8}\sin^4\theta - 3\sin^2\theta + 1\right) \\
G_1(0) &= \frac{15}{2}\gamma_e^4\hbar^2 S(S+1)\sum_j r_{ij}^{-6}\left(\frac{1}{2}\sin^2\theta - \frac{3}{8}\sin^4\theta\right) \\
G_2(0) &= \frac{3}{4}\gamma_e^4\hbar^2 S(S+1)\sum_j r_{ij}^{-6}\left(\frac{3}{8}\sin^4\theta + \cos^2\theta\right)
\end{aligned}
$$

Table 2.6: The dipolar factors G_m for a hexagonal spin lattice

$$
\begin{aligned}
\zeta_0 &= \frac{\frac{1}{4}(3\cos^2\theta - 1)^2}{\frac{1}{4}(3\cos^2\theta - 1)^2 + \frac{9}{8}\sin^4\theta}\,\frac{(\sum_j r_{ij}^{-3})^2}{\sum_j r_{ij}^{-6}} \\
\zeta_1 &= \frac{\frac{1}{4}\sin^2\theta\cos^2\theta}{\frac{1}{2}\sin^2 - \frac{3}{8}\sin^4\theta}\,\frac{(\sum_j r_{ij}^{-3})^2}{\sum_j r_{ij}^{-6}} \\
\zeta_2 &= \frac{\frac{1}{4}\sin^4\theta}{\frac{3}{8}\sin^4\theta + \cos^2\theta}\,\frac{(\sum_j r_{ij}^{-3})^2}{\sum_j r_{ij}^{-6}}
\end{aligned}
$$

Table 2.7: The constants ζ_m for a hexagonal spin lattice

finite temperatures on the relaxation-function. The EPR experiments on a great variety of magnetic 1-d and 2-d systems reveal a strongly temperature dependent linewidth. A remarkable feature is that this variation is linear as long as the influence of long-range order is insignificant. The usual relaxation processes (direct, Raman and Orbach process) do not predict such a linear behaviour. Therefore the attention has been focussed on the temperature dependence of the spin-correlation functions and the various exchange interactions.

The relaxation function of a 3-d magnetic system can be approximated as

$$
-\ln\phi(t) \approx \sqrt{\frac{\pi}{2}}\frac{G_0(0)t}{\omega_{ex}} \tag{2.87}
$$

In this expression both ω_{ex} and $G_0(0)$ are temperature dependent. The characteristic short-time decay-rate ω_{ex} varies only weakly with temperature [22]. Therefore the variation of the relaxation function is due to $G_0(0)$ which in turn is proportional to

$$
\frac{\sum_q |F_q^{(0)}|^2\langle\hat{S}_{qz}(\tau)S_{-qz}\rangle^2}{\langle S_{0z}S_{0z}\rangle} \tag{2.88}
$$

The two-spin correlation function $\langle S_{0z}S_{0z}\rangle$ is connected with the static magnetic susceptibility [13]. As a consequence the initial temperature dependence of $\langle S_{0z}S_{0z}\rangle$ is given by

$$
\langle S_{0z}S_{0z}\rangle_T = \langle S_{0z}S_{0z}\rangle_\infty\left(1 - \frac{T_\theta}{T}\right)^{-1} \tag{2.89}
$$

T_θ in this expression is the Weiss-temperature which is defined as

$$
T_\theta = \frac{2S(S+1)}{3k}\sum_j J_{ij} \tag{2.90}
$$

Richards [13] showed that the temperature dependence of the numerator of expression 2.88 is quite a bit weaker than that of $\langle S_{0z}S_{0z}\rangle$, because of the presence of the dipolar factors $|F_q^{(0)}|^2$. If we include this variation we obtain as expression for the variation of the relaxation function :

$$\frac{[-\ln\phi(t)]_T}{[-\ln\phi(t)]_\infty} = \left(1 - \frac{3}{4}\frac{T_\theta}{T}\right) \tag{2.91}$$

Because a ferromagnetic system has a positive Weiss-temperature the relaxation-function $\phi(t)$ will decay slower upon lowering the temperature. Consequently the linewidth of a 3-d ferromagnetically coupled system will decrease upon lowering the temperature, whereas it will increase if the coupling is antiferromagnetic.

For low-dimensional systems the main contribution to the relaxation function arises from the long-time spin diffusion contribution. In this case $\phi(t)$ can be approximated as

$$-\ln\phi(t) \approx \frac{G_0(0)\zeta_0\, t}{K\omega_{ex}} \ln\left(\frac{t}{t_0}\right) \tag{2.92}$$

The terms $G_0(0)$ and ζ_0 have the largest temperature dependence. But, whereas the temperature dependence of $G_0(0)$ varies as the temperature dependence of the inverse of $\langle S_{0z}S_{0z}\rangle$, the temperature variation of ζ_0 is proportional to that of $\langle S_{0z}S_{0z}\rangle^2$. The factor K also varies with the temperature due to the diffusion constant D. This results in the following temperature dependence for a 2-d magnetic system:

$$\frac{[-\ln\phi(t)]_T}{[-\ln\phi(t)]_\infty} = \frac{\langle S_{0z}S_{0z}\rangle_T}{\langle S_{0z}S_{0z}\rangle_\infty}\left(\frac{D_T}{D_\infty}\right)^{-\frac{d}{2}} \tag{2.93}$$

Hence, apart from any temperature dependence of the diffusion constant, the linewidth in 2-d magnetic systems with a ferromagnetic exchange interaction will increase, because the relaxation function will decay faster upon lowering the temperature. For systems with an antiferromagnetic exchange interaction it will decrease. This temperature effect is increased by the temperature dependence of D which is approximately proportional to the inverse of $\langle S_{0z}S_{0z}\rangle$ at high temperatures.

The preceding results are based on analysis of the influence of temperature on the time-correlation functions made by Richards [13]. Other authors tried to explain the anomalous temperature behaviour by a dependence of the various exchange interactions on temperature. The earliest model that produces a very linear T-dependence is the "phonon modulated antisymmetric exchange model" proposed by Castner and Seehra [23]. This model was applied to the $(RNH_3)_2CuX_4$ by Willett and Wong [24] and a good agreement was found. However, this model can't be true in general, because there ary many compounds with a small or absent antisymmetric-exchange interaction, which also show a remarkable strong linear temperature dependence. Examples of such compounds are $(CH_3NH_3)_2\ MnCl_4$ and the alkali-biphenyl systems. Another cause of the linear temperature variation might be that the isotropic exchange is temperature dependent. This is shown in the work of Kennedy [25], who observed a change in J of a factor of five, and Manoharan [26]. Zaspel and Drumheller [27] used an Einstein independent oscillator model to describe the temperature dependence of the isotropic exchange interaction in $(MX_4)_2$ dimers and $CrBr_3$. Using their model the temperature dependence of these compounds can be explained only partially.

In conclusion we can state that the remarkable linear temperature dependence of the EPR-linewidth remains unsolved up to now. There are several possibilities to explain this peculiar temperature dependence but none of these possibilities is able to predict the correct behaviour for all low-dimensional magnetic systems.

Bibliography

[1] C.P. Slichter.
Principles of Magnetic Resonance.
Springer Verlag (Berlin), 1980.

[2] J.E. Wertz and J.R. Bolton.
Electron Spin Resonance.
Chapman and Hall (New York), 1986.

[3] J.J. Mooij.
Single Crystals of Alkali-Aromatic ion-pairs.
PhD thesis, University of Nijmegen, 1976.

[4] J.H. van Vleck.
Physical Review, 74:1168, 1948.

[5] P.W. Anderson and P.R. Weiss.
Review of Modern Physics, 25:269, 1953.

[6] A. Lagendijk and H. de Raedt.
Physical Review B, 16:293, 1977.

[7] A. Lagendijk.
Physical Review B, 18:1322, 1978.

[8] A. Lagendijk.
Journal of the Physical Society of Japan, 46:784, 1979.

[9] H. Benner.
Untersuchung der Spindiffusion in magnetisch niedrigdimensionalen Systemen mit Hilfe der Elektronenspinresonanz.
PhD thesis, Darmstadt, 1978.

[10] H. Benner, J.-P. Boucher, J.P. Renard, and H. Seitz.
Journal of Magnetism and Magnetic Materials, 31-34:1233, 1983.

[11] R. Kubo and K. Tomita.
Journal of the Physical Society of Japan, 9:888, 1954.

[12] P.M. Richards and M.B. Salamon.
Physical Review B, 9:32, 1974.

[13] P.M. Richards.
Magnetic resonance in one and two-dimensional systems.
In K.A. Muller and A. Rigamonti, editors, *Local Properties at Phase Transitions*, page 539, North-Holland (Amsterdam), 1976.

[14] R. Kubo.
A stochastic theory of line-shape and relaxation.
In D. ter Haar, editor, *Fluctuation, Relaxation and Resonance in Magnetic Systems*, page 23, Oliver and Boyd (Edinburgh), 1961.

[15] Z.G. Soos, T.T.P. Cheung, and K.T. McGregor.
Chemical Physics Letters, 46:600, 1977.

[16] T.T.P. Cheung, Z.G. Soos, R.E. Dietz, and F.R. Meritt.
Physical Review B, 17:1266, 1978.

[17] N.N. Bogolyubov and S.V. Tyablikov.
Sovjet Physics: Doklady, 4:604, 1967.

[18] P.M. Richards.
Magnetic resonance in one and two-dimensional systems.
In H.J. Keller, editor, *Low Dimensional Cooperative Phenomena*, page 147, Plenum Press (New York), 1975.

[19] L.P. Kadanoff and P.C. Martin.
Annals of Physics, 24:419, 1963.

[20] M. Blume and J. Hubbard.
Physical Review B, 1:3815, 1970.

[21] R.A. Tahir-Kheli and D.G. McFadden.
Physical Review, 182:604, 1969.

[22] Leichner and P.M. Richards.
Physical Review B, 7:453, 1973.

[23] T.G. Castner and M.S. Seehra.
Physical Review B, 4:38, 1971.

[24] R.D. Willett and F. Waldner.
Journal of Applied Physics, 53:2680, 1982.

[25] T.A. Kennedy, S.H. Choh, and G. Seidel.
Physical Review B, 2:3645, 1970.

[26] P.T. Manoharan, J.H. Noordik, E. de Boer, and C.P. Keijzers.
Journal of Chemical Physics, 74:1980, 1981.

[27] C.E. Zaspel and J.H. Drumheller.
Physical Review B, 16:1771, 1977.

Chapter 3

Dynamic and Static Magnetic Properties of NaBp.2Tg

3.1 Introduction

For many years the alkali-biphenyl ion pairs have been an object of study. Originally, all effort was directed towards elucidating the structure of these ion pairs in solution. But since it became possible to synthesize single-crystals of these compounds the attention was drawn by the interesting magnetic properties of these substances:

- These organic compounds are paramagnetic.
- The compounds are composed of layers : Layers of paramagnetic biphenyl anions are separated by layers of diamagnetic sodium-bis-triglyme clusters.
- The large distance between the paramagnetic layers, resulting in pseudo two-dimensional magnetic properties.
- The biphenyl anions in the paramagnetic layers are arranged in different ways for the various alkali-biphenyl systems.
- The $\bar{\bar{\mathbf{g}}}$-anisotropy of these molecules is extremely small.

Although the number of systems with pseudo two-dimensional magnetic properties has increased greatly in the last few years, only a few of them are based upon organic compounds. Moreover, in most pseudo two-dimensional magnetic compounds the presence of exchange interactions in two dimensions is combined with a large $\bar{\bar{\mathbf{g}}}$-anisotropy, by which testing the theories of exchange-narrowing in two-dimensions is complicated. Therefore the title compound and related systems are well suited as model systems for the study of the spin dynamics of pseudo two-dimensional magnetic systems. The results of a series of EPR-studies on the spin dynamics of NaBp.2Tg will be discussed in the sections 3.2 and 3.3. In these sections we will also present some results of susceptibility and magnetization measurements. By a detailed analysis of the resonance field shifts and the susceptibility data we were able to determine a magnetic structure of the paramagnetic layers. This analysis and the proposed magnetic structure are the subject of the last section of this chapter.

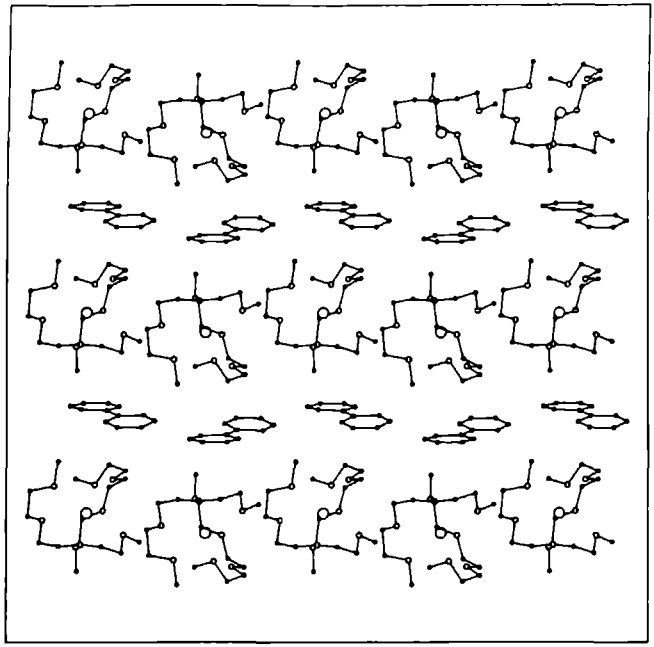

Figure 3.1: Projection of NaBp.2Tg on the *ab*-plane.

Crystal structure

Single-crystals containing sodium biphenyl ion pairs were first prepared by Canters et al. in 1970 [1]. The crystal structure of these compounds were hard to solve. In 1978 Noordik et al. [2] succeeded in solving the crystal structure of NaBp.2Tg. A picture of the crystal structure, projected on the *ab*-plane is shown in figure 3.1, and the principal crystallographic data are listed in table 3.1. It is very clear from this picture that this system can be characterized as a solvent separated ion pair, in contrast to, for example, the alkali complexes of cyclooctatetraene. In the figure one can also observe the layered structure of this compound: Layers of paramagnetic biphenyl anions are separated by layers of diamagnetic $(Na.2Tg)^+$ clusters. The distance between the paramagnetic layers amounts 11.4 Å, which is much larger than the shortest C–C distance (3.5 Å) between

$C_{28}H_{46}NaO_8$	Monoclinic, $P2_1$
$a = 11.721(2)$ Å	$Z = 2$
$b = 13.425(2)$ Å	$D_x = 1.21$ Mg m^{-3}
$c = 9.555(2)$ Å	$M_r = 533.7$
$\beta = 103.08°$	(cell dimensions at 150 K)
$V = 1464.5$ Å^3	

Table 3.1: Crystal data of NaBp.2Tg.

carbon atoms of neighbouring biphenyl anions in the magnetic plane. The phenyl rings in the biphenyl anion are nearly planar; the maximum deviation of the least-squares plane is 0.023 Å and the dihedral angle is 7.3°. This dihedral angle is composed of a torsion around, as well as a bending of the central C–C bond. The central C–C bond is somewhat shorter than the corresponding C–C bond in the neutral biphenyl. The $(Na.2Tg)^+$ cation consists of a Na^+ cation coordinated to the eight oxygen atoms of the two surrounding triglyme molecules. Due to the presence of these bonds the Na^+ cation is strongly stabilized which makes the formation of a single crystal possible.

Experimental

A $\sim$ 0.8 M solution containing NaBp.2Tg was prepared by standard techniques under high vacuum [1]. Single crystals were obtained by cooling this solution at a rate of 1 K/h from about 293 K to 273 K. The NaBp 2Tg crystals are darkly blue and form rectangular shaped plates. Because of their low-melting point and because of their sensitivity to air and moisture the crystals were mounted in small glass capillaries in a helium atmosphere in a glove box at a temperature of about 253 K. The quality of the crystals was checked by Weissenberg photographs. The positions of the crystal-axes for the EPR experiments were determined on a CAD-4 diffractometer. The EPR measurements were carried out on a Varian E-12 spectrometer in a homebuilt bath-cryostat which contained two independent, mutually orthogonal rotation axes: one of these rotation axis being the sample holder, the other axis being the magnet. By this construction we were able to measure the EPR spectra for all orientations of the magnetic field without remounting the crystal. The required dial-positions for any desired orientations of the crystal could be calculated by means of the FORTRAN program CRYORO on the basis of the initial alignment of the crystal. The magnetic field was measured with a Bruker B-NM12 Gauss meter and the frequency was measured with a HP 5246L electronic counter in connection with a HP 5255A frequency converter. The electron spin echo measurements were performed on a homebuilt ESE-spectrometer. The details of this instrument were previously described by Reijerse [3].

MOLECULAR PHYSICS, 1984, VOL. 52, No. 1, 195–206

3.2 Spin diffusion in the quasi-two-dimensional magnetic system bis[1,2-bis(2-methoxyethoxy)ethane] sodium biphenylide A temperature dependent E.S.R. study

by M. C. M. GRIBNAU, R. MURUGESAN†, H. VAN KEMPEN and E. DE BOER

Research Institute for Materials, University of Nijmegen, Toernooiveld, 6525 ED Nijmegen, The Netherlands

(*Received* 8 *September* 1983 ; *accepted* 6 *January* 1984)

The exchange narrowed E.S.R. line of single crystals of the quasi-two-dimensional magnetic system bis[1,2-bis(2-methoxyethoxy)ethane] sodium biphenylide (NaBp . 2Tg) is studied at 9·4 GHz as a function of temperature from 295 to 1·2 K. At 77 K the linewidth has the characteristic $(3\cos^2\theta-1)^2$ dependence and the resonance line is non-lorentzian except for the magic angle $\theta=\cos^{-1}(1/\sqrt{3})$. These facts are interpreted in terms of spin diffusion in this two-dimensional magnetic system. At 1·2 K the two-dimensional anomalies are lost and the linewidth and lineshape behave as expected for a three-dimensional magnetic system. The temperature dependence of the linewidth and the linewidth anisotropy indicates that at 1 5 K a crossover takes place from two-dimensional to three-dimensional behaviour. Susceptibility measurements from 270–1·1 K point to a ferromagnetic coupling at high temperatures and an antiferromagnetic coupling at low temperatures. From magnetization measurements it could be concluded that at about 1 1 K the spins in the magnetic planes are antiferromagnetically ordered.

1. INTRODUCTION

Electron spin resonance continues to be one of the most important techniques to study spin dynamics in low dimensional magnetic systems [1–4]. The importance of $q\to 0$ modes in such systems can be studied in the exchange narrowed E.S.R. line which exhibits a frequency dependent linewidth (ΔB_{pp}), a characteristic angular dependence of the form $\Delta B_{pp}\approx(3\cos^2\theta-1)^2+\text{constant}$ and a deviation from lorentzian lineshapes. Many of the studies of spin diffusion effects in such low dimensional systems pertained mainly to high temperatures. Much work has to be done both experimental and theoretical, to understand the temperature dependence of the exchange narrowed E.S.R. line in these systems. In a pioneering work Richards and Salamon have quantitatively accounted for the temperature dependence of the linewidth and linewidth anisotropy of the two-dimensional antiferromagnet K_2MnF_4 [5]. The theory considers the dipolar perturbation as the sole source of the line broadening and it does not introduce any adjustable parameters. However,

† Present address : Department of Chemistry, Washington University, St. Louis, Missouri 63130, U.S.A.

as pointed out by them, when the available low temperature data of the ferromagnets K_2CuF_4 [6] and $NiCl_2$ [7] are analysed in the light of their theory, considerable contradiction between theory and experiment was noticed. It was further pointed out that the disagreement may be associated with the non-*S*-state character of the magnetic ions of these materials, for which non-dipolar broadening can also be an important factor. Hence an *S*-state magnetic ion which has mainly dipolar and exchange interactions will be an ideal candidate for a temperature dependent E.S.R. study. The quasi-two-dimensional magnetic crystals of alkali metal biphenyl salts form a series of model examples for the above purpose. We have shown in our recent publications [8, 9] that at high temperatures both the linewidth and lineshape of NaBp . 2Tg can be quantitatively accounted for in terms of RS theory which takes into account the dominance of $q \to 0$ modes, leading to a long time decay of spin correlation functions. In this paper we report the temperature dependent E.S.R. study of NaBp . 2Tg and susceptibility and magnetization measurements on it at low temperatures (1·1 to 4·2 K).

2. Experimental

The crystals of NaBp . 2Tg are highly sensitive to moisture and air. They were prepared under high vacuum, sealed in capillary tubes under a helium atmosphere and aligned with the aid of a Weisenberg Camera as described elsewhere [8]. E.S.R. measurements were carried out on a Varian E12 spectrometer. The low temperature measurements (below 4·2 K) were carried out by evaporating liquid helium in a bath cryostat. The temperatures were determined by measuring the helium vapour pressure. Measurements between 4·2 K and 77 K were made after complete evaporation of all the helium by letting the dewar warm up to liquid N_2 temperature (time 1–2 hours). Subsequently the measurements between 77 K and room temperature were carried out during warming up of the dewar after all the liquid N_2 was evaporated. In the bath cryostat the crystal could be rotated along two mutually orthogonal axes. Hence by judicious combination of these two axes, one could obtain any particular orientation, if the initial alignment of the crystal is known.

Magnetization measurements were performed on powder samples. For the higher temperatures ($> 3{\cdot}5$ K) a vibrating sample magnetometer mounted on a flow cryostat [10] was used while for the lower temperatures ($< 4{\cdot}2$ K) we used a similar magnetometer together with a liquid helium bath cryostat. The susceptibilities were derived from measurements in an external field of 0·1 Tesla for the low and in a field of 1·2 Tesla for the high temperature range.

3. Crystal structure and magnetic properties

NaBp . 2Tg crystallizes in the space group P_{2_1}, with the unit cell parameters, $a = 11{\cdot}721$, $b = 13{\cdot}425$, $c = 9{\cdot}555$ (Å), and $Z = 2$ [11]. The magnetic ions (biphenyl anions) are situated in one layer which is formed by the *bc* plane of the crystal. The midpoints of the biphenyl anions form nearly a hexagonal lattice. The magnetic susceptibility measurements at high temperatures indicate a ferromagnetic exchange interaction between the neighbours in the magnetic plane. Applying molecular field theory it was found that the exchange

interaction between neighbouring spins is equal to $J/k = 2{\cdot}3$ K [8]. It was also noticed that the susceptibility deviates from the Curie–Weiss law below 100 K. In an attempt to fit the low temperature data to a two-dimensional ferromagnetic high temperature series expansion (HTS) we found that the measured susceptibility contained some contributions from antiferromagnetic interactions. In order to make possible an analysis of the low temperature data we have extended the earlier susceptibility measurements to lower temperatures by using a low temperature magnetometer.

4. Results and discussion

4.1. *Linewidths and lineshapes*

Figure 1 presents the angular dependence of the peak-to-peak width of the derivative line measured at 9·4 GHz and at three different temperatures.

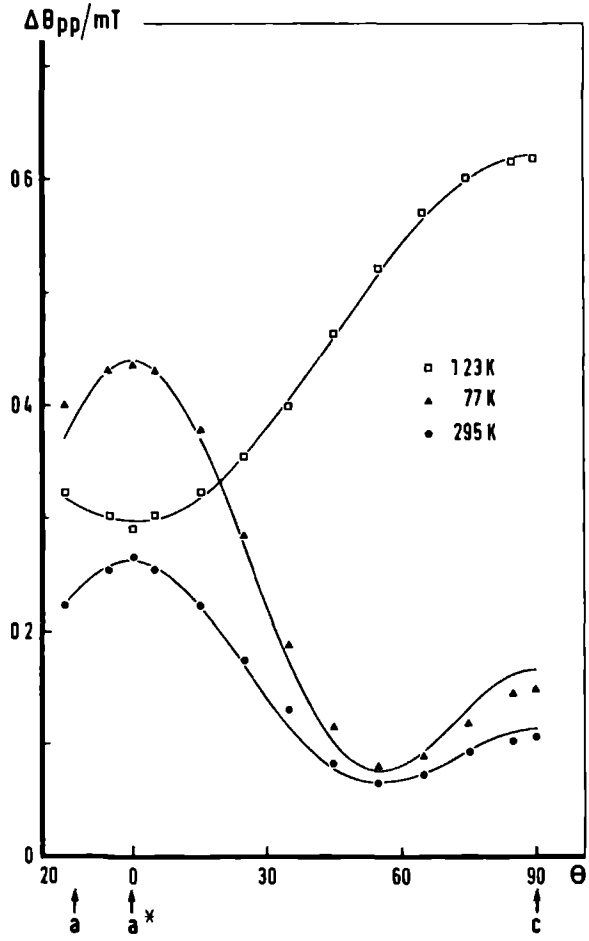

Figure 1. Angular dependence of ΔB_{pp} in the a^*c plane at 295, 77 and 1·2 K. The solid lines are least squares fits (see text).

The measurements are made with the magnetic field in the a^*c plane. The linewidths at 295 and 77 K show the characteristic angular dependence described by $\Delta B_{pp}(\theta) = a + b(3\cos^2\theta - 1)^2$ with $a = 0{\cdot}064$ and $0{\cdot}079$ mT and $b = 0{\cdot}050$ and $0{\cdot}092$ mT for 295 and 77 K, respectively (least squares fits). It is well established that in two-dimensional magnetic systems the angular dependence of the form $\Delta B_{pp}(\theta) \approx a + b(3\cos^2\theta - 1)^2$ (where θ is the angle between the applied field **B** and the normal to the two-dimensional magnetic plane) is due explicitly to the importance of spin diffusion in the long time behaviour of the spin correlation function [5, 8]. Following the theory of Richards and Salamon (RS) for a two-dimensional magnetic system we have earlier shown that the linewidth variation at 295 K could be theoretically calculated on an absolute basis without any adjustable parameters in the realm of the infinite temperature approximation [8]. Comparison of 295 and 77 K data in figure 1 reveals (i) there is an increase in the linewidth for all the orientations at 77 K and (ii) the anisotropy of the linewidth also increases as seen from the values of b ($0{\cdot}050$ mT for 295 K and $0{\cdot}092$ mT for 77 K). A qualitative interpretation of these results is straight forward in terms of dominance of the wave vector $q \to 0$ modes in the long time decay of spin correlation functions in a two-dimensional magnetic system. For $NaBp.2Tg$ with a ferromagnetic coupling between the spins at high temperatures, the $q \to 0$ modes should grow in strength as the temperature is lowered which in turn will be reflected as enhanced two-dimensional anomalies. It is gratifying to note that the results given in figure 1 conform to the expectations.

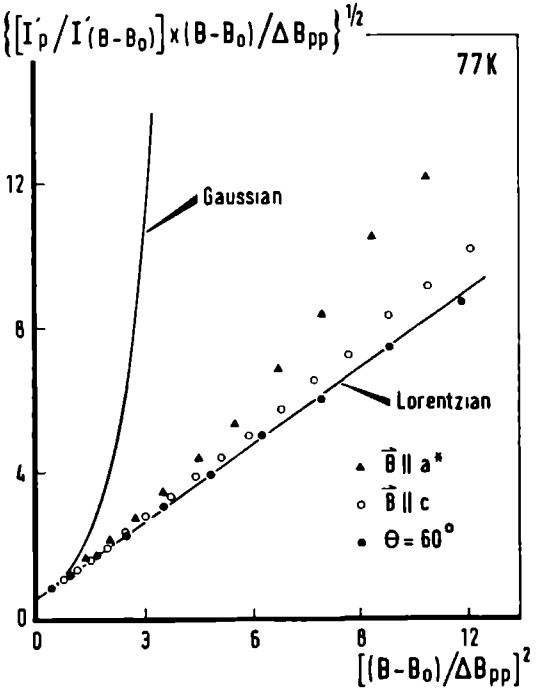

Figure 2. Lineshape analysis of the first derivative curve at 77 K and 9·4 GHz.

Another two-dimensional anomaly in the exchange-narrowed E.S.R. line is the deviation from lorentzian lineshape of the resonance line. We have analysed the E.S.R. lineshapes at 77 K for three typical orientations of $\mathbf{B}\|a^*$ ($\theta=0°$), $\mathbf{B}\|c(\theta=90)$ and $\mathbf{B}$ making an angle of 60° with the normal to the two-dimensional magnetic plane. The results are presented in figure 2, by plotting the ratio of $[I'_p\times(B-B_0))/I'_{(B-B_0)}\times\Delta B_{pp}]^{1/2}$ against $[(B-B_0)/\Delta B_{pp}]^2$ where I'_p is half of the peak-to-peak height of the derivative line. Such a plot gives a straight line with a slope of $1/\sqrt{2}$ and intercept of 0·5303 for a lorentzian lineshape. A gaussian line which falls of rapidly in the wings is also included for the sake of comparison. RS theory predicts a lorentzian lineshape for $\theta=\cos^{-1}(1/\sqrt{3})$, because at this angle the secular terms of the dipolar perturbation vanish. For other orientations one finds deviations from the lorentzian lineshape, the deviation being maximum for that orientation where the applied field $\mathbf{B}$ and the normal to the magnetic plane are parallel ($\mathbf{B}\|a^*$). The results in figure 2 are in accordance with this prediction, thereby indicating that the long time behaviour of spin correlation functions are operative at this temperature.

Interestingly the angular dependence of the linewidth at 1·2 K differs from what is observed at 77 and 295 K. It follows the equation $\Delta B_{pp}(\theta)$ (expressed in mT) $=-0.028+0{\cdot}325\ [1+\cos^2(\theta-90)]$ which is the characteristic behaviour for a three-dimensional magnetic system when secular as well as non-secular dipolar terms contribute to the linewidth [12]. It is also noted that the maximum linewidth no longer occurs for $\mathbf{B}\|a^*$, perpendicular to the magnetic plane, but for $\mathbf{B}\|c$, the axis lying in the magnetic plane.

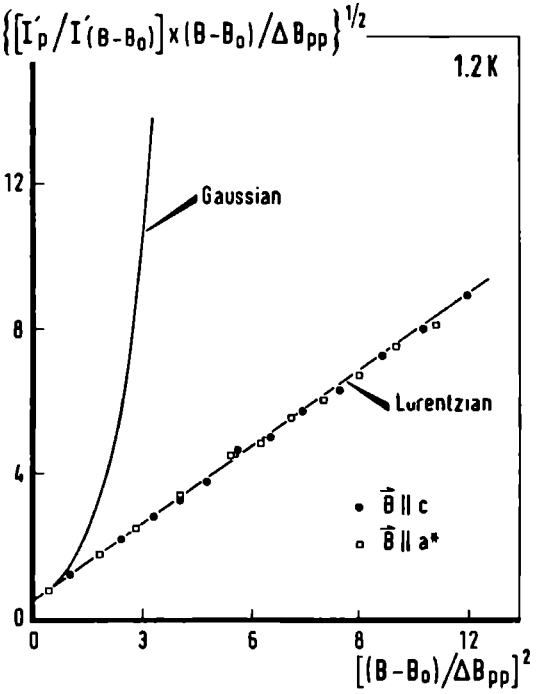

Figure 3. Lineshape analysis of the first derivative curve at 1·2 K and 9·4 GHz.

Further evidence for the three-dimensional magnetic nature of the system at 1·2 K comes from the lineshape analysis. The result of this is given in figure 3. For all orientations of the magnetic field the lineshape is lorentzian thereby indicating that the diffusive nature of the spin correlation functions are no longer operative and that an interplane coupling exists. The conclusion from the linewidth and lineshape analysis is that at 1·2 K the system behaves as a three-dimensional magnetic system and that spin diffusion effects are no longer dominant.

4.2. *Temperature dependence of* ΔB_{pp}

The values of ΔB_{pp} for the three representative orientations are plotted as a function of temperature in figure 4. As expected [3] for a two-dimensional magnetic system with ferromagnetic coupling between the spins we find an increase in the linewidth as the temperature is lowered from 295 K to 77 K, this increase being marked for the $\mathbf{B} \| a^*$ orientation, an orientation where the two-dimensional anomaly is expected to show its maximum effect. The maximum linewidth is observed at about liquid N_2 temperature, below this temperature the linewidth decreases sharply. In § 4.3 where the susceptibility data will be discussed we shall return to this point.

Figure 4 further shows a sudden increase in linewidths below 1·5 K for all the three orientations. The turning point is clearly seen in figure 5 for $\mathbf{B} \| a^*$, where the linewidth data are plotted only for the temperature range of 1·2 to 4 K. We also analysed the linewidth anisotropy as a function of temperature for some orientations in the a^*c plane. The results are illustrated in figure 6.

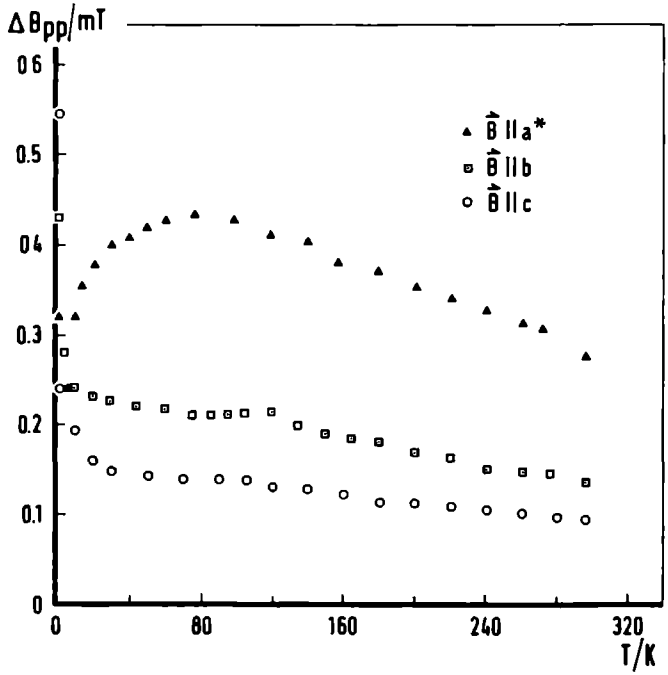

Figure 4. Temperature dependence of the linewidth for three typical orientations.

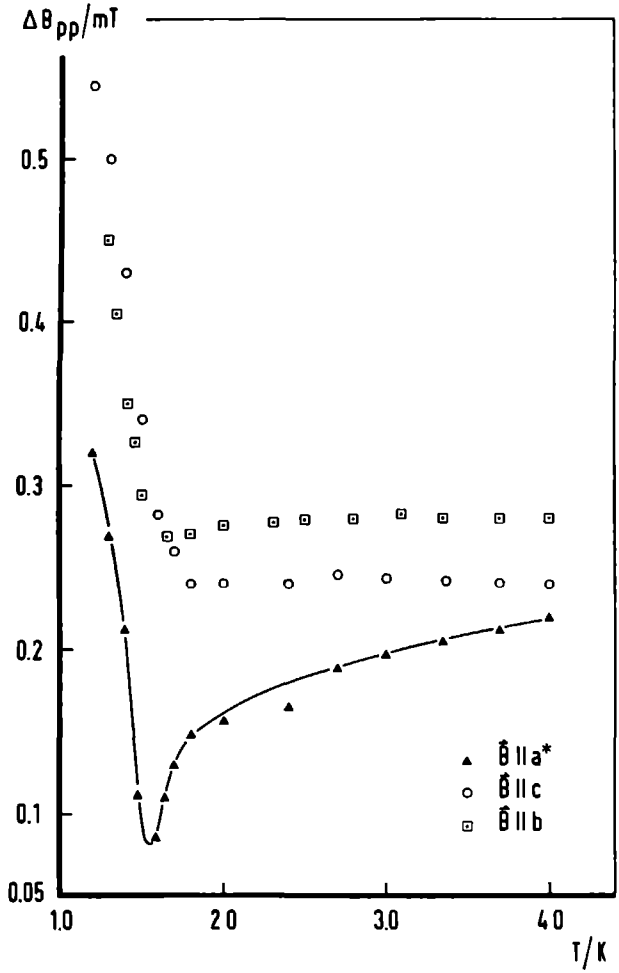

Figure 5. Expanded version of the linewidth below 4 K showing rapid change at 1·5 K.

The extrema observed at 1·5 K are interpreted as a result from a crossover from two-dimensional to three-dimensional behaviour. Further it is seen that the ratio $\Delta B_{pp}(\theta=0)/\Delta B_{pp}(\theta=60)$ approaches the value of unity at $T=3{\cdot}5$ K, revealing that there is no longer a minimum near $\theta=\cos^{-1}(1/\sqrt{3})$ as the ' crossover temperature ' is approached [4]. This implies that the dominance of $q\to 0$ modes decreases rapidly on approaching the latter temperature. The dipolar correlation functions $g(\tau)$ are no longer long lived and the importance of short time contributions to $g(\tau)$ increases. Under such conditions both the secular and non-secular parts of the dipolar interaction become equally important. This leads to an angular linewidth behaviour of the form $\Delta B_{pp}\approx [1+\cos^2(\theta-90)]$, as shown in figure 1, for $T=1{\cdot}2$ K.

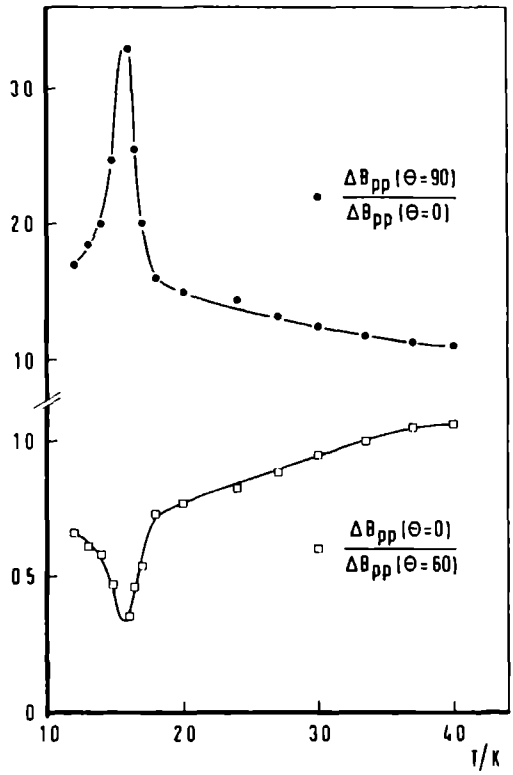

Figure 6. Temperature dependence of linewidth anisotropy in a^*c plane showing sharp change near 1·5 K.

4.3. *Magnetic susceptibility*

In an earlier publication [8] it was shown that the susceptibilities measured from 90 to 270 K fulfil the Curie–Weiss law. A positive Weiss constant of 6·9 K was obtained, which yielded for the exchange constant between nearest neighbours, using the molecular field theory, a value of $J/k = 2{\cdot}3$ K. Figure 7 exhibits the susceptibilities measured from 1·1 to 16 K. At 2·4 K a broad maximum is observed, which indicates that the spins align themselves antiferromagnetically. From these results one may be tempted to conclude that in the magnetically ordered state a ferromagnetic order exists in the magnetic planes and that the planes themselves are mutually antiferromagnetically coupled by an interplane exchange constant $J' < J$. However, figure 8 demonstrates that this cannot be true. At 4·2 K the magnetization increases linearly with the field up to 4 Tesla, at 1·1 K, the magnetization increases somewhat stronger than linearly with the field. This latter behaviour is characteristic for a strongly coupled antiferromagnet and therefore, because J' is believed to be small, rules out the possibility for the spin arrangement just mentioned. Thus we arrive at the interesting conclusion that at high temperatures a ferromagnetic coupling exists between the spins in the magnetic plane, whereas at low temperatures these spins are antiferromagnetically ordered.

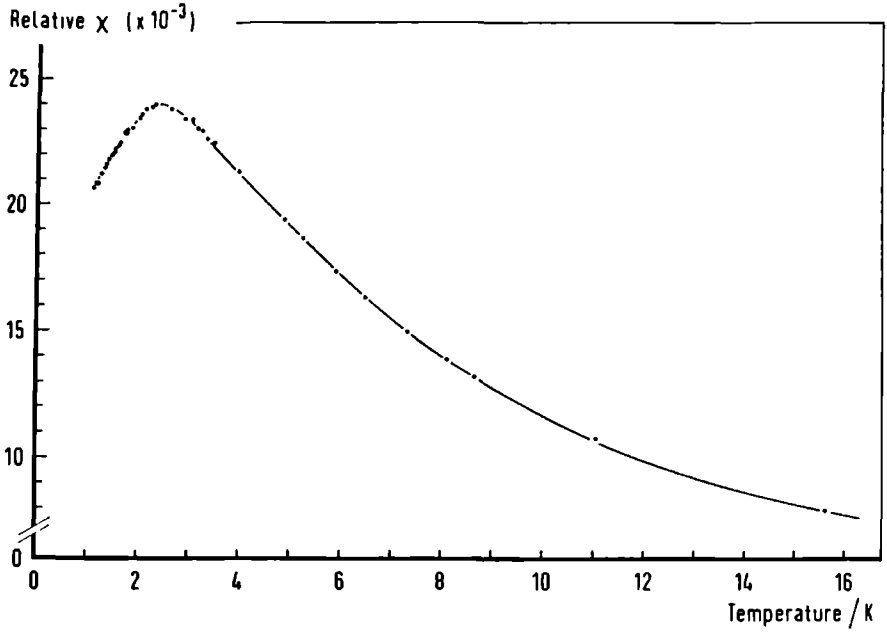

Figure 7. Relative susceptibility versus temperature for a powder sample.

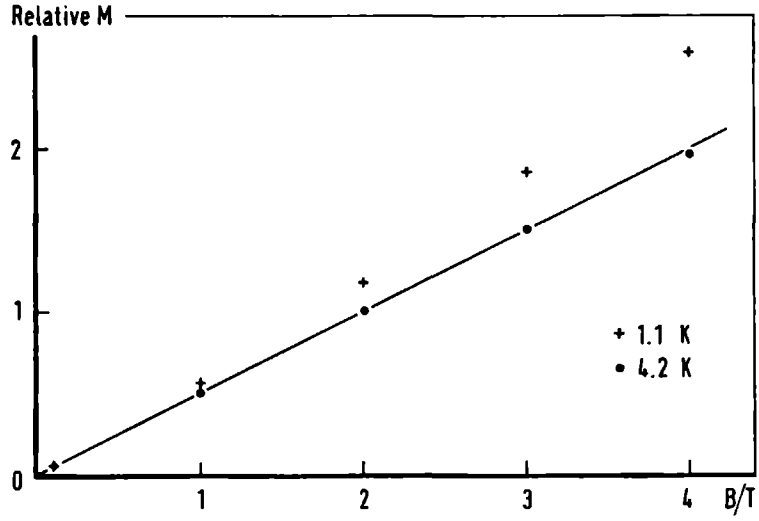

Figure 8. Relative magnetization versus field for 1·1 and 4·2 K.

There are at present several ways to explain this behaviour. First of all we note that the exchange constant J depends critically on the distance between and on the orientation of the paramagnetic biphenyl anions. For example, in a recent publication by van Hemert *et al.* [13] on the Heisenberg exchange interaction between O_2 molecules it was shown that the exchange constant could be

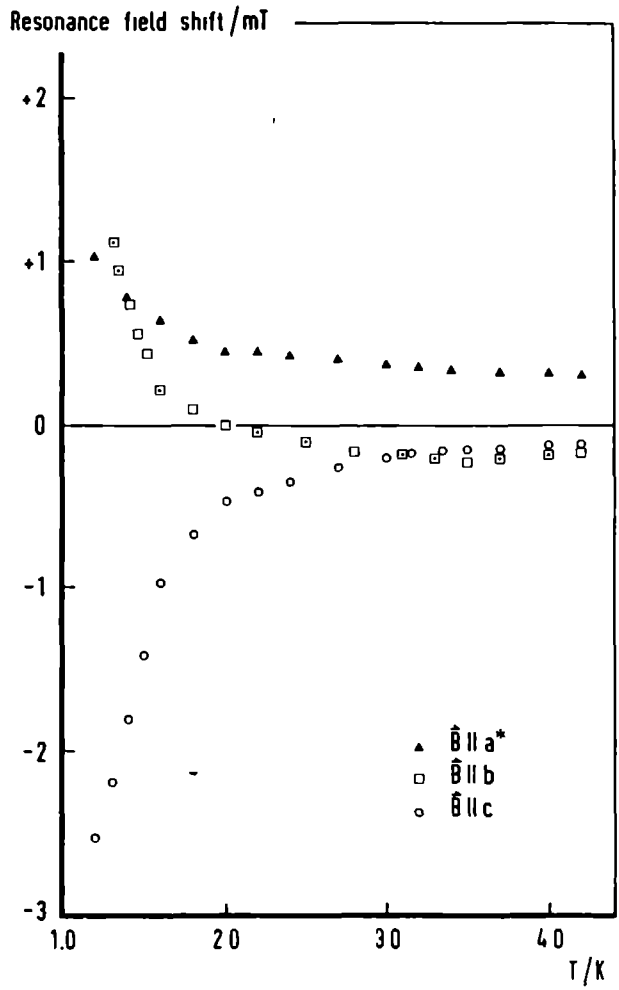

Figure 9. Resonance field shift for representative orientations in the temperature range of 1·2–4 K. The solid line corresponds to the g_{iso} value at 295 K.

negative as well as positive, depending on the orientation of the O_2 molecules. It was found that J can be described by a steeply exponential function, comparable with a power law of R^{-14}. Figure 2 of [8] illustrates how the six nearest biphenyl anions are oriented in the magnetic plane. Two different type of orientations can be distinguished, whereas the distance between the central biphenyl anion and its six nearest neighbours vary from 8·039 Å to 9·555 Å. Therefore exchange coupling constants between neighbouring spins can exist with different signs. At high temperature from the Curie–Weiss constant an averaged positive exchange constant was derived. In the above reasoning this means that the positive interactions dominate over the negative exchange interactions. Nevertheless at low temperature an antiferromagnetic structure may evolve, when a negative exchange constant (even when smaller than the also present positive one) is present.

Another possibility, which accounts also for our observation, is that the effective exchange constant will change sign when the temperature and consequently the distances and average orientations of the biphenyl anions is changed.

Finally an explanation may hold which was pointed out for the first time by Nagaev and Kovalenko [14]. They showed for EuSe that the short range order above the transition point is of different type from the long range order below the transition point (an ' order–alien disorder phase transition '). They attributed this to the different temperature dependence of the Heisenberg and of the non-Heisenberg exchange, as a result of which the high temperature properties may be determined by the former and the low temperature properties by the latter. We are planning calculations to decide between these alternatives.

The E.S.R. results discussed in § 4.1 have shown that below 1·5 K the system behaves as a three-dimensional magnetic system. Thus below this temperature an effective interplane exchange coupling exists of which the sign is unknown. From experiments on other two-dimensional magnetic systems [15, 16, 17] it can be inferred that the interplane exchange constant is most likely negative and about 10^2–10^6 times smaller than the intraplane exchange constant.

In § 4.2 we discussed the temperature dependence of ΔB_{pp} and noted that ΔB_{pp} for $\mathbf{B} \| a^*$ decreases as the ' crossover temperature ' of 1·5 K is reached from above. This effect can now be ascribed to the antiferromagnetic exchange interaction in the magnetic planes, becoming dominant at low temperatures, since for a two-dimensional magnetic system with antiferromagnetic coupling between the spins the linewidth should decrease on lowering the temperature [2]. These effects are not observed along the b and c directions, where spin diffusion is less pronounced (see figure 2).

4.4. *Resonance field shift*

We have also analysed the resonance field at low temperatures for different orientations. The results are plotted in figure 9. The resonance field is found to change considerably for all the three orientations. This kind of resonance field shift has been observed earlier [18, 19] in both one-dimensional and two-dimensional antiferromagnets. It is attributed to the magnetic dipolar interactions among short range ordered spins in the chains or in the magnetic plane.

The authors are grateful to Mr. C. Beers and Mr. A. A. K. Klaassen for their skilful assistance in carrying out the experiments and to Mr. B. van Noordwijk for constructing the low temperature magnetometer. Valuable discussions with Dr. C. P. Keijzers and Dr. O. Takizawa are gratefully acknowledged.

References

[1] Richards, P. M., 1975, *Low Dimensional Cooperative Phenomena*, edited by H. J. Keller (Plenum Press).

[2] Richards, P. M., 1976, *Local Properties at Phase Transitions*, edited by K. A. Muller and A. Rigamonti (North-Holland).

[3] Cheung, T. T. P., Soos, Z. G., Dietz, R. E., and Merrit, F. R., 1978, *Phys. Rev.*, **17**, 1266.

[4] Drumheller, J. E., 1982, *Magn. Res. Rev.*, **7**, 123.
[5] Richards, P. M., and Salamon, M. B., 1974, *Phys. Rev.* B, **9**, 32.
[6] Yamada, Y., and Ikebe, M., 1972, *J. phys. Soc. Japan*, **33**, 1334.
[7] Birgenean, R. J., Rupp, L. W., Jr., Guggenheim, H. J., and Lindgard, P. A., 1973, *Phys. Rev. Lett.*, **30**, 1252.
[8] Takizawa, O., Srinivasan, R., and de Bofr, E., 1981, *Molec. Phys.*, **44**, 677.
[9] Murugesan, R., and de Boer, E., 1983, *Chem. Phys. Lett.*, **95**, 301.
[10] Perfnboom, J. A. A. J., 1981, *Physica* B, **107**, 589.
[11] Noordik, J. H., Beurskens, P. T., van den Hark, Th. E. M., and Smits, J. M. M., 1979, *Acta crystallogr.* B, **35**, 621.
[12] Van Vleck, J. H., 1948, *Phys. Rev.*, **74**, 1168.
[13] Van Hemert, M. C., Wormer, P. E. S., and van der Avoird, A., 1983, *Phys. Rev. Lett.* (submitted).
[14] Nagaev, E. L., and Kovalenko, A. A., 1983, *Soviet Phys. JETP*, **52**, 460.
[15] Takizawa, O., 1976, *Bull. chem. Soc. Japan*, **49**, 583.
[16] Shmimizu, M., and Ajiro, Y., 1980, *J. phys. Soc. Japan*, **48**, 414.
[17] de Jongh, L. J., 1976, *Physica* B, **82**, 247.
[18] Nagata, K., and Tazuke, Y., 1972, *J. phys. Soc. Japan*, **32**, 337.
[19] Boucher, J. P., 1980, *J. Magn. magn. Mater.*, **15–18**, 687.

3.3 Pseudo 2-*d* Magnetism in Sodium Biphenyl Bis-Triglyme†

M.C.M. Gribnau and E. de Boer
Department of Molecular Spectroscopy
University of Nijmegen

The dynamic and static magnetic properties of the pseudo two-dimensional system NaBp.2Tg (Bp=biphenyl, Tg = triglyme) are discussed. Above 4.2 K the anisotropy of the EPR linewidth reveals the presence of spin diffusion. The analysis of the EPR spectra in combination with susceptibility and magnetization measurements shows that the low-temperature ordered state is antiferromagnetic in nature. However, above 80 K, ferromagnetic exchange interactions are dominant. More generally, the applicability of pulse EPR techniques to pure magnetic systems is considered.

Introduction

The electron paramagnetic resonance (EPR) spectra of low-dimensional magnetic systems exhibit special features brought about by spin diffusion [4]. The single crystal of NaBp.2Tg (Bp = biphenyl= $C_{12}H_{10}$, Tg = triglyme = $CH_3(CH_2CH_2O)_3CH_3$) is a typical example of a pseudo two-dimensional (2-*d*) magnetic system. In figure 3.2 the projection of the unit cell is given on the *ac*-plane. The crystal belongs to the space group P_{2_1}, with $a = 11.721(2), b = 13.425(2), c = 9.555(2), \beta = 103.08(4)$ and $Z = 2$ [5,6]. The magnetic ions (biphenyl anions) are situated in one layer which is formed by the *bc*-plane. The magnetic planes are separated by a layer of Na.2Tg clusters, the oxygen atoms of Tg are coordinated to the sodium ions, almost in a spherical geometry. The large separation of the magnetic planes (11.4 Å) gives the system two-dimensional magnetic properties. The NaBp.2Tg system is interesting for low dimensional physics, because of its extremely small $\bar{\mathbf{g}}$-anisotropy. Only the dipolar, exchange and isotropic Zeeman interactions are present. In this review it will be shown that EPR offers a powerful method of monitoring the pseudo two-dimensional character of this system [7,8,9].

Theoretical Background

The EPR spectra of pure magnetic compounds in general show only one exchange-narrowed resonance line. The shape of this line is equal to the Fourier transform of the relaxation function $\phi(t)$. The relaxation theory of Kubo and Tomita [10] supplies the following expression for $\phi(t)$:

$$\phi(t) = \exp\left\{-\int_0^t \psi(\tau)(t-\tau)d\tau\right\} \tag{3.1}$$

† Published in: *Electronic Magnetic Resonance of the Solid State*, Edited by J.A. Weil, Ottawa, 1987

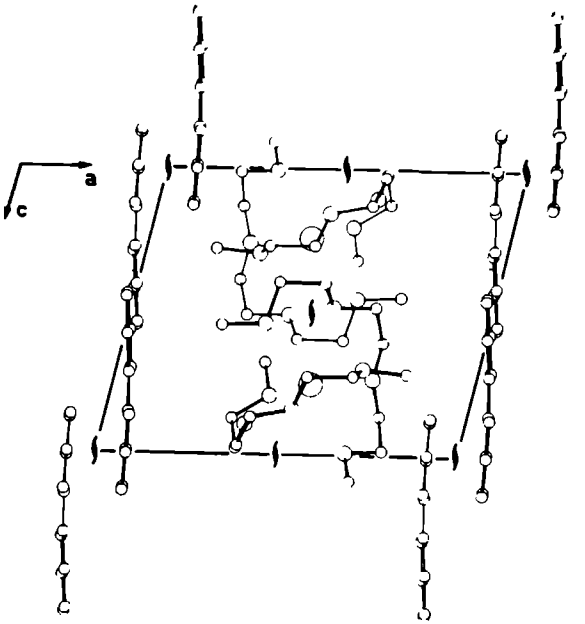

Figure 3.2: Crystal structure of NaBp.2Tg projected onto the *ac*-plane.

The function $\psi(\tau)$ contains the decay of the spin correlations. It is common to assume a fast decay of $\psi(\tau)$. Then, making a Taylor expansion for short times, one can derive

$$\psi(\tau) = \left\langle \Delta\omega^2 \right\rangle \exp\left(-\frac{\omega_{ex}^2 \tau^2}{2} \right) \tag{3.2}$$

with $\langle \Delta\omega^2 \rangle$ the Van Vleck second moment [11] of the resonance line and $\omega_{ex} = J_{ex}/\hbar$ the exchange frequency. After integration we get

$$\phi(t) = \exp\left(-\sqrt{\frac{\pi}{2}} \frac{\langle \Delta\omega^2 \rangle t}{\omega_{ex}} \right). \tag{3.3}$$

This expression shows that the shape of the resonance line will be Lorentzian and that the angular dependence of the first-derivative peak-peak linewidth will be proportional to the second moment:

$$\Delta B_{pp} = \sqrt{\frac{2\pi}{3}} \frac{\langle \Delta\omega^2 \rangle}{\gamma_e \omega_{ex}}, \tag{3.4}$$

where $\gamma_e = g\mu_B/\hbar$. The second moment is given by [12]

$$\left\langle \Delta\omega^2 \right\rangle = \frac{3}{2} \gamma_e^4 \hbar^2 S(S+1) \sum_k \frac{(1 + \cos^2 \theta_{jk})}{r_{jk}^6} \quad \text{for} \quad \omega_{ex} > \omega_0 \tag{3.5}$$

or

$$\left\langle \Delta\omega^2 \right\rangle = \frac{3}{4} \gamma_e^4 \hbar^2 S(S+1) \sum_k \frac{(1 - 3\cos^2 \theta_{jk})^2}{r_{jk}^6} \quad \text{for} \quad \omega_{ex} < \omega_0 \tag{3.6}$$

where θ_{jk} is the angle between the magnetic field and the vector $\vec{r}_{jk}$ connecting the spins j and k. Here, $\theta_{jk} \approx 90^0 - \theta$ with θ the angle between the magnetic field and the normal to the magnetic plane; $\omega_0 = \gamma_e B_0$ is the Zeeman angular frequency.

The preceding expressions do not properly describe the experimental results in low-dimensional systems. This has been attributed to the neglect of the slow decay of the $q \approx 0$ spin correlations due to spin diffusion [4,13]. Including these slow decay correlations we can write for $\psi(\tau)$ for intermediate times

$$\psi(\tau) = \left\langle \Delta\omega^2 \right\rangle \left(\frac{\tau_c}{\tau}\right)^{d/2}, \tag{3.7}$$

where τ_c is a correlation time and integer d the magnetic dimension. Integrating, using the method of Richards and Salamon [13], gives us for a two-dimensional system the relaxation function

$$\phi(t) = \exp\{-Pt - Qt\ln t\}. \tag{3.8}$$

In 2-d systems the contribution of the Q-term is dominant. It has the following angular dependence:

$$Q \sim (1 - 3\cos^2\theta)^2. \tag{3.9}$$

Now, we are able to predict that the lineshape of the resonance line will be non-Lorentzian except at the magic angle $\theta = \arccos\left(\frac{1}{\sqrt{3}}\right)$, because in that case $Q \approx 0$. A second consequence is the change in the angular dependence of ΔB_{pp}. From the relaxation function one may derive for ΔB_{pp}

$$\Delta B_{pp} = \alpha + \beta(1 - 3\cos^2\theta)^2. \tag{3.10}$$

In contrast to 3-d magnetic behaviour the maximum of the linewidth is perpendicular to the magnetic plane and there is a minimum at the magic angle.

Experimental Evidence for Spin Diffusion Behaviour

As pointed out in the previous section the slow decay of the spin correlations results in an anomalous angular dependence of the linewidth and a non-Lorentzian lineshape of the resonance line. In this section the experimental data of our measurements at 300 K and 9.4 Ghz will be presented [7,8]. One should remember that the a^* axis is perpendicular to the magnetic plane, whereas the b and c-axes are in the magnetic plane. In figure 3.3 the first-derivative EPR linewidth is shown as a function of the orientation of the magnetic field for the three crystallographic planes, together with the results of two calculations. The dashed line gives the second moment of the resonance line, which is proportional to the linewidth in a 3-d magnetic system (compare formula 3.6). There is no agreement with the experimental points. In the second calculation spin diffusion behaviour is also included (solid line). The calculation is based upon the theory of Richards and Salamon [13] and is valid for a pseudo two-dimensional system. It is noteworthy that no fitting parameters are used. The only input data are the exchange parameters in the plane, obtained from susceptibility measurements and the spin structure. In the calculations it was assumed that the spins form a hexagonal lattice, which is true to a good approximation if they are localized at the centers of the biphenyl molecules. It is clear from figure 3.3 that the second calculation agrees nicely with the experimental points. If the delocalisation of the unpaired electron over the molecule is taken into account, the agreement between experiment and theory is even better [7].

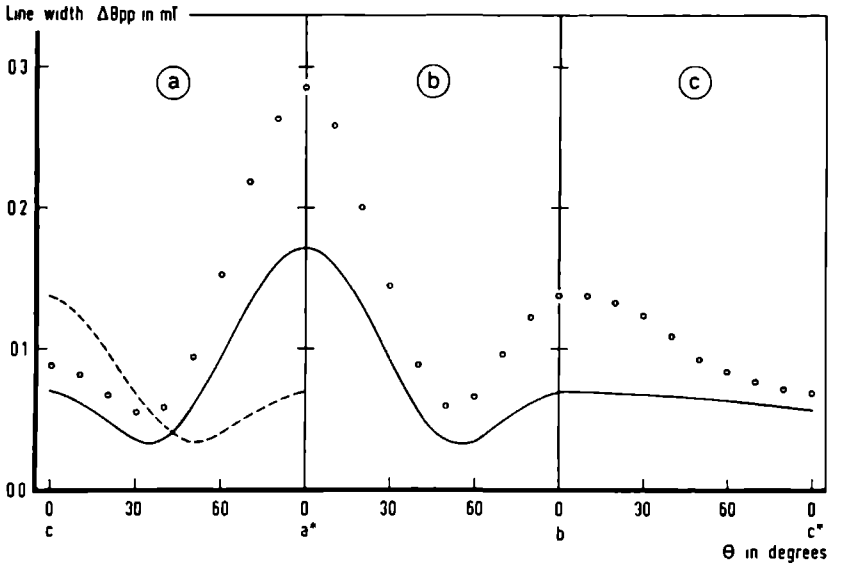

Figure 3.3: Experimental (o) and calculated (—) angular dependence of ΔB_{pp} at 295 K for the three crystallographic planes. The dashed line (- -) gives the second moment of the resonance line on an arbitrary scale.

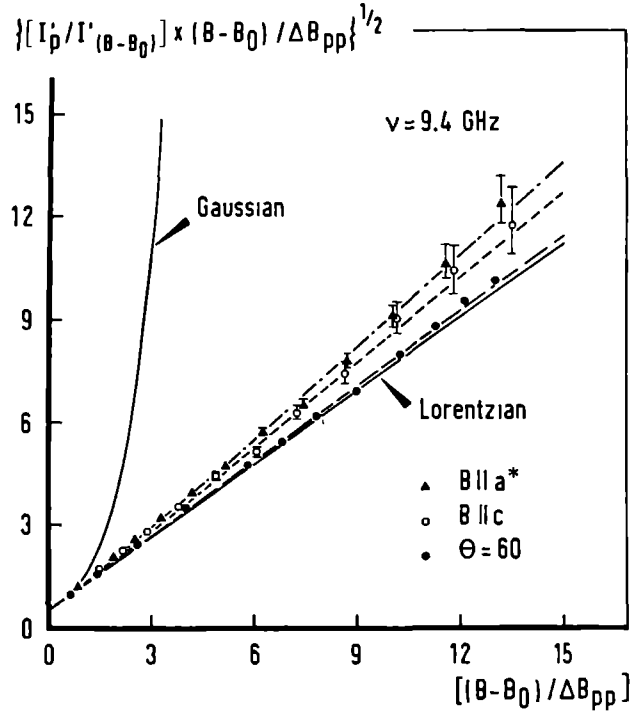

Figure 3.4: Lineshape analysis at 295 K and 9.4 GHz. The calculated lineshapes for different orientations are given by the lines: (— —) for $\theta = 60°$, (- - -) for $\vec{B}//c$ and (- · - · -) for $\vec{B}//a^*$. For $\theta = 54.74°$ the calculated line falls right on top of the Lorentzian line.

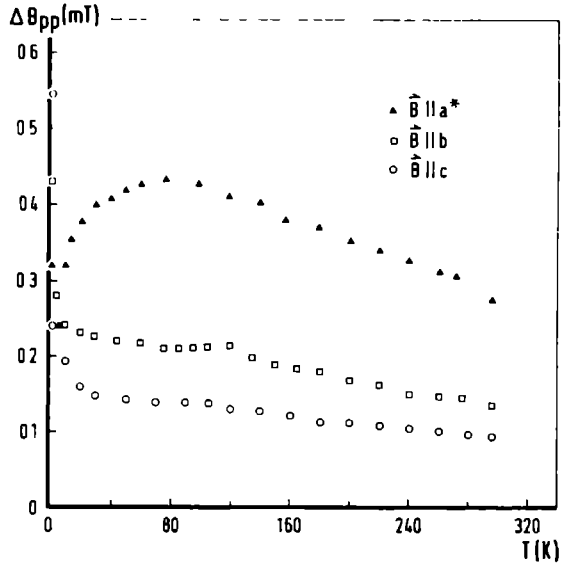

Figure 3.5: Temperature dependence of ΔB_{pp} measured along the a^*, b and c-axes.

In figure 3.4 the results of a lineshape analysis at three angles are presented. It is clear that the lineshape is non-Lorentzian except at the magic angle. So, both predicted consequences of the slow decay of the spin correlation functions are present and they clearly show the pseudo two-dimensional character of NaBp.2Tg.

Temperature Dependence of the EPR Resonance Line

Next to the EPR experiments at room temperature, we also measured the EPR resonance line as a function of the temperature [9]. In figure 3.5 the temperature dependence of ΔB_{pp} along the three crystallographic axes is shown. Figure 3.6 is an expanded version showing the same data below 4 K. The angular dependence of ΔB_{pp} in the a^*c plane at 295, 77 and 1.23 K is plotted in figure 3.7. These data reveal some important new facts. First of all we notice that upon lowering the temperature from 300 to about 80 K the spin diffusion effects become more pronounced. At room temperature the angular dependence may be represented as $\Delta B_{pp} = \alpha + \beta(3\cos^2\theta - 1)^2$ with $\alpha = 0.064$ and $\beta = 0.050$ mT. At 77 K we find $\alpha = 0.079$ and $\beta = 0.092$ mT. This clearly shows an increased importance of slow decaying $q \approx 0$ modes. The same conclusion could be drawn from a lineshape analysis, showing greater deviations from the Lorentzian lineshape at 77 K than at 300 K [9]. The more pronounced two-dimensional character upon lowering the temperature is typical of a ferromagnetically coupled system as has been pointed out by Richards [4]. In the case of a ferromagnetic coupling between the spins, the $q \approx 0$ modes grow in strength as the temperature is lowered, which in turn will be reflected as enhanced two-dimensional anomalies.

Below 80 K the linewidth starts to decrease. Following Richards again, this points

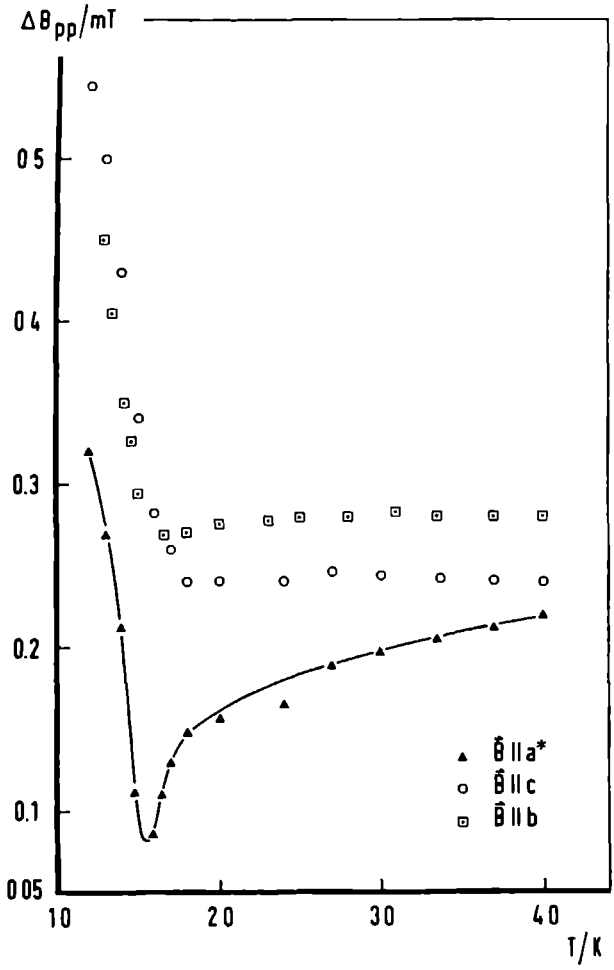

Figure 3.6: Temperature dependence of ΔB_{pp} along the a^*, b and c-axes below 4 K, showing rapid change at 1.5 K.

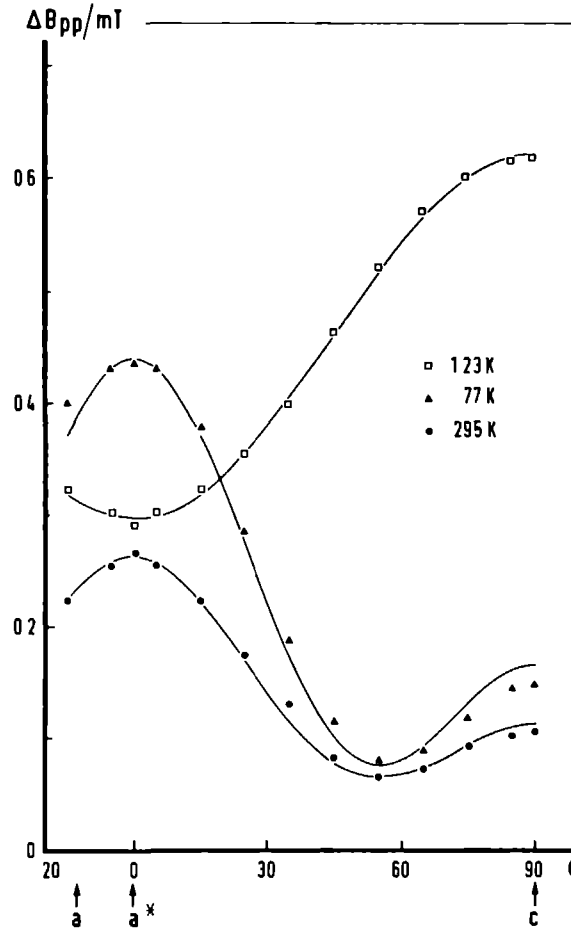

Figure 3.7: Angular dependence of ΔB_{pp} at 295, 77 and 1.23 K. The solid lines are least-squares fits (see text).

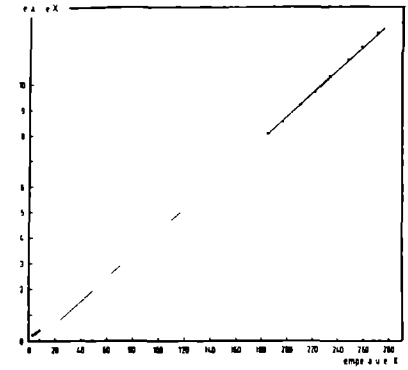

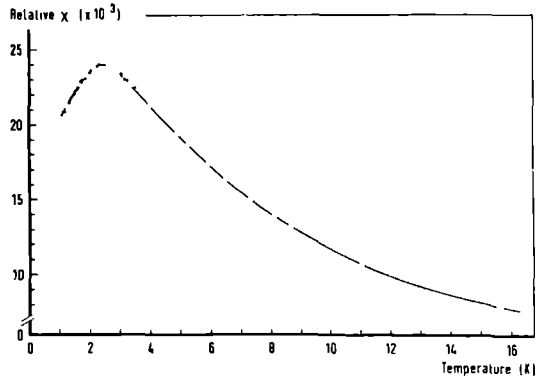

Figure 3 8 (a) Relative χ^{-1} *versus* T and (b) χ *versus* T for a powder sample

to the presence of antiferromagnetic couplings between the spins The effects of spin diffusion remain present until about liquid helium temperature The puzzling fact that the dominant coupling is ferromagnetic above that temperature will be discussed in connection with the magnetic susceptibility measurements

In figure 3 6 we observe a clear minimum at 1 5 K Below this temperature the linewidth increases rapidly This minimum is interpreted as resulting from a cross-over from two dimensional to three-dimensional behaviour Linewidth measurements [9] in the three crystallographic planes show that at 1 23 K the c-axis is the unique axis, compared with a^*-axis uniqueness at higher temperatures Moreover, the resonance line is Lorentzian at all orientations and its position is shifted due to the presence of an internal field which is a result of increased order These results will be discussed in terms of the antiferromagnetic resonance theory [14]

Susceptibility and Magnetization Measurements

The results of the magnetic susceptibility measurements on a powder sample are presented in figure 3.8a [7]. After correction for diamagnetic contributions we obtain a positive Weiss-temperature of 6.9 K. Using molecular field theory, with 6 nearest-neighbours, we obtain a ferromagnetic nearest-neighbour exchange parameter J_{intra}/k of 2.3 K. Below about 100 K the susceptibility deviates from the Curie-Weiss law. The low-temperature data are plotted in figure 3.8b [9]. A broad maximum is observed at 2.4 K indicating an antiferromagnetic coupling of the spins. Now one is faced with the problem that both the EPR and susceptibility measurements suggest a ferromagnetic coupling above 100 K and an antiferromagnetic coupling below that temperature. It is tempting to conclude that the magnetically-ordered state consists of ferromagnetically-coupled planes, which are mutually coupled by a small antiferromagnetic interplane exchange interaction J_{inter} with $|J_{inter}| \ll J_{intra}$. This kind of magnetic structure is well known and occurs for example in tanol suberate [15]. However, magnetization measurements at 4.2 K up to 4 T show a linear increase of the magnetization, whereas the same measurements at 1.1 K show an increase somewhat stronger than linear with the field. The latter behaviour is characteristic for systems with strong antiferromagnetic interactions. However, this is in contradiction with the assumption $|J_{inter}| \ll J_{intra}$ which is a necessity for the presence of pseudo two-dimensional behaviour.

Another explanation might be that the effective exchange parameter will change sign when the temperature and consequently the distances and average orientations of the biphenyl anions are changed. A consequence of this assumption would be that at some intermediate temperature one of the exchange constants would be zero and therefore a different angular dependence of the linewidth should be observed.

The most reasonable explanation at the moment is that in the magnetic plane several exchange constants are present. It is well known that the exchange parameter J depends critically on the distance between and the orientations of the magnetic ions. In the magnetic plane two completely different types of orientations can be distinguished. We assume that one of the types has a positive exchange coupling parameter whereas the other one has a negative exchange interaction. The susceptibility results at high temperatures are a function of the average of these constants which is positive. At lower temperatures an antiferromagnetic structure evolves because of the presence of the negative exchange constant. This assumption is also in agreement with the behaviour of the EPR linewidth: at $T \geq 80$ K the ferromagnetic interactions are dominant and so the $q \approx 0$ modes increase; below 80 K the antiferromagnetic couplings become dominant, resulting in a decrease of the $q \approx 0$ modes.

Results of Pulse-EPR

All results presented up to now are from CW-EPR experiments, sampling the frequency domain A more direct way to get information about the decay of the relaxation function $\phi(t)$ is to perform time-domain measurements. In principle this can be done by pulse-EPR [16,17]. Therefore, we did some pulse experiments at 10 K on a single crystal of NaBp.2Tg at an arbitrary orientation. In figure 3.9 the free induction decay (FID) observed after a 20 ns, $\pi/2$ pulse is shown. In contrast to NMR, observing a FID in

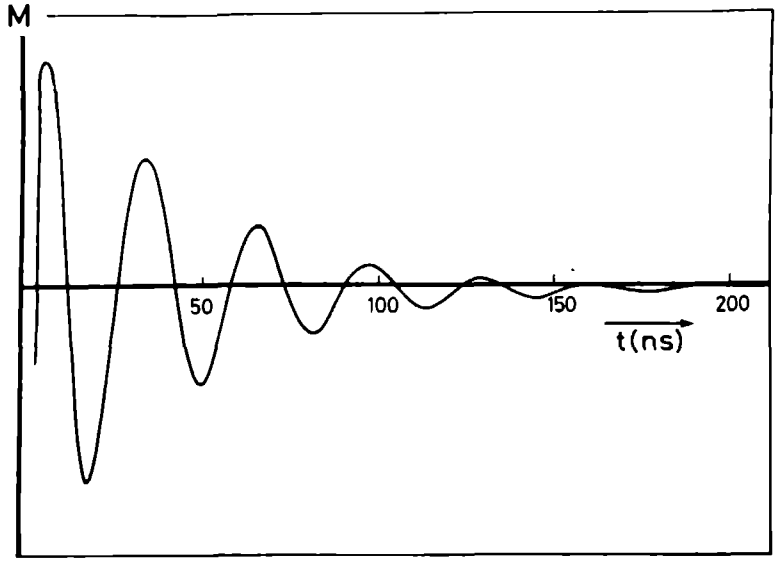

Figure 3.9: The observed FID after a 20 ns $\pi/2$ pulse showing the magnetization (M) as a function of time.

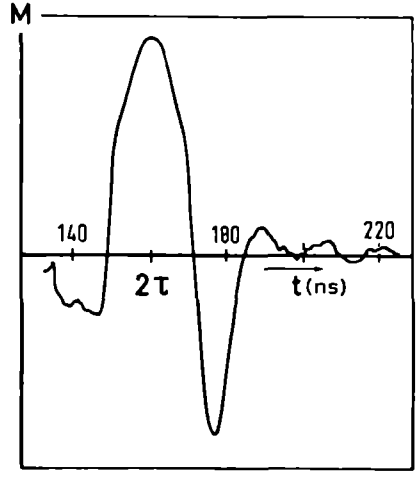

Figure 3.10: The magnetization as a function of the time after the second pulse for a two-pulse sequence (τ = 150 ns, $\pi/2$ = 20 ns) showing a mixture of a FID and an echo.

EPR is a rare event. This is a result of the long dead-time (100 ns. in our experiments), which is needed to protect the detector. The oscillations in the FID are a consequence of the magnetic field being slightly off-resonance. Fitting the FID to an exponential decay provides us with the spin-spin relaxation time $T_2 = 41$ ns. Converting this value to the field/frequency domain gives us $\Delta B_{pp} = 1.6$ Gauss. This value lies nicely in the range of values for ΔB_{pp} obtained with CW-EPR: $1.0 < \Delta B_{pp} < 3.0$. It is clear that we observe a FID, not because of slow relaxation, but because of the extremely strong signal of the pure magnetic system NaBp.2Tg, so that the FID can be observed for a relatively long time.

In a pure magnetic system the resonance line is a result of a cooperative phenomenon. Therefore, it is a homogeneously broadened line. This also appears from the calculations where one computes the total experimentally observed linewidth correctly. Consequently one expects no echo from a $\pi/2 - \tau - \pi - \tau$ pulse experiment, because a requirement for an echo is an inhomogeneously broadened resonance line. This was also observed experimentally. However, if there is no inhomogeneous broadening in the system itself we may create inhomogeneties by adding a strong magnetic field gradient. In figure 3.10 the result is presented of a two-pulse sequence in combination with a magnetic field gradient of about 150 Gauss/cm. The signal shown consists of a mixture of an echo and a FID. The distance between the signal and the first pulse was 2τ. Moreover, the signal changed completely upon removal of the first pulse.

Finally we performed a $\pi - \tau - \pi/2$ experiment and measured the intensity of the FID as a function of τ. This gives an estimate of the spin-lattice relaxation time T_1. We found $T_1 \approx 100$ ns.

In conclusion we can say that pulse-EPR is in principle a useful technique because the relaxation function $\phi(t)$ is measured directly. In practice it is only suitable for pure systems with long relaxation times, or, equivalently, an extremely sharp resonance line must be observed in CW-EPR. In the case of NaBp.2Tg this condition is not fulfilled. Nice examples of this are the fluoranthenyl cation salts investigated by Sigg et al. [16] and Maresch et al. [17].

Acknowledgment

Part of this work was carried out under the auspices of the Netherlands Foundation of Chemical Research (SON) and with the aid of of the Netherlands Organization for the Advancement of Pure Research (ZWO).

3.4 The Magnetic Intra-Layer Structure in NaBp.2Tg

In the last two sections we analyzed the dynamic magnetic properties of NaBp 2Tg as monitored by cw-EPR From the results of the angular dependence of the EPR-linewidth and lineshape we were able to conclude that NaBp 2Tg is a pseudo two dimensional magnetic system This confirmed the expectations we had on the basis of the crystal structure In these sections we also discussed the temperature dependence of the susceptibility and EPR resonance linewidth The susceptibility data above 80 K yield, after correction for diamagnetic contributions, a positive Weiss-temperature of 6 9 K Using molecular field theory with 6 nearest neighbours, one obtains a ferromagnetic nearest neighbour exchange constant of 2 3 K However, below approximately 80 K the susceptibility starts to deviate from the Curie-Weiss law The low-temperature data show a broad maximum at 2 4 K This maximum is the result of one or more antiferromagnetic couplings between the spins The temperature dependence of the EPR resonance linewidth was found to agree with these results Above 80 K the linewidth increases, indicating a ferromagnetic exchange interaction, whereas below that temperature it starts to decrease This decrease points towards the presence of antiferromagnetic couplings We explained these results by assuming that several exchange coupling constants are present in the magnetic plane It is well known that the exchange constant strongly depends on the distance and relative orientations of the magnetic ions In the magnetic plane one can distinguish three different pairs of biphenyl anions (compare figure 3 11)

We supposed that one or two of these pairs are coupled by a ferromagnetic interaction, whereas the other one or two have a negative, antiferromagnetic exchange coupling The susceptibility results at high temperatures are a function of the average of these parameters, which is positive At lower temperatures an antiferromagnetic structure evolves because of the presence of the negative exchange constant By assuming that several exchange constants are present in the magnetic plane and that at least one of them is ferromagnetic and that at least one of them is antiferromagnetic one is able to explain the experimental observations In this section we will focus our attention on the static magnetic properties of NaBp 2Tg and especially on the exchange interactions in the paramagnetic layer of biphenyl anions We will analyze the results of the susceptibility measurements by means of a mean field model As a result of this analysis we will propose a magnetic structure for the exchange coupled layers in NaBp 2Tg

EPR Resonance Field Shifts

The position of the EPR resonance field line is almost independent upon the temperature above 4 K It shows only minor variations due to the $\overline{\overline{\mathbf{g}}}$-anisotropy However, below 4 K the resonance position shows appreciable shifts upon cooling The measured shift along the three crystallographic axes at X-band frequency is shown in figure 3 12 If the external magnetic field B_0 is oriented along the a^* or b-axes the resonance position shows an upfield shift, whereas it shows an downfield shift for B_0 parallel to the c axis The origin of this shift in concentrated magnetic systems has been attributed to the increase of short range order in the spin system [18] For a Heisenberg linear chain antiferro

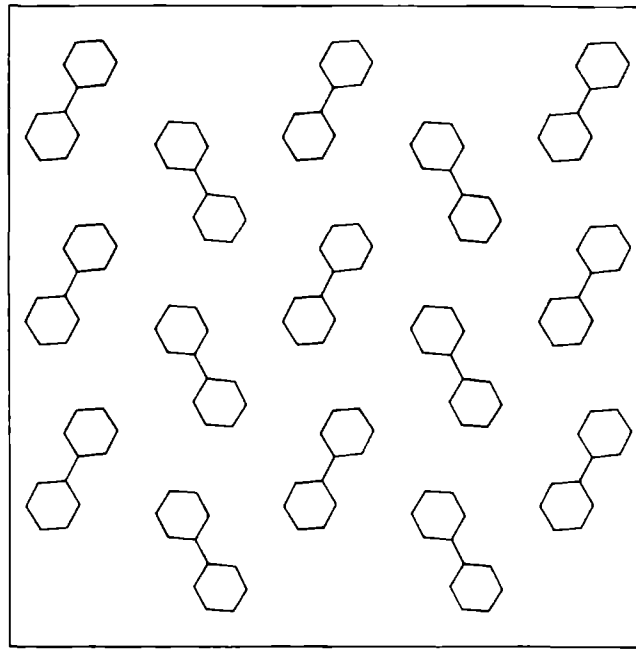

Figure 3.11. The arrangement of the biphenyl anions in the magnetic plane.

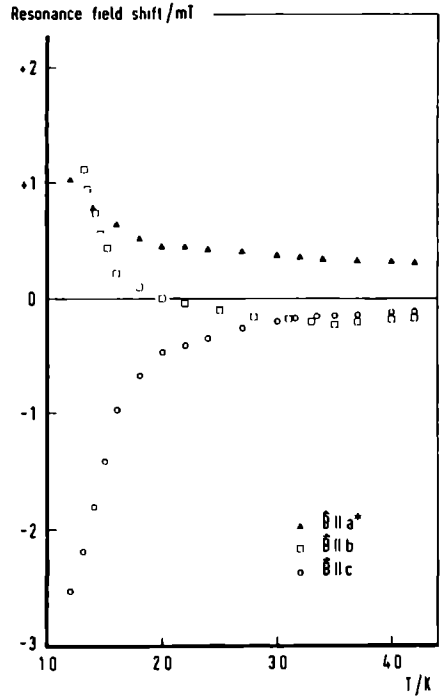

Figure 3.12: EPR-Resonance field shift

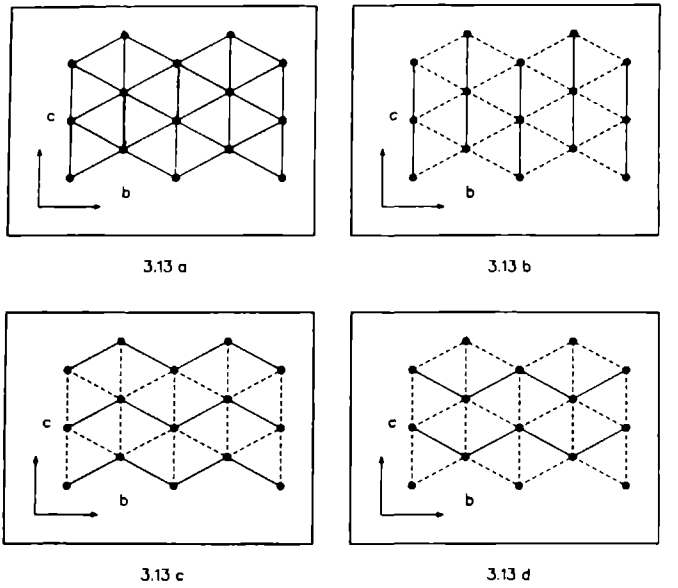

Figure 3.13: Four possible spin structures in the magnetic plane. a: All couplings ferromagnetic. b: Ferromagnetic couplings parallel to the c-axis. c,d: Ferromagnetic couplings parallel to the b-axis.

magnet one can calculate this resonance field shift, but for two-dimensional magnetic systems like NaBp.2Tg this calculation is difficult. Therefore, we will restrict ourselves to a qualitative analysis. Following the analysis Takizawa has given for the di-p-anisyl nitric oxide (DANO) crystal [19] the downfield shift along the c-axis suggests that this is the spin-hard axis, whereas the upfield shifts along the a^* and b-axes suggest that these axes are spin-easy axes. As mentioned above, the resonance field shift is caused by dipolar interaction among short range ordered spins. We calculated the influence of this interaction on the spin energy for four different spin structures. These spin structures are presented in figure 3.13. The ferromagnetic interactions are denoted by solid lines, whereas the antiferromagnetic interactions are indicated by dotted lines. In the calculations we assumed that the electron spins are oriented parallel or antiparallel to the external magnetic field. All spin-spin interactions within a distance of 40Å from a particular electron spin were taken into account. The results are listed in table 3.2. If all biphenyl anions are coupled by a ferromagnetic interaction (fig. 3.13a) the a^*-axis becomes the spin-hard axis. In the case that the spin system consists of antiferromagnetically coupled chains of ferromagnetically coupled spins parallel to the c-axis (fig. 3.13b) the b-axis becomes the spin-hard axis. If we finally assume that the chains of ferromagnetically coupled spins lie parallel to the b-axis (fig. 3.13c and 3.13d) we find the spin-hard axis in the direction of the c-axis. In the last case there are two possible arrangements; the difference between these arrangements being the slightly different distances between the biphenyl anion pairs. If we compare the results of the calculations with the experimental

		Direction B_0		
		$//a^*$	$//b$	$//c$
Structure 3.13 a	Localized	49.3	-31.7	-18.1
	Delocalized	62.8	-43.8	-19.0
Structure 3.13 b	Localized	-16.0	30.3	-14.3
	Delocalized	-17.6	43.1	-25.5
Structure 3.13 c	Localized	-10.4	-5.6	16.0
	Delocalized	-12.6	-9.2	21.8
Structure 3.13 d	Localized	-6.7	-19.8	26.5
	Delocalized	-15.3	-15.0	30.2

Table 3.2: Energies for four spin arrangements in 10^{-4} cm^{-1}. The energies are calculated by a localized and a delocalized point-dipole approximation.

data we can exclude the structures 3.13a and 3.13b, because the calculated resonance field shifts are different in sign for the external magnetic field along the a^* and b-axes, whereas the experimental resonance field shifts have the same sign along these axes. For the other two spin structures the calculated field shifts along the a^* and b axes are in the same direction. Moreover, the calculations predict for these structures that the c-axis will become the spin-hard axis in agreement with our interpretation of the experimental results. In conclusion, the calculations suggest that positive as well as negative exchange constants are present in the magnetic plane; the positive interactions forming a zig-zag chain parallel to the b-axis. From the above discussed calculations we cannot discriminate between the structures 3.13c and 3.13d.

Temperature dependence of the susceptibility

Now, we have established a spin structure for NaBp.2Tg, we are able to analyze the temperature dependence of its powder susceptibility. In this analysis we will assume that only nearest-neighbour interactions are present. In spite of this simplification the analysis remains difficult. It is severely complicated by the following facts:

- The nearest neighbour interactions are of the Heisenberg type: $\mathcal{H}_{ex} = -2\sum_{i<j} J_{ij}\vec{\mathbf{S}}_i \cdot \vec{\mathbf{S}}_j$.
- The spin lattice is two-dimensional.
- The spin lattice has a hexagonal structure.
- In the spin structure ferromagnetic as well as antiferromagnetic couplings are present.

The removal of one or two of these complicating factors would greatly facilitate the analysis. For example, in the case of a 2-d square planar lattice with only one Heisenberg-type exchange coupling we could have used a high temperature series for the susceptibility [20,21]. As such a specific highly accurate method is not available for our case, we will analyze the results by means of the very general mean field model [22]. In these mean field methods one normally introduces the following simplifications:

1. The infinite spin system is reduced to a finite number of spins.
2. Within this cluster the exchange couplings of the infinite lattice are retained.
3. The spins outside this cluster but linked to spins of this cluster are included by means of effective or internal fields.
4. An extra relation or requirement is used for the determination of these internal fields.

There are a large number of possible effective field models, which differ in so far as the extra relations or requirements are concerned. The following methods are relevant for the discussion of the susceptibility data of NaBp.2Tg[22]:

The Weiss molecular field model

This method is the simplest effective field method : The cluster of spins which are explicitly taken into account is limited to one spin. The neighbouring spins of this central spin are taken into account by an effective field for which one assumes that it is proportional to the magnetization of these neighbouring spins or more precisely, to the expectation value of their spin-moment. The relations are finally closed by the requirement that the expectation value of the central spin is equal to that of the neighbouring ones, in the case of a ferromagnetic exchange coupling. In the situation of an antiferromagnetic coupling one assumes that the total spin structure is composed of a number of sublattices and one uses the same procedure for each of these sublattices. The molecular field model can be described with the following formulas:

$$\mathcal{H}_i = g\mu_B(\vec{\mathbf{B}}_0 + \sum_{j\neq i}\vec{\mathbf{B}}_{eff,ij})\cdot\vec{\mathbf{S}}_i \tag{3.11}$$

$$\vec{\mathbf{B}}_{eff,ij} = -2\frac{J_{ij}\left\langle\vec{\mathbf{S}}_j\right\rangle}{g\mu_B} \tag{3.12}$$

$T > T_c$: Paramagnetic phase

$$\left\langle\vec{\mathbf{S}}_i\right\rangle = \left\langle\vec{\mathbf{S}}_j\right\rangle \tag{3.13}$$

$T < T_c$: Long Range Ordered Phase

$$\left\langle\vec{\mathbf{S}}_i\right\rangle = \pm\left\langle\vec{\mathbf{S}}_j\right\rangle \begin{cases} + & \text{for ferromagnetic couplings} \\ - & \text{for antiferromagnetic couplings} \end{cases} \tag{3.14}$$

This model predicts the presence of a long range ordered state below a certain temperature, the critical temperature T_c, for 3-d as well as 1-d and 2-d Heisenberg systems. This ordered magnetic state is well established for 3-d magnetic systems. However, it can be

proven that 1-d Heisenberg magnets exhibit only short range order at finite temperatures, whereas there is firm evidence that this is also true for 2-d Heisenberg magnets. Moreover, the predicted critical temperatures for 3-d systems is about 50% too high. In spite of these deficiences, the molecular field model is a very useful method for the description of complicated spin systems.

The Oguchi model

This method is an extension of the molecular field model. The cluster of spins which are explicitly taken into account is expanded from one to two spins. The equations which correspond with this model are

$$\begin{aligned}
\mathcal{H}_{12} &= g\mu_B(\vec{\mathbf{B}}_0 + \sum_{j\neq 1,2} \vec{\mathbf{B}}_{eff,1j}) \cdot \vec{\mathbf{S}}_1 \\
&\quad + g\mu_B(\vec{\mathbf{B}}_0 + \sum_{j\neq 1,2} \vec{\mathbf{B}}_{eff,2j}) \cdot \vec{\mathbf{S}}_2 \\
&\quad - 2J_{12}\vec{\mathbf{S}}_1 \cdot \vec{\mathbf{S}}_2 \qquad (3.15) \\
\vec{\mathbf{B}}_{eff,ij} &= -2\frac{J_{ij}\left\langle \vec{\mathbf{S}}_j \right\rangle}{g\mu_B} \qquad (3.16) \\
T > T_c &: \text{Paramagnetic phase} \\
\left\langle \vec{\mathbf{S}}_i \right\rangle &= \left\langle \vec{\mathbf{S}}_j \right\rangle \\
T < T_c &: \text{Long Range Ordered Phase} \\
\left\langle \vec{\mathbf{S}}_i \right\rangle &= \pm \left\langle \vec{\mathbf{S}}_j \right\rangle
\end{aligned}$$

This model predicts a long range ordered magnetic state for the 3-d and 2-d Heisenberg magnets. The predicted critical temperatures are slightly lower than those of the molecular field model. The Oguchi model predicts correctly that there is no stable long-range ordered state for a 1-d Heisenberg magnet. Another improvement of this model with respect to the molecular field model is that short range order can be described. Furthermore, it predicts that the ground state of an antiferromagnet is not completely saturated which is in agreement with experimental observations.

The correlated effective field model

The results of the above mentioned methods can be improved by the correlated effective field method which was developed by Lines [23,24]. In the molecular field and the Oguchi model the spin-spin interaction $\vec{\mathbf{S}}_i \cdot \vec{\mathbf{S}}_j$ between spins which are situated at the boundary of the cluster and spins which are outside the cluster is replaced by an effective field. This effective field is based on a decoupling of this spin-spin interaction according to $\vec{\mathbf{S}}_i \cdot \vec{\mathbf{S}}_j \approx \vec{\mathbf{S}}_i \cdot \left\langle \vec{\mathbf{S}}_j \right\rangle + \left\langle \vec{\mathbf{S}}_i \right\rangle \cdot \vec{\mathbf{S}}_j$. In this way the correlation between the spins is completely neglected which leads to effective fields which are too large. In the correlated effective field model this spin-spin interaction is approximated as $\vec{\mathbf{S}}_i \cdot \{\left\langle \vec{\mathbf{S}}_j \right\rangle - \alpha \left\langle \vec{\mathbf{S}}_i \right\rangle\} + \vec{\mathbf{S}}_j \cdot \{\left\langle \vec{\mathbf{S}}_i \right\rangle - \alpha \left\langle \vec{\mathbf{S}}_j \right\rangle\}$ where α is a correlation parameter. By this approach the correlations between the electron spins are included to some extent. Lines determined the parameter α from a self-consistency relation which was constructed from the static susceptibility [23,24], whereas Suzuki [25] constructed this self-consistency relation from the transverse dynamic susceptibility. Suzuki also showed that this correlation parameter is related to the nearest-neighbour spin correlation for systems in the

paramagnetic phase: $\alpha_{ij} = \left\langle \vec{S}_i \cdot \vec{S}_j \right\rangle / S(S+1)$.

The constant coupling method

Another effective field model is the constant coupling method. This model is due to Kasteleijn and van Kranendonk [26,27,28]. It is based on a comparison of the molecular field and Oguchi model: It requires that the thermal average of the explicitly included spins as calculated by the molecular field method (equation 3.11) and the Oguchi method (equation 3.15) is the same if one uses in both models the same effective fields arising from each of the neighbouring spins which are only implicitly included in the calculations. Consequently there is no longer a linear relationship between the effective field experienced by a spin and the thermal average of its neighbour (compare 3.12 and 3.16). Although there is no well established physical justification for this procedure, it works out very well. It predicts the critical temperature for a 3-d Heisenberg magnet very accurately. The absence of a long range ordered magnetic state in linear and square planar Heisenberg magnets is also predicted correctly. However, it predicts the presence of an ordered magnetic state for a planar hexagonal system, which is in disagreement with the experimental observations. This incorrect result is a consequence from the fact that only two spins are explicitly included in the Oguchi part of this model. If this two spin part is extended to three spins, the constant coupling model predicts the behaviour of a spin system with a hexagonal lattice correctly as well. The following equations are relevant in the constant coupling model:

$$\mathcal{H}_1 = g\mu_B(\vec{B}_0 + \sum_{j\neq 1} \vec{B}_{eff,1j}) \cdot \vec{S}_1 \tag{3.17}$$

$$\mathcal{H}_2 = g\mu_B(\vec{B}_0 + \sum_{j\neq 2} \vec{B}_{eff,2j}) \cdot \vec{S}_2 \tag{3.18}$$

$$\begin{aligned} \mathcal{H}_{12} = {} & g\mu_B(\vec{B}_0 + \sum_{j\neq 1,2} \vec{B}_{eff,1j}) \cdot \vec{S}_1 \\ & + g\mu_B(\vec{B}_0 + \sum_{j\neq 1,2} \vec{B}_{eff,2j}) \cdot \vec{S}_2 \\ & - 2J_{12}\vec{S}_1 \cdot \vec{S}_2 \end{aligned} \tag{3.19}$$

$$\left\langle \vec{S}_i \right\rangle_{\mathcal{H}_i} = \left\langle \vec{S}_i \right\rangle_{\mathcal{H}_{12}} \qquad \text{for} \quad i = 1,2 \tag{3.20}$$

As most other effective field methods the results for an antiferromagnet are not as good as the results for a ferromagnet. At temperatures much below the critical temperature the constant coupling method breaks down for an antiferromagnet: at $T = 0$ there remains no sublattice magnetization.

The effective field method applied to NaBp.2Tg

In our analysis of the powder susceptibility of NaBp.2Tg, we will assume a hexagonal lattice with three different couplings which is in agreement with the spin structure of figure 3.13c and 3.13d. The calculations will be performed on a cluster of three electron spins. The other spins in the lattice will be included by means of an effective field. The exchange paths and the exchange coupling constants between the spins 1,2 and 3 are indicated in figure 3.14. One can characterize the method we used for our calculations

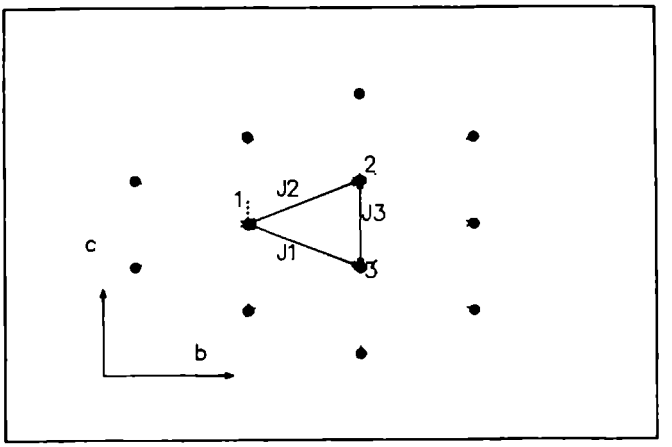

Figure 3 14: Spin cluster used in the effective field method. Solid lines with arrows indicate couplings which are explicitly taken into account Dotted lines indicate the interactions which are included by means of an effective field.

as a constant coupling type calculation based on a correlated effective field method. The computations were performed according to the following procedure.

- We assume that the magnetic layer of biphenyl anions in NaBp 2Tg can be described as a 2-d hexagonal system coupled by three different Heisenberg exchange interactions. One generally assumes that for such 2-d magnetic systems no long range ordering takes place at finite temperatures. Therefore, we assumed that $\langle \vec{S}_1 \rangle = \langle \vec{S}_2 \rangle = \langle \vec{S}_3 \rangle$ at all temperatures (paramagnetic phase).
- As input parameters the three exchange coupling constants J_1, J_2 and J_3 are supplied to the program as well as some reasonable initial values for effective fields.
- The thermal averages for the spins 1,2 and 3 are calculated by the following iterative procedure for a given value of the external magnetic field $\vec{B}_0$.
  - The Hamilton matrix for the three spin cluster is constructed using the effective fields $\vec{B}_{eff,1}$, $\vec{B}_{eff\,2}$ and $\vec{B}_{eff,3}$ and the input parameters for the three exchange couplings J_1, J_2 and J_3 and subsequently diagonalized
  - In the next step the eigenvalues and eigenvectors of the Hamilton-matrix are used for the construction of the density matrix.
  - Using this density matrix the thermal averages $\langle \vec{S}_i \rangle$ and $\langle \vec{S}_i \ \vec{S}_{i'} \rangle$ are computed. Thereupon, the correlation parameters $\alpha_{ii'}$ are calculated according to $\alpha_{ii'} = \langle \vec{S}_i \cdot \vec{S}_{i'} \rangle / S(S+1)$.
  - From the above calculated thermal averages for the spins 1,2 and 3 the corresponding total effective fields $\vec{B}_{total,i} = \sum_{j \neq i} \vec{B}_{eff,ij}$ are calculated on the basis of the spin Hamiltonian given in equation 3 11.

– From these total effective fields $\vec{\mathbf{B}}_{total,i}$ the effective fields $\vec{\mathbf{B}}_{eff,1}$, $\vec{\mathbf{B}}_{eff,2}$ and $\vec{\mathbf{B}}_{eff,3}$ of the spins 1,2 and 3 of the three spin cluster are calculated according to the following partition scheme:

$$\vec{\mathbf{B}}_{eff,1} = \frac{J_1(1-\alpha_{12}) + J_2(1-\alpha_{13}) + 2J_3(1-\alpha_{23})}{2J_1(1-\alpha_{12}) + 2J_2(1-\alpha_{13}) + 2J_3(1-\alpha_{23})}\vec{\mathbf{B}}_{total,1} \tag{3.21}$$

$$\vec{\mathbf{B}}_{eff,2} = \frac{J_1(1-\alpha_{12}) + 2J_2(1-\alpha_{13}) + J_3(1-\alpha_{23})}{2J_1(1-\alpha_{12}) + 2J_2(1-\alpha_{13}) + 2J_3(1-\alpha_{23})}\vec{\mathbf{B}}_{total,2} \tag{3.22}$$

$$\vec{\mathbf{B}}_{eff,3} = \frac{2J_1(1-\alpha_{12}) + J_2(1-\alpha_{13}) + J_3(1-\alpha_{23})}{2J_1(1-\alpha_{12}) + 2J_2(1-\alpha_{13}) + 2J_3(1-\alpha_{23})}\vec{\mathbf{B}}_{total,3} \tag{3.23}$$

In the case that $J_1 = J_2 = J_3$ one finds $\vec{\mathbf{B}}_{eff,i} = \frac{2}{3}\vec{\mathbf{B}}_{total,i}$ which is in agreement with the assumed model.

This procedure is repeated until convergence is reached for the values of $\vec{\mathbf{B}}_{eff,i}$.

- Then the magnetization is calculated by means of the relation

$$\vec{\mathbf{M}}_B = -\mu_B \sum_i \bar{\bar{\mathbf{g}}} \left\langle \vec{\mathbf{S}}_i \right\rangle . \tag{3.24}$$

- Finally the susceptibility is calculated according to

$$\chi = \frac{\vec{\mathbf{M}}_B - \vec{\mathbf{M}}_{B=0}}{B}. \tag{3.25}$$

By means of this procedure we calculated the powder susceptibility of NaBp.2Tg for a number of temperatures between 11 and 260 K. By a systematic variation of the exchange coupling constants we fitted the calculated susceptibility to the experimental values. The best agreement was reached for $J_1 = 13.8$ K, $J_2 = 0$ K and $J_3 = -6.9$ K. A picture of the fit is shown in figure 3.15. We observe that the agreement between the experimental data and calculated results is very satisfying.

Discussion

The calculated values for the exchange constants J_1, J_2 and J_3 should be considered with care: They are, of course dependent on the specific assumptions made and on the effective field model used. If we had been able to include the experimental susceptibility data in the temperature region from 1.2 to 11 K the reliability of the calculations would be improved. However, this is impossible because the model predicts long range order at about 10 K in contrast with the experimental observations. This unphysical behaviour is a consequence of the presence of antiferromagnetic interactions in the spin system under study. Nevertheless, we believe that the results from the preceding analysis are qualitatively correct. The calculations of the exchange constants for the different biphenyl anion pairs (see chapter 7) showed that the exchange coupling between the spins 2 and 3 is antiferromagnetic, whereas the coupling between the spins 1 and 2 exhibits the most ferromagnetic character. This picture is in line with the calculated values for J_1, J_2 and J_3 derived from the susceptibility data. Therefore, we conclude that the paramagnetic layer in NaBp.2Tg consists of zig-zag chains of ferromagnetically coupled spins along the *b*-axis, which are mutually coupled to each other in an antiferromagnetic fashion.

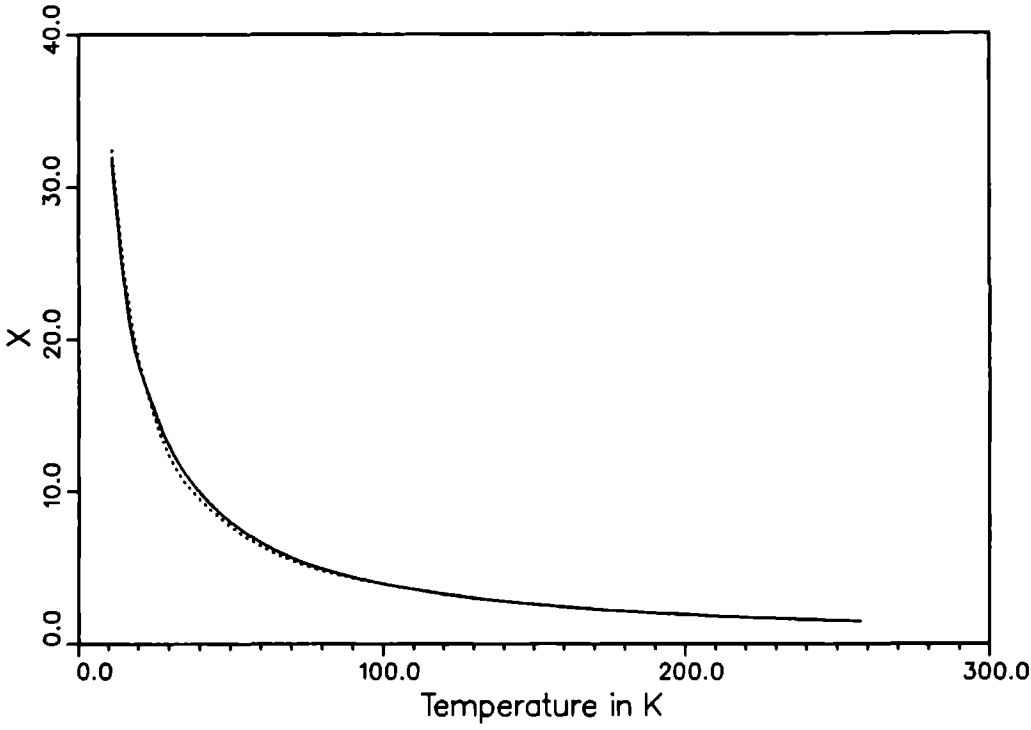

Figure 3.15: Experimental and calculated powder susceptibility in the temperature range of 11 to 260 K for $J_1 = 13.8$ K,$J_2 = 0$ K and $J_3 = -6.9$ K.

Bibliography

[1] G.W. Canters, A.A.K. Klaassen, and E. de Boer.
Journal of Physical Chemistry, 74:3299, 1970.

[2] J.H.Noordik, J. Schreurs, R.O. Gould, J.J. Mooij, and E. de Boer.
Journal of Physical Chemistry, 82:1105, 1978.

[3] E.J. Reijerse.
Electron Spin Echo Spectroscopy on Transition Metal Compounds.
PhD thesis, University of Nijmegen, 1986.

[4] P.M. Richards.
Magnetic resonance in one and two-dimensional systems.
In K.A. Muller and A. Rigamonti, editors, *Local Properties at Phase Transitions*, page 539, North-Holland (Amsterdam), 1976.

[5] J.H. Noordik, P.T. Beurskens, Th.E.M. van den Hark, and J.M.M. Smits.
Acta Crystallographica B, 35:621, 1979.

[6] E. de Boer and M.C.M. Gribnau.
Preprints, Division of Petroleum Chemistry, American Chemical Society, 31:769, 1986.

[7] O. Takizawa, R. Srinivasan, and E.de Boer.
Molecular Physics, 44:677, 1981.

[8] R. Murugesan and E. de Boer.
Chemical Physics Letters, 95:301, 1983.

[9] M.C.M. Gribnau, R. Murugesan, H. van Kempen, and E. de Boer
Molecular Physics, 52:195, 1984.

[10] R. Kubo and K. Tomita.
Journal of the Physical Society of Japan, 9:888, 1954.

[11] J.H. van Vleck.
Physical Review, 74:1168, 1948.

[12] K.T. McGregor and Z.G. Soos.
Journal of Chemical Physics, 64:2506, 1976.

[13] P.M. Richards and M.B. Salamon.
Physical Review B, 9:32, 1974.

[14] M.C.M. Gribnau and E. de Boer.
Chemical Physics Letters, to be published.

[15] A. Benoit, J. Flouquet, B. Gillon, and J. Schweizer.
Journal of Magnetism and Magnetic Materials, 31-34:1155, 1983.

[16] J. Sigg, Th. Prisner, H. Brunner, D. Schweitzer, and K.H. Hausser.
Physical Review B, 27:5366, 1983.

[17] G.G. Maresch, M. Mehring, J.U. von Schutz, and H.C. Wolf.
Chemical Physics, 85:333, 1985.

[18] K. Nagata and Y. Tazuke.
Journal of the Physical Society of Japan, 32:337, 1972.

[19] O. Takizawa.
Bulletin of the Chemical Society of Japan, 49:583, 1976.

[20] G.S. Rushbrooke and P.J. Wood.
Molecular Physics, 1:257, 1958.

[21] G.A. Baker, H.E. Gilbert. J. Eve, and G.S. Rushbrooke.
Physics Letters, 25A:207, 1967.

[22] J.S. Smart.
Effective Field Theories of Magnetism.
Studies in Physics and Chemistry, W.B.Saunders Company (Philadelphia), 1950.

[23] M.E. Lines.
Physical Review B, 9:3927, 1974.

[24] M.E. Lines and M. Eibschütz.
Physical Review B, 11:4583, 1975.

[25] N. Suzuki.
Journal of the Physical Society of Japan, 45:1791, 1978.

[26] P.W. Kasteleijn and J. van Kranendonk.
Physica, 22:317, 1956.

[27] P.W. Kasteleijn and J. van Kranendonk.
Physica, 22:367, 1956.

[28] P.W. Kasteleijn and J. van Kranendonk.
Physica, 22:387, 1956.

Chapter 4

Magnetic Properties of RbBp.2Ttg

4.1 Introduction

Bis(tetraglyme)rubidiumbiphenyl (RbBp.2Ttg) is the second member of the family of alkali-biphenyl ion pairs which will be discussed in this thesis. The structure of this compound consists of solvent separated ion pairs on the analogy of the structure of NaBp.2Tg. However, the Rb^+-cation does not fit into the cage formed by the eight oxygen atoms of two triglyme ether molecules, because it has a larger ionic radius than the Na^--cation, [1]. In order to form a stable Rb^+ glyme cluster one has to complex Rb^+ with two tetraglyme molecules. In the resulting cluster the Rb^+ cation is coordinated to the ten oxygen atoms of the complexing ether molecules. The first single crystals of RbBp.2Ttg were prepared by de Boer and coworkers in 1970 [2] and their crystal structure was solved by Noordik et al. in 1976 [3]. They are monoclinic and belong to the spacegroup $C2/c$ with eight biphenyl anions in the unit cell. The principal crystal data are listed in table 4.1. The phenyl rings in the biphenyl anions are planar within experimental error, but the two rings have a dihedral angle of 9.4°. This dihedral angle can be contrasted with an angle of 0° in the neutral biphenyl molecule in the crystalline state. It can be explained on the basis of the increased bond order of the central C–C bond in the biphenyl anion [3]. As a result of this increased bond order the central C–C bond is shortened which results in an increase of the ortho hydrogen repulsion and a change of the dihedral angle. In figure 4.1 a picture of the crystal structure is presented. From this picture it is very clear that RbBp.2Ttg has a layered structure:

$C_{32}H_{54}O_{10}Rb$	Monoclinic, C2/c
a = 30.68(3) Å	Z = 8
b = 9.79(1) Å	d_x = 1.31 Mg m^{-3}
c = 23.71(2) Å	M_r = 684.5
β = 103.34(6)°	(cell dimensions at 150 K)
V = 6909 Å^3	

Table 4.1: Crystal data of RbBp.2Ttg.

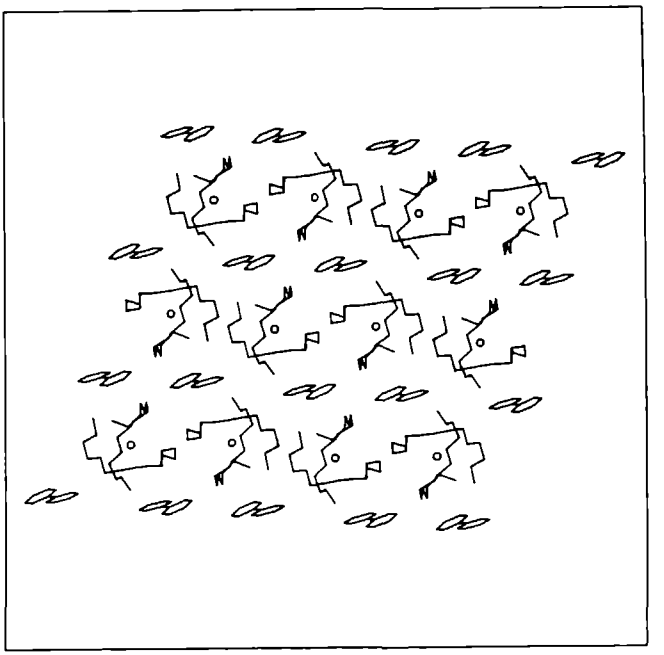

Figure 4.1: Projection of RbBp.2Ttg on the $n, a + c$ plane.

paramagnetic layers consisting of biphenyl anions are separated by diamagnetic layers of $(Rb.2Ttg)^+$ clusters. These layers are oriented parallel to the $b, a + c$ plane. The normal to this plane will be indicated by the vector $\vec{\mathbf{n}}(= \vec{\mathbf{b}} \times (\vec{\mathbf{a}} + \vec{\mathbf{c}}))$. The distance between the paramagnetic layers amounts to approximately 11 Å. This distance is much larger than the shortest intermolecular C C distance which equals 3.3 Å. Therefore, one expects that RbBp.2Ttg behaves as a pseudo two-dimensional magnet just like NaBp.2Tg. However, RbBp.2Ttg and NaBp.2Tg show significant differences as regards the structure of the paramagnetic layer: the arrangement of the biphenyl anions in these crystals is shown in figure 4.2. In NaBp.2Tg the distances between one anion and its six nearest neighbours are approximately the same (see figure 3.11), but in RbBp.2Ttg the nearest neighbour is located at 7.5 Å, whereas the next nearest neighbour is situated at a distance of 9.8 Å. This suggests that the paramagnetic layer in RbBp.2Ttg is constructed from exchange coupled biphenyl anion pairs. With this picture in mind we are able to understand the results of the susceptibility measurements on a RbBp.2Ttg powder carried out by Mooij [3]. He showed that the temperature dependence of the powder susceptibility of RbBp.2Ttg can be described with the singlet–triplet model using an exchange parameter $J_{ex} = -13$ K. This result confirms the above mentioned idea of a paramagnetic layer consisting of strongly exchange coupled anions, which are mutually coupled by weaker exchange interactions. In the present chapter we will discuss the magnetic properties of RbBp.2Ttg as probed by EPR and compare these results with those of NaBp.2Tg.

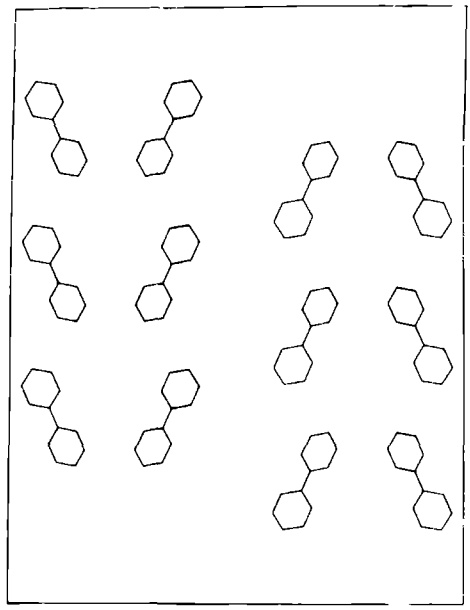

Figure 4.2: The arrangement of the biphenyl anions in RbBp.2Ttg.

4.2 Two-Dimensional Magnetism

Because of the layered structure of RbBp.2Ttg we expected that this concentrated spin system would behave as a pseudo two-dimensional magnetic system. The dynamic magnetic properties of such pure paramagnets can be fruitfully monitored by EPR: from the orientational dependence of the resonance linewidth and lineshape one can establish the magnetic dimension of these systems. Thus, we studied the EPR-resonance line of RbBp.2Ttg at 293 and 77 K in the X-band frequency regime. At both temperatures one single exchange-narrowed resonance line is observed. The orientational dependence of the first-derivative peak-peak linewidth of this resonance line for three orthogonal planes at 77 K is presented in figure 4.3. We observe that the linewidth exhibits a maximum if the magnetic field is perpendicular to the magnetic plane which is in agreement with the theoretical predictions made in chapter 2 for a magnetic 2-d system. The structure of the magnetic layer of RbBp.2Ttg has in zero order approximation a hexagonal symmetry, just like NaBp.2Tg, as may be seen in figure 4.2, but the deviations from this idealized structure are, however, much larger than in NaBp.2Tg [4]. For a planar hexagonal structure with magnetic interactions in three dimensions , one expects for the case that $\omega_{ex} > \omega_0$ that the angular dependence of the linewidth is proportional to the sum of the secular and non-secular contributions of the second moment:

$$\Delta B_{pp} = \sqrt{\frac{2\pi}{3}} \left\{ \frac{M_2^{(0)} + M_2^{(1)} + M_2^{(2)}}{\gamma \omega_{ex}} \right\}. \tag{4.1}$$

This results in the following angular dependence of the resonance linewidth:

$$\Delta B_{pp} = \sqrt{\frac{2\pi}{3}} \left\{ \frac{c_0(3\cos^2\theta - 1)^2 + c_1 \sin^2\theta \cos^2\theta + c_2 \sin^4\theta}{\gamma\omega_{ex}} \right\}. \quad (4.2)$$

where

$$c_0 = \frac{3}{16}\gamma^4\hbar^2 S(S+1)\sum_j r_{ij}^{-6}$$

$$c_1 = \frac{21}{4}\gamma^4\hbar^2 S(S+1)\sum_j r_{ij}^{-6}$$

and

$$c_2 = \frac{15}{8}\gamma^4\hbar^2 S(S+1)\sum_j r_{ij}^{-6}. \quad (4.3)$$

The angle θ in this relation is the angle between the normal to the magnetic plane ($\vec{\mathbf{n}}$ for RbBp.2Ttg and $\vec{\mathbf{a}}^*$ for NaBp.2Tg) and the direction of the external magnetic field. If, however, the magnetic interactions are limited to one or two dimensions one no longer can use the above equation for the description of the angular dependence of the linewidth because the effects of spin diffusion become manifest. Richards and Salamon [5] have shown that in 2-d magnetic systems the presence of spin diffusion results in a slow decay of the dipolar correlation function by which the contribution of the secular term is enhanced. This can be written as

$$\Delta B_{pp} = \sqrt{\frac{2\pi}{3}} \left\{ \frac{\rho(\theta)\ M_2^{(0)} + M_2^{(1)} + M_2^{(2)}}{\gamma\omega_{ex}} \right\} \quad (4.4)$$

where $\rho(\theta)$ is the angular dependent enhancement factor. The extra contribution to the secular term has an angular dependence of $(3\cos^2\theta - 1)^2$. As the angular dependence of the linewidth is dominated by this extra contribution due to the spin diffusion mechanism one can describe the orientational dependence of the linewidth with the relation of Richards and Salamon [5,6]

$$\Delta B_{pp} = \alpha + \beta(3\cos^2\theta - 1)^2 \quad (4.5)$$

However, a more precise representation of the angular dependence would be

$$\Delta B_{pp} = m_0(3\cos^2\theta - 1)^2 + m_1 \sin^2\theta\cos^2\theta + m_2 \sin^4\theta \quad (4.6)$$

as can be seen from equation 4.2. The ratio of the parameters m_0, m_1 and m_2 equals 3:84:30 for a 3-d magnetic system. In low-dimensional systems the parameter m_0 should be enhanced. We fitted the two sets of experimental linewidth data to the equation 4.5 and 4.6. The optimized values for α and β as well as the optimized values for m_0, m_1 and m_2 are listed in table 4.2. The corresponding data for NaBp.2Tg are given in table 4.3 for reasons of comparison [4,7]. The values of both sets of parameters clearly show that the contribution of the $(3\cos^2\theta - 1)^2$ term is enhanced. This confirms our expectations that the magnetic interactions in RbBp.2Ttg are limited to the magnetic plane. The linewidth for the case that the magnetic field is perpendicular to the magnetic plane increases by about 10% upon lowering the temperature from 293 K to 77 K. This effect

plane	T	α	β	m_0	m_1	m_2
nb	293	0.106	0.090	0.116	0.176	0.123
nb	77	0.110	0.115	0.129	0.175	0.129
$n(a+c)$	293	0.120	0.084	0.114	0.361	0.097
$n(a+c)$	77	0.136	0.094	0.128	0.495	0.077

Table 4.2: Experimental linewidth parameters for RbBp.2Ttg. Temperatures in Kelvin, the linewidth parameters in mT.

plane	T	α	β	m_0	m_1	m_2
a^*b	293	-	-	-	-	-
a^*b	77	0.116	0.081	0.111	0.232	0.113
a^*c	293	0.064	0.050	0.065	0.225	0.039
a^*c	77	0.080	0.091	0.110	0.315	0.035

Table 4.3: Experimental linewidth parameters for NaBp.2Tg. Temperatures in K, the linewidth parameters in mT.

is reflected in increased values of the β and m_0 at 77 K as compared to their values at 293 K (see table 4.2). This temperature effect is, however, much smaller than in NaBp.2Tg where the linewidth increased by about 50% in this temperature range [7]. The small increase of the linewidth points to the presence of weak ferromagnetic interactions in the magnetic layer of RbBp.2Ttg.

Apart from the orientational dependence of the linewidth, the presence of spin diffusion becomes also manifest in the lineshape of the exchange narrowed resonance line. Van Vleck [8] and Kubo and Tomita [9] predicted a Lorentzian lineshape for 3-d magnets, whereas deviations from the Lorentzian lineshape were predicted by Richards [5] for 2-d systems. The extent of the deviations depends on the strength of the exchange interactions in the magnetic plane. Only at the magic angle $\theta = 55°$ the resonance line should be purely Lorentzian. We analyzed the lineshape of the EPR resonance line for four different orientations. The results are shown in figure 4.4. In the case of RbBp.2Ttg one observes significant deviations from the Lorentzian lineshape only if the magnetic field is perpendicular to the magnetic plane. In the case of NaBp.2Tg one could also observe these deviations if the magnetic field vector lies in the plane of the biphenyl anions [10]. From this result we again conclude that RbBp.2Ttg is a pseudo two-dimensional magnetic system and that the interactions in the magnetic plane are weaker than in NaBp.2Tg.

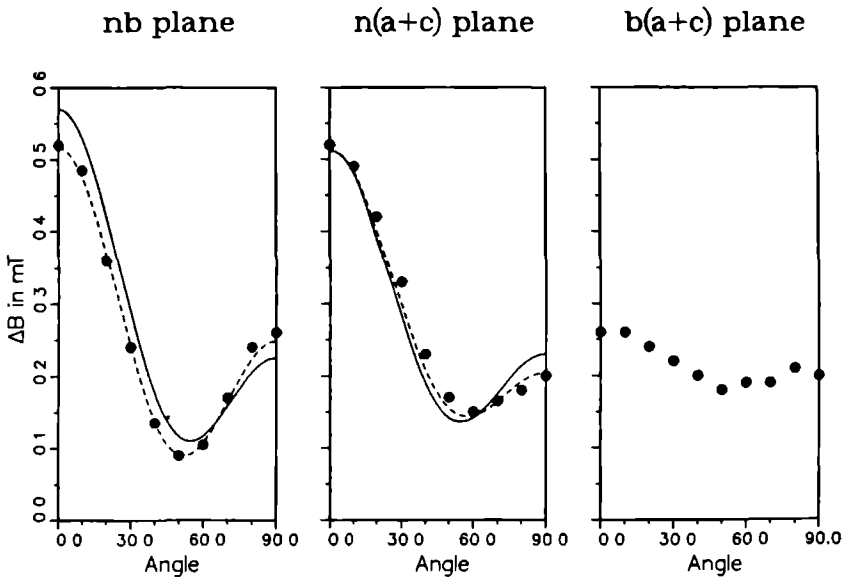

Figure 4.3: Orientational dependence of the first derivative peak-peak linewidth for RbBp.2Ttg at 77 K in three crystallographic planes. The orientational behaviour is shown only over 90° since the behaviour of the linewidth is symmetric with respect to the chosen experimental axes. The solid line indicates the fitted angular dependence with equation 4.5 and the dashed line gives the fit on the basis of equation 4.6

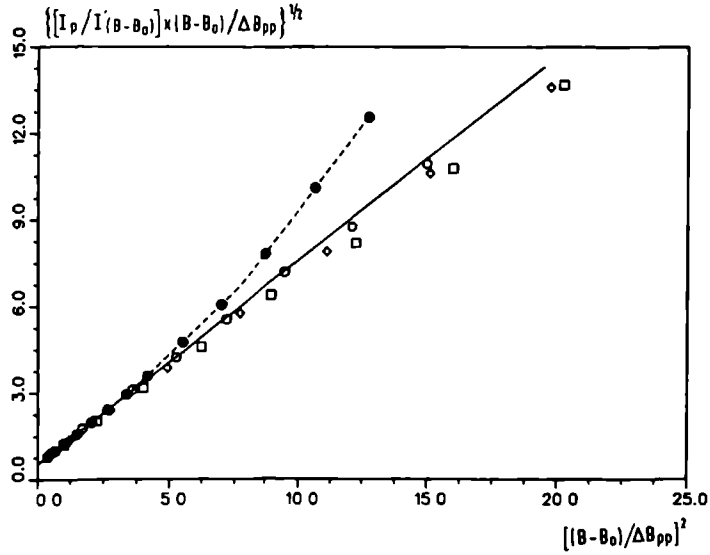

Figure 4.4: Lineshape analysis of RbBp.2Ttg at 77 K for four orientations of the external magnetic field: • : $\vec{B}_0 // \vec{n}$; ○ : $\vec{B}_0 // \vec{b}$; □ : $\vec{B}_0 // \vec{a} + \vec{c}$ and ◇ : $\theta = 55°$ (the magic angle).

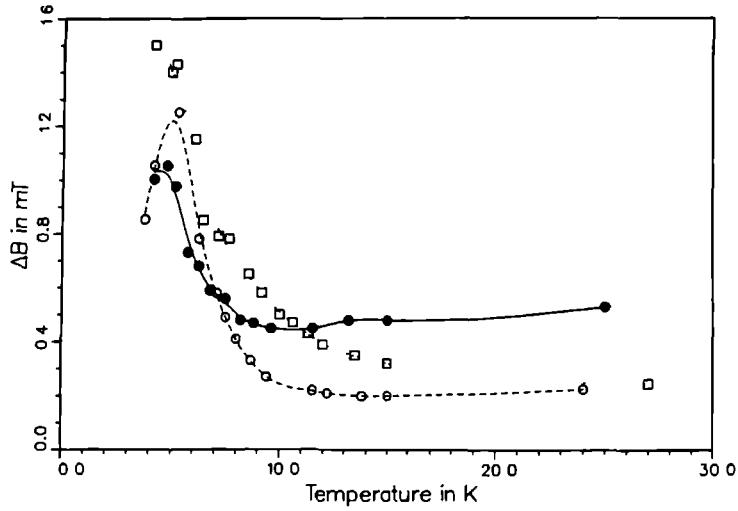

Figure 4.5: Temperature dependence of the linewidth of RbBp.2Ttgfor three orientations of the external magnetic field: • : $\vec{B}_0//\vec{n}$; ○ : $\vec{B}_0//\vec{b}$ and □ : $\vec{B}_0//\vec{a}+\vec{c}$.

4.3 The Transition to a Singlet–Triplet System

The temperature dependence of the first-derivative linewidth for three selected orientations of the magnetic field below 25 K is presented in figure 4.5. This figure shows that the angular dependence of the linewidth at 25 K is qualitativily the same as at 77 and 295 K. The largest linewidth is observed for $\vec{B}_0//\vec{n}$. The minimal linewidth was measured for the angle $\theta = 55°$ (the magic angle). A second maximum was observed when the external magnetic field vector is situated in the magnetic plane. This orientational dependence of the linewidth points to the presence of spin diffusion at this temperature and from this one can conclude that RbBp.2Ttg is still a two-dimensional magnetic system at 25 K. The linewidth behaviour of RbBp.2Ttg changes rapidly upon a further lowering of the temperature. Below 11 K the largest linewidth is found for the magnetic field vector in the magnetic plane instead of perpendicular to it. This means that RbBp.2Ttg behaves no longer as a 2-*d* magnetic system below about 11 K. As may be seen from figure 4.5 the linewidth for the magnetic field vector in the spin plane decreased when the temperature was lowered from 5 K. Together with this change the intensity of the EPR line diminished A plot of the integrated intensity versus the temperature is shown in figure 4.6. It shows that there is a sharp fall in the EPR intensity in the temperature region from about 13 to about 4 K. Below 4 K the intensity increased again. In this paragraph we will only discuss the observed phenomena in the temperature range from 18 to 4 K. The experimental observations below about 4 K will be the subject of the next section. We will start the interpretation of the experimental results by recalling the powder susceptibility of RbBp.2Ttg (figure 4.7). Mooij [3] showed that the behaviour of the susceptibility as

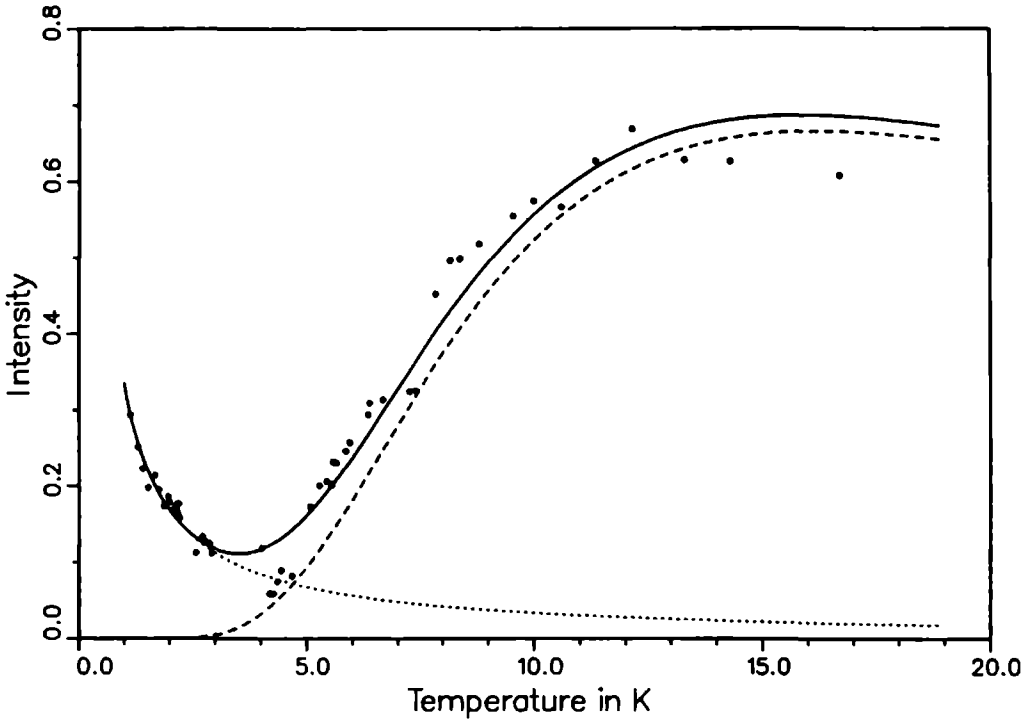

Figure 4.6: Integrated intensity of the resonance line of RbBp.2Ttg for the external magnetic field parallel to the b-axis as a function of temperature. The contribution of the spins in the triplet state is given by the dashed line, whereas the contribution of the doublet state spins is given by the dotted line. The sum of both contributions is indicated by the solid line.

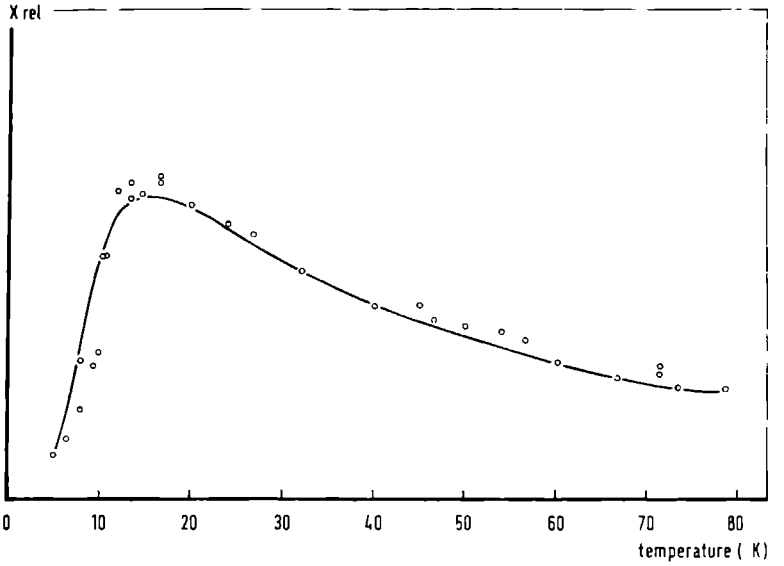

Figure 4.7: Temperature dependence of the powder susceptibility of RbBp.2Ttg.

a function of the temperature can be described with the singlet–triplet model using an exchange parameter of -13 K. This result of Mooij can be correlated with the crystal structure as determined by X-ray diffraction which shows that the layer of paramagnetic biphenyl anions is composed of strongly interacting biphenyl anion pairs (compare figure 4.2). In this picture the decrease of the EPR intensity upon cooling below about 13 K can be understood as a depopulation of the triplet states of an exchange coupled dimer with a singlet ground state. This behaviour is not unexpected as the intensity of the EPR resonance line is closely related to the paramagnetic susceptibility. The relative decrease of the linewidth for the magnetic field perpendicular to the spin plane can now be interpreted as a consequence of a transition from a pseudo two-dimensional magnetic system to a exchange coupled singlet-triplet spin system. Upon lowering the temperature the number of dimers in the singlet state increases and as a consequence a dilution of the paramagnetic spin system occurs. One effect of this apparent dilution is the disappearance of the enhancement of the $(3\cos^2\theta - 1)^2$ term due to spin diffusion in equation 4.2. This finally results in a change of the orientation for which one observes the largest linewidth: below 11 K it is not observed for the magnetic field vector perpendicular to the plane of the biphenyl anions but for the magnetic field vector in the plane of these anions. Another effect of this transition from a concentrated paramagnetic system to a diluted spin system is the increase of the linewidth of the EPR resonance line below 18 K. As the occupation number of the triplet state diminishes the average exchange interaction between the various biphenyl dimers decreases. This results in a decrease of the exchange narrowing effect and an increase of the linewidth of the EPR resonance line.

4.4 Defects in the RbBp.2Ttg Crystal

The magnetic layer structure of RbBp.2Ttg suggests that one should be able to observe EPR signals of isolated biphenyl anion pairs in the triplet state upon continued cooling. This seems to be confirmed by the decrease of the resonance linewidth for the magnetic field vector in the plane of the biphenyl anions below about 4.5 K. Moreover, the single resonance line starts to split below about 3 K. The splitting could be attributed to hyperfine interactions. The observed EPR spectra for three orthogonal directions of the magnetic field are shown in figure 4.8. The spectra show some well resolved splittings with a coupling constant of 0.12 mT. This value is equal to the hyperfine coupling constants of the ortho protons in an isolated biphenyl anion. However, in an exchange coupled dimer one expects a hyperfine interaction of about 0.06 mT, because the spin density of each electron on each of the carbon atoms of the dimer is only half as large as the spin density on the carbon atoms in the isolated monomers. This means that the experimentally observed EPR signal at 1.2 K is not due to an biphenyl anion pair in the triplet state, but to an biphenyl anion monomer in a doublet state. This conclusion is confirmed by the temperature dependence of the intensity of the EPR resonance line below about 4 K. If the signal at 1.2 K would be due to an exchange-coupled dimer in the triplet state with a singlet ground state, the intensity of this signal should decrease upon a decrease of the temperature from 4 to 1.2 K. The experimentally observed intensity increase in this temperature region, demonstrates that this assumption is not correct (see figure 4.6), and points towards a system in the doublet state. This conclusion is also confirmed by the observation of asymmetric resonances at 4.2 K. An example of a spectrum with asymmetric resonances is shown in figure 4.9. It can be explained by assuming that it consists of two signals with different origins: a signal from the transitions inside the triplet manifold of exchange coupled dimers and a signal from isolated biphenyl anions in the doublet state. The asymmetric signal cannot arise from the two different resonances within the triplet manifold, because these transitions will result in a symmetric signal: the resonance positions are slightly different, but the transition probabilities are almost the same.

Once, we understood the experimental EPR spectra we became interested in the origin of these isolated anions. Therefore, we analyzed the temperature dependence of the intensity of the EPR signal and furthermore, we simulated the experimental spectra at 1.2 K for three orthogonal directions of the external magnetic field. As discussed in the preceding paragraphs, the EPR signals arise from two different sources: part of the signal is due to the transitions within the triplet manifold of an exchange coupled $S = 1/2$ dimer, whereas the other part of the signal arises from the isolated biphenyl anions in the doublet state. The total intensity I of both signals may be described with

$$I = aI_{ST} + bI_D \tag{4.7}$$

where a and b are fitting parameters. The intensity I_{ST} of $N_d(= \frac{1}{2}N_{spins})$ dimers of the singlet-triplet system is given by

$$I_{ST}(T) = \frac{1}{2}\frac{2\pi}{\hbar}g^3\mu_B^3 B_0 B_{1x}^2 N_d \frac{e^{\frac{g\mu_B B_0}{kT}} - e^{-\frac{g\mu_B B_0}{kT}}}{1 + e^{\frac{g\mu_B B_0}{kT}} + e^{-\frac{g\mu_B B_0}{kT}} + e^{-\frac{2J}{kT}}} \tag{4.8}$$

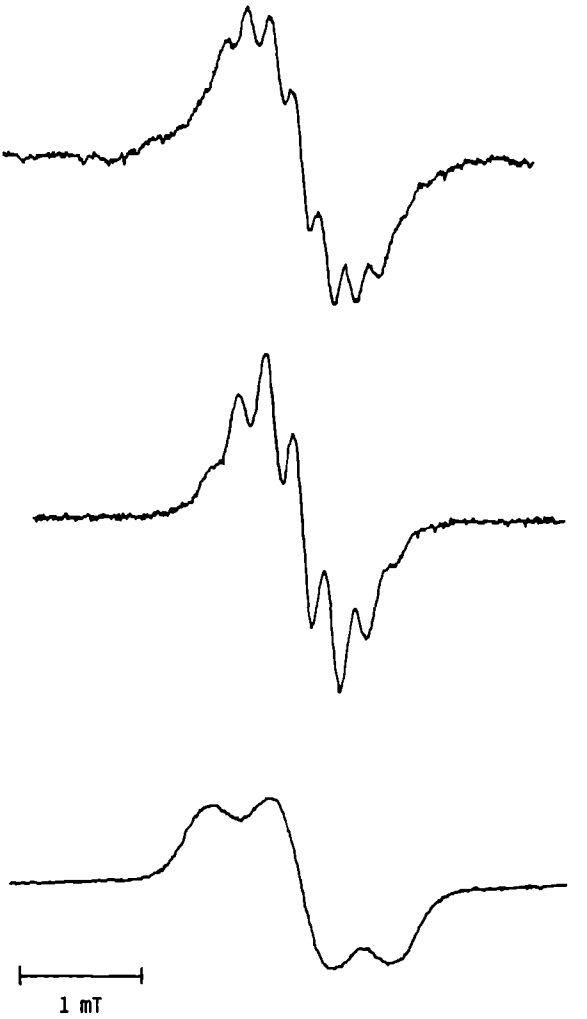

Figure 4.8: Experimental spectra of RbBp.2Ttg at 1.2 K for the external magnetic field along three orthogonal directions showing the presence of hyperfine interactions. Top: n axis, middle: b axis and bottom $a + c$ axis.

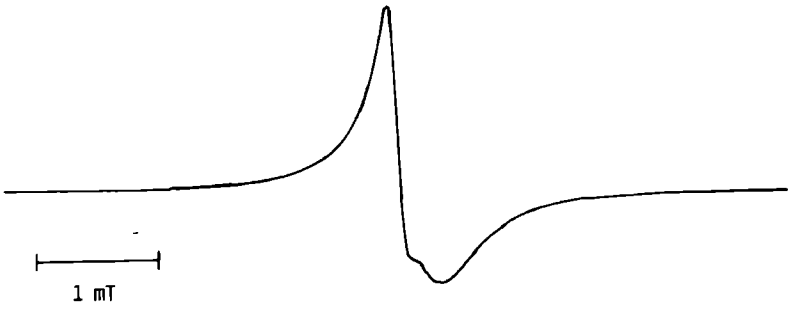

Figure 4.9: Asymmetric EPR-resonance signal in RbBp.2Ttg at 4.2 K.

whereas the intensity of a doublet signal I_D arising from N_{spins} may be described with the relation

$$I_D(T) = \frac{1}{4}\frac{2\pi}{\hbar} g^3 \mu_B^3 B_0 B_{1x}^2 N_{spins} \frac{e^{\frac{g\mu_B B_0}{2kT}} - e^{-\frac{g\mu_B B_0}{2kT}}}{e^{\frac{g\mu_B B_0}{2kT}} + e^{-\frac{g\mu_B B_0}{2kT}}} \tag{4.9}$$

The solid line in figure 4.6 represents the best fit to the experimental data. From this fit we obtained that $a = 98.4\%$ and $b = 1\ 6\%$, which means that 1.6% of the signal arises from isolated spins in the doublet state. This result shows that the concentration of spins in the doublet state is quite low, which can be interpreted as though the spins in the doublet state are due to defects in the crystal structure of RbBp.2Ttg.

At this point one is faced with the question whether these signals are due to distortions at the surface of the crystals, or whether they originate from the bulk of the crystal. We performed our measurements on a crystal of dimensions 0.5 x 0.5 x 1 mm^3. If we use the above calculated concentration of spins in the doublet state, the sample should contain $2.9 \cdot 10^{17}$ isolated electron spins. On the contrary, one surface-layer of a crystal of these dimensions contains ca. $3.6 \cdot 10^{13}$ biphenyl anions. Even if we extend the surface from 1 to 10 layers the number of biphenyl anions remains too small to account for the experimentally observed concentration of unpaired electrons in the doublet state. Therefore, we conclude that these doublets predominantly occur in the bulk of the crystal. Another important question concerns the orientation of these defects: do they follow a random distribution or do they occur only in some well defined positions. Supposing that the latter situation is true we attempted to simulate the experimental spectra of figure 4.8 on the basis of the following assumptions:

- The signal arises from unpaired electrons localized on biphenyl anions.
- The orientations of these biphenyl anions are the same as those in the crystal structure. This means that there are four possible orientations for the defect-biphenyl anions, but only two of these orientations are significantly different.

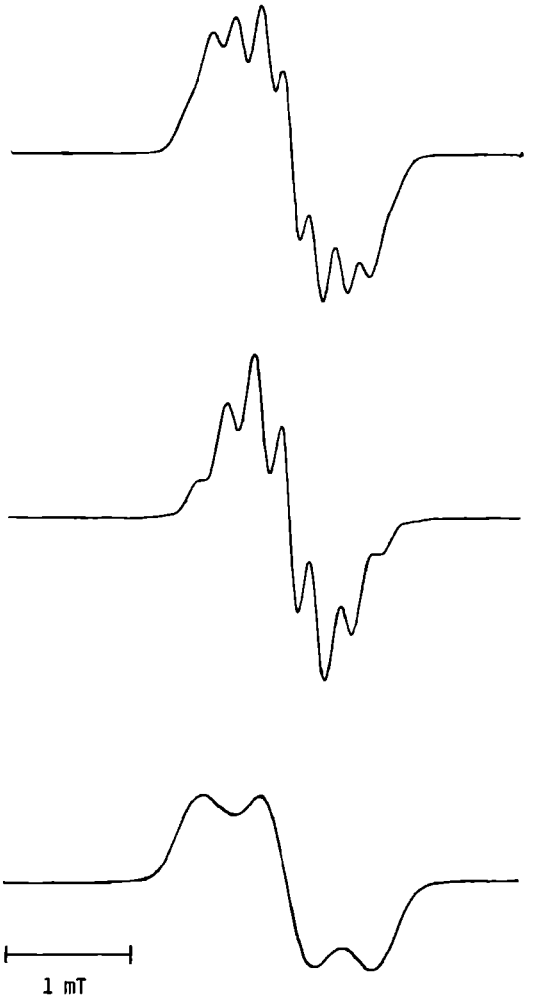

Figure 4.10: Simulated spectra of RbBp.2Ttg at 1.2 K for the external magnetic field along three orthogonal directions. The simulations used a first derivative Gaussian lineshape with a peak-peak linewidth of 0.25 mT. Top: n axis, middle: b axis and bottom $a + c$ axis.

- For each possible defect-orientation an EPR spectrum is calculated with the simulation program MAGRES [11] as follows:
  - The spins in the doublet state are described with the spin-Hamiltonian:

$$\mathcal{H} = \mu_B \vec{B}_0 \cdot \overline{\overline{g}} \cdot \vec{S} + \sum_{i=1}^{6} \vec{S} \cdot \overline{\overline{A}}_i \cdot \vec{I}_i - \sum_{i=1}^{6} \gamma_N \hbar \vec{B}_0 \cdot \vec{I}_i. \tag{4.10}$$

    where $\vec{I}_i$ denotes one of the ortho- or para-proton spins of the biphenyl anion. The hyperfine interaction with the meta-protons is neglected because this interaction is almost an order of magnitude smaller than the hyperfine interactions between the unpaired electron and the other proton spins [12].
  - The components of the $\overline{\overline{g}}$ tensor were taken from Mooij [13].
  - The $\overline{\overline{A}}$-tensor for each of the ortho- and para-protons was calculated by combining the data of Möbius [12] for the isotropic hyperfine couplings with the data for the anisotropic hyperfine interactions in a C–H fragment and the spin densities on the carbon atoms of the biphenyl anion, given by Hirota [14] and Hendriks [15], respectively.

$$\overline{\overline{A}}_i = a_{\text{Möbius}} + \rho_{i,\text{Hendriks}} \overline{\overline{A}}_{\text{Hirota}} \tag{4.11}$$

  - A Gaussian as well as a Lorentzian linewidth of 0.25 mTesla was used.
- The total spectrum is obtained by a summation of the spectra corresponding to the four different orientations of the defect, each orientation occurring with the same probability.

In figure 4.10 the simulations are shown using a Gaussian linewidth. An excellent agreement exists between the experimental and the simulated spectra. Hence, we conclude that the orientations of the defect are indeed equal to the four crystallographically different orientations of the biphenyl anions in the single crystal. Simulations with Lorentzian linewidths were clearly inferior to the simulations using Gaussian linewidths. This is an indication that exchange between the defect and other species is absent.

The question arises how are the defects produced. The single crystals of RbBp.2Ttg are crystallized from solutions of biphenyl anions, which are obtained by reduction of neutral biphenyl with Rb:

$$C_{12}H_{10} + Rb \rightleftharpoons C_{12}H_{10}^{-} + Rb^{+}$$

The standard reduction potentials E_0 of Rb and biphenyl are almost equal (E_0(Rb) - E_0(biphenyl) $\approx$ 0.1 eV [16]), so that a slight amount of neutral molecules remains in solution. We expect that these neutral biphenyl molecules will incorporate into the RbBp.2Ttg crystal structure. In order to keep the crystal electrically neutral a positive charge should be absent as well. We think that this will occur by the absence of complete $Rb(Ttg)_2^+$ clusters as there is no reason for the two tetraglyme molecules to participate in the crystal when their Rb^+ cation is absent. Near the holes created by these absent clusters a local distortion of the lattice occurs. We now assume that a neutral biphenyl molecule will move into this empty space as sketched in figure 4.11. As a result of this displacement this neutral biphenyl molecule no longer interacts with the neighbouring

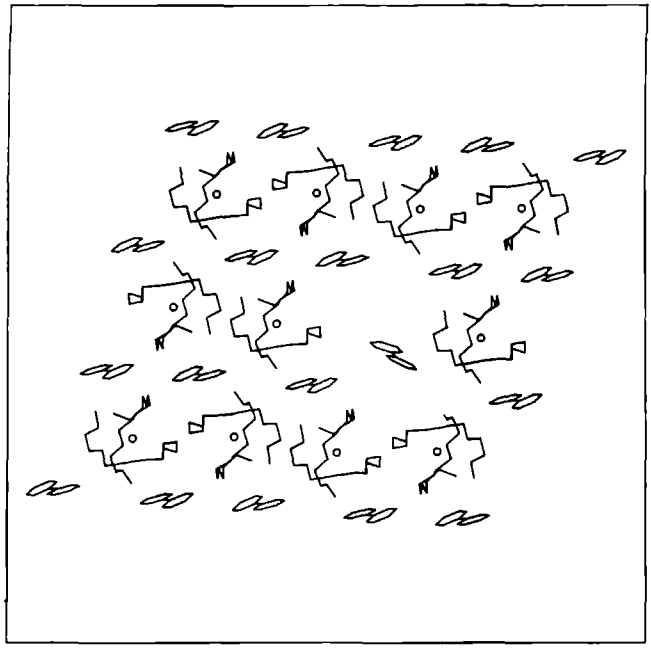

Figure 4 11: Schematic picture of a part of RbBp.2Ttg crystal showing a defect.

biphenyl anions. This leaves one biphenyl anion without an associate, it becomes an isolated biphenyl anion in the doublet state, which is still oriented according to the crystal structure. This picture explains also that a simulation with a Gaussian linewidth is better than with a Lorentzian linewidth.

4.5 The Double-Quantum Transition

As may be noticed from figure 4.6 the number of biphenyl anion pairs in the triplet state is quite low at 4.2 K. As a consequence of this low concentration the average triplet-triplet interaction between neighbouring biphenyl anion dimers will be quite small. It is well-known that in isolated triplet state systems one can observe apart from the $\Delta m_s = \pm 1$ transitions other transitions. In order to establish the isolated triplet character of the spin system in RbBp.2Ttg at 4.2 K we searched for these extra transitions. For the clarity of the discussion we first formulate the spin-Hamiltonian valid for a biphenyl anion pair in the triplet state.

$$\mathcal{H} = \mu_B \sum_{i=1,2} \vec{\mathbf{B}}_0 \cdot \overline{\mathbf{g}}_i \cdot \vec{\mathbf{S}}_i + (\vec{\mathbf{S}}_1 + \vec{\mathbf{S}}_2) \cdot \overline{\overline{\mathbf{D}}} \cdot (\vec{\mathbf{S}}_1 + \vec{\mathbf{S}}_2) \tag{4.12}$$

where $\overline{\mathbf{D}}$ is the zero field splitting (ZFS) tensor and where we have neglected all hyperfine interactions present. The ZFS tensor arises in this system from the dipolar interaction between the unpaired electrons. As the unpaired electrons are well seperated in space one can calculate this interaction by means of a delocalized point-dipole model (compare, for instance, chapter 9). The calculated eigenvalues in 10^{-4} cm^{-1} and the principal

directions are

D_1 = 21.3 , $//\vec{\mathbf{n}}$ axis

D_2 = 14.6 , $//\vec{\mathbf{b}}$ axis

D_3 = -35.9 , $//\vec{\mathbf{a}} + \vec{\mathbf{c}}$ axis

The first extra signal which one may observe in a triplet-state system is the so called half field transition. This signal is the result of a single quantum transition between the $m_s = |+1>$ and $|-1>$ states of the triplet. The strength of this signal depends upon the extent by which the $|+1>$ and $|-1>$ levels of the triplet are mixed: The higher the degree of mixing the stronger the half field resonance. As the ZFS tensor is very small with respect to the Zeeman interaction the mixing of the mentioned energy levels will be very limited and, therefore, we expected that the intensity of the half field transition will be too small to be observed. Nevertheless, we tried to detect the half field resonance, but according to our expectations we didn't succeed.

Another new resonance which may be observed in triplet state systems is the double-quantum transition. It is a transition from the $|\pm 1>$ state to the $|\mp 1>$ state by the absorption of two microwave quanta. This process occurs via an intermediate level which may be virtual. The direction of the oscillating microwave field should be equal to that of the normal single-quantum resonances.i.e. perpendicular to the static magnetic field. By means of second order time dependent perturbation theory one can derive that the transition probability of this resonance is equal to

$$P_{mn} = \frac{1}{4\hbar^2} \frac{|<\phi_m|V|\phi_k>|^2 |<\phi_k|V|\phi_n>|^2}{(\omega_{mk}-\omega)^2(\omega_{mn}-2\omega)^2} \sin^2\left\{\frac{(\omega_{mn}-2\omega)}{2}t\right\}. \qquad (4.13)$$

This equation shows that the transition probability of the signal is maximal if the intermediate level $|k>$ is situated exactly in the middle of the initial and final spin states. From the above expression one can also deduce that the transition probability of the double-quantum signal is proportional to B_1^4. As a consequence of this B_1^4 dependence the intensity of the detected signal is proportional to $P^{3/2}$, where P denotes the microwave power level. For a single quantum transition the measured signal is proportional to $P^{1/2}$. This means that we can discriminate between a single and double quantum transition by measuring its intensity as a function of the microwave power level. In figure 4.12 we show two experimental EPR-spectra at 4.2 K: The top one was measured with a microwave power level of 20 mW and a gain factor of 400, whereas the one at the bottom was measured with a power level of 50 mW and a gain factor of 3.2. It is clear that two different resonances are observed, as may be seen from the completely different linewidths. We attributed the uppermost signal to the single quantum transitions in the triplet dimer and in the doublet monomer and the lowermost signal to the double quantum transition in the triplet manifold. Careful inspection of the latter spectrum reveals that the normal single-quantum resonances are present as well, but because of their larger linewidth their peak-height is much smaller than that of the double-quantum transition. In order to check our assignment we determined the intensity of the EPR signal as a function of the power level. The intensity was obtained by integrating the derivative EPR absorption two times. The resulting data are shown in figure 4.13. We observe that below 15 mW the intensity increases according to $P^{0.5}$, whereas the intensity

Figure 4.12: Experimental EPR spectra of RbBp.2Ttg at 4.2 K for the same orientation showing the double quantum transition: at the top $P = 20$ mW and a gain factor of 400, at the bottom $P = 50$ mW and a gain factor 3.2

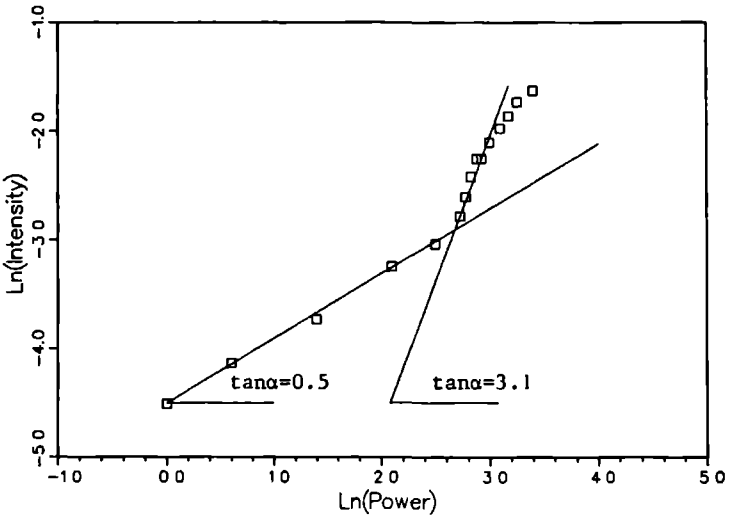

Figure 4.13: EPR signal intensity as a function of the microwave power level at 7 K. Below 15 mW the slope equals 0.5, slightly above 15 mW the slope is equal to 3.1

just above 15 mW is proportional to $P^{3.1}$. The results supports our view that the new resonance is a double quantum transition, although the power dependence is somewhat different from the predicted value.

We also measured the microwave power level at which the onset of the double quantum resonance was observed as a function of the orientation in three orthogonal planes. Since in our oscillating setup the oscillating $\vec{\mathbf{B}}_1$ field does not remain perpendicular to the static external field $\vec{\mathbf{B}}_0$ on rotation of the magnet, the measured power levels were corrected with a factor $\sin^2 \delta$, where δ is the angle between the $\vec{\mathbf{B}}_0$ and $\vec{\mathbf{B}}_1$. These corrected results are presented in figure 4.14. Inspection of expression 4.12 learns that the probability of the double quantum transition is largest and consequently the less power is needed to observe it - if the intermediate level $|0>$ lies exactly between the initial and final energy levels. This is the case as the ZFS tensor is equal to zero. One can calculate from the ZFS tensor that this occurs for an angle of 48° from the n axis in the $n, a+c$ plane and for an angle of 43° from the b axis in the $b, a+c$ plane. For both planes it occurred at an angle of 40° in reasonable agreement with the predicted values. According to the calculated $\bar{\mathbf{D}}$ components the behaviour of the double quantum transitions with respect to the power in the nb plane should be different from that in the $n(a+c)$ and $b(a+c)$ planes. However, as one may notice from figure 4.14 the experimental results do not agree with our expectations. A similar behaviour was observed as in the two other planes, only the amplitude of the angular variation is smaller. This extraordinary behaviour in the nb plane cannot be explained by including the hyperfine interaction in the spin-Hamiltonian as the separation between the intermediate level and the two other levels are changed in a symmetric way. A possible explanation could be the presence of double-quantum transitions in a tetramer consisting of two pairs of biphenyl anions, the

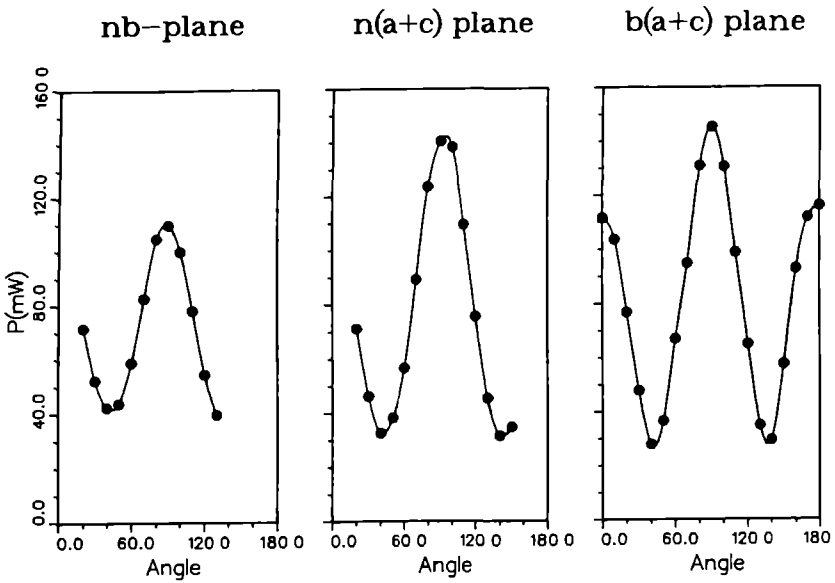

Figure 4.14: The microwave power level at which the double quantum transition appears as a function of the orientation for three crystallographic planes (T=4.2 K).

connection axis of these dimers being the b axis. The ZFS tensor components between the two $S = 1$ spins in such a tetramer are equal to

D_1 = 11.3 , $//\vec{n}$ axis

D_2 = -15.1 , $//\vec{b}$ axis

D_3 = 3.8 , $//(\vec{a} + \vec{c})$ axis

which means that this ZFS goes through zero if the magnetic field vector rotates in the nb plane. However, the concentrations of such tetramers at 4.2 K is so low (0.01%), that this explanation is also not very likely. Thus, although we were able to give detailed picture of the magnetic behaviour of RbBp.2Ttg as a function of the temperature, there still remains something to be solved.

4.6 Conclusion

The above presented results show that RbBp.2Ttg is a very interesting system. The crystal structure shows that it is composed of paramagnetic layers of biphenyl anions, the distance between the layers being much larger than the shortest C C distance in the magnetic layer. Therefore, one expects that this compound should exhibit 2-d magnetic properties. These properties can indeed be found by means of EPR: Above about 25 K the low-dimensional magnetic character of RbBp.2Ttg is reflected in the angular dependence of the linewidth which shows basically a $(3\cos^2\theta \quad 1)^2$ dependence and in deviations from

a Lorentzian lineshape. Both results are in agreement with theoretical predictions made for 2-d systems. A more precise inspection of the structure of the magnetic layer reveals that one of the neighbouring anions is much nearer than all other biphenyl ions. This would mean that the paramagnetic layer consists of exchange coupled biphenyl anion dimers. This idea is confirmed by the experimental data below 25 K. These data are in agreement with a singlet–triplet model with a singlet ground state. Furthermore we were able to observe the double quantum transition of the triplet state of these biphenyl anion dimers. Finally we also detected signals from isolated biphenyl anions in the doublet state. At 1.2 K we observed the hyperfine interactions of these doublet state ions. We determined their concentration and concluded that they occur in the bulk of the crystal. Furthermore, we simulated a few experimental spectra at 1.2 K. The simulations permitted us to conclude that these isolated biphenyl anions are oriented according to the crystal structure.

Bibliography

[1] E. de Boer, A.A.K. Klaassen, J.J. Mooij, and J.H. Noordik.
Pure and Applied Chemistry, 51:73, 1979.

[2] G.W. Canters, A.A.K. Klaassen, and E. de Boer.
Journal of Physical Chemistry, 74:3299, 1970.

[3] J.J. Mooij, A.A.K. Klaassen, E. de Boer, H.M.L. Degens, Th.E.M. van den Hark, and J.H.Noordik.
Journal of the American Chemical Society, 98:680, 1976.

[4] O. Takizawa, R. Srinivasan, and E.de Boer.
Molecular Physics, 44:677, 1981.

[5] P.M. Richards and M.B. Salamon.
Physical Review B, 9:32, 1974.

[6] P.M. Richards.
Magnetic resonance in one and two-dimensional systems.
In K.A. Muller and A. Rigamonti, editors, *Local Properties at Phase Transitions*, page 539, North-Holland (Amsterdam), 1976.

[7] M.C.M. Gribnau, R. Murugesan, H. van Kempen, and E. de Boer.
Molecular Physics, 52:195, 1984.

[8] J.H. van Vleck.
Physical Review, 74:1168, 1948.

[9] R. Kubo and K. Tomita.
Journal of the Physical Society of Japan, 9:888, 1954.

[10] R. Murugesan and E. de Boer.
Chemical Physics Letters, 95:301, 1983.

[11] C.P. Keijzers, E.J. Reijerse, P. Stam, M.F. Dumont, and M.C.M. Gribnau.
Journal of the Chemical Society, Faraday Transactions I, 1987:3493, 1987.

[12] K Möbius.
Zeitschrift für Naturforschung A, 20:1102, 1965.

[13] J.J. Mooij.
Single Crystals of Alkali-Aromatic ion-pairs.
PhD thesis, University of Nijmegen, 1976.

[14] N. Hirota, C.A. Hutchison, and P.Palmer.
Journal of Chemical Physics, 40:3717, 1964.

[15] B.M.P. Hendriks.
Nuclear Magnetic Relaxation in Solutions of of Alkali Aromatic Ion Pairs.
PhD thesis, University of Nijmegen, 1973.

[16] E. de Boer.
Electronic structure of alkali metal adducts of aromatic hydrocarbons.
In F.G.A. Stone and R. West, editors, *Advances in Organometallic Chemistry*, page 115, Academic Press (New York), 1964.

Chapter 5

The Dynamic Magnetic Properties of KBp.2Ttg

5.1 Introduction

The last compound which will be discussed in the first part of this thesis is bis(tetraglyme)-potassiumbiphenyl (KBp.2Ttg). This substance was discovered by de Boer and coworkers as well [1]. The crystal structure of this compound was solved by Noordik et al. in 1977 [2]. In spite of the similarity in chemical composition of KBp.2Ttg with NaBp.2Tg and RbBp.2Ttg the structure of KBp.2Ttg is not isomorphous with either of these two. The X-ray diffraction data revealed a monoclinic crystal structure of the spacegroup Cc, with a unit cell which is half that of RbBp.2Ttg and twice that of NaBp.2Tg. The principal crystal data are listed in table 5.1 and a picture of the crystal structure is shown in figure 5.1. Just as in the sodium and rubidium analogues the ions occur in the crystals as solvent separated ion pairs. The molecular structure of KBp.2Ttg is essentially the same as that of RbBp.2Ttg, but, as a consequence of the smaller unit cell, the K^+ and the $C_{12}H_{10}^-$ ions are situated on symmetry elements. As a result of this special position the biphenyl anions must be planar in contrast with a dihedral angle of 9.4° in RbBp.2Ttg. The K^+ ions are coordinated by the ten oxygens in the two surrounding tetraglyme molecules. We note that the average value of the K–O separation in KBp.2Ttg is 0.085 Å shorter than the Rb–O separation in RbBp.2Ttg, while the difference in ionic radii is 0.14 Å[3,2]. This means that the K^- cation has more space left in the cage formed by the coordinating oxygen atoms than the Rb^+ cation. This is reflected in the lower melting point of KBp.2Ttg (~ 40°C) as compared to RbBp.2Ttg (~ 55°C) [4]. The biphenyl anions in KBp.2Ttg are arranged in a plane parallel to the ab plane (bc in NaBp.2Tg and $b, a + c$ in RbBp.2Ttg) and a picture of a projection of the biphenyl anions on this plane is shown in figure 5.2. One observes that the packing is different from the packing in NaBp 2Tg as well as the packing in RbBp.2Ttg. In RbBp.2Ttg there exists a pair of biphenyl molecules, related by a twofold axes, having a distance between their centres of 7 58 Å, which is much shorter than the distance of 9.79 Å to the next nearest neighbours. In NaBp.2Tg each molecule is approximately hexagonally surrounded by its neighbours at distances of 8.04, 8.60 and 9 56 Å. In KBp.2Ttg each anion is also approximately hexagonally surrounded by its neighbours, but now at distances of 9.65 and 9.69 Å. This means that the deviations in KBp.2Ttg from a hexagonal lattice are much smaller than in

$C_{32}H_{54}KO_{10}$	Monoclinic, Cc
$a = 9.654(3)$ Å	$Z = 4$
$b = 16.803(9)$ Å	$d_x = 1.03$ Mg m^{-3}
$c = 21.845(7)$ Å	$M_r = 637.8$
$\beta = 96.03°$	(cell dimensions at 120 K)
$V = 3465$ Å^3	

Table 5.1: Crystal data of KBp.2Ttg.

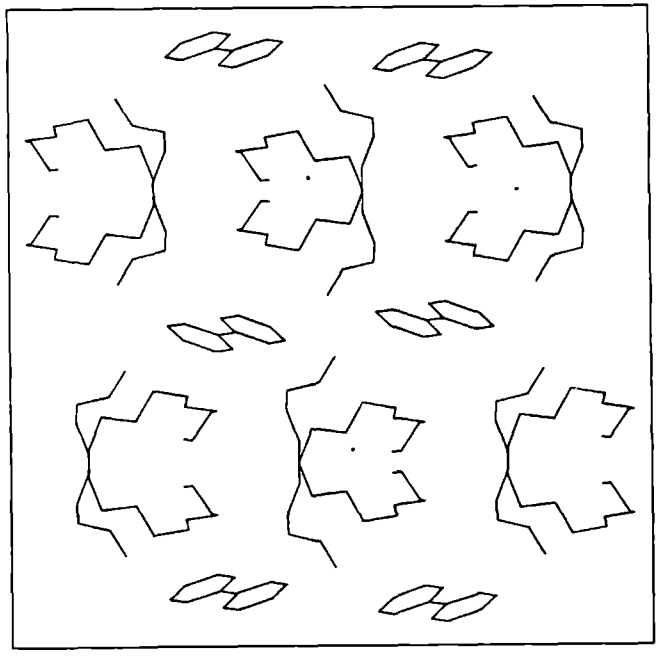

Figure 5.1: Crystal structure of KBp.2Ttg projected on the c^*b plane.

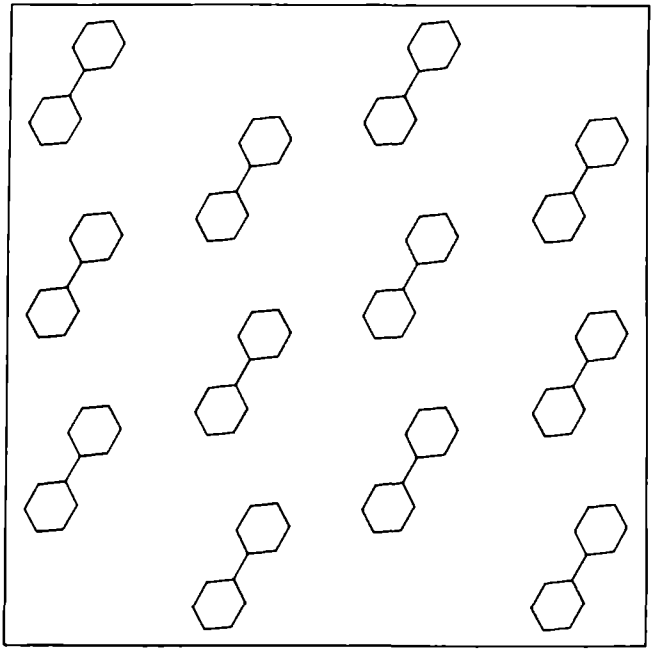

Figure 5.2: Projection of the biphenyl molecules in KBp.2Ttg on the *ab*-plane.

NaBp.2Tg. The main difference in the arrangement of the biphenyl anions in KBp.2Ttg and NaBp.2Tg concerns the orientation of the anions. In KBp.2Ttg all anions within the same paramagnetic layer have the same orientation, but these orientations alternate over the different layers. In NaBp.2Tg all magnetic layers are constructed in the same way, but inside one layer two distinct orientations can be distinguished.

5.2 Pseudo 2-*d* Magnetic Behaviour at 77 K

As discussed above KBp.2Ttg has a layered structure: layers of paramagnetic biphenyl anions are separated by layers of diamagnetic $K(Ttg)_2^+$ clusters. As the distance between the paramagnetic layers is much larger than the shortest C–C distance in the magnetic plane, we expected that this compound would behave as a pseudo 2-*d* magnetic system. The theoretical aspects of the behaviour of the EPR linewidth and lineshape in such systems were discussed in chapter 2. In the chapters 3 and 4 we presented the experimental results on NaBp.2Tg and RbBp.2Ttg and we demonstrated that these systems can be characterized as pseudo 2-*d* magnetic systems. In this chapter we will present some experimental results concerning the magnetic properties of KBp.2Ttg and subsequently discuss them. We will limit ourselves to some results at 77 K, because the experimental spectra at lower temperatures (4.2 and 1.2 K) unfortunately showed irreproducable resonance lines. We attributed this bad behaviour to the poor quality of our crystals: the $K(Ttg)_2^+$ cluster in these crystals is less well stabilized as compared to the $Na(Tg)_2^+$ and $Rb(Ttg)_2^+$ clusters in NaBp.2Tg and RbBp.2Ttg, respectively, which makes the preparation of KBp.2Ttg single crystals much harder than the preparation of single crystals of

compound	plane	α	β	ρm_0	m_1	m_2
KBp.2Ttg	c^*b	0.076	0.070	0.090	0.175	0.074
	c^*a	0.068	0.073	0.089	0.215	0.049
NaBp.2Tg	a^*b	0.116	0.081	0.111	0.232	0.113
	a^*c	0.080	0.091	0.110	0.315	0.035
RbBp.2Ttg	nb	0.110	0.115	0.129	0.175	0.129
	$n(a+c)$	0.136	0.094	0.128	0.495	0.077

Table 5.2: Experimental linewidth parameters for KBp.2Ttg, NaBp.2Tg and RbBp.2Ttgat 77 K. All linewidth parameters are expressed in mT.

the other two alkali biphenyl compounds.

We previously discussed that the relaxation function in 2-d magnetic systems contains apart from the contributions from Gaussian random processes a contribution which originates from spin diffusion. This latter contribution results in a resonance linewidth which has a characteristic $(3\cos^2\theta \quad 1)^2$ angular dependence, where θ is the angle between the normal to the magnetic plane and the external magnetic field. It may be described by the relation of Richards and Salamon [5]

$$\Delta B_{pp} = \alpha + \beta(3\cos^2\theta - 1)^2 \tag{5.1}$$

or by the more precise expression

$$\Delta B_{pp} = \rho m_0(3\cos^2\theta - 1)^2 + m_1 \sin^2\theta\cos^2\theta + m_2 \sin^4\theta \tag{5.2}$$

where ρ is an angular independent enhancement factor. One can derive that in magnetic 3-d systems which are composed of spin layers with a hexagonal structure the enhancement factor should be equal to 1 and that the ratio of the parameters m_0, m_1 and m_2 should equal 3:84:30. However, in low-dimensional systems the parameter rho should be greater than 1, because of the contribution of spin diffusion to the relaxation function. The experimentally measured first derivative peak-peak EPR linewidths at 77 K in the X-band frequency region are shown in figure 5.3. One observes a significant anisotropy if the plane of rotation includes the c^* axis which is the normal to the magnetic plane. The largest linewidth is measured for the magnetic field vector parallel to this axis. The resonance linewidth exhibits a minimum if the orientation of the external magnetic field makes an angle $\theta = 55°$ (the magic angle) with this c^* axis. We analyzed the experimental data by fitting them to the expressions 5.1 and 5.2. The results of this analysis are presented in table 5.2. The corresponding data for NaBp.2Tg and RbBp.2Ttg are given as well. If we compare the values ρm_0 in the c^*b and c^*a plane with those of m_1 and m_2 we can calculate a value of 12.5 for the enhancement factor ρ. This means that the angular dependence of the resonance linewidth is dominated by the contribution which arises from the spin diffusion mechanism, which in turn means that KBp.2Ttg is a 2-d magnetic system at 77 K.

The presence of spin diffusion becomes not only visible in the $(3\cos^2\theta - 1)^2$ dependence of the EPR linewidth, but it can also be observed in deviations from the lineshape from

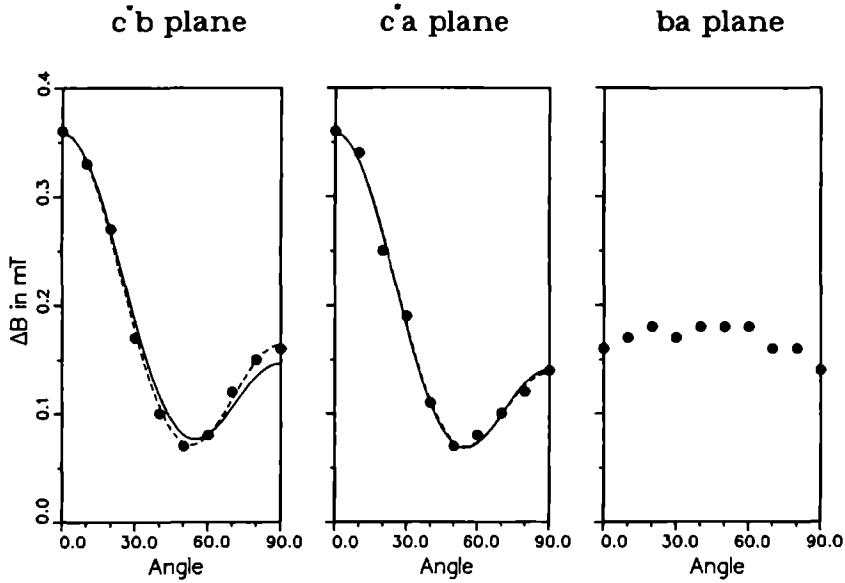

Figure 5.3: Orientational dependence of the first derivative peak-peak linewidth for KBp.2Ttg at 77 K in three crystallographic planes. The orientational behaviour is shown only over 90° since the behaviour of the linewidth is symmetric with respect to the chosen experimental axes. The solid line indicates the fitted angular dependence with equation 5.1 and the dashed line gives the fit on the basis of equation 5.2

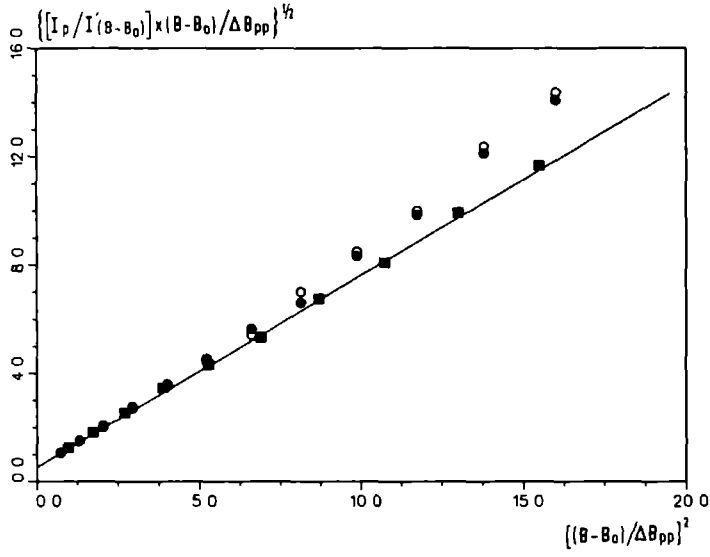

Figure 5.4. Lineshape analysis of KBp.2Ttg at 77 K for three orientations of the external magnetic field: • : $\vec{B}_0 // \vec{c}^*$, ○ : $\vec{B}_0 // \vec{b}$ and ◇ : $\theta - 55°$ (the magic angle).

Lorentzian (compare chapter 2). This feature was predicted by Richards [5] and it has been observed in many pseudo 2-*d* magnetic systems. These deviations are, however, much harder to observe than the characteristic angular dependence of the linewidth which was discussed above. We analyzed the lineshape of KBp.2Ttg at 77 K for three orientations of the external magnetic field $\vec{B}_0$: $\vec{B}_0 // \vec{c}^*(\theta = 0°), \vec{B}_0 // \vec{b}(\theta = 90°)$ and for $\vec{B}_0$ at the magic angle $\theta = 55°$. The results of this lineshape analysis are given in figure 5.4. The lineshape of a perfect Lorentz-line is indicated in this figure by the solid line. One clearly observes that the lineshape is non-Lorentzian for $\theta = 0°$ and $\theta = 90°$. For the magic angle the resonance lineshape is close to Lorentzian. These results confirm the presence of spin diffusion in KBp.2Ttg at 77 K.

Bibliography

[1] G.W. Canters, A.A.K. Klaassen, and E. de Boer.
Journal of Physical Chemistry, 74:3299, 1970.

[2] J.H.Noordik, J. Schreurs, R.O. Gould, J.J. Mooij, and E. de Boer.
Journal of Physical Chemistry, 82:1105, 1978.

[3] J.J. Mooij, A.A.K. Klaassen, E. de Boer, H.M.L. Degens, Th.E.M. van den Hark, and J.H.Noordik.
Journal of the American Chemical Society, 98:680, 1976.

[4] E. de Boer, A.A.K. Klaassen, J.J. Mooij, and J.H. Noordik.
Pure and Applied Chemistry, 51:73, 1979.

[5] P.M. Richards and M.B. Salamon.
Physical Review B, 9:32, 1974.

Part II

The Calculation of Spin-Spin Interactions

Chapter 6

The spin-Hamiltonian

The second part of this thesis will be directed towards the calculation of some spin-spin interactions. These spin-spin interactions can be real, in case they occur in the actual physical Hamiltonian, or they may be fictitious and only be present in the spin-Hamiltonian. Therefore, we will start with a discussion of the concept and the use of the spin-Hamiltonian in EPR-spectroscopy.

6.1 The Concept of the Spin-Hamiltonian

The resonance lines of an EPR spectrum are due to transitions between various electron spin energy levels. These lines often occur in groups due to the presence of nuclear spins, which cause splittings which are relatively small. The main features — positions and intensities — of these resonances depend upon the microwave frequency ω which is used for the excitation of the various transitions and upon the strength and orientation of the external magnetic field B. By a systematic variation of these experimental parameters a lot of experimental data can be accumulated. However, the insight into the properties of the compound under study is easily obscured by such a large amount of data, especially because these data are interdependent. Therefore, an effective Hamiltonian is used, which is called the spin-Hamiltonian. The only purpose of this effective Hamiltonian is to describe all experimental spectra with a limited number of parameters. This is accomplished by constructing a Hamiltonian which *implicitly* contains all relevant physical interactions. No explicit statements are made about the fundamental physical interactions. We will discuss the interactions and parameters which occur in the spin-Hamiltonian in the paragraphs 6.2 and 6.3. If one wants to interpret the obtained parameters in order to obtain insight into the physical properties of the system, one has to relate the parameters of the spin-Hamiltonian with the contributions of the actual Hamiltonian. These relations will be discussed in general terms in paragraph 6.4. As it is the purpose of this part of this thesis to describe these relations and their calculation for some of the spin-spin interactions, some of them will be discussed in more detail in the following chapters. For a more extensive discussion of the various aspects of the spin-Hamiltonian formalism the reader is referred to the extensive literature on this subject [1,2,3,4,5,6,7,8].

General Procedure

The main characteristics of the spin-Hamiltonian can be summarized as follows Every paramagnetic centre with one or more unpaired electrons is attributed an effective electron spin S, which can differ from the value that one expects on account of the number of unpaired electrons of that centre This difference is due to the fact, that the unpaired electrons are no longer free but bound and that they interact with each other and with the other electrons and nuclei As a consequence, the number of energy-levels that is reached in a certain experiment can differ from the number of energy levels that is reached in a free electron system The energy levels that are reached, are described as a $2S + 1$ manifold After the assignment of an effective spin, a spin-Hamiltonian is constructed (see below) which contains operators based on the effective electron spins S, the nuclear spins I and the external magnetic field B Apart from these operators it contains a limited number of parameters Once the spin Hamiltonian is constructed one can obtain a matrix-representation of this Hamiltonian by choosing an appropriate set of basis-functions By diagonalizing this matrix representation the eigenvalues and eigenvectors can be calculated The differences of the eigenvalues yield the positions of the resonance lines For the calculation of the intensities of the transitions one also needs the eigenvectors A simulated spectrum is constructed by convolution of the calculated stick spectrum with a lineshape and this spectrum is compared with the experimental one By changing the various parameters of the spin-Hamiltonian the simulated spectrum is varied until complete agreement with the experimental spectrum is obtained If *all* relevant physical parameters are implicitly contained in the spin Hamiltonian, it is possible to obtain a perfect agreement between the experimental and the simulated spectra The result of this procedure is not only a significant reduction of the data, but the parameters of the spin-Hamiltonian are also independent of the specific conditions of the measurements This implies that measurements in different places under different circumstances can be compared easily and meaningfully However, one should realize that the parameters still can depend upon other experimental circumstances such as the temperature Examples of such systems are compounds with a structural or spin phase-transition

6.2 The Interactions in the Spin-Hamiltonian

The determination of the value of the effective spin can be a problem If no other information is available it has to be guessed from the experimental spectra If n principal resonance-lines are observed one can try to describe the experimental spectra with an effective spin $S = n/2$ If this is impossible the effective spin is increased in steps of a half, until the match is successful The maximum effective electron spin, in case of no orbital degeneracy, is given by $S = m/2$, where m is the number of unpaired electrons of the paramagnetic centre One always has to bear in mind that the effective spin can depend upon the experimental circumstances such as temperature and microwave frequency In case the structure of the compound is known one can obtain the values for the nuclear spins I from the NMR periodic table Otherwise one has to determine the values of the nuclear spins I in the same way as the electron spins

Once one knows the effective electron spin one is able to construct the appropriate spin-Hamiltonian The terms one needs for a complete description of the spin Hamil-

1/2 :	BS,
1 :	BS, S^2
3/2 :	BS, S^2, BS^3
2 :	BS, S^2, BS^3, S^4,
5/2 :	BS, S^2, BS^3, S^4, BS^5

Table 6.1: Spin operators for various effective spins S

tonian depend on the value of the effective electron spin. This may be seen as follows: The dimension of the spin-Hamiltonian matrix equals $N \times N$ where $N = 2S + 1$. If we use an operator algebra the corresponding Hamilton matrix can be constructed from $N \times N$ basis-operators. For instance, for a spin $S = 1/2$ system one needs $2 \times 2 = 4$ basis-operators. These are the identity operator E and the spin operators S_x, S_y and S_z. Because of the requirement of invariance to time-reversal these spin-operators are coupled to the external magnetic field according to $\vec{\mathbf{B}} \cdot \vec{\mathbf{S}}$. For a $S = 1$ system one needs $3 \times 3 = 9$ basis operators. Apart from the four above mentioned operators one needs five more. These five operators are quadratic in nature and are indicated by S^2. They consist of linear combinations of the various products of the three spin operators like $S_xS_y + S_yS_x$. For systems with $S > 1$ one needs even more terms in the spin-Hamiltonian. The terms one needs for the complete description of an effective spin $S \leq 5/2$ are listed in table 6.1. In practice, the higher order terms in the electron spin like BS^3 are often neglected because the coefficients are small [9].

Up to now we have only discussed the case of an isolated site with one or more unpaired electrons. In undiluted spin-systems such as alkali-biphenyl single-crystals the unpaired electrons are so close to each other, that they no longer can be regarded as independent. Therefore, the spin-Hamiltonian of such systems should contain, apart from the above mentioned terms which describe an isolated one-site electron spin system, also terms which represent the interaction between the electron spins located on different sites. The most general form of a spin-Hamiltonian in which the coupling between electron spins is included is obtained by taking the direct product of the spin-Hamiltonians which describe the isolated effective electron-spins. It should be noted that the number of terms increases very rapidly as the number of sites increases. In general only the terms which are bilinear in the effective electron spins like $\vec{\mathbf{S}}_1 \cdot \vec{\mathbf{S}}_2$ are retained in the spin-Hamiltonian, but also higher order terms like $(\vec{\mathbf{S}}_1 \cdot \vec{\mathbf{S}}_2)^2$ are sometimes included [10,11,12,13].

If one also includes the nuclear spins the number of terms increases rapidly. One has to include terms which describe the interaction of the nuclear spins with the magnetic field, with the effective electron spins and with other nuclear spins. We start with noticing that the effective nuclear spins hardly differ from the actual nuclear spins, because the excited states are very high in energy. Therefore one never talks about an effective nuclear spin. The terms one needs for the description of the interaction of the nuclear spin with the magnetic field are similar to those which describe the interaction of the effective electron spin with the magnetic field and are obtained by replacing S by I in table 6.1. As a consequence of the almost pure spin character of the nuclear spins the higher order terms

in the nuclear spin are never considered. For a complete description of the interaction between the nuclear spin and the (effective) electron spin in the spin-Hamiltonian we have to include all terms which occur in the direct product of the effective electron spin and the nuclear spin. Normally only the principal term, i.e. the one which is bilinear in the effective electron spin and the nuclear spin, $\vec{\mathbf{S}} \cdot \vec{\mathbf{I}}$, is taken into account. If more than one nuclear spin is present one should include terms which represent the interaction between the different nuclear spins. However, because the interactions between the nuclear spins turn out to be very small on the EPR-energy scale, these terms are in general neglected. Only in some double resonance experiments like ENDOR, these terms are needed [14].

6.3 The Parameters of the Spin-Hamiltonian

In the previous section we have only discussed the operators which occur in the various terms of the spin-Hamiltonian. In this section we will pay attention to the parameters in these terms. These parameters occur in general in matrices, which are designated as tensors, although it is well-known that some of these tensors, as for instance the hyperfine tensor, do not obey the transformation rules of actual tensors. The amount of information we can derive from the measurements depends on the physical state of the sample. If one assumes symmetrical tensors only 6 independent elements remain to be determined. These elements can be obtained from single-crystal studies. After diagonalization the principal values and principal axes of the tensors are obtained which contain important chemical information. In powders or glasses only the principal values can be obtained, the directions of the principal axes in the molecular frame remain unknown. If one performs the experiments on liquids only the isotropic values of the various tensors can be found, because the random rotations of the paramagnetic molecules are normally fast with respect to the EPR-time scale. If this condition is not fulfilled, as for instance in viscous solvents, we are in the slow-motion regime where we can obtain anisotropic information as well.

The principal term in the spin-Hamiltonian of a magnetic resonance experiment describes the interaction of the effective electron spin or nuclear spin with the magnetic field. It is called the electron or nuclear Zeeman interaction. The electron Zeeman interaction is given by

$$\mathcal{H}_{eZ} = \mu_B \vec{\mathbf{B}} \cdot \bar{\mathbf{g}} \cdot \vec{\mathbf{S}} \tag{6.1}$$

For a free electron the $\mathbf{g}$-tensor is isotropic and has a value of approximately 2.0023. The g-value in organic radicals is almost isotropic and equal to this free electron value. For inorganic systems significant isotropic and anisotropic contributions build up. The deviations become larger as the atoms become heavier. The strength of the electron Zeeman coupling depends upon the magnetic field used. At 0.3 Tesla it is approximately equal to 0.3 cm^{-1}. This energy corresponds with the X-band microwave frequency. The nuclear Zeeman term is given by

$$\mathcal{H}_{NZ} = -\gamma\hbar \vec{\mathbf{B}} \cdot (\bar{\bar{\mathbf{1}}} - \bar{\sigma}) \cdot \vec{\mathbf{I}} \tag{6.2}$$

in the spin-Hamiltonian. The tensor $\bar{\bar{\sigma}}$ is called the chemical shift tensor and it is of the order 10^{-5} for protons. Because the effects of the chemical shift tensor are too small to be

observed in EPR-experiments it is neglected in the EPR spin-Hamiltonian. The nuclear Zeeman term is three orders of magnitude smaller than the electron Zeeman interaction.

In case of a spin-system with an effective spin $S \geq 1$ there appears a quadratic term in S in the spin-Hamiltonian as shown in the previous section. This quadratic term is called the Zero Field Splitting (ZFS), because it splits the electron spin energy levels even in zero magnetic field. The corresponding parameters are contained in the Zero Field Splitting tensor $\overline{\overline{\mathbf{D}}}$. The ZFS contribution to the spin-Hamiltonian is described by

$$\mathcal{H}_{ZFS} = \vec{\mathbf{S}} \cdot \overline{\overline{\mathbf{D}}} \cdot \vec{\mathbf{S}} \tag{6.3}$$

The strength of the ZFS can vary widely. It ranges from 1.10^{-3}cm^{-1} in organic systems up to 10 cm^{-1} in inorganic systems which contain tetrahedrally coordinated Co(II) [15]. Just like an effective spin $S \geq 1$ gives rise to a quadratic term S^2 in the spin-Hamiltonian the spin-Hamiltonian for a nuclear spin $I \geq 1$ contains a quadratic term in I^2. It is called the (nuclear) quadrupole interaction and it is described by

$$\mathcal{H}_Q = \vec{\mathbf{I}} \cdot \overline{\overline{\mathbf{Q}}} \cdot \vec{\mathbf{I}} \tag{6.4}$$

where $\overline{\overline{\mathbf{Q}}}$ is the quadrupole tensor. A typical value for the quadrupole interaction is $1 \cdot 10^{-4}$ cm^{-1} in Cu-complexes.

In many systems one encounters the case of effective electron spins at different paramagnetic centres which interact with each other. Examples of such systems are pure paramagnetic systems like NaBp.2Tg and RbBp.2Ttg (see part I) and singlet-triplet systems like Cu-Cu dimers. In principle, one can couple all effective electron spins of the different centres to an overall effective spin and describe the experimental spectra with this overall spin. However, because the interactions between the various spins are relatively weak it is common use to construct the spin-Hamiltonian for these systems from an effective spin for each centre and to add extra terms to this Hamiltonian which describe the interaction between the effective spins. Depending on the physical background of the interactions the following terms are added to the spin-Hamiltonian:

$$\mathcal{H}_{ex} = \vec{\mathbf{S}}_1 \cdot \overline{\overline{\mathbf{J}}}_{12} \cdot \vec{\mathbf{S}}_2, \tag{6.5}$$

$$\mathcal{H}_{dip} = \vec{\mathbf{S}}_1 \cdot \overline{\overline{\mathbf{D}}}_{12} \cdot \vec{\mathbf{S}}_2. \tag{6.6}$$

where the subscripts 1 and 2 refer to the centres on which the effective spins are localized. The first expression is used to describe spin-spin interactions which arise from the "exchange"-coupling. The origin of this interaction will be discussed in general terms in the next section. At this point we only notice that it often reduces to the isotropic term

$$\mathcal{H}_{ex} = -2J\vec{\mathbf{S}}_1 \cdot \vec{\mathbf{S}}_2 \tag{6.7}$$

which is called the Heisenberg exchange interaction. The parameter J is called the exchange constant. Just like the ZFS, the strength of the exchange interaction can vary widely. It ranges from 1.10^{-4} cm^{-1} to values of the order of 1000 cm^{-1}. The second equation is used to describe interactions which are due to the dipolar interactions between the magnetic moments of the electron spins. It has a value in the order of 1.10^{-2} cm^{-1}. In analogy to the couplings between the effective electron spins there are couplings between

nuclear spins as well. These couplings are very small and they can safely be neglected in the spin-Hamiltonian.

The last term we will discuss in this section is called the hyperfine interaction. It is written as

$$\mathcal{H}_{hf} = \vec{\mathbf{S}} \cdot \overline{\overline{\mathbf{A}}} \cdot \vec{\mathbf{I}} \tag{6.8}$$

where $\overline{\mathbf{A}}$ is the hyperfine tensor. This coupling results in a splitting of each electron spin energy level in $2I + 1$ energy levels. In principle one can describe all $(2S + 1)(2I + 1)$ energy levels with an effective spin S' which is given by

$$S' = 2SI + S + I \tag{6.9}$$

However, the mixing of the electron spin energy levels due to the electron spin-nuclear spin coupling is very small as the hyperfine interaction is normally weak as compared to the electron Zeeman coupling. This means that the main result of the presence of the nuclear spins is a splitting of each electron spin level in an electron spin manifold. This can be described much easier with the above given equation than by a total electron spin S' as given in equation 6.9. Moreover, the use of a hyperfine coupling tensor is also much closer to the underlying physical mechanisms. The value of the hyperfine interaction ranges from 1.10^{-4}cm^{-1} to about 1.10^{2}cm^{-1}.

6.4 The Physical Background of the Parameters of the Spin-Hamiltonian

If one has obtained a set of parameters with which the the experimental spectra can be described satisfactorily, one has reached the stage of interpretation of the experimental results. The interpretation can be accomplished in two ways. Firstly, one can use relations which correlate the parameters of the spin-Hamiltonian with properties of the substance under study. An example of such a relation is the well known Weissman-McConnell relation [16,17] by which proton hyperfine interactions in aromatic systems are connected with spin-densities on the adjacent carbon atoms. Other examples are the Hatfield-Hodgson equation which establishes a linear relationship between the exchange constant J and the Cu-O-Cu angle ϕ in oxygen-bridged copper dimers [18,19,20] and the expressions of Bencini and coworkers by which the spin-orbit contribution to the ZFS of these oxygen-bridged compounds is related with their Cu-Cu distance [21,22].

A second method to interpret the experimental parameters is to calculate values for them from theoretical expressions which originate from the actual physical Hamiltonian. Examples of such theoretical expressions are the Ramsey formula for the chemical shift tensor in NMR and the expressions for $\overline{\mathbf{g}}$ [23,24,25] and $\overline{\overline{\mathbf{A}}}$ [26,27]. This approach requires a clear insight in the underlying physical mechanisms of the various interactions. In the following we will focus our attention on these mechanisms.

$\overline{\overline{\mathbf{g}}}$: The Zeeman interaction originates from the interaction of an unpaired electron with the external magnetic field. The g-factor which occurs in this interaction is due to relativistic effects [28]. Using quantum-electrodynamics one can derive a value $g_{free} = 2.00231922$ for a free electron. In atoms and molecules the electrons are no longer free but

bound to the nuclei and therefore they do not only have a spin-angular momentum but also an orbital angular momentum. For free atoms one can employ the Landé formula to obtain the g-factor for the Zeeman splittings appropriate to each of the atomic energy levels in a magnetic field. Since the ground state of most molecules and radicals has zero angular momentum, one might expect that the g-factor in these cases is precisely the free-electron value. However, small amounts of the excited states are mixed into the ground state of such systems by means of the spin-orbit interaction. These contributions result in a change of the effective magnetic moment of the ground state and are reflected in the g-tensor.

$\overline{\overline{\mathbf{D}}}$: The ZFS originates mainly from two different physical interactions, which cannot be distinguished experimentally. There is a first order contribution from the dipole-dipole interaction between the unpaired electrons at one site. There is also a second order contribution which arises from the spin-orbit interaction. This latter contribution is sometimes also called the "pseudo dipolar interaction" or the "anisotropic exchange interaction". However, these names are absolutely incorrect if judged from the physical origin of this interaction. The spin-orbit coupling contributes only if an exchange interaction is operative in the excited electronic states of the system [29,30,31]. The contribution from the spin-orbit coupling to the ZFS will be discussed in chapter 8. As any tensor this ZFS-tensor can be divided into a symmetric and an antisymmetric part. The antisymmetric part is only present if a centre of symmetry is absent. Moriya [32] showed that the order of the antisymmetric part can be estimated as $(\Delta g/g).J$, whereas the symmetric part is of the order $(\Delta g/g)^2.J$, where J is the exchange interaction in the ground state. In organic systems like triplet-state naphtalene [33,34,35,36] the main contribution arises from the dipole-dipole coupling, because the spin-orbit coupling in these systems is very small. In inorganic complexes such as Cu-Cu dimers [37] both contributions are about equally important, whereas the spin-orbit contribution dominates in complexes with even heavier atoms such as Ag-Ag dimers [29].

$\overline{\mathbf{Q}}$: Although the quadrupole tensor looks very much like the ZFS the physical background is completely different. The quadrupole tensor arises from a coupling between the nuclear quadrupole moment and the electric field gradient at the site of the nucleus due to all surrounding electrons, the ligands and the lattice. In case of a spherical charge distribution this contribution equals zero because the electric field gradient at the position of the nucleus is zero.

$\overline{\overline{\mathbf{A}}}$: There are several physical mechanisms which contribute to the hyperfine interaction. We will only mention the principal ones. For s-electrons a first order term is present which originates from the spin-orbit interaction [28]. It is called the Fermi-contact interaction and is related to the density of the unpaired electron at the nucleus. For non-s electrons there is a first order contribution that arises from the magnetic dipole interaction between the electron and the nuclear spin. There are also second order effects; the most inportant of these is due to the combined effect of the orbital-Zeeman interaction and the spin-orbit coupling. The calculation of the hyperfine tensor will be discussed in more detail in chapter 10.

$\overline{\mathbf{J}}$: The exchange coupling constant J, or in case of anisotropic exchange interactions the exchange coupling tensor $\overline{\mathbf{J}}$, is used if a direct or indirect exchange interaction contributes to the spin-spin coupling. These exchange interactions are quantum-mechanical

effects due to the antisymmetric nature of the n-electron wavefunction. If the atoms on which the electron spins are located are nearest neighbours one talks about direct exchange. If the exchange interaction takes place via the orbitals of an intermediate atom one speaks of indirect or superexchange. An example of this case is the exchange interaction between two Mn^{2+} ions via an O^{2-} atom in MnO_2. It are exactly these exchange interactions which give rise to the presence of ferro-, ferri- and antiferromagnetism. In the next chapter we will discuss the origin of the exchange interaction in detail. In our discussion we will only regard the bilinear Heisenberg term in the exchange interaction but in principle also higher order terms are possible like for instance the biquadratic exchange term $j(\vec{\mathbf{S}}_1 \cdot \vec{\mathbf{S}}_2)^2$. Anderson [38,39,40] used a perturbation treatment and showed that (a) these higher order terms appear only for ions with more than one unpaired electron and (b) that they are of the order of 1% of the bilinear term. Herring [41] used a modified Heitler-London method to prove the validity of the Heisenberg Hamiltonian assuming only that the real Hamiltonian does not contain spin-variables and that the separated monomers have no orbital degeneracy. As Anderson, he concluded that the higher order terms are in principle present but that they are negligibly small. These theoretical results of Anderson and Herring have been confirmed by various experimental data [12,10,13,11] as well as ab-initio calculations [42,43]. Therefore we can truncate the spin-Hamiltonian after the bilinear term. At this point we should also note that the Heisenberg Hamiltonian is only appropriate for ions in orbital singlet states. For the coupling of ions in orbitally degenerate states, as e.g. Ti^{3+} in a trigonal ligand field, Hamiltonians are to be used which contain orbital parameters that cannot be collected in an overall J [44,45,46].

Bibliography

[1] C.P. Keijzers.
De spin-Hamiltoniaan (Lecture Notes).
Department of Molecular Spectroscopy, University of Nijmegen, 1981.

[2] A. Abragam and B. Bleaney.
Electron Paramagnetic Resonance of Transition Ions.
Dover Publications (New York), 1986.

[3] A. Carrington and A.D. McLachlan.
Introduction to Magnetic Resonance.
Harper and Row (London), 1967.

[4] C.P. Slichter.
Principles of Magnetic Resonance.
Springer Verlag (Berlin), 1980.

[5] J.E. Wertz and J.R. Bolton.
Electron Spin Resonance.
Chapman and Hall (New York), 1986.

[6] G.E. Pake.
Paramagnetic Resonance.
W.A. Benjamin (New York), 1962.

[7] Ch.P. Poole and H.A. Farach.
The Theory of Magnetic Resonance.
Wiley-Interscience (New York), 1972.

[8] J.S. Griffith.
The Theory of Transition Metal Ions.
Cambridge University Press (Cambridge), 1961.

[9] J.C.M. Henning and J.H. den Boef.
Physical Review B, 18:60, 1978.

[10] A. Beutler, H.U. Güdel, T.R. Snellgrove, G. Chapuis, and K.J. Schenk.
Journal of the Chemical Society, Dalton Transactions, 1979:983, 1979.

[11] D.E. Bolster, P. Gütlich, W.E. Hatfield, S. Kremer, E.W. Müller, and K. Wieghardt.
Inorganic Chemistry, 22:1725, 1983.

[12] U. Falk, A. Furrer, J.K. Kjems, and H.U. Güdel.
Physical Review Letters, 52:1336, 1984.

[13] H U Gudel
Inelastic neutron scattering from clusters
In R D Willett, D Gatteschi, and O Kahn, editors, *Magneto-Structural Correlations in Exchange Coupled Systems*, page 297, D Reidel (Dordrecht), 1985

[14] D Snaathorst
Single Crystal EPR and Proton ENDOR studies of Copper Dithiolate Complexes
PhD thesis, University of Nijmegen, 1982

[15] R F Wielinga, H W J Blote, J A Roest, and W J Huiskamp
Physica, 34 223, 1967

[16] S I Weissman
Journal of Chemical Physics, 25 890, 1956

[17] H M McConnell
Journal of Chemical Physics, 24 764, 1956

[18] W E Hatfield
Inorganic Chemistry, 22 833, 1983

[19] W H Crawford, H W Richardson, J R Wasson, D J Hodgson, and W E Hatfield
Inorganic Chemistry, 15 2107, 1976

[20] D J Hodgson
Progress in Inorganic Chemistry, 19 173, 1975

[21] A Bencini, M di Vaira, A C Fabretti, D Gatteschi, and C Zanchini
Inorganic Chemistry, 23 1620, 1984

[22] A Bencini, D Gatteschi, and C Zanchini
Inorganic Chemistry, 24 700, 1985

[23] C P Keijzers, H J M de Vries, and A van der Avoird
Inorganic Chemistry, 11 1338, 1972

[24] C P Keijzers and E de Boer
Molecular Physics, 29 1007, 1975

[25] C P Keijzers and E de Boer
Molecular Physics, 29 1743, 1975

[26] C P Keijzers and E de Boer
Journal of Chemical Physics, 57 1277, 1972

[27] C P Keijzers, G F M Paulussen, and E de Boer
Molecular Physics, 29 973, 1975

[28] J E Harriman
Theoretical Foundations of Electron Spin Resonance
Academic Press (New York), 1978

[29] J G M van Rens and E de Boer
Chemical Physics Letters, 31 377 1975

[30] C P Keijzers
Spin-spin interactions in weakly interacting dimers

In M.C.R. Symons, editor, *Electron Spin Resonance, Specialist Periodical Reports*, page 1, Royal Society of Chemistry (London), 1987.

[31] M.C.M. Gribnau and C.P. Keijzers.
Inorganic Chemistry, 26:3413, 1987.

[32] T. Moriya.
Physical Review, 120:91, 1960.

[33] C.A. Hutchison Jr. and B.W. Magnum.
Journal of Chemical Physics, 29:952, 1958.

[34] C.A. Hutchison Jr. and B.W. Magnum.
Journal of Chemical Physics, 34:908, 1961.

[35] J.H. van der Waals and M.S. de Groot.
Molecular Physics, 2:333, 1959.

[36] M.S. de Groot and J.H. van der Waals.
Molecular Physics, 3:190, 1960.

[37] J.G.M. van Rens, E. van der Drift, and E. de Boer.
Chemical Physics Letters, 14:113, 1972.

[38] P.W. Anderson.
Physical Review, 115:2, 1959.

[39] P.W. Anderson.
Theory of magnetic exchange interactions : exchange in insulators and semiconductors.
In F. Seitz and D. Turnbull, editors, *Solid State Physics*, page 99, Academic Press (New York), 1963.

[40] P.W. Anderson.
Exchange in insulators : superexchange, direct exchange and double exchange.
In G.T. Rado and H. Suhl, editors, *Magnetism*, page 25, Academic Press (New York), 1963.

[41] C. Herring.
Review of Modern Physics, 34:631, 1962.

[42] M.C. van Hemert, P.E.S. Wormer, and A. van der Avoird.
Physical Review Letters, 51:1167, 1983.

[43] P.E.S. Wormer and A. van der Avoird.
Journal of Chemical Physics, 81:1929, 1984.

[44] M. Drillon and R. Georges.
Physical Review B, 26:3882, 1982.

[45] B. Leuenberger and H.U. Güdel.
Molecular Physics, 51:1, 1984.

[46] B. Leuenberger, H.U. Güdel, and A. Furrer.
Chemical Physics Letters, 126:255, 1986.

Chapter 7

The Calculation of the Exchange Constant of the Weakly Coupled Biphenyl Anion Dimer

7.1 The Heisenberg Exchange Interaction

The subject of this chapter is the calculation of the exchange constant J which occurs in the Heisenberg exchange interaction:

$$\mathcal{H}_{ex} = -2J_{ex}\vec{\mathbf{S}}_1 \cdot \vec{\mathbf{S}}_2 \tag{7.1}$$

It is well-known that this exchange interaction follows from the antisymmetrical nature of the n-electron wavefunction. The basic concepts of this interaction were developed by Heisenberg [1] and Dirac [2] in 1928. Their work formed the basis of subsequent theoretical work on the various kinds of magnetism, such as ferro-, ferri- and antiferromagnetism and it has resulted in a clear understanding of the fundamental aspects of magnetism. There are two principal mechanisms of the exchange interaction between two paramagnetic ions or radicals which lead to the above mentioned spin-dependent coupling of their magnetic moments. These are the direct exchange interaction which acts between two neighbouring spin-centres and the indirect or super-exchange mechanism between two non-neighbouring paramagnetic particles. In the last case the exchange interaction is propagated by one- or multi-atom bridges.

It would be highly desirable for organic-, inorganic- and biochemists that the theoretical chemists would be able to calculate the exchange constant fast and accurately, since it could give insight into, for instance, the pathways of electron transfer in biological electron transport chains. It could also be used as a guideline for the preparation of new, interesting polymetallic complexes or one- and two- dimensional magnetic exchange systems with magnetic properties that can be predicted, both in nature and in magnitude. However, although the fundamentals of the Heisenberg exchange interaction are well-understood for most systems it is still a problem to calculate the coupling constant J_{ex}. This is a consequence of the lack of an analytical solution to the many electron problem in quantum mechanics. In the past, several methods have been developed to tackle this problem. With these methods it is, in principle, possible to obtain reliable values for J_{ex}. However, these methods are only applicable to systems with relatively

few electrons, such as the O_2-O_2 dimer (32 electrons) [3] , due to the heavy demands on computing power. Consequently, one can only obtain values for J_{ex} for large systems like the biphenyl anion dimer (166 electrons) by approximate methods. The interest in these approximate methods has recently been renewed by the work of Kahn and coworkers [4]. In this chapter we will show the derivation of some expressions for the exchange constant by means of the Valence-Bond method and subsequently we will apply these formulas to the biphenyl anion dimer. Although we realize that the Valence-Bond method is highly approximate, it might give us a key to the interpretation of the experimental results on NaBp.2Tg and RbBp.2Ttg.

7.2 The Heisenberg Exchange Constant for a Localized Two-Electron Dimer

In order to arrive at an expression for the exchange constant we will consider a system of two identical paramagnetic particles having one unpaired electron each, in addition to their closed shell cores [5,6,7]. In our derivation we will use the independent particle model and neglect the role of the closed shell core electrons. Furthermore we will assume that the atoms are situated at fixed positions at a distance R_{ab}. Under these conditions the Hamiltonian of this system in atomic units can be expressed as

$$\mathcal{H} = \mathcal{H}_a + \mathcal{H}_b + \mathcal{H}_{ab} \tag{7.2}$$

where

$$\mathcal{H}_a = -\frac{\vec{\nabla}_1^2}{2} - \frac{Z}{r_{1a}}, \tag{7.3}$$

$$\mathcal{H}_b = -\frac{\vec{\nabla}_2^2}{2} - \frac{Z}{r_{2b}}. \tag{7.4}$$

The symbol Z in these equations denotes the effective charges of the ion cores. The orbitals which satisfy the one-electron Schrödinger equations are ϕ_a and ϕ_b:

$$\mathcal{H}_a\phi_a(1) = E_a\phi_a(1), \tag{7.5}$$

$$\mathcal{H}_b\phi_b(2) = E_b\phi_b(2) \tag{7.6}$$

where E_a and E_b are the energy eigenvalues. $\mathcal{H}_{ab}$ is the interaction Hamiltonian which has the form

$$\mathcal{H}_{ab} = \frac{Z^2}{R_{ab}} - \frac{Z}{r_{1b}} - \frac{Z}{r_{2a}} + \frac{1}{r_{12}}. \tag{7.7}$$

In this expression the mutual repulsion of the two ion cores is indicated by Z^2/R_{ab}. The second and the third term represent the attractive potentials on electron 1 due to ion b and electron 2 due to ion a, respectively. The last term is the mutual Coulomb repulsion between the two electrons. It will be clear that the above equations contain no explicit dependence on the spin-variables of the two electrons. This spin dependence enters implicitly into the problem when we fulfill the requirement for fermion wavefunctions: antisymmetry under interchange of fermions. Hereto the following two-electron Valence-Bond orbitals are constructed:

$$\phi_+ = N_+\{\phi_a(1)\phi_b(2) + \phi_b(1)\phi_a(2)\}, \tag{7.8}$$

$$\phi_- = N_-\{\phi_a(1)\phi_b(2) - \phi_b(1)\phi_a(2)\} \tag{7.9}$$

where the normalisation constants N_+ and N_- are given by

$$N_\pm = \frac{1}{\sqrt{(2 \pm 2{S_{ab}}^2)}}. \tag{7.10}$$

S_{ab} is the overlap integral $< \phi_a(1)|\phi_b(1) >$. By combination of the spatial orbitals ϕ_+ and ϕ_- ,the spin wavefunctions and the demand for antisymmetry one can contruct two functions: the singlet ψ_S and the triplet ψ_T wave-functions:

$$\psi_T = \begin{cases} \phi_-\alpha\alpha & \text{for } |S, M_S >= |1, 1 > \\ \phi_-\frac{1}{\sqrt{2}}(\alpha\beta + \beta\alpha) & \text{for } |S, M_S >= |1, 0 > \\ \phi_-\beta\beta & \text{for } |S, M_S >= |1, -1 > \end{cases} \tag{7.11}$$

and

$$\psi_S = \phi_+\frac{1}{\sqrt{2}}(\alpha\beta - \beta\alpha) \quad \text{for } |S, M_S >= |0, 0 > \tag{7.12}$$

The energies of the triplet states are calculated by first order perturbation theory according to

$$E_T = \frac{< \psi_T|\mathcal{H}|\psi_T >}{< \psi_T|\psi_T >} =< \phi_- \ |\mathcal{H}|\phi_- > . \tag{7.13}$$

The simplification to the second expression is possible because the Hamiltonian $\mathcal{H}$ contains no spin-dependent operators. In a similar way the energy of the singlet state is calculated. After substitution of the functions for the singlet and triplet states one can calculate the first order interaction energies which are defined by

$$\begin{aligned} \Delta E_{S,T} &= < \psi_{S,T}|\mathcal{H}|\psi_{S,T} > - < \phi_a|\mathcal{H}_a|\phi_a > - < \phi_b|\mathcal{H}_b|\phi_b > \\ &= E_{S,T} - E_a - E_b. \end{aligned} \tag{7.14}$$

This results in the following expressions :

$$\Delta E_T = \frac{Q - J}{1 - {S_{ab}}^2} + \frac{1}{R_{ab}}, \tag{7.15}$$

$$\Delta E_S = \frac{Q + J}{1 + {S_{ab}}^2} + \frac{1}{R_{ab}}. \tag{7.16}$$

where the symbols Q and J denote the Coulomb integral and the exchange integral, respectively. They can be expressed as

$$Q =< \phi_a^2(1)\frac{1}{r_{12}}\phi_b^2(2) > -2 < \phi_b^2(1)\frac{1}{r_{1a}} >, \tag{7.17}$$

$$J =< \phi_a(1)\phi_b(2)\frac{1}{r_{12}}\phi_b(1)\phi_a(2) > -2S_{ab} < \phi_a(1)\phi_b(1)\frac{1}{r_{1b}} > . \tag{7.18}$$

At this point we introduce the symbols $\overline{Q}$ and $\overline{J}$:

$$\overline{Q} \equiv \frac{1}{2}(\Delta E_S + \Delta E_T) = \frac{Q - JS_{ab}^2}{1 - S_{ab}^4} + \frac{1}{R_{ab}}, \tag{7.19}$$

$$\overline{J} \equiv \frac{1}{2}(\Delta E_S - \Delta E_T) = \frac{J - QS_{ab}^2}{1 - S_{ab}^4}. \tag{7.20}$$

These symbols allow us to write the energies of the two spin states in an even more compact form as

$$\Delta E_{2S+1} = \overline{Q} - \{S(S+1) - 1)\}\,\overline{J} \tag{7.21}$$

where S represents the total spin quantum number. This relation can also be written as:

$$\begin{aligned} \Delta E_{2S+1} &= \overline{Q} - \tfrac{1}{2}(1 + 4\vec{\mathbf{S}}_1 \cdot \vec{\mathbf{S}}_2)\overline{J} \\ &= \overline{Q} - \tfrac{1}{2}\overline{J} - 2\overline{J}\vec{\mathbf{S}}_1 \cdot \vec{\mathbf{S}}_2 \end{aligned} \tag{7.22}$$

where $\vec{\mathbf{S}}_1$ and $\vec{\mathbf{S}}_2$ are the spin operators of the individual spins. If we compare this expression with the exchange term of the spin-Hamiltonian :

$$\mathcal{H}_{ex} = -2J_{ex}\vec{\mathbf{S}}_1 \cdot \vec{\mathbf{S}}_2 \tag{7.23}$$

we notice that this spin-Hamiltionian is able to describe the energy separation between the two spin states if we take the exchange constant J_{ex} of the spin-Hamiltonian equal to $\overline{J}$ of the actual physical Hamiltonian. This means that the requirement that the total wave-function is antisymmetric with respect to electron exchange results in an energy separation of the singlet and the triplet state of the dimer and that this energy-separation can be reproduced by the exchange term of the spin-Hamiltonian.

The value of the exchange constant J_{ex} depends strongly upon the overlap-integral S_{ab}. If the overlap between the orbitals is zero — which may be caused by accidental orthogonality — the exchange constant is equal to:

$$J_{ex} = \overline{J} = < \phi_a(1)\phi_b(2)\frac{1}{r_{12}}\phi_b(1)\phi_a(2) > . \tag{7.24}$$

Since this integral is positive, the exchange constant becomes necessarily positive as well and the triplet state is energetically the most stable one. In this case the nature of the exchange coupling is indicated as ferromagnetic. However, normal chemical bonds contain electron pairs of opposite spin and therefore an antiferromagnetic contribution, by which the singlet state is stabilized with respect to the triplet, should be present as well. This antiferromagnetic contribution appears in the situation of non-orthogonal orbitals and the terms which contain the overlap-integrals do contribute as well. If the values of the overlap integral are relatively small we can neglect the higher order terms S_{ab}^2 and S_{ab}^4. Then we can approximate the exchange constant as

$$J_{ex} = \overline{J} \approx < \phi_a(1)\phi_b(2)\frac{1}{r_{12}}\phi_b(1)\phi_a(2) > -2S_{ab} < \phi_a(1)\phi_b(1)\frac{1}{r_{1b}} > . \tag{7.25}$$

It should be noted that now both positive and negative values are possible for the effective exchange coupling constant J_{ex}. This implies that the nature of the spin-spin coupling can be both ferro- and antiferromagnetic which is in agreement with experiment.

7.3 The Heisenberg Exchange Constant for Two Multi-Centre One-Electron Systems

The system we considered up to now consisted of two unpaired electrons located on two identical paramagnetic ions. The energies of the singlet and the triplet states of this symmetric two-electron system can be described with the exchange term of the spin-Hamiltonian and we derived an expression for the exchange constant J_{ex}. In the derivation of this formula we neglected the influence of the closed shell core orbitals. In this section we will consider a dimer consisting of two molecules which may be different. On each of the monomers there is one unpaired electron, which may be delocalized over the complete molecule. For this system we will derive a formula for the exchange coupling between these unpaired electrons within the framework of the Valence-Bond method However, in contrast to our previous derivation we will include the influence of the closed shell orbitals as well.

The Hamilton operator of this dimer is given by:

$$\mathcal{H} = \mathcal{H}_a + \mathcal{H}_b + \mathcal{H}_{ab} \tag{7.26}$$

with

$$\mathcal{H}_a = -\frac{\vec{\nabla}_1^2}{2} - \sum_{\alpha \in a} \frac{Z_\alpha}{r_{1\alpha}} + \sum_{i \subset a} < \psi_i(3) | \frac{1}{r_{13}} (1 - P_{13}) | \psi_i(3) > + \sum_{\alpha_1, \alpha_2 \in a} \frac{Z_{\alpha_1} Z_{\alpha_2}}{R_{\alpha_1 \alpha_2}}, \tag{7.27}$$

$$\mathcal{H}_b = -\frac{\vec{\nabla}_2^2}{2} - \sum_{\beta \in b} \frac{Z_\beta}{r_{2\beta}} + \sum_{j \in b} < \psi_j(3) | \frac{1}{r_{23}} (1 - P_{23}) | \psi_j(3) > + \sum_{\beta_1, \beta_2 \in b} \frac{Z_{\beta_1} Z_{\beta_2}}{R_{\beta_1 \beta_2}} \tag{7.28}$$

and

$$\begin{aligned} \mathcal{H}_{ab} = & \sum_{\alpha \in a, \beta \in b} \frac{Z_\alpha Z_\beta}{R_{\alpha\beta}} - \sum_{\beta \in b} \frac{Z_\beta}{r_{1\beta}} - \sum_{\alpha \in a} \frac{Z_\alpha}{r_{2\alpha}} + \frac{1}{r_{12}} \\ & + \sum_{i \subset b} < \psi_i(3) | \frac{1}{r_{13}} (1 - P_{13}) | \psi_i(3) > \\ & + \sum_{j \in a} < \psi_j(3) | \frac{1}{r_{23}} (1 - P_{23}) | \psi_j(3) > . \end{aligned} \tag{7.29}$$

The summations in these expression run over all atoms α and β of the two molecules a and b and the factor Z_α is the effective charge of the core of atom α. The closed shell orbitals are indicated by ψ_i and ψ_j. The unity operator is designated by 1 and the permutation operator by P_{ij}. The solutions of the Schrödinger-equation are again denoted by ϕ_a for molecule a and ϕ_b for molecule b. Using the expressions of the singlet and triplet wavefunctions of the previous section we can calculate the energies of these states. We obtain the same equations for the energies if we define the coulomb integral Q and the exchange integral J in a slightly different way as:

$$
\begin{aligned}
Q &= <\phi_a^2(1)\frac{1}{r_{12}}\phi_b^2(2)> - \sum_{\beta\in a} <\phi_a^2(1)\frac{Z_\beta}{r_{1\beta}}> - \sum_{\alpha\in b} <\phi_b^2(1)\frac{Z_\alpha}{r_{1\alpha}}> \\
&\quad + <\phi_a^2(1)\left(\sum_{i\in b} <\psi_i(3)|\frac{1}{r_{13}}(1-P_{13})|\psi_i(3)>\right)> \\
&\quad + <\phi_b^2(1)\left(\sum_{j\in a} <\psi_j(3)|\frac{1}{r_{13}}(1-P_{13})|\psi_j(3)>\right)> \qquad (7.30) \\
J &= <\phi_a(1)\phi_b(2)\frac{1}{r_{12}}\phi_b(1)\phi_a(2)> - S_{ab}\sum_{\alpha\in a,b} <\phi_a(1)\phi_b(1)\frac{Z_\alpha}{r_{1\alpha}}> \\
&\quad + S_{ab} <\phi_a(1)\phi_b(1)\left(\sum_{i\in a,b} <\psi_i(3)|\frac{1}{r_{13}}(1-P_{13}|\psi_i(3)>\right)> \qquad (7.31)
\end{aligned}
$$

From these equations we can obtain the experimental exchange constant if we equate J_{ex} with $\overline{J}$ as was shown in the expressions 7.22 and 7.23. We should note that the expression for $\overline{J}$ contains only the electrostatic and exchange interactions between the unperturbed monomer charge distributions. If we want to describe the behaviour of the dimer also at larger distances we have to include the induction and dispersion contributions which are second order in the energy. They result in a Van der Waals attraction at larger distances. The calculation of the first order interaction energy between two monomers with open shells is not straightforward if closed shell orbitals are present as well, because the closed shell orbitals of the two monomers are non-orthogonal. One can solve this problem by the following orthogonalization procedure [3]: First the MO's of each monomer are divided into a group of closed shell orbitals and a group of open shell orbitals. Then, we notice that it is allowed to orthogonalize the closed shell orbitals of the two monomers. Moreover, we can remove the components of the closed shell MO's from the open shell functions, without changing the total dimer wavefunction, by means of a Gram-Schmidt orthogonalization. In this way we have created new closed shell orbitals which are orthogonal with respect to all other orbitals, whereas the open shell orbitals are only orthogonal with respect to the closed shell functions. The open shell orbitals must remain non-orthogonal with respect to each other. If we orthogonalize the open shells we implicitly include charge transfer configurations in our dimer function and the contributions from these configurations must be removed explicitly by a configuration interaction treatment for a correct calculation of the exchange constant.

7.4 The Calculations

In chapter 3 we discussed the results of the EPR and susceptibility measurements on NaBp.2Tg. The experimental data strongly suggested the presence of ferromagnetic as well as antiferromagnetic interactions in the paramagnetic layers of biphenyl anions. Although it is known that the exchange constant depends heavily upon the distance and relative orientation of the paramagnetic centres, the presence of intra-layer couplings of different sign is rather rare in the literature. In order to get more insight in this situation we decided to calculate the exchange interaction between the various possible dimer pairs in NaBp.2Tg. We also computed the exchange constant for the biphenyl anion

pair in RbBp.2Ttg. As the exchange constant of this system is known quite accurately from susceptibility measurements, the calculated value for this system can be used as an indicator for the quality of our computational results.

We tried to get information regarding the sign and magnitude of the exchange constant via two approaches. They both use the monomer wavefunctions as the starting point. In the first approach we calculated the overlap integral as this might be an indicator for the sign of the exchange constant. The second apporach is the computation of the complete expression for $\bar{J}$ as given by the equation 7.20.

The Calculation of the Monomer Wavefunctions

Although the biphenyl molecule (82 electrons) is already quite a large system for the calculation of molecular orbitals by the ab-initio SCF technique, several authors have performed them [8,9] Almlöf, for example, studied the geometry of the biphenyl molecule within the framework of the LCAO-MO method using a Gaussian basisset of double zeta quality and determined the rotation barriers and equilibrium conformation. However, performing an ab-initio SCF calculation on the mono-anion of the biphenyl molecule is quite impossible. It is metastable in the gas-phase and the odd electron is readily ejected from the molecule. This behaviour is reflected in the results of the ab-initio calculations. The unpaired electron is always found in the most diffuse orbital and therefore the orbital coefficients and the properties of the anion depend completely upon the basisset. In contrast to the biphenyl anion in the gas-phase, the anion and even the dianion [10] is stable in alkali-biphenyl solutions in ethers and it is also possible to synthesize single crystals containing the anion. This is possible because the odd electron in these systems is stabilized by the presence of the positive charges of the alkali metal cations complexed with polyethers. Therefore, it is possible to compute the MO of the unpaired electron of the biphenyl anion if we include the neighbouring alkali cation aggregates as well. However, such a calculation is out of reach at the level of the ab-initio SCF method. Therefore, we choose a much simpler but also much faster semi-empirical Extended Hückel method for the calculation of the MO's of the anion. As this method uses some selected chemical information — the Valence State Ionization Potentials — the energies are often better calculated than by the ab-initio method with a minimal basisset. Another advantage (of our implementation) is the use of Slater type orbitals (STO-s) as basisfunctions, instead of Gaussian type orbitals (GTO-s), which result in a better description of the radial dependence of the wavefunctions. The main disadvantage of the Extended Hückel method is the neglect of electron-electron correlation. However, this is advantageous in our case as it allows us to calculate stable molecular orbitals for an isolated biphenyl anion. The basissets we used for the various calculations are the single, double and quadruple zeta functions from Clementi and Roetti [11]. The orbital coefficients c_i and exponents ζ_i are listed in table 7.1. The Wolfsberg-Helmholtz parameter and the VSIP's were taken as usual [12,13].

The Calculation of the Overlap Integral

The equations 7.20 and 7.25 show that the sign and magnitude of the exchange constant J_{ex} depend heavily upon the overlap integral S_{ab}. If the overlap integral equals zero, due

Carbon					
		2s		2p	
		c_i	ζ_i	c_i	ζ_i
$1-\zeta$		1.0	1.60833	1.0	1.56788
$2-\zeta$	: 1	0.761532	1.83068	0.802638	1.25656
	: 2	0.263024	1.15282	0.259459	2.73045
$4-\zeta$	: 1	0.08099	1.05749	0.282409	0.98073
	: 2	0.75045	1.52427	0.546969	1.44361
	: 3	0.33549	2.68435	0.231950	2.60051
	: 4	−0.14765	4.20096	0.010250	6.51003

Hydrogen		
	c	ζ
$1-\zeta$	1.0	1.0

Table 7.1: Basisfunctions for Carbon and Hydrogen

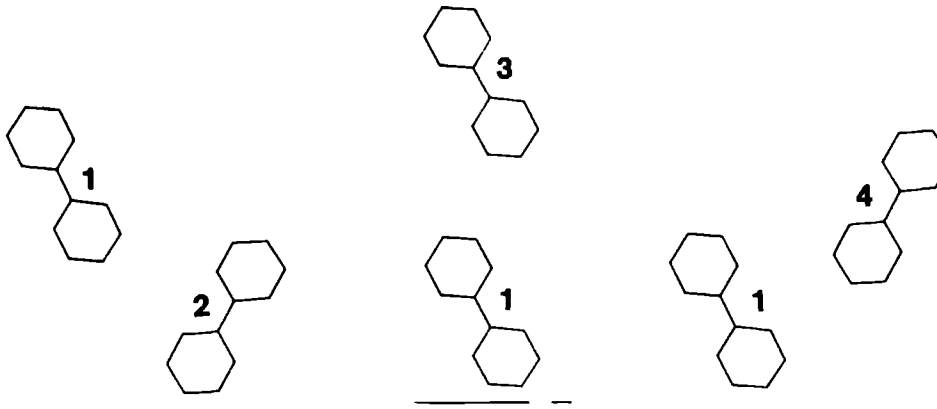

Figure 7.1: The three dimer configurations

to orthogonal MO's, the exchange constant is equal to the two-electron exchange integral and the coupling between the unpaired electrons is always ferromagnetic in nature. On the other hand, if an overlap integral is present, the second contribution dominates in general and the character of the coupling becomes antiferromagnetic. Therefore we planned to calculate the overlap integral as a function of the relative orientation of the biphenyl anions. If the magnitude of this integral should vary strongly with the relative orientations of the anions we are tempted to conclude that ferromagnetic as well as antiferromagnetic couplings exist between the monomers.

As the interaction depends strongly upon the relative distances *and* orientations of the monomers we should in principle calculate the overlap integral varying all degrees of freedom. As we are only interested in the dependence of the integral on the intermolecular orientation we will fix the intramolecular distances and "only" five degrees of freedom remain. For a reasonable description of this 5-dimensional hypersurface we need to calculate N^5 points where N is about 5. Although the calculation of each point is quite fast the complete calculation would still cost too much time. Therefore we restricted the calculations to those orientations we are interested in: the three dimer configurations which occur in the crystal structure of NaBp.2Tg. These three pairs are shown in figure 7.1. As we were interested in the influence of deformations from the ideal symmetry we also did the calculations for an idealized molecule in which D_{2h} symmetry was assigned to each of the two biphenyl anions and the anions were arranged in a coplanar fashion in the dimer. The first approximation seems quite reasonable as the dihedral angle between the two benzene fragments in the biphenyl anions of NaBp.2Tg is only 7.3°. The second approximation may be subject to stronger criticism as the angle between the least-squares plane of the biphenyls and the magnetic plane is about 11° degrees. The computation of the overlap integral occurred in three stages: We started with the computation of the MO's of the monomers. Subsequently we calculated the overlap integrals over atomic orbitals for our dimer configuration and finally the overlap integrals between the MO's of the unpaired electrons were calculated by a two-index transformation of the overlap integrals of the atomic orbitals.

The results are tabulated in table 7.2. If we compare the values of the single zeta calculations for the idealized and the crystal structure in this table we observe large differences, although the trend is the same. This clearly shows that the non-coplanarity of the anions contributes significantly to the overlap integral. These single-zeta results suggest that the coupling of pair 1-4 has more ferromagnetic character than the other two pairs. If we expand our basisset from single-zeta to double-zeta and eventually to quadruple-zeta we notice two changes. 1. The absolute magnitude of the integrals increases. This is the result of a slower decay of the wavefunctions in the long range region. 2. The relative differences between the three configurations become smaller and finally disappear completely. This indicates that the nature of the exchange interaction will be the same for all three pairs. It is clear that our results depend on the choice of the basisset. It seems reasonable to expect that the quadruple-zeta basisfunction describes the radial dependence of the wavefunctions better than the single zeta orbital. This implies that we are not able to draw conclusions from the calculated overlap integrals as they are approximately equal for the three dimers.

Overlap integrals for idealized structure		
Dimer	R_{cc}	$1-\zeta$
$1-2$	7.965	0.242
$1-3$	9.555	0.126
$1-4$	8.532	0.063

Overlap integrals for crystal structure				
Dimer	R_{cc}	$1-\zeta$	$2-\zeta$	$4-\zeta$
$1-2$	8.040	0.146	0.370	0.366
$1-3$	9.555	0.097	0.310	0.327
$1-4$	8.601	0.050	0.250	0.358

Table 7.2: The overlap integral S_{ab} for the three dimer configurations. R_{cc} denotes the distance between the centres of the bridging C-C bonds of the two biphenyl anions.

Complete Calculation of the Exchange Integral

As it is impossible to draw conclusions about the possibility of exchange interactions of different type in NaBp.2Tg from the overlap integrals, we calculated the complete expression of formula 7.20 for the exchange constant. The procedure we used consisted of several steps. As in the above case we started with the calculation of the monomer wavefunctions with the Extended Hückel MO-method. We performed the calculations on the crystal structures and on a D_{2h}-structure for each of the biphenyl anions. For all calculations we used the quadruple zeta basis functions of Clementi and Roetti [11] (table 7.1). In a first approximation we reduced our dimer to a two-electron system neglecting the contribution of the closed shell core orbitals. A problem which we encountered in the evaluation of the one-electron nuclear attraction integrals was the value of the effective charge Z_a of the carbon atoms. In zero-order we should attribute a value of zero to it, as the sum of the closed shell core electrons equals the total nuclear charge. However, as it is possible to synthesize a stable anion in the solid state there seems to be some attraction which means that the effective charge must be greater than zero. This is not unexpected as it is well-known that the screening of the nuclear charge by the core electrons is incomplete for the outer electrons. It is common use to equate the effective charge with the exponent of the single-zeta STO's. This would result in a value for the effective charge of a neutral carbon atom of 1.56788 (= the exponent of the $2p_z$-orbital) However, we think that this value is too large for the effective charge which is felt by the unpaired electron in a biphenyl anion and that a more reasonable value lies somewhere between 0.0 and 1.56788. We arbitrarily choose a value of 1.0.

The calculation of the one- and two-electron integrals was another problem we met. It is well-known that these integrals, especially the three- and four-centre contributions,

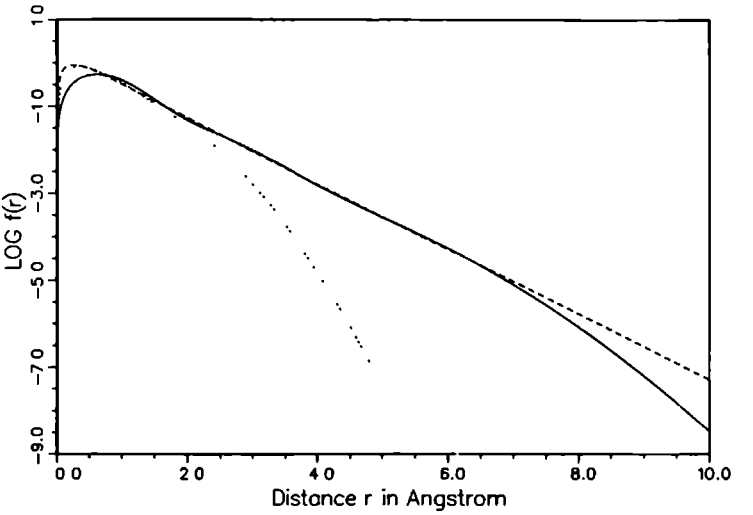

Figure 7.2: Comparison of our (—) and Stewart's expansion (···) of 4-ζ Slater orbital (- - -) of the carbon $2p_z$ functions in three Gaussian functions.

	Long range expansion		Stewart expansion	
	coefficients	exponents	coefficients	exponents
1	0.819712	0.386934	0.162395	2.25977
2	0.243160	0.107660	0.566171	0.57996
3	0.025177	0.044617	0.422307	0.19691

Table 7.3: Coefficients and exponents for 3-GTO fit to 4-ζ STO in the range $1.0 < R < 7.0$ Å. The data of Stewart are listed for reference.

are hard to calculate if one uses Slater type orbitals as basisfunctions. Therefore we expanded the STO's into GTO's. Although the number of basisfunctions becomes much larger by this expansion, the complete calculation is still faster, because the calculation of the individual integrals is much faster. The expansion of STO's into GTO's requires special attention. Many authors calculated expansion coefficients, but they all optimized their coefficients for the region around the nucleus, where the electron density is maximal. We, in contrast, are interested in the long-range region where the overlap between the dimer orbitals is maximal. Therefore, we determined a set of exponents and coefficients ourselves. Each contracted STO was expanded into three GTO's. The coefficients and exponents were obtained by minimizing the error function

$$\epsilon = \int_{1\mathring{A}}^{7\mathring{A}} \left\{ \frac{|\sum_{i=1}^{3} N_i c_i r e^{-\alpha_i r^2} - \sum_{j=1}^{4} N_j c_j r e^{-\zeta_j r}|}{\sum_{j=1}^{4} N_j c_j r e^{-\zeta_j r}} \right\}^{1/2} dr \qquad (7.32)$$

The expansion coefficients and exponents are listed in table 7.3 together with those of Stewart [14] which are optimized for the region near the nucleus. A picture of the fit is shown in figure 7.2. It is clear that the expansion of Stewart is closer to the contracted STO near the nucleus whereas our expansion is better suited for the long range region.

Using this set of exponents and coefficients we calculated all one- and two-centre integrals. The calculations were performed with the ATMOL integral package [15]. The coefficients of the $2s$ functions on carbon and the $1s$ functions on hyfrogen as calculated with the extended Hückel method were small. Therefore, we included only the $2p$-orbitals on the carbon atoms in the calculations of the one- and two-electron integrals. This gave us 72 contracted orbitals for the dimer instead of 116 for a complete basisset containing all valence orbitals. The required integrals over the molecular orbitals were obtained by a transformation of the integrals over the atomic orbitals. We finally calculated the exchange constant by selecting the required integrals over the MO's from the integral files.

The results for the various cases are given in table 7.4. We first notice that the overlap integrals of our expanded functions agree within 10% with the values of the extended Hückel program. This indicates that the 3-GTO expansion of the STO's is sufficiently accurate. Furthermore, we notice that, although the exchange integral dominates in the exchange constant, the contribution of the Coulomb term should be included as well. The results for the calculations on the D_{2h} and the crystal-structure of NaBp.2Tg differ significantly. These differences are the result of different overlap- and exchange-integrals. The value of the Coulomb-integral is approximately the same for all structures. The results indicate that the exchange-coupling in the biphenyl dimer 1-3 is antiferromagnetic, whereas it has a rather high degree of ferromagnetic character in the pair 1-2. The results in the pair 1-4 depend on the structure but they indicate an antiferromagnetic coupling somwhat weaker than in the dimer 1-3. The calculations on the biphenyl anion dimer in RbBp.2Ttg show that the exchange coupling in this system is antiferromagnetic, which is in agreement with experiment. However, the value of the experimental (-13 K, [16]) and calculated (-1.1 K) exchange constant differ by an order of magnitude. This discrepancy shows that the quality of the calculation is quite poor. We were also interested in the

D_{2h}-structure for NaBp.2Tg				
pair	S	J	QS^2	$J_{ex} \approx J - QS^2$
$1-2$	0.302	-0.047	-0.055	0.008
$1-3$	0.391	-0.130	-0.085	-0.045
$1-4$	0.358	-0.079	-0.075	-0.004

D_{2h}-structure for RbBp.2Ttg				
pair	S	J	QS^2	$J_{ex} \approx J - QS^2$
$1-2$	1.225	-1.181	-0.093	-1.088

crystal-structure for NaBp.2Tg				
pair	S	J	QS^2	$J_{ex} \approx J - QS^2$
$1-2$	0.334	-0.061	-0.047	-0.014
$1-3$	0.337	-0.095	-0.042	-0.052
$1-4$	0.336	-0.087	-0.045	-0.042

Table 7.4: The exchange constant J_{ex} for NaBp.2Tg and RbBp.2Ttg. S in 10^{-3}, J, QS^2 and $J_{ex} \approx J - QS^2$ in Kelvin.

D_{2h}-structure for NaBp.2Tg				
pair	V_{ab}	F_{ab}	J : open shells	J : open shells + closed shells
1 – 2	−1.004	0.917	−0.047	0.041
1 – 3	−1.223	1.132	−0.130	0.010
1 – 4	−1.085	1.022	−0.079	0.036

D_{2h}-structure for RbBp.2Ttg				
pair	V_{ab}	F_{ab}	J : open shells	J : open shells + closed shells
1 – 2	−3.707	3.460	−1.181	0.157

Table 7.5: One-electron integrals for the open shell two-electron approximation (V_{ab}) and the open shell two-electron approximation including closed shell contributions (F_{ab}). The values for the contribution of the exchange integral J to the exchange constant J_{ex} are listed as well. V_{ab}, F_{ab} in 10^{-3} a.u., J in Kelvin.

effects of the presence of the closed shell orbitals. Therefore, we also calculated the exchange-integral including the closed shell functions. The results are listed in table 7.5. Inspection of this table shows that the principal effect of the presence of the closed shell orbitals is a shift of the exchange coupling in the positive direction. This result is in agreement with the results of Wormer and Van der Avoird [3] in their calculation on the O_2-O_2 dimer. However, the order of magnitude is not changed by the inclusion of the closed shell orbitals.

Conclusions and possible Improvements

Unfortunately, we are not able to draw firm conclusions about the exchange coupling parameter on the basis of the above mentioned results. However, if we focus our attention on the trends of the calculations we can state that different exchange interactions will be present in the alkali-biphenyl single-crystals. The results strongly suggest an antiferromagnetic interaction in the 1-3 dimer Furthermore, it is suggested that the nature of the exchange constant in dimer 1-2 is more ferromagnetic than in the other two pairs.

Nevertheless, these rather poor results raise the question whether it is possible to improve the calculation of two-electron properties like, for instance, the exchange constant, or not. In order to answer this question we will first repeat the assumptions and approximations we made in the course of our calculation:

- The electrons behave as independent particles.
- The one-electron spin orbitals can be written as a product of a spin- and an orbital wavefunction.

- The correlation between the electrons can be neglected.
- The Na (or Rb) cations, by which the biphenyl anions are stabilized, as well as the polyethers are neglected.
- The molecular orbitals can be calculated by the extended Hückel method.
- Each STO can be expanded into 3 GTO's.
- The carbon $2s$ as well as the hydrogen $1s$ contributions to the MO's of the unpaired electrons may be neglected.

The first change in our calculational procedure should be the inclusion of all valence orbitals. This can be fulfilled rather easily as it only requires small changes in the input file, but it is limited by the amount of available CPU-time. A second, more drastic change would be the inclusion of the neighbouring cations and polyethers in the calculations. This change will greatly increase the dimension of the problem, but it will also result in a better agreement with the physical situation of our system. If one is only interested in the exact value of the exchange coupling one has to perform calculations in which the electron-electron correlations are included like CI [17,3]. However, this type of calculations is absolutely impossible on systems of intermediate size like the biphenyl anion dimer. Therefore, we think that approximate calculations remain necessary in the study the calculation of two-electron properties of larger systems, because it is very important to extent our understanding of the exchange phenomena for the design of new compounds with interesting properties. This means that if the presently available methods do not suffice, one should try to extend them or one should try to develop new approximate methods, based on other assumptions, which may yield better results. In the mean time one should especially study the trends in the exchange constants in a series of substances, instead of concentrating on the absolute value of the exchange constant of a single compound.

Bibliography

[1] W. Heisenberg.
Zeitschrift fur Physik, 49:619, 1928.

[2] P.A.M. Dirac.
Proceedings of the Royal Society A, 123:714, 1929.

[3] P.E.S. Wormer and A. van der Avoird.
Journal of Chemical Physics, 81:1929, 1984.

[4] O. Kahn.
Design of polymetallic systems exhibiting expected magnetic properties.
In *Magneto-Structural Correlations in Exchange-Coupled Systems*, page 57, D.Reidel (Dordrecht), 1985.

[5] P.-O. Lowdin.
Review of Modern Physics, 34:80, 1962.

[6] K.P. Sinha and N. Kumar.
Interactions in magnetically ordered solids.
Oxford University Press (Oxford), 1980.

[7] R. McWeeny and B.T. Sutcliffe.
Methods of Molecular Quantum Mechanics.
Academic Press (London), 1969.

[8] J. Almlőf.
Chemical Physics, 6:135, 1974.

[9] R. Stőlevik and Ő. Thingstad.
Journal of Molecular Structure, 106:333, 1984.

[10] K. Lűhder.
Zeitschrift für Chemie, 9:387, 1969.

[11] E. Clementi and C. Roetti.
Atomic Data and Nuclear Data Tables.
Volume 14, Academic Press (New York), 1974.

[12] C.P. Keijzers, H.J.M. de Vries, and A. van der Avoird.
Inorganic Chemistry, 11:1338, 1972.

[13] C.P. Keijzers and E. de Boer.
Molecular Physics, 29:1007, 1975.

[14] R.F. Stewart.
Journal of Physical Chemistry, 52:431, 1970.

[15] V.R. Saunders and M.F. Guest.
ATMOL.
SERC Daresbury Laboratory, Warrington (United Kingdom).

[16] J.J. Mooij, A.A.K. Klaassen, E. de Boer, H.M.L. Degens, Th.E.M. van den Hark, and J.H.Noordik.
Journal of the American Chemical Society, 98:680, 1976.

[17] M.-F. Charlot, O. Kahn, M. Chaillet, and C. Larrieu.
Journal of the American Chemical Society, 108:2574, 1986.

Chapter 8

The Spin-Orbit Contribution to the Zero Field Splitting Tensor in Weakly Interacting $S = 1/2$ Dimers†

M.C.M. Gribnau and C.P. Keijzers
Department of Molecular Spectroscopy
Research Institute of Materials
University of Nijmegen

Sir:

It is the purpose of this correspondence to clarify the role of the spin-orbit coupling in the Zero Field Splitting (ZFS) tensor of weakly interacting $S = 1/2$ dimers. Moriya [1,2] was the first to derive an analytical expression for this contribution in infinite crystals. In recent years much experimental work [3,4] has been done in order to establish the magnitude of the spin-orbit contribution (which is also called "pseudo-dipolar interaction" or "anisotropic exchange") to the ZFS in weakly coupled copper dimers with oxygen [5,6,7,8,9], sulphur [9,10], fluorine [11], chlorine [12,13] and nitrogen [14,15,16] based bridges. The ZFS consists of two contributions which cannot be measured independently: the dipole-dipole interaction and the spin-orbit contribution. Therefore, the procedure to obtain the spin-orbit contribution is to subtract the calculated dipole-dipole interaction from the experimental ZFS tensor. In the interpretation of the spin-orbit contribution using the theory of Moriya approximations are necessary which are, however, not always valid. In the course of time, the approximate method of interpretation developed a momentum of its own. We have the impression that authors do not always realize that they are using approximate expressions instead of the original exact one of Moriya. The value of the interpretations may, therefore, be very limited. In the following we will first summarize the theory of Moriya. Subsequently we will clarify the nature of the approximations on the basis of an alternative derivation.

† Published in *Inorganic Chemistry* 26:3413,1987

Moriya [1,2] included spin-orbit coupling into Anderson's theory of superexchange [17,18]. Using a third order perturbation treatment in which both the spin-orbit and the isotropic exchange act as perturbations, he derived an expression that was reformulated for dimeric systems by Kanamori [19,20]. It contains terms such as

$$\frac{< g_1 g_2|\vec{\mathbf{L}}_1 \cdot \vec{\mathbf{S}}_1|e_1 g_2 >< e_1 g_2|\mathcal{H}_{ex}|e_1 g_2 >< e_1 g_2|\vec{\mathbf{L}}_1 \cdot \vec{\mathbf{S}}_1|g_1 g_2 >}{(E_e - E_g)^2} \tag{8.1}$$

Here g_1 and g_2 represent the orbital singlet ground states of the monomers with energy E_g, and e_1 is an excited state monomer orbital of energy E_e. The approximation mentioned above is that the term in $\mathcal{H}_{ex}$ is replaced by a simple two-electron exchange integral, while, in fact , it represents a singlet-triplet splitting of an excited state. This approximation is analogous to approximating the singlet-triplet splitting of the dimer ground state by a simple exchange integral. However, Anderson [17,18], and more recently Kahn and coworkers [21], have shown that the singlet-triplet splitting ($2J_0$ in the effective Heisenberg spin-Hamiltonian $-2J_0\vec{\mathbf{S}}_1 \cdot \vec{\mathbf{S}}_2$) in the ground state may, in first order, be calculated according to:

$$2J_0 \;=\; 4tS + 2(j - kS^2) \tag{8.2}$$

where t, S are the one-electron integrals and j, k are two-electron integrals. The approximation $2J_0 = 2j$ is correct only if the monomer orbitals are orthogonal. This means that the approximation mentioned above is valid only if the orbitals e_1 and g_2 are orthogonal, which is highly unlikely for bridged dimers. This orthogonality may be strict as the result of the molecular symmetry or it may be accidental. Both cases are discussed by Kahn and coworkers [22,23].

An analytical expression analogous to the one of Moriya may be derived by second order instead of third order perturbation theory [4,10]. This is a consequence of the fact that we are no longer dealing with an infinite lattice but instead with two spins each with $S = 1/2$. Therefore, it is possible to start from ground and excited singlet ($|\psi_S^n >$) and triplet ($|\psi_T^n >$) states in which the exchange interactions have been included to the highest accuracy possible. The resulting singlet-triplet splitting in the state n is defined as $2J_n$, where J_n is the effective exchange constant in the spin-Hamiltonian $-2J_n\vec{\mathbf{S}}_1 \cdot \vec{\mathbf{S}}_2$. The spin-orbit perturbation is $\mathcal{H}_{SO} = \zeta_1\vec{l}_1 \cdot \vec{s}_1 + \zeta_2\vec{l}_2 \cdot \vec{s}_2$ where ζ_i is the one-electron spin-orbit coupling constant. The second order energy correction to the three triplet ground state functions may be calculated by diagonalizing the matrix with elements

$$E_{ij}^{(2)} \;=\; \sum_n \sum_\sigma \frac{< \psi_{T_i}^0|\mathcal{H}_{SO}|\psi_\sigma^n >< \psi_\sigma^n|\mathcal{H}_{SO}|\psi_{T_j}^0 >}{E_T^0 - E_\sigma^n} \tag{8.3}$$

where the summation σ runs over all (four) spin states of the excited states n. After some algebra this may be written as[¶]

$$E_{ij}^{(2)} \;=\; 2\sum_n \sum_{\alpha,\beta=x,y,z} < \psi_T^0|\zeta_1 l_{1\alpha}|\psi_T^n >< \psi_T^n|\zeta_2 l_{2\beta}|\psi_T^0 > \times$$
$$\left\{ \frac{< T_i|S_{1\alpha}S_{2\beta} - \delta_{\alpha\beta}|T_j >}{E_n + 2J_n} - \frac{< T_i|S_{1\alpha}S_{2\beta} + \delta_{\alpha\beta}|T_j >}{E_n} \right\} \tag{8.4}$$

By comparison with the matrix elements within the ground state triplet manifold of the spin-Hamiltonian $\vec{S}_1 \cdot \vec{\vec{D}}_{SO} \cdot \vec{S}_2$ and after omitting an isotropic contribution, one obtains the tensor elements:

$$\mathbf{D}_{SO,\alpha\beta} = 2\sum_n < \psi_T^0|\zeta_1 l_{1\alpha}|\psi_T^n >< \psi_T^n|\zeta_2 l_{2\beta}|\psi_T^0 > \left\{\frac{1}{E_n + 2J_n} - \frac{1}{E_n}\right\} \quad (8.5)$$

In case $|J_n| \ll E_n$ this can also be written as

$$\mathbf{D}_{SO,\alpha\beta} = -4\sum_n < \psi_T^0|\zeta_1 l_{1\alpha}|\psi_T^n >< \psi_T^n|\zeta_2 l_{2\beta}|\psi_T^0 > \frac{J_n}{{E_n}^2} \quad (8.6)$$

This expression is equivalent to the one derived by Moriya and it shows that the spin-orbit coupling contributes to the ZFS provided that the singlet-triplet splitting in the excited states is not zero. Moreover, this alternative derivation clearly shows that J_n in formula 8.6 is not a simple two-electron exchange integral but instead is the singlet-triplet separation in the excited state. Therefore, we think it dangerous that in recent articles the effective exchange has been treated as a simple exchange integral.

In this context we think it worthwhile to mention another aspect of the analyitcal expression for J_0 mentioned above: the model upon which this expression is based is a two electron description. The effects of the doubly occupied orbitals in the dimer are neglected. They play a role only in so far as they influence the energies and delocalization of the unpaired electron functions. Wormer and Van der Avoird [24] tested this approximation on the O_2-O_2 dimer (two spins $S = 1$). They compared the results of an extensive all electron calculation with a four electron model and found that the orientational dependencies of J_0 are qualitatively the same but quantitatively not so ! The much more economic four electron model turns out to be quite inaccurate. This was also found by Charlot et al. [25] on a model system for azido-bridged copper dimers. A full CI calculation including all core levels was needed in order to understand the behaviour of the singlet-triplet separation in these systems.

In conclusion, we think it is now clear that the spin-orbit term will contribute to the ZFS if an effective exchange interaction is present in the excited states, and that this effective exchange interaction represents a singlet-triplet splitting and is not equal to a simple two-electron exchange integral. Furthermore, extensive all electron calculations are needed in order to obtain quantitatively correct results for the singlet-triplet splittings.

Acknowledgment. This investigation was supported in part by the Netherlands Foundation for Chemical Research (SON) with financial aid from the Netherlands Organization for the Advancement of Pure Research (ZWO).

¶ The isotropic part of expression (4) of *Inorganic Chemistry* 26:3413,1987 is in error. The correct equation is given in expression 8.4.

Bibliography

[1] T. Moriya. Weak ferromagnetism.
In G.T. Rado and H. Suhl, editors, *Magnetism*, page 85, Academic Press (New York), 1963.

[2] T. Moriya.
Physical Review, 120:91, 1960.

[3] R.D. Willett, D. Gatteschi, and O. Kahn, editors.
Magneto-Structural Correlations in Exchange-Coupled Systems.
D.Reidel (Dordrecht), 1985.

[4] C.P. Keijzers. Spin-spin interactions in weakly interacting dimers.
In *Electron Spin Resonance, Specialist Periodical Reports*, page 1, Royal Society of Chemistry (London), 1987, M.C.R. Symons, editor.

[5] A. Bencini, D. Gatteschi, and C. Zanchini.
Inorganic Chemistry, 24:700, 1985.

[6] A. Ozarowski and D. Reinen.
Inorganic Chemistry, 25:1704, 1986.

[7] L. Banci, A. Bencini, and D. Gatteschi.
Journal of the American Chemical Society, 105:761, 1983.

[8] G.F. Kokoszka, H.C. Allen, and G.J. Gordon.
Journal of Chemical Physics, 46:3013, 1967.

[9] J.G.M. van Rens, E. van der Drift, and E. de Boer.
Chemical Physics Letters, 14:113, 1972.

[10] J.G.M. van Rens and E. de Boer.
Chemical Physics Letters, 31:377, 1975.

[11] M.A. Hefni, N.M. McConnell, F.J. Rietmeijer, M.C.M. Gribnau, and C.P. Keijzers.
Molecular Physics, 57:1283, 1986.

[12] C. Chow and R.D. Willett.
Journal of Chemical Physics, 59:5903, 1973.

[13] A. Bencini, D. Gatteschi, and C. Zanchini.
Inorganic Chemistry, 24:704, 1985.

[14] M.L. Boillot, Y. Journaux, A. Bencini, D. Gatteschi, and O. Kahn.
Inorganic Chemistry, 24:263, 1985.

[15] T.R. Felthouse and D.N. Hendrickson.
Inorganic Chemistry, 17:444, 1978.

[16] A. Bencini, D. Gatteschi, C. Zanchini, J.G. Haasnoot, R. Prins, and J. Reedijk.
Inorganic Chemistry, 24:2812, 1985.

[17] P.W. Anderson. Exchange in insulators : superexchange, direct exchange and double exchange.
In G.T. Rado and H. Suhl, editors, *Magnetism*, page 25, Academic Press (New York), 1963.

[18] P.W. Anderson.
Physical Review, 115:2, 1959.

[19] J. Kanamori. Anisotropy and magnetostriction of ferromagnetic and antiferromagnetic materials.
In G.T. Rado and H. Suhl, editors, *Magnetism*, page 127, Academic Press (New York), 1963.

[20] J. Owen and E.A. Harris. Pair spectra and exchange interactions.
In S. Geschwind, editor, *Electron Spin Resonance*, page 427, Plenum Press (New York), 1972.

[21] J.J. Girerd, Y. Journaux, and O. Kahn.
Chemical Physics Letters, 82:534, 1981.

[22] O. Kahn. Design of polymetallic systems exhibiting expected magnetic properties.
In *Magneto-Structural Correlations in Exchange-Coupled Systems*, pages 57–85, D.Reidel (Dordrecht), 1985.

[23] M.-F. Charlot, Y. Journaux, O. Kahn, A. Bencini, D. Gatteschi, and C. Zanchini.
Inorganic Chemistry, 25:1061, 1986.

[24] P.E.S. Wormer and A. van der Avoird.
Journal of Chemical Physics, 81:1929, 1984.

[25] M.-F. Charlot, O. Kahn, M. Chaillet, and C. Larrieu.
Journal of the American Chemical Society, 108:2574, 1986.

Chapter 9

The Calculation of the Dipolar Interaction

9.1 Introduction

As stated in chapter 6 the ZFS tensor is the (tensor-)sum of two other tensors, which arise from completely different physical mechanisms: the spin-orbit coupling and the electron-electron dipolar interaction. In chapter 8 we discussed the calculation of the spin-orbit contribution and there we showed that this interaction only contributes to the ZFS if singlet-triplet splittings are present in the excited states of the system. The results of a study on the calculation of the singlet-triplet splitting were given in chapter 7. From the poor results of these calculations we can conclude that a reliable calculation of the singlet-triplet splitting of the ground state of intermediate and large molecules is still out of reach. This implies that a reasonably accurate calculation of the singlet-triplet splitting in the excited states is quite impossible, which in turn means that we are not able to calculate the spin-orbit contribution to the ZFS. Therefore, it has become almost standard practice to start the analysis of the ZFS by calculating the dipolar contribution. Subsequently, one attributes the difference between the experimental ZFS tensor and the calculated dipolar tensor to the spin-orbit interaction. It will be clear that this procedure can only be successful if the dipolar interaction can be calculated with sufficient accuracy. In this chapter we will discuss the problems which arise in the calculation of the contribution of the dipolar tensor to the ZFS. Furthermore, we will present two computer-programs by which the contributions of the one- and two-centre integrals to the dipolar tensor elements can be calculated. In this way one is able to compute the dipolar tensor with sufficient accuracy and after the above mentioned calculation of the spin-orbit interaction from the experimental ZFS, one can start with the interpretation of the results in order to gain chemical insight.

The General Expression for the Dipolar Tensor Elements

The dipolar coupling tensor originates from the interaction between two localized magnetic dipoles. The classical theory of magnetism supplies the following expression for the energy of two magnetic point-dipoles $\vec{m}_1$ and $\vec{m}_2$ at a distance r_{12} [1].

$$E = \frac{\vec{m}_1 \cdot \vec{m}_2}{{r_{12}}^3} - 3\frac{(\vec{m}_1 \cdot \vec{r}_{12})\ (\vec{m}_2 \cdot \vec{r}_{12})}{{r_{12}}^5} \tag{9.1}$$

The quantum-mechanical analogue of this equation is obtained by replacing the classical quantities by quantum-mechanical operators. The energy is replaced by the Hamilton operator and the magnetic dipole moment is related to the electron spin operator according to [2]

$$\vec{m}_i = -\mu_B \bar{\bar{g}}_i \vec{S}_i. \tag{9.2}$$

if one assumes that the $\bar{g}$-tensor is fixed. These changes result in the expression

$$\mathcal{H}_{dip} = \mu_B^2 \left\{ \frac{\vec{S}_1 \bar{g}_1^T \bar{g}_2 \vec{S}_2}{{r_{12}}^3} - 3\frac{(\vec{S}_1 \bar{\bar{g}}_1^T \vec{r}_{12})(\vec{S}_2 \bar{\bar{g}}_2^T \vec{r}_{12})}{{r_{12}}^5} \right\} \tag{9.3}$$

which can be rewritten as

$$\mathcal{H}_{dip} = \vec{S}_1 \bar{\bar{g}}_1^T \bar{\bar{\bar{D}}}_{12} \bar{\bar{g}}_2 \vec{S}_2 \tag{9.4}$$

where the elements of the dipole-dipole operator $\widehat{D}_{12}$ are given by

$$\widehat{D}_{12,\alpha\beta} = \mu_B^2 \left\{ \frac{\delta_{\alpha\beta}}{{r_{12}}^3} - 3\frac{r_{12,\alpha} r_{12,\beta}}{{r_{12}}^5} \right\} \tag{9.5}$$

and the indices α and β run over the coordinates x, y and z. As the dipolar interaction is only weak as compared to the electronic interactions one can calculate its contribution to the energy by first order perturbation theory:

$$\Delta E^{(1)} = < \psi_T | \mathcal{H}_{dip} | \psi_T > \tag{9.6}$$

$$= < \phi_T \sigma_T | \vec{S}_1 \bar{\bar{g}}_1^T \bar{\bar{\bar{D}}}_{12} \bar{\bar{g}}_2 \vec{S}_2 | \phi_T \sigma_{T'} > \tag{9.7}$$

$$= \mu_B^2 \sum_{\alpha,\beta} < \sigma_T | (\vec{S}_1 \bar{\bar{g}}_1^T)_\alpha < \phi_T | \frac{\delta_{\alpha\beta}}{{r_{12}}^3} - 3\frac{r_{12,\alpha} r_{12,\beta}}{{r_{12}}^5} | \phi_T > (\bar{g}_2 \vec{S}_2)_\beta | \sigma_{T'} > \tag{9.8}$$

By comparison of this term with the first order energy contribution of the spin-Hamiltonian $\vec{S}_1 \cdot \bar{\bar{D}} \cdot \vec{S}_2$ one can derive the following expression for the dipolar interaction tensor

$$\bar{\bar{D}} = \bar{\bar{g}}_1^T < \bar{\bar{\bar{D}}}_{12} > \bar{g}_2. \tag{9.9}$$

For the calculation of this expression one has to evaluate the matrix-elements of the two-electron operator $\widehat{D}_{12}$. If one assumes that the triplet function can be described by Valence-Bond orbitals according to

$$\begin{aligned} \psi_T(1,2) &= \phi_T(1,2)\sigma_T(1,2) \\ &= \frac{1}{\sqrt{2}} \{\phi_I(1)\phi_{II}(2) - \phi_I(2)\phi_{II}(1)\}\, \sigma_T(1,2) \end{aligned} \tag{9.10}$$

where ϕ_I and ϕ_{II} denote the one-electron molecular orbitals and the three triplet spin functions are represented by $\sigma_T(1,2)$, then the tensor elements of the dipole-dipole interaction reduce to

$$< \widehat{D}_{12,\alpha\beta} > = < \psi_T(1,2)|\frac{\delta_{\alpha\beta}}{{r_{12}}^3} - 3\frac{r_{12,\alpha}r_{12,\beta}}{{r_{12}}^5}|\psi_T(1,2) > \quad (9.11)$$

$$= < \phi_I(1)\phi_{II}(2)|\frac{\delta_{\alpha\beta}}{{r_{12}}^3} - 3\frac{r_{12,\alpha}r_{12,\beta}}{{r_{12}}^5}|\phi_I(1)\phi_{II}(2) >$$

$$- < \phi_I(1)\phi_{II}(2)|\frac{\delta_{\alpha\beta}}{{r_{12}}^3} - 3\frac{r_{12,\alpha}r_{12,\beta}}{{r_{12}}^5}|\phi_{II}(2)\phi_I(1) > . \quad (9.12)$$

Subsequently, one can expand the molecular orbitals in sets of atomic orbitals according to

$$\phi_I(1) = \sum_A \sum_{a\in A} c_{Ia}\phi_a^A(1). \quad (9.13)$$

where the summations run over the atomic orbitals a centered on atom A. By substitution of this expression for both molecular orbitals one arrives at the equation

$$< \widehat{D}_{12,\alpha\beta} > = \sum_{A,B,C,D\, a\in A, b\in B, c\in C, d\in D} (c_{Ia}c_{IIb}c_{Ic}c_{IId} - c_{Ia}c_{IIb}c_{Id}c_{IIc}) \times$$

$$< \phi_a^A(1)\phi_b^B(2)|\frac{\delta_{\alpha\beta}}{{r_{12}}^3} - 3\frac{r_{12,\alpha}r_{12,\beta}}{{r_{12}}^5}|\phi_c^C(1)\phi_d^D(2) > \quad (9.14)$$

This is the final expression one has to evaluate for the calculation of the contribution of the electron-electron dipolar interaction to the ZFS. It clearly shows that each tensor element consists of a sum of one-,two-,three- and four-centre integrals. The calculation of these integrals is not completely straightforward, especially as regards the multi-centre terms. In the following we will first discuss the point-dipole approximation to this equation and subsequently we will outline two methods to calculate the one- and two-centre integrals.

The Point-Dipole Approximation

The expression 9.14 is often simplified by assuming that the electrons are localized in well separated regions in space. If this assumption is valid one can replace the distance r_{12} between the two electrons by its average value $< r_{12} >$ in each integral. This results in

$$< \widehat{D}_{12,\alpha\beta} > \approx \sum_{A,B,C,D\, a\in A, b\in B, c\in C, d\in D} (c_{Ia}c_{IIb}c_{Ic}c_{IId} - c_{Ia}c_{IIb}c_{Id}c_{IIc}) \times$$

$$< \phi_a^A(1)\phi_b^B(2)|\phi_c^C(1)\phi_d^D(2) > \left\{\frac{\delta_{\alpha\beta}}{< r_{12} >^3} - 3\frac{< r_{12} >_\alpha < r_{12} >_\beta}{< r_{12} >^5}\right\} \quad (9.15)$$

$$\approx \sum_{A,B} \sum_{a\subset A, b\in B} (c_{Ia}^2 c_{IIb}^2 - c_{Ia}c_{IIa}c_{Ib}c_{IIb}) \left\{\frac{\delta_{\alpha\beta}}{R_{AB}^3} - 3\frac{R_{AB,\alpha}R_{AB,\beta}}{R_{AB}^5}\right\} \quad (9.16)$$

In the derivation of the second expression we approximated the average distance $< r_{12} >$ by R_{AB}. It will be clear that this relation diverges if atom B equals atom A. Therefore,

one assumes that the one-center contribution may be neglected, which is indeed true if the unpaired electrons are located on different monomers. Under these circumstances the value of the term $c_{Ia}c_{IIa}c_{Ib}c_{IIb}$ will also be small with respect to $c_{Ia}^2 c_{IIb}^2$ and therefore it can be neglected. These approximations finally result in the expression

$$< \widehat{D}_{12,\alpha\beta} > \approx \sum_{A,B \neq A} \left(\sum_{a \in A} c_{Ia}^2 \right) \left(\sum_{b \in B} c_{IIb}^2 \right) \left\{ \frac{\delta_{\alpha\beta}}{R_{AB}^3} - 3 \frac{R_{AB,\alpha} R_{AB,\beta}}{R_{AB}^5} \right\} \tag{9.17}$$

which is known as the point-dipole approximation. By this relation the contribution of the dipolar interaction to the ZFS tensor can be calculated in an easy and convenient way. However, this point-dipole approximation is only valid in a limited number of cases. In systems in which the unpaired electrons are delocalized on the same atoms, as, for instance, in halide bridged copper dimers [3,4,5,6,7], one no longer can neglect the one-centre contributions. In these systems one can also doubt the correctness of the replacement of the distance r_{12} in the dipolar operator by its average value. Therefore one also should calculate the two-electron integrals exactly. At this point we will tacitly assume that the contributions of the three- and four-centre integrals are small and therefore can be neglected. This assumption will be valid for atoms which are far apart. However, it still has to be verified for atoms which are close to each other, such as the copper and halide-bridge atoms of the above mentioned systems. If one doesn't want to neglect the contributions of these integrals completely, one can use as a first approximation, for instance, a Mulliken-type approximation [8]:

$$< ab|\hat{O}(1,2)|ss > \approx \frac{S_{ab}}{2}(< aa|\hat{O}(1,2)|ss > + < bb|\hat{O}(1,2)|ss >) \tag{9.18}$$

to approximate them. However, in this work we will neglect these multi-centre terms.

In order to be able to analyze the ZFS-tensor of more complex systems like the halide-bridged copper dimers we designed the computer programs DIPONE and DIPTWO. These programs enable the user to calculate the one- and two-centre contributions to the dipolar tensor of an arbitrary system in the triplet state. In principle, the one- and two-centre contributions to the dipolar tensors for systems in a higher spin-state can be calculated as well. In these systems the tensor elements of the dipolar interaction are the expection value of n-electron wave functions, instead of 2-electron functions as in the triplet state. If one assumes that the n-electron functions can be described as combination of products of one-electron molecular orbitals, these tensor elements reduce to a sum of two-electron terms because of the two-electron character of the dipolar operator and the orthogonality of the one-electron molecular orbitals. These two electron terms can be evaluated by the mentioned programs.

9.2 The Calculation of the One-Centre Contribution

The contribution of the one-centre integrals to the dipolar tensor is given by

$$\begin{aligned} < \widehat{D}_{12,\alpha\beta}^{1-centre} > = & \sum_{A} \sum_{a,b,c,d \in A} (c_{Ia}c_{IIb}c_{Ic}c_{IId} - c_{Ia}c_{IIb}c_{Id}c_{IIc}) \times \\ & < \phi_a^A(1)\phi_b^A(2)|\frac{\delta_{\alpha\beta}}{{r_{12}}^3} - 3\frac{r_{12,\alpha}r_{12,\beta}}{{r_{12}}^5}|\phi_c^A(1)\phi_d^A(2) > \end{aligned} \tag{9.19}$$

The integrals which occur in expression 9.19 may be calculated with the FORTRAN program DIPONE. This program is based on the formulas for the one-centre two-electron spin-spin integrals derived by Matcha, Kern and Schrader[9]. We note that each tensor-element is calculated by a summation of two terms : a term due to the electron-electron dipolar operator and a term from a delta function operator [10,11,12]. This delta-function term is needed to obtain the correct values for the dipolar tensor elements. It is a consequence of the derivation which was used by these authors. One can also derive expressions for the tensor-elements without this delta-function contribution as has been pointed out by Geller [13].

By the formulas of Matcha, Kern and Schrader [9] one can calculate the tensor elements of the *spherical* dipolar interaction tensor on the basis of *complex* Slater type orbitals. In order to keep our computer program compatible with the other programs of our department: The extended Hückel program [14] for the calculation of the electronic structure of molecules as well as the $\overline{\overline{\mathbf{g}}}$, $\overline{\overline{\mathbf{A}}}$ and $\overline{\overline{\mathbf{Q}}}$ tensors of the spin-Hamiltonian and MAGRES [15] for the simulation of ESR,NMR,ENDOR and ESEEM spectra as well as the optimization of spin-Hamiltonian parameters from a set of experimental spectra, we like to obtain the tensor elements of the *cartesian* dipole-dipole tensor on the basis of *real* Slater type functions. This means that we had to perform two transformations. The first conversion concerns the basis-functions of the integrals. We prefer the normalized real Slater type atomic orbitals which are defined as

$$\chi_{nlm}(r,\theta,\phi) = k_n r^{n-1} e^{-\zeta r} S_{lm}(\theta,\phi), \tag{9.20}$$

where the normalization constant k_n is defined as

$$k_n = \frac{(2\zeta)^{n+1/2}}{\sqrt{(2n)!}}. \tag{9.21}$$

and the functions $S_{lm}(\theta,\phi)$ denote the tesseral harmonics. The normalized complex Slater type functions differ in so far from their real counterparts as that the real tesseral harmonics are replaced by complex spherical harmonics $Y_{lm}(\theta,\phi)$. These functions are related to each other according to

$$\begin{aligned} S_{l,|m|} &= \frac{1}{\sqrt{2}}\left\{(-1)^{|m|}Y_{l,|m|} + Y_{l,-|m|}\right\} \\ S_{l,0} &= Y_{l,0} \\ S_{l,-|m|} &= \frac{-i}{\sqrt{2}}\left\{(-1)^{|m|}Y_{l,|m|} - Y_{l,-|m|}\right\}. \end{aligned} \tag{9.22}$$

The second transformation is related to the calculated dipolar tensors. In our program the spherical dipolar tensor is calculated. A spherical tensor is a tensor which is calculated on the basis of complex spherical harmonics, whereas a cartesian tensor is calculated on the basis of the functions x, y and z [16]. One can convert the calculated spherical dipolar tensor into a cartesian tensor by a simple transformation. The necessary conversions are performed inside the program.

The main features of DIPONE can be summarized as follows. The program is written in FORTRAN and it is able to compute the following three types of one-centre electron-electron dipolar integrals:

1. All possible integrals $< \phi_{nlm}(1)\phi_{n'l'm'}(2)|\frac{\delta_{\alpha\beta}}{r_{12}^3} - 3\frac{r_{12\,\alpha}r_{12\,\beta}}{r_{12}^5}|\phi_{n'',l'',m''}(1)\phi_{n''',l''',m'''}(2) >$, where ϕ_{nlm} denotes a complex Slater type orbital characterized by the quantum numbers n, l and m (Spherical option) These integrals are calculated with the expressions of Matcha, Kern and Schrader [9] The necessary equations are listed in the appendix of this chapter

2 The integrals $< \phi_a(1)\phi_b(2)|\frac{\delta_{\alpha\beta}}{r_{12}^3} - 3\frac{r_{12\,\alpha}r_{12\,\beta}}{r_{12}^5}|\phi_c(1)\phi_d(2) >$ over all combinations of real STO's (Cartesian option) These integrals are computed by a combination of dipolar integrals on the basis of complex STO's

3 The integrals over molecular orbitals according to the expression 9 19 (MO-option) These integrals are calculated by combining the necessary integrals over real STO's

To prevent incorrect results due to programming errors we paid much attention to the debugging of the program The output of the fundamental integrals over the complex Slater orbitals were carefully compared with the results of Pritchard and Kern [17] The results of the other integrals were checked by comparing them with the output of the fundamental integrals over the complex STO's

9.3 The Calculation of the Two-Centre Integrals

The contribution of the two-centre integrals is given by

$$\begin{aligned} < \widehat{D}_{12\,\alpha\beta}^{2-centre} > \;=\; & \sum_{A\;B\neq A} [AA|\widehat{D}_{12}|AB] + [AA|\widehat{D}_{12}|BA] \\ & + [AB|\widehat{D}_{12}|AA] + [AA|\widehat{D}_{12}|BB] \\ & + [AB|\widehat{D}_{12}|AB] + [AB|\widehat{D}_{12}|BA] \\ & + [AB|\widehat{D}_{12}|BB] \end{aligned} \tag{9 23}$$

with

$$\begin{aligned} [AB|\widehat{D}_{12}|CD] \;=\; & \sum_{a\subset A\;b\subset B\;c\in C\;d\in D} (c_{Ia}c_{IIb}c_{Ic}c_{IId} - c_{Ia}c_{IIb}c_{Id}c_{IIc}) \times \\ & < \phi_a^A(1)\phi_b^B(2)|\frac{\delta_{\alpha\beta}}{r_{12}^3} - 3\frac{r_{12\,\alpha}r_{12\,\beta}}{r_{12}^5}|\phi_c^C(1)\phi_d^D(2) > \end{aligned} \tag{9 24}$$

In principle one can compute the contributions of the two-centre integrals in the same way as the one-centre integrals, because Matcha, Kern and Schrader [9] also derived expressions for the two-centre integrals over complex Slater functions However, these expressions are even more complex as the one-centre formula's and they are not completely exact, i e they require a numerical integration procedure over two dimensions Moreover, the number of possible combinations of two-centre terms is very large which would result in highly time-consuming computations Therefore, we decided to calculate the two-centre contributions by numerical methods The advantage of this approach is that we have to perform the integration only once, since we can include the

contribution of all atomic orbitals at the same time. A disadvantage is that we have to perform a numerical integration in six dimensions which requires a lot of integration points. Nevertheless, we expect that the numerical integration is quite a bit faster than a summation of all combinations of two-centre integrals.

Each matrix-element can be calculated by the summation of a number of integrals of the type

$$I_{\alpha\beta} = \iiint d\vec{\mathbf{r}}_1 \iiint d\vec{\mathbf{r}}_2 f_1(\vec{\mathbf{r}}_1) f_2(\vec{\mathbf{r}}_2) \left\{ \frac{\delta_{\alpha\beta}}{{r_{12}}^3} - 3\frac{r_{12,\alpha} r_{12,\beta}}{{r_{12}}^5} \right\} \tag{9.25}$$

where $f_1(\vec{\mathbf{r}}_1)$ and $f_2(\vec{\mathbf{r}}_2)$ are products of one-electron functions like

$$\left\{ \sum_{a \in A} c_{Ia} \phi_a^A(1) \right\} \left\{ \sum_{c \in C} c_{IIc} \phi_c^C(1) \right\} \tag{9.26}$$

The analytical integration of the expression 9.25 is performed by a weighted summation over the function values for a selected grid of integration points. The integration over the six-dimensional space of the two-electrons can be divided into two integrations over three dimensions for each electron. One can use a different grid for each electron or one can use the same grid for both electrons. The first choice is simpler as the electrons never coincide, i.e. one never has to evaluate the integrand for $\vec{\mathbf{r}}_{12} = 0$. Although this approach seems very attractive, it turns out to be less favourable, because the integration converges only very slowly upon increasing the number of integration points. The better, much faster converging method uses the same integration grid for both electrons. In this case, one has to take care of the singular points, i.e. the points for which $\vec{\mathbf{r}}_{12} = 0$ and the two-electron operator goes to infinity. Because of the antisymmetric character of the triplet wavefunction the contributions of these volume elements should remain finite, as has been shown by McConnell [18]. Therefore, we can simply skip these integration points. The correctness of this procedure was confirmed by comparing the results of the numerically integrated one-centre contributions (calculated with DIPTWO) with the values of the exactly integrated one-centre contributions (calculated with DIPONE).

The numerical integrations were performed by means of two Gauss-quadrature methods [19,20,21]. These methods require only a small number of integration points for highly accurate results. The integration in these methods is performed according to the scheme

$$\int_a^b W(x) f(x) dx \approx \sum_{i-1}^{N} w_i f(x_i). \tag{9.27}$$

The weight function $W(x)$ and thereby the weights w_i and the abscissas x_i are chosen as to make the integration exact for a certain class of functions. The integration is exact if $f(x)$ is a polynomial of degree less or equal to $2N - 1$. In regions where we expect an exponentially decaying function we used the Gauss-Laguerre method with adjusted weights ($W(x) = \exp(-bx)$), whereas we used the Gauss-Legendre method ($W(x) = 1$) in area's where the functions change more slowly. The values for the weights w_i and the abscissas x_i can be calculated or, alternativily, be found in tables [22]. The Gauss-Laguerre integration with adjusted weights contains an adjustable parameter b. This parameter influences the convergence rate. As a first approximation one can take two

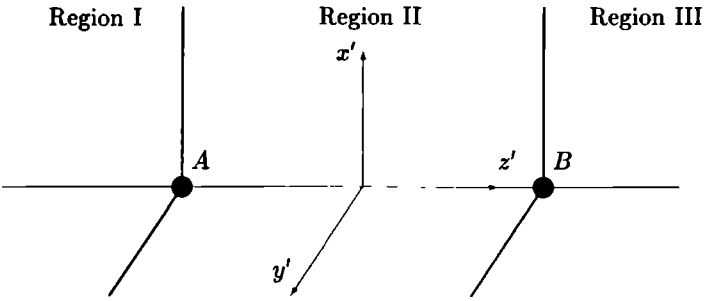

Figure 9.1: Definition of the x', y', z'-axis system for the numerical integration procedure for the two-centre integrals.

times the average of the exponents of the STO's for this parameter. A better method is to calculate the one-centre contributions exactly for the two atoms and compare these values with the results of the numerical integration procedure for different b and N and to take the value for b which gives the best agreement for the lowest value of N.

The computational procedure which is followed in the program DIPTWO can be summarized as follows:

- A local axis system x', y', z' which is connected to the two atoms A and B is calculated. In this local axis system the z' axis lies parallel to the $\vec{\mathbf{R}}_{AB}$-axis, whereas the other two directions are chosen perpendicular to this axis.

- The local axis system is divided into three regions as sketched in figure 9.1. The boundaries of these regions are tabulated in table 9.1. For each direction of each region a suitable integration method is taken. Then the number of integration points is chosen and the values of the weights w_i and abscissas x_i are calculated. The methods we used for the various directions are listed in table 9.1 together with the number of integration points needed.

- For each integration point the value of the one-electron molecular orbitals is calculated according to expression 9.13. In order to obtain an impression about the quality of the numerical integration we also computed the one-electron integrals $< \phi_a(1)|\phi_a(1) >$ and $< \phi_b(2)|\phi_b(2) >$ for all orbitals on the atoms A and B. These integrals are normally equal to 1 within parts of a percent for the light atoms and within a few percent for the double zeta orbitals of transition-metal atoms.

- Finally the actual integration is performed by a weighted summation over six dimensions. For both electrons the same integration grid is used. The singular points are simply skipped.

Region	Integration method	N
I		
$-\infty < x' < \infty$	2 × Gauss-Laguerre	2 × 6
$-\infty < y' < \infty$	2 × Gauss-Laguerre	2 × 6
$-\infty < z' < -\frac{1}{2}R_{AB}$	1 × Gauss-Laguerre	1 × 6
II		
$-\infty < x' < \infty$	2 × Gauss-Laguerre	2 × 6
$-\infty < y' < \infty$	2 × Gauss-Laguerre	2 × 6
$-\frac{1}{2}R_{AB} < z' < \frac{1}{2}R_{AB}$	Gauss-Legendre	12
III		
$-\infty < x' < \infty$	2 × Gauss-Laguerre	2 × 6
$-\infty < y' < \infty$	2 × Gauss-Laguerre	2 × 6
$\frac{1}{2}R_{AB} < z' < \infty$	1 × Gauss-Laguerre	1 × 6

Table 9.1: Boundaries of the three integration regions and the Gauss-quadrature used in the different directions of these regions. N is an estimate of the number of integration points needed.

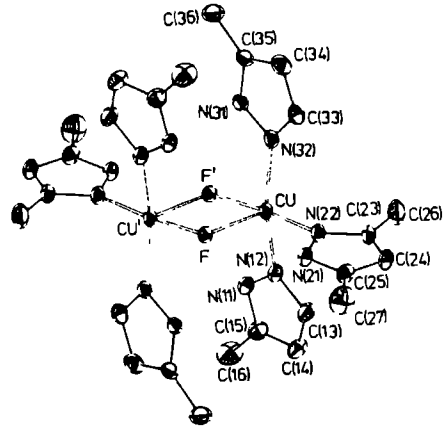

Figure 9.2: ORTEP-drawing of the structure of $[Cu_2F_2(dmpz)_2(mpz)_4](BF_4)_2$ -cation.

MO	Occupation	Symmetry	Energy	Cu-coefficients	F-coefficients
87	2	g	-10.54	$0.70d_{zz}$	
88	2	u	-10.45	$0.70d_{zz}$	
89	2	u	-10.40	$0.24d_{yz} + 0.65d_{xy}$	
90	2	g	-10.38	$0.26d_{yz} + 0.65d_{xy}$	
91	2	u	-10.36	$0.64d_{yz} - 0.24d_{xy}$	
92	2	g	-10.31	$0.63d_{yz} - 0.25d_{xy}$	
93	2	g	-10.17	$0.10s + 0.68d_{z^2}$	$-0.09p_z$
94	2	u	-10.04	$0.12s + 0.68d_{z^2}$	
95	1	g	-7.20	$0.62d_{x^2-y^2} + 0.17p_z$	$0.09p_z + 0.14p_x$
96	1	u	-6.73	$0.64d_{x^2-y^2} + 0.05p_z$	$0.11s - 0.14p_x$
97	0	u	-4.25	$0.10d_{x^2-y^2} - 0.19p_z$	

Table 9.2: Energies (eV), occupation numbers, symmetry (g = gerade, u = ungerade) and main coefficients of the highest occupied molecular orbitals of $[Cu_2F_2(dmpz)_2(mpz)_4](BF_4)_2$.

9.4 The Dipolar Contribution to the ZFS-Tensor in Halide Bridged Copper Dimers

We will use the above described programs DIPONE and DIPTWO for the calculation of the dipolar contributions to the ZFS of bridged transition-metal compounds. These systems are used for the study of the interactions between unpaired electrons. The activities in this field have resulted in a large number of EPR studies on bridged copper(II)-dimers [3,23,24,4,5,25,6,26,27]. In these studies special attention was paid to the isotropic exchange constant J_{ex}, which is connected to the singlet-triplet splitting of the ground state and the ZFS of the lowest triplet state. These spin-Hamiltonian parameters depend on the nature of the bridging ligands and, within a series of equal bridges, are dependent on the details of the molecular structure. In non-bridging dimers, which consist of two separated monomers the largest principal value of the ZFS is expected along the Cu-Cu' direction. This direction was indeed found in studies on the dimers of copper(II)bis(diethyldithiocarbamate) [28] and copper(II)bis(malconitriledithiolate) [29]. However, in all bridged dimers, the largest principal value of the ZFS tensor was reported to be oriented perpendicular to the Cu-Cu' axis. This unexpected orientation was attributed to the spin-orbit contribution of the ZFS. However, before one can justify this conclusion one should carefully calculate the dipolar contribution, because the ZFS can be affected to a large extent if the two unpaired electrons are significantly delocalized, because of the $r_{12}{}^{-3}$ dependence of the dipole-dipole interaction. In this paragraph we will analyze the dipolar tensor of a fluoride bridged copper(II)-dimer $[Cu_2F_2(dmpz)_2(mpz)_4](BF_4)_2$.

Moreover, we will discuss some results of a model study on two chloride bridged copper dimers.

$[Cu_2F_2(dmpz)_2(mpz)_4](BF_4)_2$

Single crystals of $[Cu_2F_2(dmpz)_2(mpz)_4](BF_4)_2$ were recently grown by Ten Hoedt et al. [30]. A picture of the crystal structure of this compound — which was solved by the same authors — is shown in figure 9.2. The two copper atoms are located at a distance of 3.131 Å. They are connected by two asymmetric fluoride bridges: The shorter Cu-F' distance is equal to 1.904 Å, whereas the longer Cu-F distance equals 2.258 Å. The F-Cu-F' angle is 83° and the Cu-F-Cu' angle equals 97°. We calculated the electronic structure of this compound with a semi-empirical extended-Hückel calculation [7,14]. We defined the shorter Cu-F axis as the z-axis. The y-axis was taken perpendicular to the Cu_2F_2-plane. The two parameters in the Hamilton matrix were taken equal to those which were obtained by optimizing the results for the monomeric copper(II)bis(diethyldithiocarbamate) [31]. The data of the most relevant orbitals are listed in table 9.2. Using these data the $\overline{\mathbf{g}}$-tensor of the triplet state was calculated. This calculated tensor showed a very satisfactory agreement with the experimental one [7], indicating that the calculated MO's describe the molecule reasonably well. The picture that emerges from this extended Hückel calculation is that the unpaired electrons are located in the copper $3d_{x^2-y^2}$ orbitals with very little delocalization to the fluoride bridges. This implies that the Cu-Cu' interaction is still the largest contribution to the dipolar part of the ZFS-tensor. The one-centre F contributions will be small whereas the one-centre Cu and the two-centre Cu-F integrals can be larger. The calculated contributions of the one- and two-centre dipolar integrals are presented in table 9.3. The data in this table show that the two-centre contributions are dominating. The fluor one-centre integrals are negligibly small whereas the copper one-centre integrals contribute approximately 10% of the total dipolar interaction. Surprisingly, the largest principal value is hardly affected by the delocalization as opposed to the asymmetry parameter $|(D_2 - D_3)/D_1|$ which increases from 0 to 0.19. The difference between the calculated and experimental tensor is still large. Depending on the sign of the experimental tensor the difference tensor is roughly { +271(∼Cu-Cu', +180, -451(∼⊥)} or { 885(∼Cu-Cu'), -636, -249(∼⊥)}. This difference is often attributed to the spin-orbit contribution to the ZFS. As shown in chapter 8 this contribution is approximately equal to $2J_n\lambda^2/\Delta E^2$, where $2J_n$ are the singlet-triplet splittings in the excited states, λ the spin-orbit couplings parameter (828 cm^{-1} for copper $3d$-electrons) and ΔE the excitation energy $E_n - E_0$ which is of the order of 10^4 cm^{-1}. The singlet-triplet splittings in the excited states are rarely known and, therefore, they are usually assumed to be of the same order of magnitude as the corresponding splitting in the ground state, ~ 0.75 cm^{-1} in $[Cu_2F_2(dmpz)_2(mpz)_4](BF_4)_2$ [7]. Using the mentioned values one can estimate that the spin-orbit contribution is of the order of $50 \cdot 10^{-4}$ cm^{-1}, much smaller than either of the two possible difference tensors. Therefore, the spin-orbit contribution can only explain the difference between the experimental and calculated ZFS tensor if the singlet-triplet splitting in the first few excited states is an order of magnitude larger than in the ground state.

		Calculated				Experimental			
		Principal values	Principal axes			Principal values	Principal axes		
			Cu-Cu'	F-Cu	⊥		Cu-Cu'	F-Cu	⊥
A	D_1	−566	0	37	90				
	D_2	283	90	†					
	D_3	283	90	†					
B_1	D_1	−64	53	16	92				
	D_2	30	38	74	84				
	D_3	34	87	90	174				
B_2	D_1	−12	3	40	90				
	D_2	1	93	130	90				
	D_3	11	90	89	1				
B_3	D_1	−551	6	32	90				
	D_2	246	96	58	90				
	D_3	305	90	90	0				
B_4	D_1	−578	9	28	90	∓307	12	28	85
	D_2	228	99	62	90	±408	101	65	74
	D_3	350	90	89	1	∓101	92	102	16

†Axial tensor: the angles are undefined

Table 9.3: Calculated and experimental dipolar tensor of $[Cu_2F_2(dmpz)_2(mpz)_4](BF_4)_2$ for the spin-Hamiltonian $\vec{S} \cdot \overline{\overline{D}} \cdot \vec{S}$. A: Unpaired electrons localized on copper . B: Unpaired electrons delocalized (equation 9.17). B_1: One centre Cu (DIPONE). B_2: One-centre F (DIPONE). B_3: Total two-centre contribution (DIPTWO). B_4: Summed one- and two-centre contributions by tensor-addition. Principal axes in degrees, principal values in $10^{-4}cm^{-1}$.

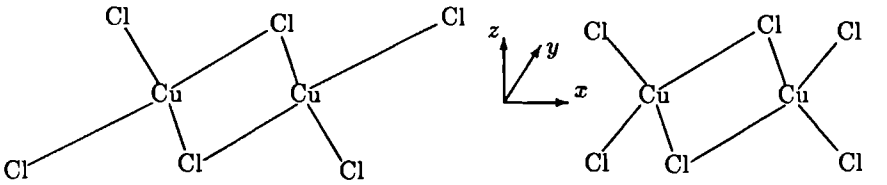

Figure 9.3: The structures of the two $Cu_2Cl_6^{2-}$ model systems

MO	Symmetry	Cu-coefficients	μ-Cl-coefficients
Planar coordinated structure			
1	u	$0.61d_{xy} + 0.05p_y$	$0.38p_x$
2	g	$0.63d_{xy} + 0.02p_y$	$-0.16s + 0.30p_y$
Tetrahedrally coordinated structure			
1	u	$0.63d_{xy} + 0.13p_y$	$0.05s - 0.30p_y$
2	g	$0.64d_{x^2-y^2} + 0.13p_z$	$-0.23p_z$

Table 9.4: Symmetry (g = gerade, u = ungerade) and main coefficients of the single occupied molecular orbitals of two model structures of $Cu_2Cl_6^{2-}$.

Two $Cu_2Cl_6^{2-}$ model systems

The above results on $[Cu_2F_2(dmpz)_2(mpz)_4](BF_4)_2$ suggest that the dipolar tensor is only changed to a minor degree if one calculates the one- and two-centre contributions as exactly as possible instead of by the point-dipole approximation. In order to show that this isn't true in all cases, we performed a set of calculations on two $Cu_2Cl_6^{2-}$ anions. For the first anion we assumed a D_{2h} structure with all atoms in the xy-plane. We arbitrarily took a Cu-Cu distance of 3.4 Å, whereas the distances for the four Cu-μ-Cl bonds were taken as 1.55 Å. For the second structure we used the same atom-atom distances. The only difference concerns the four terminating chloride atoms which were rotated by 90 degrees. In the first structure each copper atom is approximately square-planar coordinated by the chloride atoms and in the second structure the copper atoms are approximately tetrahedrally coordinated by the chloride anions. The two structures are shown in figure 9.3. In analogy to our calculations on the fluoride bridged copper(II)-dimer we started our analysis by calculating the one-electron MO's with an extended Hückel calculation. Subsequently, we calculated the one- and two-centre contributions for these model systems with the programs DIPONE and DIPTWO. The coefficients of the MO's of the unpaired electrons are tabulated in table 9.4. In the planar structure both unpaired electrons are located in d_{xy}-orbitals; they are significantly delocalized onto the bridging chloride atoms. In the tetrahedral compound one unpaired electron is located in a d_{xy} orbital, whereas the other electron occupies a $d_{x^2-y^2}$-function. In this structure the unpaired electrons are also significantly delocalized towards the bridging chloride atoms. In table 9.5 the

calculated one- and two-centre dipolar terms are listed. The two-centre contributions were calculated by three different methods: 1. A localized point-dipole approximation. Here, we assumed that the electrons remain localized on the two copper atoms; every copper atom bears one unpaired electron. 2. A delocalized point-dipole approximation. In this case the dipolar contribution was calculated according to equation 9.17. 3. A calculation using numerical integration. This calculation was carried out with the program DIPTWO ($N_{\text{Legendre}} = 12, N_{\text{Laguerre}} = 9, b = 4.75$). The calculated direction of the vector belonging to the largest principal value lies for all three cases of both structures along the x-axis. However, the magnitude of the principal values and especially the the asymmetry parameter of the tensors show significant variations. The magnitude of the largest principal value of the last calculation agrees within about 10% with the localized point-dipole calculation. The deviations from the delocalized point-dipole calculations are, however, much larger. The asymmetry parameter changes from 0 for the localized electron approximation via 0.87 for the delocalized electron approximation to 0.60 for the tensor obtained by numerical integration. For the other structure these values are 0, 0.38 and 0.15, respectively. From these results we can conclude that the only methods which yield reliable values for the two-centre terms are based on (numerical) integration of the terms in expression 9.23. As regards the one-centre contributions, these terms are completely neglected in the point-dipole calculations. The data in table 9.5 clearly show that this neglect isn't correct. In the planar structure the bridging chloride atoms contribute about 20% of the total dipolar tensor. The contribution of the copper one-centre terms is very small. This picture is completely different for the tetrahedral structure. In this case the copper one-centre term is so large that the total dipolar tensor is completely dominated by this term. The largest principal value lies along the x-axis, but is of the opposite sign as compared to the two-centre terms. The large value for this one-centre term is due to the fact that the two molecular orbitals of the two unpaired electrons are dominated by atomic orbitals of different symmetry. The conclusion of these calculations is that in bridged transition-metal dimers one cannot calculate the dipolar tensor with one of the point-dipole approximations. The one-centre as well as the two-centre terms should be calculated by integration of the various terms.

	Planar structure			Tetrahedral structure		
	x	y	z	x	y	z
Localized point-dipole approximation						
Cu–Cu	−883.2	441.6	441.6	−883.2	441.6	441.6
Delocalized point-dipole approximation						
Cu-Cu	−529.6	264.8	264.8	−313.0	156.5	156.5
All	−1001.8	64.4	937.3	−587.4	181.8	405.4
One-centre contributions (DIPONE)						
Cu	1.1	−4.0	2.9	10772.0	−5385.5	−5386.5
μ-Cl	−101.4	−35.6	137.0	42.2	−19.7	−22.4
One-centre contributions (DIPTWO)						
Cu	0.9	−3.9	3.0	18006.0	−9002.5	−9003.5
μ-Cl	−107.5	−38.0	145.5	44.8	−21.0	−23.8
Two-centre contributions (DIPTWO)						
Cu–Cu	−572.0	275.9	296.1	−324.9	172.0	152.9
All	−845.6	171.5	674.1	−798.7	338.3	460.4
Total dipolar tensor (DIPONE + DIPTWO)						
All	−1046.2	92.3	953.9	20829.7	−10472.1	−10357.4

Table 9.5: Calculated one and two centre contributions to the dipolar tensors for a planar and tetrahedrally coordinated Cu_2Cl_6 model system for the spin-Hamiltonian $\vec{S}_1 \cdot \overline{\vec{D}} \cdot \vec{S}_2$. Principal values in 10^{-4}cm ^{1}.

9.5 Conclusion

The study described in this chapter was inititated in order to explain the anomalous direction of the largest principal value of the ZFS tensor in halide bridged copper dimers. It will be clear from the above mentioned results that we haven't reached our goal:The direction of the largest principal value of the dipolar tensor was found to lie parallel to the x-axis for $[Cu_2F_2(dmpz)_2(mpz)_4](BF_4)_2$ as well as the two $Cu_2Cl_2^{2-}$ model systems. instead of perpendicular to this axis. From these results one could conclude that the anomalous direction is a consequence of a large contribution from the spin-orbit coupling to the ZFS tensor. However, if we recall the results of van Rens and de Boer on a sulphur bridged copper dimer and a sulphur bridged silver dimer we note that ZFS in the copper dimer could be well explained by the dipolar interaction, whereas only about 50% of the splitting in the silver dimer was due to the contribution of the spin-orbit interaction. This

difference is the result of the increased value of the spin-orbit parameter for silver (λ = 1794 cm^{-1} for the 4*d* electrons) as compared to copper (λ = 828 cm^{-1} for 3*d* electrons). Of course, the structures of these sulphur bridged compounds show important differences as compared to the halide bridged copper dimers. But, if we estimate the strength of the spin-orbit contribution for these halide bridged dimers we obtain a value which is an order of magnitude too small. Therefore, one can conclude that the spin-orbit interaction gives only rise to a significant contribution to the ZFS, if the singlet-triplet splittings of the first few low-lying excited states is an order of magnitude larger than in the ground state. An alternative to this explanation might be that the excited states are mixed into the ground state by configuration interaction and that as a result of this mixing significant one-centre contributions to the dipolar tensor arise, which do not point along the Cu-Cu' axis. However, at the moment we are not able to draw definite conclusions as regards the origin of the anomalous direction of the largest principal value of the ZFS.

Appendix

The basic integrals that are calculated are the expectation values of the spherical tensor-elements $< \mathcal{H}_{ss}^{-\alpha\alpha'} >$ [9,17]. Every matrix element of this tensor can be expressed as a sum of products over the functions $G_\kappa^{-\alpha\alpha'}$ and $H_{\zeta_1\zeta_2}^\kappa$:

$$\begin{aligned} < \mathcal{H}_{ss}^{-\alpha\alpha'} > &= \sum_{\kappa_{min1,2}}^{\kappa_{max1}} [G_\kappa^{-\alpha\alpha'}(\kappa+1,\kappa-1,m'-m-\alpha)H_{\zeta_1\zeta_2}^\kappa(n_1,n_2) \\ &+ \sum_{\kappa_{min2,2}}^{\kappa_{max2}} G_\kappa^{-\alpha\alpha'}(\kappa-1,\kappa+1,m'-m-\alpha)H_{\zeta_2\zeta_1}^\kappa(n_2,n_1)] \end{aligned} \tag{9.28}$$

The limits on the summation over κ are given by

$$\begin{aligned} \kappa_{min1} &= \text{maximum}\{|l-l'|-1, |l''-l'''|+1, |m''-m'''|+1\}, \\ \kappa_{max1} &= \text{minimum}\{l+l'-1, l''+l'''+1\}, \\ \kappa_{min2} &= \text{maximum}\{|l-l'|+1, |l''-l'''|-1, |m-m'|+1\}, \\ \kappa_{max2} &= \text{minimum}\{l+l'+1, l''+l'''-1\}. \end{aligned}$$

and the terms $n_1, n_2, \zeta_1, \zeta_2$ are defined as

$$\begin{aligned} n_1 &= n''+n''', \\ n_2 &= n+n', \\ \zeta_1 &= \zeta''+\zeta''', \\ \zeta_2 &= \zeta+\zeta'. \end{aligned}$$

The function $G_\kappa^{-\alpha\alpha'}$ is related to the functions $T_\kappa^{-\alpha\alpha'}$ according to

$$\begin{aligned} G_\kappa^{-\alpha\alpha'}(\lambda,\lambda',q) &= (-)^{m''+m'+\alpha'} k(n'',n''';\zeta'',\zeta''') T_\kappa^{-\alpha\alpha'}(\lambda,\lambda',q) \times \\ &\sqrt{\frac{1}{2}(2l''+1)(2\lambda'+1)(2l'''+1)} \times \\ &\begin{pmatrix} l'' & \lambda' & l''' \\ m'' & -(\alpha'+q) & -m''' \end{pmatrix} \begin{pmatrix} l'' & \lambda' & l''' \\ 0 & 0 & 0 \end{pmatrix}. \end{aligned} \tag{9.29}$$

The constant $k(n,n';\zeta,\zeta')$ in this expresssion is equal to

$$k(n,n';\zeta,\zeta') = \frac{(2\zeta)^{n+1/2}(2\zeta')^{n'+1/2}}{\sqrt{(2n)!(2n')!}} \tag{9.30}$$

and the functions $T_\kappa^{-\alpha\alpha'}$ are given by

$$\begin{aligned} T_\kappa^{-\alpha\alpha'}(\lambda,\lambda',q) &= k_n(2\kappa+1)\sqrt{2\kappa(\kappa+1)(2\lambda+1)(2l+1)(2l'+1)} \times \\ &\begin{pmatrix} \kappa & 1 & l \\ q & \alpha & -(\alpha+q) \end{pmatrix} \begin{pmatrix} \kappa & 1 & \lambda' \\ q & \alpha' & -(\alpha'+q) \end{pmatrix} \times \end{aligned}$$

$$\begin{pmatrix} l & \lambda & l' \\ m & (\alpha+q) & -m' \end{pmatrix} \begin{pmatrix} l & \lambda & l' \\ 0 & 0 & 0 \end{pmatrix}. \tag{9.31}$$

By the above expressions one can calculate the function $G_{\kappa}^{-\alpha\alpha'}$. It is apparent from the selection rules on the $3-j$ symbols that the matrix elements vanish whenever $m'-m-\alpha \neq m''-m'''-\alpha'$. The other function one needs for the calculation of the dipolar tensor elements is $H^{\kappa}_{\zeta_1,\zeta_2}(n_1,n_2)$. It may be calculated by evaluation of the expression

$$H^{\kappa}_{\zeta_1\zeta_2}(n_1,n_2) = \zeta_1^{-n_1-\kappa}\zeta_2^{-n_2+\kappa+1}\overline{H}(n_1+\kappa, n_2-\kappa-1, \zeta_2/\zeta_1) \tag{9.32}$$

where

$$\overline{H}(p,q,s) = (p-1)!(q-1)!B_{(1+s)^{-1}}(p,q). \tag{9.33}$$

Here, the function $B_{(1+s)^{-1}}(p,q)$ is the incomplete beta function, which can be calculated with the equation

$$B_{(1+s)^{-1}}(p,q) = \frac{(p+q-1)!}{(p-1)!}\sum_{i=0}^{\infty}\frac{(-)^i(1+s)^{-(p+i)}}{(p+i)!(q-i-1)!i!} \tag{9.34}$$

As noted in section 9.1 one has to add a delta function contribution in order to obtain correct results. This contribution is given by

$$\begin{aligned} D_O^{-\alpha\alpha'} &= \frac{8}{3}(K\pi)\sqrt{6\pi}(-)^{\alpha+\alpha'}\begin{pmatrix} 1 & 1 & 2 \\ \alpha' & -\alpha & (\alpha-\alpha') \end{pmatrix} \times \\ &\quad \delta(m'-m-\alpha, m''-m'''-\alpha') \times \\ &\quad \frac{(n_1+n_2-2)!}{(\zeta_1+\zeta_2)^{n_1+n_2-1}}\sum_{\bar{l}_{min},2}^{\bar{l}_{max}}\sum_{\bar{l}'_{min},2}^{\bar{l}'_{max}} S^{-\alpha\alpha'}(\bar{l},\bar{l}') \end{aligned} \tag{9.35}$$

The limits on the summations are given by

$$\begin{aligned} \bar{l}_{min} &= \text{maximum}\{|l-l'|, |m-m'|\}, \\ \bar{l}_{max} &= l+l', \\ \bar{l}'_{min} &= \text{maximum}\{|l''-l'''|, |m''-m'''|\}, \\ \bar{l}'_{max} &= l''+l'''. \end{aligned}$$

The constant K is equal to the products of the normalization-constants k_n :

$$K = k_n k_{n'} k_{n''} k_{n'''} \tag{9.36}$$

and the function $S^{-\alpha\alpha'}(\bar{l},\bar{l}')$ is given by

$$\begin{aligned} S^{-\alpha\alpha'}(\bar{l},\bar{l}') &= \tilde{S}^{-\alpha\alpha'}(\bar{l},\bar{l}')(-)^{m''+m'''}\sqrt{\frac{5(2\bar{l}+1)(2\bar{l}'+1)}{4\pi}} \times \\ &\quad \begin{pmatrix} \bar{l}' & 2 & \bar{l} \\ m''-m''' & \alpha-\alpha' & m-m' \end{pmatrix}\begin{pmatrix} \bar{l}' & 2 & \bar{l} \\ 0 & 0 & 0 \end{pmatrix} \end{aligned} \tag{9.37}$$

where the function $\tilde{S}^{-\alpha\alpha'}(\bar{l},\bar{l}')$ is given by

$$\tilde{S}^{-\alpha\alpha'}(\bar{l},\bar{l}') = (-)^{m'+m''}\sqrt{\frac{(2l+1)(2\bar{l}+1)(2l'+1)(2l''+1)(2\bar{l}'+1)(2l'''+1)}{16\pi^2}}\times$$
$$\begin{pmatrix} l & l & l' \\ -m & m-m' & m' \end{pmatrix}\begin{pmatrix} l & \bar{l}' & l' \\ 0 & 0 & 0 \end{pmatrix}\times$$
$$\begin{pmatrix} l'' & \bar{l}' & l''' \\ -m'' & m''-m''' & m''' \end{pmatrix}\begin{pmatrix} l'' & l' & l''' \\ 0 & 0 & 0 \end{pmatrix}. \qquad (9.38)$$

Bibliography

[1] J.D. Jackson.
Classical Electrodynamics.
Wiley (New York), 1962.

[2] A. Abragam and B. Bleaney.
Electron Paramagnetic Resonance of Transition Ions.
Dover Publications (New York), 1986.

[3] G.F. Kokoszka, H.C. Allen, and G.J. Gordon.
Journal of Chemical Physics, 46:3013, 1967.

[4] T.R. Felthouse and D.N. Hendrickson.
Inorganic Chemistry, 17:444, 1978.

[5] L. Banci, A. Bencini, and D. Gatteschi.
Journal of the American Chemical Society, 105:761, 1983.

[6] M.L. Boillot, Y. Journaux, A. Bencini, D. Gatteschi, and O. Kahn.
Inorganic Chemistry, 24:263, 1985.

[7] M.A. Hefni, N.M. McConnell, F.J. Rietmeijer, M.C.M. Gribnau, and C.P. Keijzers.
Molecular Physics, 57:1283, 1986.

[8] R.S. Mulliken.
Journal de Chimie et de Physique, 46:497, 1949.

[9] R.L. Matcha, C.W. Kern, and D.M. Schrader.
Journal of Chemical Physics, 51:2152, 1969.

[10] R.M. Pitzer, C.W. Kern, and W.N. Lipscomb.
Journal of Chemical Physics, 37:267, 1962.

[11] Y.-N. Chiu.
Journal of Mathematical Physics, 5:283, 1964.

[12] D.M. Schrader.
Journal of Chemical Physics, 41:3266, 1964.

[13] M. Geller.
Journal of Chemical Physics, 39:853, 1963.

[14] C.P. Keijzers and E. de Boer.
Molecular Physics, 29:1743, 1975.

[15] C.P. Keijzers, E.J. Reijerse, P. Stam, M.F. Dumont, and M.C.M. Gribnau.
Journal of the Chemical Society, Faraday Transactions I, 1987:3493, 1987.

[16] D.M. Brink and G.R. Sachtler.
Angular Momentum.
Oxford University Press (Oxford), 1962.

[17] R.H. Pritchard and C.W. Kern.
Journal of Chemical Physics, 57:2590, 1972.

[18] H.M. McConnell.
Proceedings of the National Academy of Sciences, 45:172, 1959.

[19] P.J. Davis and P. Rabinowitz.
Methods of Numerical Integration.
Academic Press, 1975.

[20] A.H. Stroud and D. Secrest.
Gaussian Quadrature Formulas.
Prentice Hall, 1966.

[21] G.H. Golub and J.H. Welsch.
Mathematics of Computations, 23:221. 1969.

[22] M. Abramowitz and I.A. Stegun.
Handbook of Mathematical Functions.
Dover Publications (New York), 1965.

[23] G.F. Kokoszka, H.C. Allen, and G.J. Gordon.
Journal of Chemical Physics, 46:3020, 1967.

[24] C. Chow and R.D. Willett.
Journal of Chemical Physics, 59:5903, 1973.

[25] A. Bencini, D. Gatteschi, J. Reedijk, and C. Zanchini.
Inorganic Chemistry, 24:207, 1985.

[26] A. Bencini, D. Gatteschi, and C. Zanchini.
Inorganic Chemistry, 24:700, 1985.

[27] A. Bencini, D. Gatteschi, and C. Zanchini.
Inorganic Chemistry, 24:704, 1985.

[28] J.G.M. van Rens and E. de Boer.
Chemical Physics Letters, 31:377, 1975.

[29] D. Snaathorst, H.M. Doesburg, J.A.A.J. Perenboom, and C.P. Keijzers.
Inorganic Chemistry, 20:2526, 1981.

[30] R.W.M. Ten Hoedt, J. Reedijk, and G.C. Verschoor.
Receuil de Travaux de Chimie de Pays-Bas, 100:400, 1981.

[31] C.P. Keijzers, H.J.M. de Vries, and A. van der Avoird.
Inorganic Chemistry, 11:1338, 1972.

Chapter 10

The Calculation of the Hyperfine Tensor

10.1 Introduction

The hyperfine interaction arises from the coupling between a nuclear spin $\vec{I}^N$ and one or more unpaired electrons. This coupling results in a splitting of each electron spin energy level in a manifold of $2I_N + 1$ energy levels, where I_N is the spin of nucleus N. The strength of the coupling is described with the tensor $\overline{\mathbf{A}}$. If the magnitude of the hyperfine interaction is larger than the inhomogeneous EPR-linewidth — which itself is the result of small unresolved hyperfine interactions — one can observe these splittings by conventional EPR spectroscopy. This is normally the case for atoms with a high spin-density such as the Cu and S-atoms in copper(II)-dithiolene complexes. For atoms with a low spin-density the splitting can be smaller than the linewidth. For these atoms one can measure the hyperfine tensor by double resonance techniques such as ENDOR and TRIPLE-resonance. These techniques are already available for many years. However, in the last few years the possibilities to determine small hyperfine interactions have increased greatly by the development of pulsed resonance techniques, like ESEEM and ESE-ENDOR, which do not have the limitations of conventional multi-resonance techniques. These new techniques renewed our interest in calculating the various contributions to the hyperfine tensor. In this section we will first describe the computational methods to calculate the main contributions to the hyperfine tensor and subsequently discuss the results of some of these calculations on copper(II)-dithiolene complexes.

Theoretical Expressions for the Hyperfine Tensor

The three principal interactions which give rise to the coupling between the effective electron spin $\vec{\mathbf{S}}$ and the nuclear spin $\vec{\mathbf{I}}^N$ of nucleus N are the electron-nuclear dipolar interaction, the spin-orbit coupling and the orbital-Zeeman interaction. The dipole-

dipole interaction (in SI-units) is given by

$$\mathcal{H}_{SI,dip} = \frac{\mu_0}{4\pi} g_e \mu_B \gamma_N \hbar \left\{ \sum_i 3\frac{(\vec{\mathbf{I}}^N \cdot \vec{\mathbf{r}}_i^N)(\vec{\mathbf{S}}^i \cdot \vec{\mathbf{r}}_i^N)}{(r_i^N)^5} - \frac{\vec{\mathbf{I}}^N \cdot \vec{\mathbf{S}}^i}{(r_i^N)^3} \right\} \tag{10.1}$$

$$= \frac{\mu_0}{4\pi} g_e \mu_B \gamma_N \hbar \sum_i \frac{1}{(r_i^N)^3} \sum_{\alpha,\beta} I_\alpha^N \hat{F}_{\alpha\beta}^{Ni} S_\beta^i \tag{10.2}$$

where the index i labels the electrons. The operator $\hat{F}^{Ni}$ is the following traceless symmetric tensor

$$\hat{F}_{\alpha\beta}^{Ni} = \begin{pmatrix} \sqrt{3}S_{2,2}^i - S_{2,0}^i & \sqrt{3}S_{2,-2}^i & \sqrt{3}S_{2,1}^i \\ \sqrt{3}S_{2,-2}^i & -\sqrt{3}S_{2,2}^i - S_{2,0}^i & \sqrt{3}S_{2,-1}^i \\ \sqrt{3}S_{2,1}^i & \sqrt{3}S_{2,-1}^i & 2S_{2,0}^i \end{pmatrix} \tag{10.3}$$

where the symbols $S_{l,m}^i$ denote the tesseral harmonics of electron i. The second interaction which should be taken into account is the spin-orbit coupling. For our purposes we will divide this interaction in a a field-dependent part $\mathcal{H}_{SO,B}$ and a field independent part $\mathcal{H}_{SO,N}$ according to

$$\mathcal{H}_{SO,B} = \frac{m_e g_e \mu_B \gamma_N}{4\pi\hbar} \sum_{k,i} \xi_k(r_i^k) \left\{ \frac{(\vec{\mathbf{S}}^i \cdot \vec{\mathbf{I}}^N)(\vec{\mathbf{r}}_i^N \cdot \vec{\mathbf{r}}_i^k) - (\vec{\mathbf{S}}^i \cdot \vec{\mathbf{r}}_i^N)(\vec{\mathbf{I}}^N \cdot \vec{\mathbf{r}}_i^k)}{(r_i^N)^3} \right\} \tag{10.4}$$

$$\mathcal{H}_{SO,N} = \frac{g_e}{2} \sum_{k,i} \xi_k(r_i^k) \vec{\mathbf{S}}^i \cdot \vec{\mathbf{L}}_i^k \tag{10.5}$$

where the index k runs over all nuclei present. Finally, the orbital-Zeeman term should be included. This interaction is given by

$$\mathcal{H}_{OZ} = \frac{\mu_0}{2\pi} \mu_B \gamma_N \hbar \sum_i \frac{\vec{\mathbf{I}}^N \cdot \vec{\mathbf{L}}_i^N}{(r_i^N)^3} \tag{10.6}$$

By combining these terms one can derive expressions for the main contributions to the hyperfine interaction. At this point one has to discriminate between the s and the non-s electrons. The only term which contributes to the hyperfine tensor of s electrons is $\mathcal{H}_{SO,B}$. This term results in an isotropic contribution to the hyperfine splitting — the Fermi contact interaction — which is given by

$$A_{\alpha\alpha}^N = \frac{2\mu_0}{3} g_e \mu_B \gamma_N \hbar \, |\phi_0(\vec{\mathbf{r}}_N = 0)|^2. \tag{10.7}$$

The term $|\phi_0(\vec{\mathbf{r}}_N = 0)|^2$ in this expression denotes the spin-density of the molecular orbital of the unpaired electron (ϕ_0) at the position of the nucleus. The hyperfine tensor of the non-s electrons consists of a first and second order contribution. The first order contribution originates from the electron-nuclear dipolar interaction $\mathcal{H}_{SI,dip}$:

$$A_{\alpha\beta}^{N(1)} = \frac{\mu_0}{4\pi} g_e \mu_B \gamma_N \hbar \left\langle \phi_0 \left| \frac{F_{\alpha\beta}^N}{(r^N)^3} \right| \phi_0 \right\rangle. \tag{10.8}$$

The main second order contribution is due to the combined interaction of the orbital Zeeman term $\mathcal{H}_{OZ}$ and the field independent term of the spin-orbit interaction $\mathcal{H}_{SO,N}$. These terms result in the anisotropic contribution

$$A_{\alpha\beta}^{N(2)} = \frac{\mu_0}{2\pi} g_e \mu_B \gamma_N \hbar \sum_{n\neq 0} \sum_{k} \frac{\left\langle \phi_0 \left| \xi_k(r^k) L_\alpha^k \right| \phi_n \right\rangle \left\langle \phi_n \left| \frac{L_\beta^N}{(r^N)^3} \right| \phi_0 \right\rangle}{\epsilon_0 - \epsilon_n}. \tag{10.9}$$

The symbol ϕ_n represents the n-th one-electron molecular orbital. The energy of this orbital is indicated by ϵ_n, whereas the energy of the MO of the unpaired electron is given by ϵ_0. This second order term is not traceless. Therefore, it gives rise to an isotropic contribution which can reach an appreciable value. It should be noted that experimentally one cannot distinguish this isotropic contribution from the isotropic contribution from the *s* electrons (equation 10.7).

The anisotropic contributions contain one-, two- and three-centre contributions. The multi-centre terms are in general small, because of the $(r^N)^{-3}$ dependence of the operator. Therefore, one can neglect these terms for atoms with a high spin-density, as the hyperfine interaction in these systems is completely determined by the one-centre term. However, for atoms with almost no spin-density the two- and three-centre terms significantly contribute to the hyperfine tensor. The multi-centre terms of the first order contribution are given by

$$\begin{aligned} A_{\alpha\beta}^{N(1),2-centre} &= \frac{\mu_0}{4\pi} g_e \mu_B \gamma_N \hbar \sum_A \sum_{a,b\in A} c_a c_b \left\langle \phi_a^A \left| \frac{F_{\alpha\beta}^N}{r_N^3} \right| \phi_b^A \right\rangle \\ &\quad + \frac{\mu_0}{4\pi} g_e \mu_B \gamma_N \hbar \sum_A \sum_{a\in A, b\in N} c_a c_b \left\langle \phi_a^A \left| \frac{F_{\alpha\beta}^N}{r_N^3} \right| \phi_b^N \right\rangle \end{aligned} \tag{10.10}$$

and

$$A_{\alpha\beta}^{N(1),3-centre} = \frac{\mu_0}{4\pi} g_e \mu_B \gamma_N \hbar \sum_{A,B} \sum_{a\in A, b\in B} c_a c_b \left\langle \phi_a^A \left| \frac{F_{\alpha\beta}^N}{r_N^3} \right| \phi_b^B \right\rangle \tag{10.11}$$

In transition-metal systems one can neglect the multi-centre second order contributions to the anisotropic hyperfine coupling, as the second order contribution has only an appreciable value for the central metal atom, for which one only needs to include the one-centre terms.

10.2 Computational procedure

The spin densities and MO-coefficients which were used in the computation of the hyperfine couplings were calculated with a semi-empirical extended-Hückel calculation [1]. The two parameters in the Hamilton matrix were taken equal to those which were obtained by optimizing the results for the monomeric copper(II)bis(diethyldithiocarbamate) [2]. The basis set for these calculations consists of single-zeta non core-orthogonalized Slater-type

orbitals (STO's), except for the copper $3d$-orbital for which a double-zeta function is used. Since the orbitals are non-core-orthogonalized these orbitals are not appropriate for the calculation of the spin density at the nucleus (isotropic hyperfine coupling) or the expectation values of r^{-3} (anisotropic coupling). In order to calculate these values one usually replaces the basis functions by core-orthogonalized double (or more) zeta STO's.

The one-centre contributions to the hyperfine tensors were calculated in the extended Hückel program itself [3]. Hereto, the expectation values of r^{-3} for the different combinations of atomic orbitals and the spin density at the nucleus, as calculated with multi-zeta core-orthogonalized STO's [4], were given as input parameters to the program. The multi-centre contributions were calculated separately [5]. For the calculations of these contributions the coefficients of tesseral d-functions, as obtained from the extended Hückel calculation, were first transformed into coefficients of cartesian d-functions. Subsequently, the single-zeta, non-core-orthogonalized STO's were extended to double-zeta core-orthogonalized STO's retaining the Hückel MO-coefficients for these extended orbitals. Finally each STO was expanded as a linear combination of 5 Gaussian-type orbitals using the coefficients and exponents of Stewart's maximum overlap fits. These expansions are substituted into the MO of the unpaired electron, and the components of the hyperfine coupling tensors are calculated with the property package of the program POLYATOM [6], which calculates all multi-centre contributions. In fact, the components of the electric field gradient tensor are calculated with this program but, since the integrals for the electric field gradient and the hyperfine interaction are identical except for a multiplication factor, it is straightforward to obtain the first-order hyperfine coupling tensor from the electric field gradient.

10.3 Calculated Hyperfine Tensors for Copper(II)-Dithiolene Complexes

We will illustrate the use of the above mentioned expressions by calculating the hyperfine tensors for some atoms in two transition-metal dithiolene complexes. The general structure of these systems is shown in figure 10.1. These systems have attracted the interest of EPR spectroscopist for many years, because of their interesting properties:

- The high covalency of the metal-sulphur bonds, which is the cause of the large delocalization of the unpaired spin density [7,8].
- The different metal oxidation states that are stabilized by these ligands and which result in various electronic configurations [9,10].
- The interesting behaviour with respect to ligand exchange reactions [11,12].
- The ability to form one-dimensional systems and π-donor-acceptor complexes [13,14,15,16,17].

In order to characterize the bonding in these systems in detail hyperfine data are needed because they provide direct information about the nature of the electronic ground state and about the extent of electron delocalization. The structure for most of these

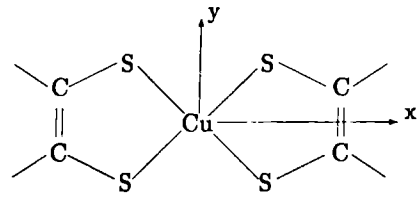

Figure 10.1: General structure of copper dithiolene complexes

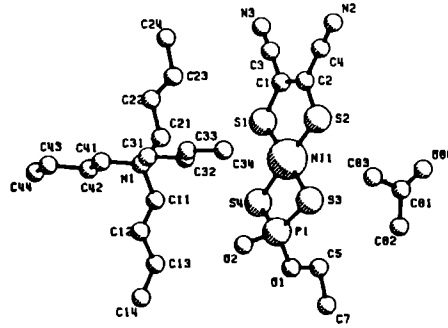

Figure 10.2: Structure of the asymmetric part of Ni(mnt)(HEtdtp)

complexes can be characterized as follows: The central copper atom is approximately square-planar coordinated by four sulphur atoms whereas the other ligand atoms are slightly out of plane [8]. This copper-sulphur plane was taken as the xy-plane in the MO-calculations with the x-axis pointing towards the bisection of the two sulphur atoms of one ligand. The picture that emerges from the extended Hückel MO-calculations on a great variety of these copper(II)-dithiolene complexes [7,8] is that about 50% of the unpaired electron is centered in the d_{xy} orbital of the copper atom. The remaining 50% is delocalized onto the four sulphur atoms. The spin density on the remaining ligand atoms is very small. In the following we will discuss the results of the calculations for (n-Bu_4)$_2$Cu(mnt)(HEtdtp)·0.7 acetone (mnt = maleonitriledithiolate and HEtdtp = monoethyldithiophosphate) [8] and (n-Bu_4)$_2$Cu(mnt)$_2$[18]. Both compounds were diamagnetically diluted by the corresponding Ni-complexes.

Cu(mnt)(HEtdtp)·0.7acetone

A picture of the structure of this compound is shown in figure 10.2 [8]. In contrast to many other copper-dithiolenes this compound has four different Cu-S bonds, which

range from 2.135 to 2.264 Å. Despite the unequality of these bonds the planarity of the copper-coordination sphere is preserved. Kirmse and coworkers were able to measure the ^{63}Cu hyperfine tensor with EPR and ENDOR. They also succeeded in measuring the ^{33}S hyperfine interactions (natural abundance 0.74%) of an not ^{33}S-enriched sample! In order to interpret their experimental results the ^{63}Cu and ^{33}S hyperfine interactions were calculated following the above mentioned procedures. For the calculations we used the structure of the Ni host molecule. Since, however, the Cu–S distances in the pure copper complexes are usually larger than the corresponding Ni–S distances [19,20,21,13] the ligands were shifted by 0.07 Å. As the spin-density on the copper and sulphur atoms is quite high, only the first and second order one-centre contributions were calculated. The results are presented in table 10.1. The anisotropic parts of the copper and sulphur hyperfine tensors agree perfectly well with experiment. This implies that the highest occupied molecular orbitals and their energies must reproduce the binding rather well. The isotropic coupling of copper is dominated by spin polarization of the inner shell s-electrons and, therefore, it cannot be calculated with this spin-restricted method. The isotropic sulphur couplings decrease rapidly with increasing copper-ligand distances. The difference between the experimental and calculated results of the hyperfine tensors for the two sulphur nuclei of the mnt-ligand suggests that this ligand should be shifted by more than 0.07 Å.

Kirmse et al. [8] also performed ^{1}H ENDOR measurements on this system. However, due to the complexity of the spectra they were not able to follow the proton resonance positions in three planes and, therefore, they couldn't determine the hyperfine tensors of the protons. However, the analysis and subsequent assignment was possible by calculating the hyperfine interactions including the multi-centre contributions of the closest protons. There are seven protons closer than 4.0 Å from the copper nucleus, all of them being intermoleculer ones: four on the n-Bu_4N^+ cation and three of one of the methyl groups of acetone. There is also an intramolecular proton at a distance of 4.09 Å from the copper atom. The theoretical tensors for these protons were calculated as described above. From these tensors the ENDOR frequencies were calculated and compared with the experimental frequencies. In this way, the hyperfine tensors for the seven intermolecular and one intramolecular proton could be determined. The results are listed in table 10.2. The signs of the principal values cannot be determined with ENDOR and therefore they are adapted to the calculated signs. At this point we want to note that calculating the hyperfine tensor with a point-charge model in which the delocalization of the unpaired electron is neglected leads to hyperfine couplings which are too large by a factor of two. As the tensors are almost axial only the axial components of the tensors are given. The correspondence between theory and experiment is good, both for the magnitude of the couplings as well as for their directions. An isotropic coupling is measured only for the intramolecular proton H_{211} which fits with the expectation that only this electron will have a direct spin-density.

		Calculated				Experimental			
		Principal values	Principal axes			Principal values	Principal axes		
			g_1	g_2	g_3		g_1	g_2	g_3
$\bar{\bar{\mathbf{g}}}$	g_1	2.088				2.090			
	g_2	2.026				2.027			
	g_3	2.023				2.024			
$\bar{\bar{\mathbf{A}}}^{Cu}$	A_1	−80.6	1	89	90	−80.6	1	90	91
	A_2	40.0	89	†		38.9	90	1	91
	A_3	40.5	91	†		41.7	89	90	1
	A_{iso}	14.0				−77.8			
$\bar{\bar{\mathbf{A}}}^{S_1}$ (mnt)	A_1	8.1	84	47	136	6.4	90	45	135
	A_2	−4.0	87	137	133	2.8	90	135	135
	A_3	−4.1	6	92	84	−3.6	0	90	90
	A_{iso}	14.7				11.8			
$\bar{\bar{\mathbf{A}}}^{S_2}$ (mnt)	A_1	8.1	95	132	138	7.2	90	135	135
	A_2	−4.0	87	138	49	−3.0	90	135	45
	A_3	−4.1	5	91	95	4.3	0	90	90
	A_{iso}	15.2				12.5			
$\bar{\bar{\mathbf{A}}}^{S_3}$ (dtp)	A_1	9.3	87	134	35	9.6	90	133	43
	A_2	−4.6	87	34	56	−3.7	90	43	43
	A_3	−4.7	4	91	94	−5.9	0	90	90
	A_{iso}	15.4				14.1			
$\bar{\bar{\mathbf{A}}}^{S_4}$ (dtp)	A_1	10.0	91	57	33	10.2	90	43	43
	A_2	−5.0	91	33	123	−3.5	90	43	133
	A_3	−5.1	1	89	90	−6.8	0	90	90
	A_{iso}	15.6				15.0			

†Axial tensor: the angles are undefined

Table 10.1: Calculated and experimental copper and sulphur hyperfine tensors of Cu(mnt)(HEtdtp)· 0.7 acetone. Principal axes in degrees relative to the principal axes of $\bar{\bar{\mathbf{g}}}$, principal values in 10^{-4}cm^{-1}.

			Calculated				Experimental			
			Principal values	Principal axes			Principal values	Principal axes		
Proton	$R_{Cu\text{-}H}$			g_1	g_2	g_3		g_1	g_2	g_3
H_{321}	3 83	A_1	0.64	75	106	23	0.67	81	110	23
		A_2	−0.30	42	123	112				
		A_3	−0.34	52	38	86				
H_{322}	3.56	A_1	0.75	84	70	159	0.74	89	72	165
		A_2	−0 36	164	102	100				
		A_3	−0.39	105	23	72				
H_{341}	3 86	A_1	0.61	78	75	20	0 57	80	68	24
		A_2	−0 29	139	124	71				
		A_3	−0.32	52	141	85				
H_{342}	3.63	A_1	0.70	81	105	163	0.72	83	95	171
		A_2	−0.34	25	110	76				
		A_3	−0.35	113	155	80				
H_{831}	3 47	A_1	0.77	85	95	173	0.83	85	103	168
		A_2	−0.38	42	131	83				
		A_3	−0 39	131	139	89				
H_{832}	3.71	A_1	0.68	79	74	160	0.67	70	81	162
		A_2	−0.33	150	114	107				
		A_3	−0 35	118	30	80				
H_{833}	3 73	A_1	0.65	80	101	15	0.68	80	96	13
		A_2	−0.32	39	126	105				
		A_3	0.33	52	38	88				
H_{211}	4.09	A_1	0.60	85	40	130	0.54	78	38	124
		A_2	−0.24	171	91	99				
		A_3	−0.35	97	50	41				
		A_{iso}					0.28			

Table 10.2: Calculated and experimental proton hyperfine couplings in Cu(mnt)(HEtdtp) ·0.7acetone. Principal axes in degrees relative to the principal axes of $\bar{\bar{\mathbf{g}}}$, principal values in 10^{-4}cm ^{1}.

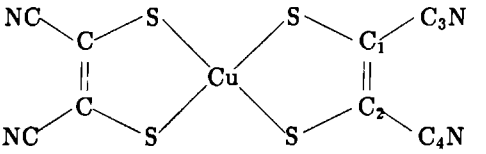

Figure 10.3: The $Cu(mnt)_2^{2-}$-anion

The ^{13}C and ^{14}N-hyperfine tensors of $Cu(mnt)_2^{2-}$

The calculated hyperfine tensors of the copper and sulphur atoms in Cu(mnt)(HEtdtp) arise only from the one-centre contributions, whereas the ^1H hyperfine interactions are only determined by the multi-centre contributions, because the spin density on the protons is zero (for the intermolecular ones) or small (for the intramolecular one). It would be interesting to compare the calculated and the experimental results for compounds in which the one-centre as well as the multi-centre terms are important. Therefore, we calculated the ^{13}C and ^{14}N hyperfine tensors in $(n\text{-}Bu_4)_2Cu(mnt)_2$: The ^{13}C and ^{14}N hyperfine tensors in this molecule consist of a one-centre part, due to a small direct spin-density on these atoms, and a multi-centre part because of the interaction of the electron spin density centered on the copper and sulphur atoms with the nuclear spins on these atoms. The ^{13}C tensors were measured by Kirmse and coworkers [7] in a single-crystal ENDOR study. The ^{14}N tensors were determined with the ESEEM-technique by Reijerse et al [18].

The ^{13}C hyperfine tensors

The structure of the anion of $Cu(mnt)_2$ is shown in figure 10.3 The hyperfine tensors were calculated for two different structures of the anion: For the first one the structure of the pure copper complex (C_i-symmetry) as determined by Soos et al. [13] was used; for the second one a structure with D_{2h}-symmetry was assumed. For the latter structure the atomic coordinates were derived from the structure of the pure Cu-complex by keeping as close as possible to the atom-atom distances. The calculated ^{13}C tensors are presented in table 10.3. From the table it is quite clear that the one-centre contributions alone cannot reproduce the experimental tensors. Although the relative order of the (absolute value of the) isotropic hyperfine couplings of C_1 and C_2 and of C_3 and C_4 is correct, the anisotropic hyperfine couplings of C_1 and C_2 are by far too small (and have the wrong sign) and those of C_3 and C_4 are too large. This concurs with the previous results that the one-centre contributions do explain the hyperfine couplings of the central metal atom and of the atoms of the first coordination sphere for copper complexes with unsaturated dichalcogeno ligands [22,3,2] but not for ligand-atoms at larger distances [5,23]. All calculated tensors depend strongly on the molecular structure. Although neither the copper molecule nor the host nickel complex has D_{2h}-symmetry it is suggested by the

experimental results that the guest molecule is close to D_{2h}-symmetry, because each tensor has one principal axis along the molecular z axis and the tensors of C_1 and C_2 and also those of C_3 and C_4 do not differ much The fact that the agreement of the calculated tensors with the experiment is better in D_{2h} symmetry than in the original structure of the copper complex suggests also that the guest molecule is forced into a higher symmetry than in its own structure

For C_3 and C_4 the calculations predict the correct sign for the hyperfine couplings and, in agreement with the experiment, the "axial" component of both tensors is located in the molecular plane It is concluded that this part of the molecular orbital of the unpaired electron is rather well reproduced by our calculations — the s density on C_3 and C_4 is $\approx$ 25 % underestimated and the p density is overestimated (30 % in D_{2h} symmetry) a result that is very satisfying for atoms at such a large distance from the paramagnetic centre The relatively large spin-density on the CN groups corresponds with the "electron-withdrawing" property that is ascribed to these groups

Close to the C_1–C_2 axis there is a nodal plane in the in the MO of the unpaired electron This explains why for C_1 and C_2 the one-centre contributions depend very critically on the structure but for any geometry they are smaller than the more-centre contributions It was predicted from these calculated results that the largest principal values of the experimental hyperfine coupling tensors of C_1 and C_2 would be negative, because if they were positive, then the one-centre contributions should dominate since the two and three-centre contributions yield a negative hyperfine coupling along z (and the maximum and positive principal value in the molecular plane) But a dominating one-centre contribution would mean a large spin-density in the p_z, which is only possible if the molecule is non-planar This, however, is highly improbable on the basis of the crystallographic structures This prediction was later confirmed by TRIPLE resonance measurements Although our spin-restricted calculations resulted in a correct prediction of the sign and yielded qualitative insight into the bonding in this complex, they were of course not able to reproduce these negative couplings quantitatively For that purpose, spin-unrestricted calculations must be performed

	Calculated						Experimental			
	1-centre	2-,3-centre	1-,2-,3-centre	Principal axes			Principal values	Principal axes		
				g_1	g_2	g_3		g_1	g_2	g_3
Crystal structure of $[Cu(mnt)_2]^{2-}$										
$C_1 : A_x$	−0.066	0.331	0.334	11	96	81	0.294	13	103	90
A_y	−0.066	−0.026	−0.081	82	13	101	0.129	77	13	90
A_z	0.131	−0.305	−0.254	98	78	14	−0.425	90	90	1
A_{iso}	0.675	0.085	0.760				−1.326			
$C_2 : A_x$	−0.098	0.335	0.332	14	85	77	0.311	15	75	90
A_y	−0.098	−0.029	−0.100	100	25	68	0.138	105	15	90
A_z	0.195	−0.306	−0.232	100	114	27	−0.448	90	90	2
A_{iso}	0.643	0.077	0.720				−1.270			
$C_3 : A_x$	−0.358	0.190	−0.184	175	86	94	−0.205	125	35	90
A_y	0.717	−0.075	0.630	85	21	110	0.325	35	55	90
A_z	−0.358	−0.116	−0.445	92	70	21	−0.120	90	90	0
A_{iso}	1.403	0.102	1.505				1.945			
$C_4 : A_x$	−0.372	0.192	−0.195	2	90	88	−0.219	118	152	90
A_y	0.745	−0.069	0.649	89	149	121	0.326	28	118	90
A_z	−0.372	−0.123	−0.454	91	121	31	−0.106	90	90	0
A_{iso}	1.295	0.095	1.390				1.854			
Assuming D_{2h}-symmetry										
$C_1 : A_x$	0.037	0.332	0.359	5	95	90	0.294	13	103	90
A_y	−0.019	−0.036	−0.048	85	5	90	0.129	77	13	90
A_z	−0.018	−0.296	−0.315	90	90	0	−0.425	90	90	1
A_{iso}	0.681	0.084	0.765				−1.326			
$C_3 : A_x$	−0.283	0.181	−0.117	174	84	90	−0.205	125	35	90
A_y	0.567	−0.087	0.495	84	6	90	0.325	35	55	90
A_z	−0.284	−0.094	−0.378	90	90	0	−0.120	90	90	0
A_{iso}	1.393	0.103	1.496				1.945			

Table 10.3: Calculated and experimental ^{13}C hyperfine tensors of $Cu(mnt)_2$ in the axis system of the $\bar{\bar{g}}$-tensor. Principal axes in degrees, principal values in 10^{-4}cm ^{1}.

The ^{14}N hyperfine tensors in $Cu(mnt)_2^{2-}$

For the calculation of the ^{14}N hyperfine splittings the structure of the $Cu(mnt)_2$ molecule was assumed to be the same as that of the nickel molecule in the host crystal with two alterations:

- The ligands were shifted by 0.06 Å along the x-axis, which results in in a copper-sulphur distance in between the metal sulfur distances of the guest and the host molecules.
- The computation of the nitrogen interactions turned out to be very sensitive to the C–N bond length and bond direction. In the host crystal the C–N bond lengths are different (1.130 and 1.147 Å) and both bonds point to the one side of the molecular plane [19]. In the pure copper crystal the C–N bond lengths are equal (1.144 and 1 143 Å), and one bond points above the plane, the other below the plane [13]. One expects that the distances are related to the copper atom, whereas the overall structure will resemble the host structure. Therefore, the C–N distances of the copper crystal and the C–N directions of the host crystal were used.

The numerical results are listed in table 10.4. Inspection of this table shows that the multicentre integrals are not dominant but still significant : approximately 20 % of the largest one-centre principal value. The effect of the two- and three-centre contribution is a reduction of (the absolute value of) A_1 and A_3, causing the calculated tensors to be nonaxial. This is in agreement with experiment. The total results for the anisotropic parts are equal to the experimental tensors, both in magnitude and direction, a result that might be somewhat fortuitous on the basis of the very crude MO-method used. The calculated isotropic hyperfine interaction is about 50% of the experimental value.

Conclusions

In the last two paragraphs we presented the results of calculations on the hyperfine tensor of the atoms in two copper(II) dithiolenes. These calculations showed that we are able to calculate this tensor with a very satisfactory agreement with experiment. For atoms with a high spin density one only needs to include the one-centre first and second order contributions. For the ligand-atoms with small spin densities only the first order contribution has to be calculated. However, in this case one also needs to include the multi-centre integrals. From the satisfactory agreement between the experimental and the calculated tensors one can conclude, especially considering the crude MO-method, that one can also calculate these couplings for systems where one is unable to measure the interactions. This result is very promising, since it means that one can calculate these tensors for very large systems, as, for instance, active centres in enzymes, for which the analysis of the experimental spectra is very hard. By combining the experimental and calculated data one can improve the analysis of the hyperfine tensors in these systems, which in turn offers the possibility to peep deeper into the molecular properties of these molecules.

		Calculated						Experimental			
		1-centre	2-,3-centre	Principal values	Principal axes			Principal values	Principal axes		
					x	y	z		A_1	A_2	A_3
$\overline{\overline{\mathbf{A}}}^{^{14}N_1}$	A_1	−0.471	0.156	−0.315	24	114	86	−0.318	34	111	65
	A_2	−0.477	−0.009	−0.483	89	80	11	−0.486	112	80	25
	A_3	0.948	−0.147	0.798	66	26	100	0.804	66	24	90
	A_{iso}	0.126	0.051	0.177				0.306			
$\overline{\overline{\mathbf{A}}}^{^{14}N_2}$	A_1	−0.420	0.147	−0.273	21	70	87	−0.249	41	63	62
	A_2	−0.426	−0.012	−0.435	90	89	9	−0.471	116	100	27
	A_3	0.846	−0.135	0.708	69	157	108	0.720	61	151	86
	A_{iso}	0.123	0.051	0.174				0.231			

Table 10.4: Calculated and experimental ^{14}N-hyperfine tensors of Cu(mnt)$_2$ in the molecular axis system and the axis system of A^{Cu}, respectively, at a temperature of 30 K. The directions of the principal axis A_1, A_2 and A_3 of the ^{63}Cu hyperfine tensor relative to the molecular axes x, y and z were not determined because the crystal was not oriented with X-ray diffraction. However, Maki et al. [24] found that $A_1 || x, A_2 || y$ and $A_3 || z$. Principal axes in degrees, principal values in MHz.

Bibliography

[1] C.P. Keijzers and E. de Boer.
Molecular Physics, 29:1743, 1975.

[2] C.P. Keijzers, H.J.M. de Vries, and A. van der Avoird.
Inorganic Chemistry, 11:1338, 1972.

[3] C.P. Keijzers and E. de Boer.
Molecular Physics, 29:1007, 1975.

[4] E. Clementi and C. Roetti.
Atomic Data and Nuclear Data Tables.
Volume 14, Academic Press (New York), 1974.

[5] C.P. Keijzers and D. Snaathorst.
Chemical Physics Letters, 69:348, 1980.

[6] D.B. Neumann, H. Basch, R.L. Kornegay, L.C. Snyder, J.W. Moskowitz, C. Hornback, and C.B. Liebmann.
QCPE, 11:199, 1974.

[7] R. Kirmse, J. Stach, U. Abram, W. Dietsch, R. Böttcher, M.C.M. Gribnau, and C.P. Keijzers.
Inorganic Chemistry, 23:3333, 1984.

[8] R. Kirmse, W. Dietsch, J. Stach, L. Golič, R. Böttcher, W. Brunner, M.C.M. Gribnau, and C.P. Keijzers.
Molecular Physics, 57:1139, 1986.

[9] J.G.M. van Rens, M.P.A. Viegers, and E. de Boer.
Chemical Physics Letters, 28:104, 1974.

[10] R.L. Schlupp and A.H. Maki.
Inorganic Chemistry, 13:44, 1974.

[11] W. Dietzsch, J. Reinhold, R. Kirmse, E. Hoyer, I.N. Marov, and V.K. Belyaeva.
Journal of Inorganic and Nuclear Chemistry, 39:41, 1977.

[12] W. Dietzsch, J. Lerchner, J. Reinhold, J. Stach, R. Kirmse, G. Steimecke, and E. Hoyer.
Journal of Inorganic and Nuclear Chemistry, 42:509, 1980.

[13] K.W.Plumlee, B.M. Hoffman, J.A. Ibers, and Z.G. Soos.
Journal of Chemical Physics, 63:1926, 1975.

[14] L.V. Interrante, K.W. Browall, H.R. Hart, I.S. Jacobs, G.D. Watkins, and S.H. Wee.
Journal of the American Chemical Society, 97:889, 1975.

[15] R.D. Schmitt, R.M. Wing, and A.H. Maki.
Journal of the American Chemical Society, 91:4394, 1979.

[16] R.M. Wing and R.L. Schlupp.
Inorganic Chemistry, 9:471, 1970.

[17] P.T. Manoharan, J.H. Noordik, E. de Boer, and C.P. Keijzers.
Journal of Chemical Physics, 74:1980, 1981.

[18] E.J. Reijerse, A.H. Thiers, R. Kanters, M.C.M. Gribnau, and C.P. Keijzers.
Inorganic Chemistry, 26:2764, 1987.

[19] A. Kobayashi and Y. Sasaki.
Bulletin of the Chemical Society of Japan, 50:2650, 1977.

[20] M. Bonamico, G. Dessy, C. Mariani, A. Vaciago, and L. Zambonelli.
Acta Crystallographica, 19:619, 1965.

[21] M. Bonamico, G. Dessy, C. Mariani, A. Vaciago, and L. Zambonelli.
Acta Crystallographica, 19:886, 1965.

[22] D. Snaathorst, H.M. Doesburg, J.A.A.J. Perenboom, and C.P. Keijzers.
Inorganic Chemistry, 20:2526, 1981.

[23] D. Snaathorst, C.P. Keijzers, A.A.K. Klaassen, E. de Boer, V.P. Chacko, and R. Gomperts.
Molecular Physics, 40:585, 1980.

[24] A.H. Maki, N. Edelstein, A. Davison, and R.H. Holm.
Journal of the American Chemical Society, 86:4580, 1964.

Summary

In this thesis the author presents a part of the results which he gathered during his four-year stay at the department of Molecular Spectroscopy of the University of Nijmegen. This research was carried out in close cooperation with the members of the technical and scientific staff under auspices of the Netherlands Foundation of Chemical Research (SON). The described measurements were mainly performed by means of the Electron Paramagnetic Resonance (EPR) technique. The thesis is divided into two parts for reasons of systematics. In the first part the results of the EPR measurements on three alkali aromatic systems are presented, whereas in the second part the calculation of four types of spin-spin interactions, which occur in the spin-Hamiltonian, are discussed.

In part I we describe the magnetic behaviour of the compounds NaBp.2Tg, RbBp.2Ttg and KBp.2Ttg (Bp= biphenyl= $C_{12}H_{10}$, Tg= triglyme= $CH_3O(CH_2CH_2O)_3CH_3$ en Ttg= tetraglyme= $CH_3O(CH_2CH_2O)_4CH_3$). The crystal structure of these substances consists of solvent-separated ion pairs. The biphenyl anions are arranged in layers. These paramagnetic layers are separated by diamagnetic layers of alkali bis-polyglyme clusters. Because of this special arrangement we expect pseudo-two-dimensional magnetic behaviour. In chapter 2 we present an outline of the theory by which one can describe the EPR line of such two-dimensional systems. We show that the angular dependence of the resonance linewidth of two-dimensional magnets differs from the angular dependence of the linewidth of three-dimensional magnetic systems. It can be described by the relation $\Delta B_{pp} = \alpha(3\cos^2\theta - 1)^2 + \beta$. The angle θ in this expression is the angle between the normal to the magnetic plane and the static magnetic field vector. Apart from this characteristic angular dependence of the resonance linewidth the resonance lineshape shows deviations from Lorentzian, except for the magic angle $\theta = \cos^{-1}(1/\sqrt{3})$. In the chapters 3,4 and 5 we present the experimental results for NaBp.2Tg, RbBp.2Ttg and KBp.2Ttg, respectively. All three mentioned compounds exhibit the predicted two-dimensional behaviour above 25 K. Furthermore, we observe differences in the behaviour of NaBp.2Tg and RbBp.2Ttg below this temperature. These differences can be traced back to differences in the arrangement of the biphenyl anions in the paramagnetic layer.

In NaBp.2Tg the distances between any biphenyl anion and its six nearest neighbours are approximately equal. As a result of this arrangement one expects a long-range ordered magnetic structure upon cooling. The experimental results support these ideas and point towards a three-dimensional magnetic structure at 1.2 K. Moreover, they show that more than one exchange coupling parameter is present in the magnetic layer. Above 80 K one observes the average of these interactions, which is positive, but below this temperature the presence of antiferromagnetic interactions becomes manifest. From an analysis of the resonance field shifts in combination with the susceptibility data we were able to propose a magnetic strcuture for the paramagnetic layers of biphenyl anions in NaBp.2Tg.

In RbBp.2Ttg one can distinguish pairs of biphenyl anions. This suggests that a number of the properties of this system may be described by means of the singlet-triplet model. The experimental data of the EPR and susceptibility measurements supported our expectations. The expectations were also confirmed by the observation of the double quantum transition within the triplet manifold at high microwave power levels at 4.2 K. Because of the singlet ground state of RbBp.2Ttg we searched for signals of isolated

biphenyl anion pairs in the triplet state. These signals were not detected. However, we observed signals with hyperfine structure, which could be ascribed to isolated biphenyl anions in the doublet state. These anions are the result of the incorporation of a small number of neutral biphenyl molecules in the crystal structure of RbBp.2Ttg. We could prove that the isolated anions in the doublet state are oriented according to the crystal structure of RbBp.2Ttg.

In the second part of this thesis we pay attention to the calculation of four spin-spin interactions which occur in the spin-Hamiltonian. The term spin-Hamiltonian refers to a method by which one can describe some of the principal features of the experimental EPR spectra by means of a limited number of parameters. In chapter 6 we start with a short overview of this method and subsequently we discuss the parameters which often occur in the spin-Hamiltonian of an EPR experiment. In the next four chapters we focus our attention on the calculation of four of these parameters.

First of all we discuss the exchange parameter J in chapter 7. This parameter occurs in the Heisenberg exchange interaction. We describe the calculation of the strength of this interaction on the basis of the Valence Bond model. Hereafter, we applied these expressions to the calculation of the exchange parameter for the different pairs of biphenyl anions, which occur in NaBp.2Tg. Although the absolute values of the calculated exchange constants are too small by an order of magnitude, the tendency of the calculations is in agreement with the experimental data of chapter 3.

In the next two chapters we discuss the calculation of the Zero Field Splitting (ZFS) tensor. This tensor is composed of two parts which have a different physical origin. One part arises from the dipolar interaction between two effective electron spins, the other part originates from the spin-orbit interaction. The contribution of the spin-orbit coupling is especially important in transition metal complexes. The expressions by which one may compute this contribution are relatively easy for a weakly coupled $S = 1/2$ dimer. Nevertheless it is not yet fully understood. Therefore, it will be discussed in chapter 8.

The second term which contributes to the ZFS tensor, the dipolar interaction between two electron spins, is the subject of chapter 9. One may calculate this tensor in a first order approximation according to the point dipole method. Although this approach suffices in many cases, especially if both the effective spins are localised on different molecules, it cannot be used under all circumstances. If the distance between the unpaired electron spins is small, one no longer can use this point-dipole approximation, but one has to calculate the distinct contributions by more exact methods. We illustrate our view by means of some calculations on halide-bridged copper(II) dimers. The calculation of the one- and two-centre contributions to the ZFS for these systems was carried out by home-written software. The main features of these programs will be discussed in this chapter as well.

Finally in chapter 10 we discuss a few calculated ^{63}Cu, ^{33}S, ^{14}N, ^{13}C en ^{1}H hyperfine tensors in copper(II) complexes. The calculated tensors show a very satisfactory agreement with the experimental ones. This result is very promising as regards the analysis of the experimental EPR spectra of large systems such as active centres in enzymes. By combining the experimental spectra of such systems with simulated ones, which are based on calculated hyperfine tensors, it will become possible to peep deeper into the molecular properties of these molecules.

Samenvatting

In dit proefschrift beschrijft de auteur een gedeelte van de onderzoeksresultaten die hij verzamelde tijdens zijn vierjarige verblijf op de afdeling Molecuul Spectroscopie van de K.U. Nijmegen. Hij verrichtte dit onderzoek in nauwe samenwerking met de technische en wetenschappelijke staf van deze afdeling onder auspiciën van de stichting Scheikundig Onderzoek Nederland (SON). De in dit proefschrift beschreven metingen werden voornamelijk verricht met behulp van de Electron Paramagnetische Resonantie (EPR) techniek. Uit het oogpunt van systematiek is het proefschrift verdeeld in twee stukken. In het eerste deel worden vooral de resultaten van de EPR metingen aan een drietal alkali-aromaat systemen beschreven, terwijl in het tweede deel de berekening van een aantal spin-spin interacties die voorkomen in de spin-Hamiltoniaan centraal staan.

In deel I beschrijven we het magnetische gedrag van de verbindingen NaBp.2Tg, RbBp.2Ttg en KBp.2Ttg (Bp= biphenyl= $C_{12}H_{10}$, Tg= triglyme = $CH_3O(CH_2CH_2O)_3$-CH_3 en Ttg= tetraglyme= $CH_3O(CH_2CH_2O)_4CH_3$). De kristalstructuur van deze verbindingen bestaat uit door oplosmiddel gescheiden ion paren, waarbij de biphenyl-anionen in een laag gerangschikt zijn. Deze paramagnetische lagen met biphenyl-anionen worden gescheiden door diamagnetische lagen waarin ieder alkali-kation gecomplexeerd is met twee polyglyme molekulen. Op grond van deze structuur verwachten we magnetisch twee-dimensionaal gedrag. In hoofdstuk 2 geven we een overzicht van de theorie waarmee we het gedrag van de EPR lijn van magnetisch twee-dimensionale systemen kunnen beschrijven. We laten zien dat de hoekafhankelijkheid van de lijnbreedte voor een dergelijk systeem verschilt van die van een magnetisch drie-dimensionaal systeem en dat die beschreven kan worden als $\Delta B_{pp} = \alpha(3\cos^2\theta - 1)^2 + \beta$. In deze uitdrukking is θ is de hoek tussen het uitwendige magneetveld en de normaal op het magnetische vlak . Verder geldt voor een magnetisch twee-dimensionaal systeem dat de lijnvorm niet langer lorentzisch is behalve bij de magische hoek $\theta = \cos^{-1}(1/\sqrt{3})$. In de hoofdstukken 3 t/m 5 worden de experimentele resultaten van respectievelijk NaBp.2Tg, RbBp.2Ttg en KBp.2Ttg gepresenteerd. Boven de 25 K vertonen alle drie de verbindingen het voorspelde magnetisch twee-dimensionale gedrag. In NaBp.2Tg en RbBp.2Ttg nemen we beneden deze temperatuur verschillen waar die we kunnen terugvoeren op verschillen in de rangschikking van de biphenyl-anionen in de paramagnetische laag.

In NaBp.2Tg zijn de afstanden van een willekeurig biphenyl-anion tot zijn verschillende buren ongeveer gelijk. Op grond hiervan verwachten we dat in deze verbinding bij afkoelen een long-range geordende magnetische structuur ontstaat. Dit wordt bevestigd door de experimentele resultaten die erop duiden dat in NaBp.2Tg een magnetische structuur met interacties in drie dimensies aanwezig is bij 1.2 K. Bovendien tonen zij aan dat er verschillende exchange interacties in de magnetische laag aanwezig zijn. Boven de 80 K nemen we alleen het gemiddelde — dat positief is — waar. Beneden deze temperatuur wordt ook de aanwezigheid van een antiferromagnetische interactie manifest. Door de richting van de verschuiving van de resonantiepositie bij 1.2 K en de gegevens van susceptibiliteitsmetingen te combineren is het mogelijk een magnetische structuur voor de paramagnetische biphenyl-anion lagen in NaBp.2Tg voor te stellen.

In het RbBp.2Ttg ligt een van de buren duidelijk dichter bij, wat suggereert dat een beschrijving van de eigenschappen van dit systeem met het singlet-triplet model mogelijk

is. Dit wordt bevestigd door de resultaten van susceptibiliteits- en EPR metingen. Een andere bevestiging is de extra lijn die we waarnemen rond de 4.2 K bij hoge microgolf-vermogens. Dit blijkt de double-quantum overgang binnen de triplet-toestand te zijn. Omdat het RbBp.2Ttg een singlet-grondtoestand heeft hebben we gezocht naar ESR-signalen van geisoleerde tripletten. Deze hebben we niet waargenomen. Wel vonden we signalen met een hyperfijn structuur die we toe konden schrijven aan de geisoleerde biphenyl-anionen in de doublet toestand. Deze anionen ontstaan door de inbouw van een gering percentage neutrale biphenyl moleculen in het kristalrooster van RbBp.2Ttg. We konden verder aantonen dat deze geisoleerde anionen georienteerd zijn volgens de kristalstructuur van RbBp.2Ttg.

In het tweede deel van het proefschrift besteden we aandacht aan de berekening van een viertal spin-spin interacties die voorkomen in de spin-Hamiltoniaan. Het begrip spin-Hamiltoniaan verwijst hier naar een methode waarmee men de voornaamste gegevens van experimentele EPR-spectra door middel van een beperkt aantal parameters op een eenvoudige en eenduidige wijze kan beschrijven. In hoofdstuk 6 geven we eerst een kort overzicht van deze methode en vervolgens bespreken we de parameters die vaak in de spin-Hamiltoniaan van een EPR experiment voorkomen. In de volgende hoofdstukken gaan we dieper in op de berekening van een aantal van deze parameters.

Allereerst besteden we in hoofdstuk 7 aandacht aan de exchange parameter J. Deze parameter komt voor in de Heisenberg exchange interactie. We beschrijven hoe men de sterkte van deze interactie kan berekenen uitgaande van het Valence Bond model. Hierna passen we de afgeleide formules toe op de berekening van de exchange interactie in de verschillende biphenyl anion paren, die voorkomen in NaBp.2Tg. Hoewel de absolute waarde van de berekende exchange parameters veel te klein is, is de trend van de berekeningen in overeenstemming met de experimentele gegevens van hoofdstuk 3.

In de volgende twee hoofdstukken staat de berekening van de nulveldsplitsings tensor centraal. Deze tensor bestaat uit twee gedeelten die een fysisch verschillende oorsprong hebben. Het ene gedeelte komt voort uit de dipolaire interactie, het andere gedeelte vindt zijn oorsprong in de spin-baan koppeling. De bijdrage van de spin-baan koppeling is met name van belang in overgangsmetaalcomplexen. De uitdrukkingen om deze laatste bijdrage te berekenen zijn relatief eenvoudig voor een zwak gekoppeld $S = 1/2$ dimeer. Toch blijkt uit de literatuur dat de essentie van de methode onvoldoende begrepen is. Hieraan besteden we aandacht in hoofdstuk 8.

De tweede term die bijdraagt tot de nulveldsplitsings tensor, de dipolaire interactie tussen twee electronen, is het onderwerp van hoofdstuk 9. Deze tensor kan in een eerste orde benadering berekend worden volgens de zogenaamde punt-dipool methode. Hoewel deze methode vaak voldoet, met name als de beide effectieve spins gelocaliseerd zijn op verschillende moleculen, is hij zeker niet altijd correct. Als de afstand tussen de effectieve electron spins klein is, kan men niet langer volstaan met de punt-dipool methode, maar moeten de verschillende bijdragen zo exact mogelijk berekend worden. We illustreren dit aan de hand van berekeningen aan een tweetal halogeen-gebrugde koper dimeren. De berekening van de zogenaamde één- en twee-center bijdragen voor deze systemen werd uitgevoerd met zelf geschreven programmatuur. De hoofdlijnen van deze programmatuur worden ook in dit hoofdstuk beschreven.

In hoofdstuk 10 tenslotte bediscussiëren we enkele berekende ^{63}Cu, ^{33}S, ^{14}N, ^{13}C en ^{1}H

hyperfijn tensoren in koper-complexen. De berekende tensoren stemmen goed overeen met de experimenteel bepaalde tensoren. Dit resultaat is zeer bevredigend en biedt perspectieven voor de analyse van de experimentele EPR spectra van grote systemen, zoals actieve centra in enzymen. Door de combinatie van de experimentele spectra van dergelijke systemen met simulaties die uitgaan van de berekende hyperfijn tensoren wordt het dan mogelijk de moleculaire eigenschappen van deze systemen beter te bestuderen.

Curriculum Vitae

De auteur van dit proefschrift werd op 18 augustus 1959 te Heerlen geboren. Na het behalen van het diploma gymnasium-β aan het Bernardinus College te Heerlen in 1977 werd in datzelfde jaar begonnen met de studie scheikunde aan de K.U. Nijmegen. Het kandidaatsexamen werd op 29 september 1980 afgelegd (cum laude) met als hoofdvakken scheikunde en natuurkunde en bijvak wiskunde. In de doctoraalfase werden bijvakstages gelopen op de afdelingen theoretische chemie bij dr. P.E.S. Wormer en prof. dr. ir. A. van der Avoird en organische chemie bij prof. dr. W.H. Laarhoven. Het onderzoek voor de hoofdvakstage werd uitgevoerd op de afdeling molecuulspectroscopie onder begeleiding van prof. dr. E. de Boer en dr. C.P. Keijzers. Het doctoraal examen werd op 27 februari 1984 afgelegd (cum laude). Voor het werk op de afdelingen molecuulspectroscopie en theoretische chemie werd de studieprijs 1984 van de faculteit wiskunde en natuurwetenschappen van de K.U. Nijmegen toegekend.

Vanaf 1 maart 1984 tot 1 maart 1988 is de auteur — als onderzoekmedewerker in dienst van SON/ZWO — verbonden geweest aan de afdeling molecuulspectroscopie van de K.U. Nijmegen bij prof. dr. E. de Boer. Op die afdeling werd het onderzoek verricht dat in dit proefschrift beschreven wordt.

In het kader van zijn onderwijstaak gaf hij colleges en werkcolleges Fasenleer en Kinetiek en werkcolleges Spectroscopische Methoden. Verder verzorgde hij onderdelen van het practicum Spectroscopie.

Stellingen

1. EPR poeder-spectra kunnen snel en nauwkeurig berekend worden door de bikubische interpolatie techniek te combineren met een volgalgoritme voor de energieniveau's dat gebaseerd is op de inproducten van de eigen-vectoren voor naburige oriëntaties.

2. De studie van Rubins en Drumheller naar het gedrag van de $\overline{\overline{g}}$-tensor in Cu^{2+} gedoopte $ZnTiF_6 \cdot 6H_2O$ kristallen is verkeerd opgezet.

   R.S. Rubins en J.E. Drumheller
   J. Chem. Phys. **86**, 6660, 1987.

3. Het is inconsequent om de susceptibileits-data van bis(N-methyl-phenazinium)bis(dicyanoethenedithiolato)cuprate(II) te analyseren in termen van een 1-*d* magnetisch systeem en tegelijkertijd de EPR lijnbreedten metingen te beschrijven in termen van een 3-*d* magnetisch systeem.

   P. Kuppusamy, B.L. Ramakrishna en P.T. Manoharan
   Inorg. Chem. **23**, 3886, 1984.

4. De conclusie van Tékély et al. dat er twee typen PMMA ketens voorkomen in een 50/50 PVF_2/PMMA blend is in tegenspraak met hun eigen experimentele resultaten.

   P. Tékély, F. Laupretre en L. Monnerie
   Polymer **26**, 1081, 1985.

5. De door Hsu et al. bepaalde backbone conformaties van drie cyclische dinucleotiden zijn gebaseerd op te weinig experimentele gegevens.

   C.-Y.J. Hsu, D. Dennis en R.A. Jones
   Nucleosides and Nucleotides **4**, 377, 1985

6. De ontwikkeling van de hoge T_c supergeleiders zal het uitvoeren van magneetveld gestuurde chemische reacties economische rendabel maken.

7. Op grond van financiele overwegingen dienen de gezamelijke Nederlandse universiteiten een inkoopbureau in de Verenigde Staten te vestigen.

8. Het moderne natuurwetenschappelijke onderzoek vertoont teveel overeenkomsten met de wereld van de popmuziek.

9. Beter een doctorsbul in de hand dan negen stellingen in de NRC.

Michiel Gribnau
Nijmegen, 22 juni 1988.